

**University of Alberta**

**A Methodology for Calculating Tonnage Uncertainty in  
Vein-Type Deposits**

by

**Michael J. Munroe**

A thesis submitted to the Faculty of Graduate Studies and Research  
in partial fulfillment of the requirements for the degree of

**Master of Science  
in  
Mining Engineering**

Department of Civil and Environmental Engineering

©Michael J. Munroe  
Spring 2012  
Edmonton, Alberta

Permission is hereby granted to the University of Alberta Libraries to reproduce single copies of this thesis and to lend or sell such copies for private, scholarly or scientific research purposes only. Where the thesis is converted to, or otherwise made available in digital form, the University of Alberta will advise potential users of the thesis of these terms.

The author reserves all other publication and other rights in association with the copyright in the thesis and, except as herein before provided, neither the thesis nor any substantial portion thereof may be printed or otherwise reproduced in any material form whatsoever without the author's prior written permission.

# Abstract

*One of the main sources of uncertainty in vein type deposits is found in the calculation of the tonnage. The boundary limits often applied to a vein type deposit are calculated from sparse data using deterministic methods that offer no measure of uncertainty. The most common method used to calculate the tonnage of a vein-type deposit is to convert the volume of the deposit defined by a wireframe model into a tonnage. Wireframe models are deterministic in nature being created from the interpretation of level plans and cross sections. These types of models have no provision for the calculation of tonnage uncertainty. One method of calculating the tonnage uncertainty in vein deposits is through the use of a distance function. This thesis presents a distance function (DF) approach that allows for the introduction of uncertainty into the modeling process by defining a zone or bandwidth that is quantifiable. This approach uses individual drillhole samples coded with a distance calculated by the DF rather than a wireframe model to estimate the vein tonnage resulting in considerable savings in time by skipping the wireframe modeling process. Three dimensional models are then extracted for probability intervals across the bandwidth. Through standardization, tonnages corresponding to any probability interval can be extracted. Modifying the distance function modifies the size and shape of the bandwidth. Two parameters are used to modify the distance function. The first parameter controls the bandwidth and is the uncertainty parameter. The second parameter controls position of bandwidth and is the bias correction parameter. With proper calibration, the values of the two parameters used to modify the distance function will result in models that are both accurate and precise. A method for full calibration of the uncertainty and bias correction parameters is presented. An example using synthetic models is also presented and demonstrates that the method does produce results that are accurate and precise within a defined tolerance.*

# Acknowledgement

I would like to express my deep appreciation to the **Centre for Computational Geostatistics (CCG)** and members at the **University of Alberta** for providing an environment in which to expand my knowledge. I would especially like to express my gratitude to **Dr. Clayton V. Deutsch** for his motivation, guidance and unrelenting patience.

# Table of Contents

<b>CHAPTER 1</b>	<b>INTRODUCTION .....</b>	<b>1</b>
1.1	The Problem.....	1
1.2	Background.....	2
1.2.1	Geometry of Vein Deposits .....	2
1.2.2	Epithermal Deposits.....	3
1.2.3	Mesothermal Deposits .....	4
1.3	Previous Work .....	5
1.4	Thesis Summary.....	6
1.4.1	Statement.....	6
1.4.2	Outline.....	6
<b>CHAPTER 2</b>	<b>FRAMEWORK FOR TONNAGE UNCERTAINTY .....</b>	<b>8</b>
2.1	Problem Setting.....	8
2.2	Criteria for Good Uncertainty .....	11
2.2.1	Unbiasedness.....	11
2.2.2	Fair Uncertainty .....	12
2.2.3	Low Uncertainty .....	14
2.3	Distance Function .....	14
2.3.1	Distance Function (DF).....	14
2.3.2	Modified Distance Function ( $DF_{mod}$ ).....	19
2.3.3	Distance Function Thresholds.....	23
2.4	Mapping of the Distance Function.....	26
2.4.1	SK Mean .....	27
2.4.2	Variogram .....	30
2.4.3	Anisotropy.....	31
2.5	Implementation Considerations .....	34
2.5.1	Procedure Summary.....	34
2.5.2	Soft Knowledge .....	35

<b>CHAPTER 3</b>	<b>PARAMETER INFERENCE .....</b>	<b>37</b>
3.1	Data and Mean .....	37
3.2	Variogram and Anisotropy .....	38
3.2.1	Theoretical Variogram Model.....	40
3.2.2	Numerical Verification .....	43
3.2.3	Comments on Multiple strings / Multiple intercepts .....	48
3.2.4	Practical Considerations.....	49
3.3	Parameter Guidelines .....	49
3.3.1	Variogram .....	49
3.3.2	Unbiasedness parameter C.....	50
3.3.3	Fairness parameter Beta.....	54
3.3.4	Anisotropy.....	55
3.3.5	Simple Kriging Interpolator .....	56
3.3.6	SK Mean .....	56
3.4	Assessing Uncertainty.....	57
3.4.1	Accuracy Plots .....	59
3.5	Calibration of Parameters .....	63
3.5.1	Objective function / criteria .....	63
3.5.2	Parameter Optimization .....	67
3.5.3	Search Strategy C/Beta Space.....	68
3.6	Implementation Considerations .....	72
3.6.1	Computational considerations.....	72
3.6.2	Practical Considerations.....	73
<b>CHAPTER 4</b>	<b>SYNTHETIC EXAMPLES.....</b>	<b>76</b>
4.1	Simulation and the Reference Models .....	76
4.1.1	Creating the Reference Models.....	76
4.1.2	Smoothing.....	80
4.2	Estimation Process .....	81
4.2.1	Drilling the Synthetic Orebodies .....	81
4.2.2	Application of the Distance Function .....	85

4.3	Calibration.....	87
4.4	Uncertainty Results.....	89
4.4.1	Drill Spacing 5 .....	90
4.4.2	Drill Spacing 10 .....	92
4.4.3	Drill Spacing 15 .....	94
4.4.4	Drill Spacing 20 .....	97
4.5	Linkages & Implementation Challenges.....	100
4.5.1	Multiple intercepts .....	101
4.5.2	Anisotropy.....	101
4.5.3	Widely Spaced Data.....	101
<b>CHAPTER 5 PRACTICAL APPLICATION.....</b>		<b>103</b>
5.1	Introduction.....	103
5.2	Methodology .....	104
5.2.1	Selection of C and $\beta$ .....	106
5.2.2	Anisotropy.....	108
5.2.3	Variogram .....	108
5.3	Results.....	108
<b>CHAPTER 6 CONCLUSION .....</b>		<b>112</b>
6.1	Conclusions.....	112
6.2	Future Work .....	113
<b>BIBLIOGRAPHY .....</b>		<b>116</b>
<b>APPENDICES.....</b>		<b>118</b>
<b>APPENDIX A: PROGRAM SUMMARY, PARAMETER FILES AND SCRIPTS.....</b>		<b>A-1</b>
<b>APPENDIX B: PROGRAM RESULTS .....</b>		<b>B-1</b>
<b>APPENDIX C: PRACTICAL EXAMPLE FIGURES .....</b>		<b>C-1</b>

# List of Tables

<b>Table 3-1:</b> Slope and intercepts by region .....	46
<b>Table 4-1:</b> Comparison of methodology drill spacing to those found in real world. .....	85
<b>Table 4-2:</b> Full Calibration Results for 5 unit drill spacing .....	87
<b>Table 4-3:</b> Full Calibration Results for 10 unit drill spacing .....	87
<b>Table 4-4:</b> Full Calibration Results for 15 unit drill spacing .....	88
<b>Table 4-5:</b> Full Calibration Results for 20 unit drill spacing .....	88
<b>Table 5-1:</b> Comparison of Optimal values of C and Beta with selected values.	107
<b>Table 5-2:</b> p-value Volumes.....	111

# List of Figures

<b>Figure 1-1:</b> Example of Cross sections and Level plans. From Dennen 1989.....	1
<b>Figure 1-2:</b> Relationship between epithermal and mesothermal ore deposits (Modified from Kessler, 1994) .....	4
<b>Figure 2-1:</b> A) DF distribution with no modification, B) Drillhole example, C) DF distribution with C modification, D) Drillhole example.....	10
<b>Figure 2-2:</b> Schematic illustration of bias; (Left) Unbiased Estimator; (Upper Right) Biased estimator – Estimate less than true value; (Lower Right) Biased estimator – Estimate greater than true value.....	12
<b>Figure 2-3:</b> An illustration of accuracy plots, (Left) fair estimate, actual proportion is equal to the assigned proportion. (Centre) unfair estimate, too many estimates fall within the assigned $p$ -interval. (Right) unfair estimate, too few estimates fall within the assigned $p$ -interval.....	14
<b>Figure 2-4:</b> Schematic of distance function. Numbers indicate the distance assigned by the DF.....	16
<b>Figure 2-5:</b> Schematic of the uncertainty bandwidth defined by C. ....	17
<b>Figure 2-6:</b> Examples of C parameters, increasing C from left to right. ....	17
<b>Figure 2-7:</b> When C=0 the uncertainty bandwidth has zero thickness. ....	18
<b>Figure 2-8:</b> When C=4 the uncertainty bandwidth has a thickness of 8, -4 to +4. ....	18
<b>Figure 2-9:</b> Effect of C on the DF and modified DF. ....	20
<b>Figure 2-10:</b> Effect of $\beta$ on the DF and modified DF.....	21
<b>Figure 2-11:</b> Effect of $\beta$ on the iso-zero surface. With increasing $\beta$ , the surface expands, with decreasing $\beta$ the surface contracts. ....	22
<b>Figure 2-12:</b> Behaviour of Beta on the distribution of a set of interpolated realizations .....	22
<b>Figure 2-13:</b> As Beta increases from 1, the iso-zero surface expands. ....	23
<b>Figure 2-14:</b> As Beta decreases from 1, the iso-zero surface shrinks.....	24

<b>Figure 2-15:</b> Uncertainty Bandwidth limits, DFmin inner limit, DFmax outer limit. ....	25
<b>Figure 2-16:</b> Schematic of uncertainty bandwidth between drillholes. ....	25
<b>Figure 2-17:</b> Effect of changing SK mean. Each realization uses the same parameters with the exception of the mean. (top) Mean = +5 units, (centre) Mean = zero, (bottom) Mean = -5 units. ....	29
<b>Figure 2-18:</b> Effect of smaller variogram ranges. ....	31
<b>Figure 2-19:</b> Effect of larger variogram ranges. ....	31
<b>Figure 2-20:</b> Example of geometric anisotropy in a tabular vein oreshoot. ....	32
<b>Figure 2-21:</b> Geometric Anisotropy, Vs - along strike direction, Vt – thickness	33
<b>Figure 2-22:</b> Geometric anisotropy applied to DF. ....	33
<b>Figure 3-1:</b> Schematic diagram of Distance Function. Distance increases away from vein/non-vein boundary. ....	39
<b>Figure 3-2:</b> Drillhole geometry in simplified form. ....	40
<b>Figure 3-3:</b> Defined drillhole regions. ....	41
<b>Figure 3-4:</b> Z(u), Z(u+h) pairs by Region. Diagram depicts which rock types are paired and from which regions as the lag distance increases. For example, when the lag distance is between (A/2 + a/2) and (A), the lag distance is longer than the thickness of the vein therefore no vein pairs exist. This is shown on the right outer edge of the diagram, RI-RIV, RII-RIV, RIII-RIV and RIV-RIV at the bottom. ..	44
<b>Figure 3-5:</b> Schematic of experimental variogram regions with respect to the domain A. ....	45
<b>Figure 3-6:</b> Experimental variogram example for lag <i>h</i> where drillhole length A=100 and vein thickness a=20. ....	45
<b>Figure 3-7:</b> Relationship of Data (left) to variogram slopes and intercepts (right) .....	48
<b>Figure 3-8:</b> Theoretical Variogram calculated using Equation 3.7. ....	48
<b>Figure 3-9:</b> Examples of uncertainty in orebody volume. Each example is same orebody realization, and same vertical slice through the centre in the XZ plane. Distance function calculated using $\beta$ equal to one. The solid outline is the true orebody outline. ....	51

<b>Figure 3-10:</b> Examples of uncertainty using $C$ and $\beta$ combinations. Each example is same orebody realization, and same vertical XZ slice through the centre of the model. Distance function calculated using $\beta$ values from 0.25 to 2.0. The solid outline is the actual orebody. ....	53
<b>Figure 3-11:</b> - Vertical section of the true orebody in the XZ plane through centre of simulated orebody.....	54
<b>Figure 3-12:</b> Vertical section in the XZ plane. Beta = 1, base case.....	54
<b>Figure 3-13:</b> Vertical section in the XZ plane. Beta = <1, Iso-zero contracts.....	55
<b>Figure 3-14:</b> Vertical section in the XZ plane. Beta >1, Iso-zero dilates .....	55
<b>Figure 3-15:</b> The effect of changing the SK mean on the DF. Vertical sections in the XZ plane.....	57
<b>Figure 3-16:</b> Schematic showing, Bias toward underestimation (left); Unbiased (centre); Bias toward overestimation (right);.....	58
<b>Figure 3-17:</b> Accuracy and precision; A) Accurate and Precise, B) Accurate and too precise, C) Accurate and imprecise, and D) On average accurate and precise. ....	62
<b>Figure 3-18:</b> Same sample as <b>Figure 3-17</b> D, different arrangement. Both are equally precise and on average accurate. This particular situation is difficult to control and is undesirable. ....	63
<b>Figure 3-19:</b> Contour plot depicting the relationship of $O1$ to $C$ and $\beta$ .....	64
<b>Figure 3-20:</b> Contour plot depicting the relationship of $O2b$ to $C$ and $\beta$ .....	66
<b>Figure 3-21:</b> Optimization of $C$ and $\beta$ .....	67
<b>Figure 3-22:</b> Initial four points used in Full Optimization of $C$ and $\beta$ .....	69
<b>Figure 3-23:</b> Full Optimization $O1$ .....	70
<b>Figure 3-24:</b> Full Optimization $O2b$ .....	71
<b>Figure 3-25:</b> Plot of $O2$ versus number of reference models interpreted. ....	73
<b>Figure 3-26:</b> Vertical cross section example. Arrows point to the closest sample used in calculation of the DF. Colored background represents a 2D model of the DF. Hotter colors are farther away from the vein. Cold colors (Darker blues) are closer to, or located inside vein. Note that in some instances the pairs cross	

structural boundaries. Also inclined holes and an inclined deposit can cause artefacts. .... 74

**Figure 3-27:** Modeled and clipped DF shown crossing an interpreted fault (Dashed Line) on the lower three holes. However on the upper three holes the DF terminates before the fault due to the absence of vein down dip. Outline of wireframe vein shown for reference. .... 75

**Figure 4-1:** (left) unmodified unconditioned 2d surface, (right) unmodified data conditioned 2d surface showing location of conditioning data. .... 77

**Figure 4-2:** Modified conditional 2d surface, zeroed so outer fringes of area equal zero. .... 77

**Figure 4-3:** (left) Modified final conditional 2d surface, zeroed so outer fringes of area equal zero. .... 79

**Figure 4-4:** XZ Cross section through modified conditional and unconditional surfaces ..... 79

**Figure 4-5:** (top) Modified SGS surfaces without smoothing; (bottom) Modified surfaces using smoothing..... 80

**Figure 4-6:** 5-point moving average used to smooth out modified realizations. . 81

**Figure 4-7:** Drill5.exe output example. The hole is located at the centre of the 100x100 surface grid, (50, 50). The upper surface is at 104.5 and the lower surface at 89.6. The Hole number is 41. If the sample elevation  $z$ , third column, is between  $Z_u$  and  $Z_l$ ,  $VI = 1$ . .... 83

**Figure 4-8:** Drill spacing shown superimposed on Realization #1. Spacings are relative to deposit size..... 84

**Figure 4-9:** (left) Euclidean distances to samples with different VI values, negative values are  $VI = 1$ , Positive values are  $VI = 0$ . (right) Modified distances applied by the DF when  $C_p = 4$  and  $\beta = 1$ . .... 86

**Figure 4-10 :** Optimized values of C versus drill spacing ..... 89

**Figure 4-11 :** Optimized values of  $\beta$  versus drill spacing (**solid line**); Values of  $\beta$  for a constant value of  $C = 0.2$  for each drill spacing. (**dashed line**) ..... 89

**Figure 4-12:**  $C/\beta$  space for 5 unit spacing. **A)**  $C_{\min}$  end member, **B)**  $C_{\max}$  end member and **C)** optimal  $C/\beta$ . Letters refer to accuracy plots below. Full set of plots are available in Appendix B. .... 91

**Figure 4-13:** Accuracy plot for location A in **Figure 4-16**. .... 91

<b>Figure 4-14:</b> Accuracy plot for location B in <b>Figure 4-16</b> .....	92
<b>Figure 4-15:</b> Accuracy plot for location C in <b>Figure 4-16</b> .....	92
<b>Figure 4-16:</b> $C/\beta$ space for 10 unit spacing. <b>A)</b> $C_{\min}$ end member, <b>B)</b> $C_{\max}$ end member and <b>C)</b> optimal $C/\beta$ . Letters refer to accuracy plots below. Full set of plots are available in Appendix B. ....	93
<b>Figure 4-17:</b> Accuracy plot for location A in <b>Figure 4-16</b> .....	93
<b>Figure 4-18:</b> Accuracy plot for location B in <b>Figure 4-16</b> .....	94
<b>Figure 4-19:</b> Accuracy plot for location C in <b>Figure 4-16</b> .....	94
<b>Figure 4-20:</b> $C/\beta$ space for 15 unit spacing. <b>A)</b> $C_{\min}$ end member, <b>B)</b> $C_{\max}$ end member and <b>C)</b> optimal $C/\beta$ . Letters refer to accuracy plots below. Full set of plots are available in Appendix B. ....	95
<b>Figure 4-21:</b> Accuracy plot for location A in <b>Figure 4-20</b> .....	96
<b>Figure 4-22:</b> Accuracy plot for location B in <b>Figure 4-20</b> .....	96
<b>Figure 4-23:</b> Accuracy plot for location C in <b>Figure 4-20</b> .....	96
<b>Figure 4-24:</b> $C/\beta$ space for 20 unit spacing. <b>A)</b> $C_{\min}$ end member, <b>B)</b> $C_{\max}$ end member and <b>C)</b> optimal $C/\beta$ . Letters refer to accuracy plots below. Full set of plots are available in Appendix B. ....	97
<b>Figure 4-25:</b> Accuracy plot for location A in <b>Figure 4-24</b> .....	98
<b>Figure 4-26:</b> Accuracy plot for location B in <b>Figure 4-24</b> .....	98
<b>Figure 4-27:</b> Accuracy plot for location C in <b>Figure 4-24</b> .....	99
<b>Figure 4-28:</b> Uncertainty plots for final optimized C and $\beta$ for; <b>(A)</b> 5 unit spacing ( <b>top left</b> ); <b>(B)</b> 10 unit spacing ( <b>top right</b> ); <b>(C)</b> 15 unit spacing ( <b>lower left</b> ); <b>(D)</b> 20 unit spacing ( <b>lower right</b> ). ....	100
<b>Figure 4-29:</b> Simplified vertical XZ cross sectional schematic of multiple vein intercept scenario. ....	101
<b>Figure 5-1:</b> Çayeli mine location map. (reproduced from “Technical Report on Mineral Resource and Mineral Reserve Estimates, Çayeli Mine, Turkey”, RPA, March, 2006) .....	104
<b>Figure 5-2:</b> 3D View of wireframe used to calculate the p50 interval tonnage. ....	105

<b>Figure 5-3:</b> p50 Interval Indicator map of vertical section 1840N showing wireframe outline.....	106
<b>Figure 5-4:</b> The optimized values of C for drillspacing.....	106
<b>Figure 5-5:</b> The optimized values of $\beta$ for drillhole spacing. ....	107
<b>Figure 5-6:</b> Model volume results using an uncertainty constant of 0.2 and the specified beta. The red dot represents the wireframe volume. ....	110
<b>Figure 5-7:</b> Uncertainty bandwidth for C = 0.2 (left) and C=0.5 (right), vertical cross section 1840N. ....	110
<b>Figure 5-8:</b> Range of volumes (uncertainty) associated with the C=0.2, beta = 1.0 model and the C=0.5, beta = 1.6 model. The red circle represents the wireframe volume.....	111
<b>Figure 6-1:</b> Vertical cross section schematic showing two possible interpretations. A) The two intercepts in drillhole B belong to the same structure. B) The two intercepts in drillhole B belong to different structures. ....	114
<b>Figure 6-2:</b> Vertical cross section schematic showing the cross cutting relationship of two vein structures. In this example structure A is also offset by structure B.....	115

# Chapter 1

## Introduction

### 1.1 The Problem

Modeling the geometry of vein-type deposits is a time consuming and complicated exercise for the majority of the deposits. This thesis will introduce a straight forward methodology for calculating tonnage of vein deposits with a measure of uncertainty.

An understanding of the geometry of the deposit is required for reasonable modeling. The volume and tonnage are calculated from the geometry.



**Figure 1-1:** Example of Cross sections and Level plans. From Dennen 1989

Three dimensional models of vein-type deposit geometry are often made by tying together a series of deterministically interpreted geological sections. Geological interpretations are the opinions of geoscientists based on experience. It is common that a second interpretation is inconsistent with the first. These interpretations of vein geometry lead to a single solution based on the interpreter with no quantitative measure of uncertainty. The reliability of the interpretation is unknown. To

report fair and unbiased tonnage estimates it is important that tonnage uncertainty be included with the estimation process.

This thesis presents a methodology for calculating the tonnage uncertainty in vein-type deposits. A distance based algorithm is used to map the boundaries of the orebody and therefore the tonnage.

## **1.2 Background**

In the context of this thesis a vein is an irregular tabular zone of finite extent that has been filled with some material of interest. This broad definition serves well because we are interested in the physical characteristics of the deposit such as the length, width and thickness of the deposit. Multiple veins and other complex features of vein-deposits is beyond the scope of this thesis. The essential characteristics of vein-type deposits are described below.

### **1.2.1 Geometry of Vein Deposits**

Vein-type deposits vary from a single narrow structure to large brecciated zones and stockworks. Some deposits form as a set of veins confined to a single strata-bound horizon and mined as a single unit (Peters, 1976). The orientation of vein-type deposits varies from steeply plunging to flat lying. They are made up principally of quartz veins. Mineralized dykes, however, can also be included since they often display similar geometric characteristics to veins. Vein-type deposits are most commonly confined by faults, shear zones or stratigraphic units (Gilluly, 1968, Park, 1975). This is different from large disseminated orebodies where limits are more gradational and often defined on cut-off grade.

Vein-type deposits are most commonly formed by hydrothermal fluids (Gilluly, 1968, Dietrich, 1979). Vein-type deposits have well defined zones of mineralization, are generally inclined and discordant with local geology. They come in all sorts of shapes and sizes with many different levels of complexity and occur in fault or shear related zones. Vein systems occur as groups of veins which exhibit similar characteristics which are related to the same structural event.

In the context of this thesis the term orebody is synonymous with ore shoot in the sense it reflects a closed area of increased thickness with respect to the areal extent of the vein or vein system.

Vein deposits form from superheated hydrothermal fluids that ascend towards the surface from deep within the earth through faults, fractures or any low pressure conduit. As the fluids cool they react with the host rock and if pressure and temperature conditions are right, will begin to create alteration zones, precipitate minerals and possibly develop an orebody. Sometimes, vein deposits are subject to subsequent tectonic forces which rework and remobilize them resulting in complex structurally controlled orebodies.

Most vein deposits include gold and silver however vein type copper and lead-zinc deposits exist but to a much lesser degree.

The principal component of vein-type deposits is quartz (Dietrich, 1979). Quartz veins commonly occur in coarse crystalline form or as finely laminated bands parallel to the vein wall rock contact.

The general tendency is for deposits (oreshoots) to be thicker in the centre rather than have a uniform thickness in the strike direction defined as the intersection of the vein with a horizontal plane (Dickinson, 1942). Deposits often terminate abruptly, possibly caused by faulting or some other structural presence or extend for some distance and gradually pinch out. Narrow veins hosted in shear zones have an associated thickness typically in the range of 0.25 and 1.75m and up to 60m in replacement vein deposits (Peters, 1993).

Fluids moving through fractured rock in the near surface form epithermal deposits and whereas deep seated fluids form mesothermal deposits.

### **1.2.2 Epithermal Deposits**

Epithermal type deposits form at low temperatures (<250°C) and low pressure often deposited within 1-2 kilometres of the surface, Figure 1-2. Epithermal deposits are more persistent laterally than vertically and very rarely have a vertical extent greater than 600m (Panteleyev, A., 1986). Epithermal veins usually form as

vein fillings, irregular branching fissures, stockworks or zones of brecciation and breccia pipes. Epithermal deposits are not uniformly mineralized. Mineralization varies along strike and is subject to vertical zoning with only a portion of the total vein being mineralized. Precious metals dominate epithermal veins and often are host to bonanza style high grade deposits.

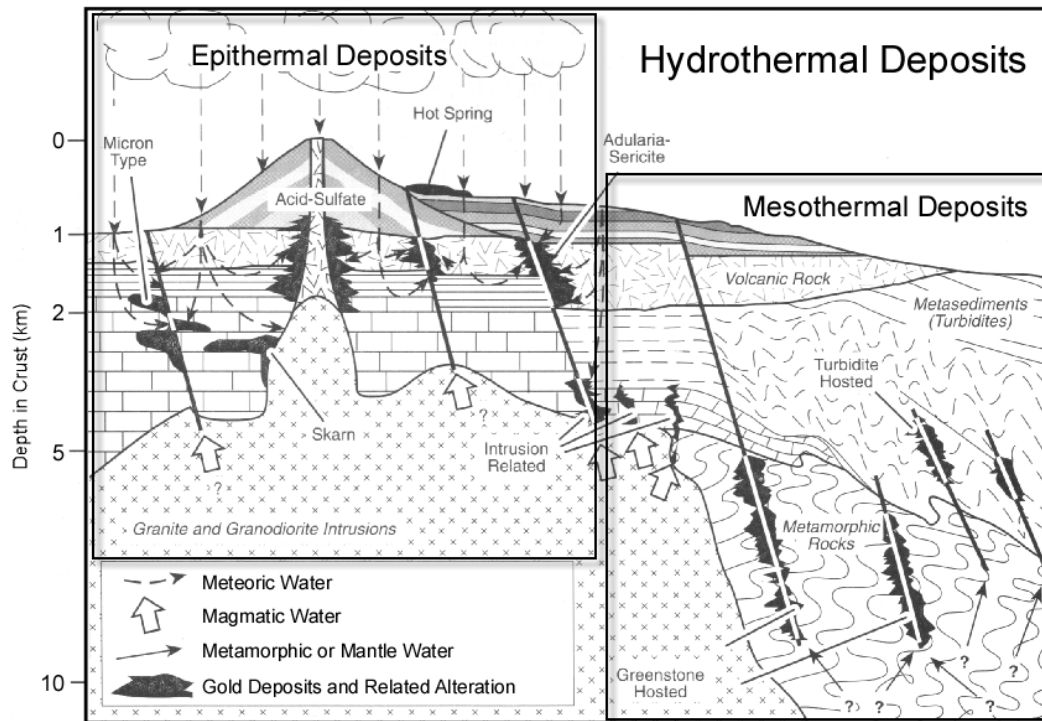


**Figure 1-2:** Relationship between epithermal and mesothermal ore deposits (Modified from Kessler, 1994)

### 1.2.3 Mesothermal Deposits

Mesothermal deposits occur at moderate temperature (>250°C) and pressure conditions that correspond to a depth in the range of 5-15 km, Figure 1-2.

Epithermal type mineralization grades into Mesothermal type mineralization. Mesothermal veins often form banded structures parallel to vein walls caused by tectonic stresses. The mineralization in mesothermal deposits can have a variety of forms and can occur in shear/fault zones, as discordant quartz veins or quartz-vein sets (stockworks) as well as in stratabound zones. Mesothermal veins occur in rock packages of all ages but are commonly hosted in metamorphosed intermediate to mafic volcanics (greenstone-hosted type) such as the deposits of the Red

Lake camp in Ontario, and sedimentary/metasedimentary rocks (slate-belt or turbidite-hosted type) such as those found in the Meguma Group in Nova Scotia (R.J. Ryan , P.K. Smith, 1997).

Each type is significant as each is associated with different styles of vein deposition from a single near vertical narrow vein to shallow dipping zones of vein sets. There is a wide and varied set of possible deposit configurations. This thesis will use simple non trivial models as the starting point for modeling the tonnage uncertainty of vein type deposits. The models will mimic the basic characteristics of vein deposits described in the previous sections.

### **1.3 Previous Work**

There is not much written on the subject of calculating tonnages, and the associated uncertainty, using distance functions. McLennan and Deutsch (2006) developed a methodology using a volume (distance) function for boundary simulation with the capability of assessing uncertainty. The method calculates uncertainty by using a spatial bootstrap to calculate separate realizations of the mean value for different p-values. The method presented here calculates uncertainty using a set of realizations interpolated from independently sampled orebodies. The orebodies are sampled using the same sampling method.

There are other methods used to model boundaries in 2D using indicator kriging to define the uncertainty bandwidth between dry wells (barren holes) and producing wells (ore holes), (Pawlowsky, Olea, and Davis, 1993). Soares (1990) showed a method of boundary assessment utilizing an indicator type approach similar to the one above but, modified by conditioning the data to the anisotropy of the global covariance. Srivastava (2005) presented a probabilistic method for modeling lens geometry using a p-field simulation; a method similar to the indicator kriging method. Shcheglov (1991) demonstrated the use of a probabilistic method based on the drillhole spacing and the number of ore holes to calculate the area of an expected orebody. No uncertainty assessment was carried out. None of the methods use a distance function as the basis for interpolation.

## 1.4 Thesis Summary

### 1.4.1 Statement

The objective of this thesis is to demonstrate a method for calculating tonnage uncertainty of vein-type deposits which is both unbiased and fair. The work focuses on non-trivial flat lying closed veins, a simple but common scenario for vein-type deposits. We will compile a set of “true” vein tonnages from a set of synthetic simulated vein structures. Using the distance function approach, the estimated volumes of the pseudo deposits will be compared to the true volumes. A set of guidelines for the parameterization of the distance function will be created from the results. From this foundation the methodology could be expanded to more complex deposits with multiple veins, veins of different orientations and veins with different continuities.

### 1.4.2 Outline

This thesis is a study on the distance function approach to calculate the tonnage of vein-type deposits with the goal of reproducing true measurements with some degree of measurable uncertainty. This thesis contains six chapters. Each chapter targets one specific aspect behind the study.

In **Chapter 2**, the framework behind tonnage uncertainty is presented and a discussion of the parameters and calibration techniques is offered.

**Chapter 3** will discuss parameter inference and will look at the various parameters used in the methodology and the values required to produce results that are unbiased and fair. The majority of this thesis deals with the calibration of the distance function parameters that will provide an estimate of the vein boundary and deposit volume that best conforms to the known geology of the deposit. The final section, *Assessing Uncertainty*, will discuss the methods used to measure the goodness of the estimation process so that estimates are unbiased and fair.

**Chapter 4** will discuss the application of the methodology to a set of synthetic deposits. The chapter begins with an overview of the methods used to create the synthetic models and the methods used to sample them. The chapter will discuss

the interpolation method used and explain how the fairness and uncertainty was derived.

**Chapter 5** will discuss some practical considerations for vein-type modeling and some of the complexities that can arise such as the impact of widely spaced data.

In closing, **Chapter 6** will discuss some conclusions and comment on future research.

# Chapter 2

## Framework for Tonnage Uncertainty

### 2.1 Problem Setting

There is a need for an unbiased and fair estimate of the tonnage of a deposit. The more widely spaced the drillholes the more uncertainty there will be in the estimated tonnage due to the increasing uncertainty in the actual location of the deposit boundary between drillholes.

The tonnage calculation is an important part of any resource calculation. Uncertainty in the calculated tonnage will have a direct impact on metal content and mine life. Little attention has been given to modeling tonnage uncertainty in vein type deposits. A model of the geometry is usually developed based on the deterministic interpretation of a set of sections and becomes the container within which grades are modeled. A central idea of this thesis is to model the tonnage uncertainty with a probabilistic model.

The uncertainty in tonnage can be quantified by using a distance function (DF) approach. The DF is based on calculated distances between specific sample locations in and between drillholes. Down-the-hole samples form a continuous string of data and result in smooth boundaries interpolated between holes. These smooth boundaries are used to calculate the tonnage uncertainty.

The DF methodology relies on the definition and implementation of two parameters with the objective of defining the optimal set of parameters needed to give a fair and unbiased representation of tonnage uncertainty. The two parameters discussed in detail later are:

- The distance function uncertainty bandwidth parameter,  $C$  and
- The distance function bias correction parameter,  $\beta$

In addition to these two parameters, selection of a suitable variogram model, simple kriging mean and modification for anisotropy will also be discussed.

The DF is the Euclidean distance between different types of samples. The distance is the shortest distance to a sample with a different rock type (vein or non-vein). The distance is a signed attribute and is given a positive sign in one rock type and a negative sign in another. The contact between samples has a distance function of zero. An isoline connecting successive 'zero' points in each drillhole defines a surface or shell. The tonnage uncertainty cannot be calculated directly using this unmodified Euclidean distance. The unmodified distance produces a single boundary as shown in Figure 2-1A and Figure 2-1B. In order to calculate tonnage uncertainty, the DF must be modified. The modified distance function,  $DF_{\text{mod}}$ , considers the uncertainty component  $C$ , and fairness component  $\beta$ , creating a range of probable vein boundaries as depicted in Figure 2-1C and Figure 2-1D. The corresponding vein tonnage uncertainty can be calculated using these different vein boundaries.

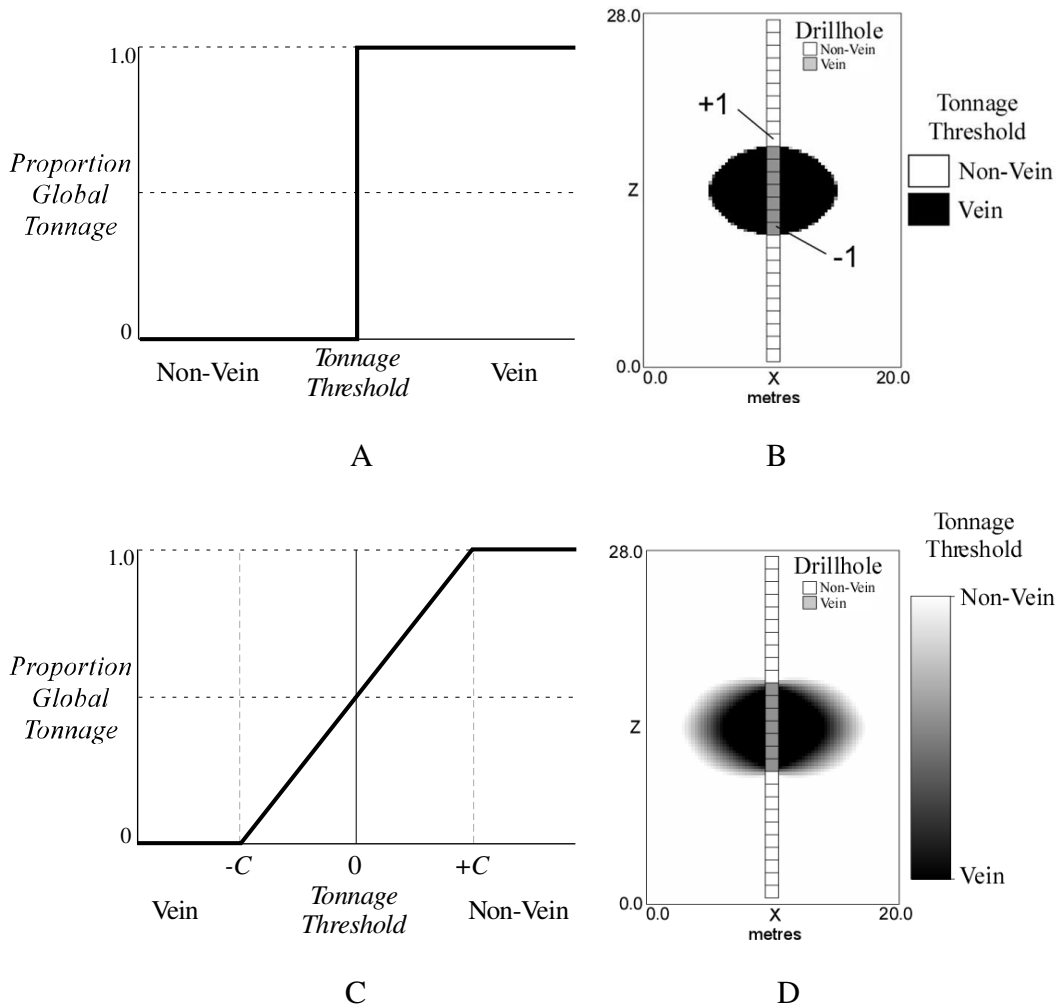


**Figure 2-1:** A) DF distribution with no modification, B) Drillhole example, C) DF distribution with C modification, D) Drillhole example

The method presented here is tested using a set of predefined, closed, 3D vein-type deposits designed specifically for this exercise. The true tonnage is extracted and tabulated from these pseudo deposits. The pseudo deposits are then sampled on a regular grid in a manner that replicates diamond drilling. The result is a rectangular array, representing the *XY* coordinates of the drillhole collar locations. The *XY* spacing of the sample locations represent drillhole spacing. At each *XY* (drillhole collar) location, a contiguous string of samples is taken in the vertical from the top of the model to the bottom and represents a completely sampled drillhole. The data recorded is the location of the sample in the model *XYZ* coordinates and an indicator for the vein type, either vein or non-vein. No other data is

required. Each sample in the dataset is then assigned a distance calculated by the modified DF,  $DF_{\text{mod}}$ . Once the sample data has been modified, the orebody is estimated using simple kriging. Simple kriging uses a variogram model and a predetermined mean value. The resulting kriged models are compared to the true tonnages. The process is iterative and repeated for different values of  $C$  and  $\beta$  until optimal values are found that produce fair and unbiased estimates. As a final step, the exercise is repeated using datasets with different drill spacing to test the robustness of the method.

Each of the aforementioned parameters is discussed in detail in the following sections. The criteria for good uncertainty must be established first.

## 2.2 Criteria for Good Uncertainty

The criteria for good uncertainty include: (1) the result needs to be unbiased, (2) the result needs to be a fair measure of uncertainty, and (3) the result must have low uncertainty.

### 2.2.1 Unbiasedness

Bias is a tendency for one particular outcome to be favoured over another. It is a measure of the expected difference between an estimate and the true value of the variable being estimated. If the estimates are on average greater than the true value, then this would indicate a bias toward over estimation. A measure is unbiased if the expected difference between the estimate and the true value is zero;

$$E\{Z^*\} = E\{Z\} \quad (2.1)$$

A cartoon showing a plot of the estimate,  $T^*$ , versus the true value,  $T$ , is shown in Figure 2-2. If the points fall along the  $45^\circ$  (1:1) line, Figure 2-2 left, the estimates are considered unbiased. If however, the estimates fall above or below the  $45^\circ$  line as depicted in the top and bottom right of Figure 2-2, the estimates are biased. Through calibration we can correct for bias in the estimates.

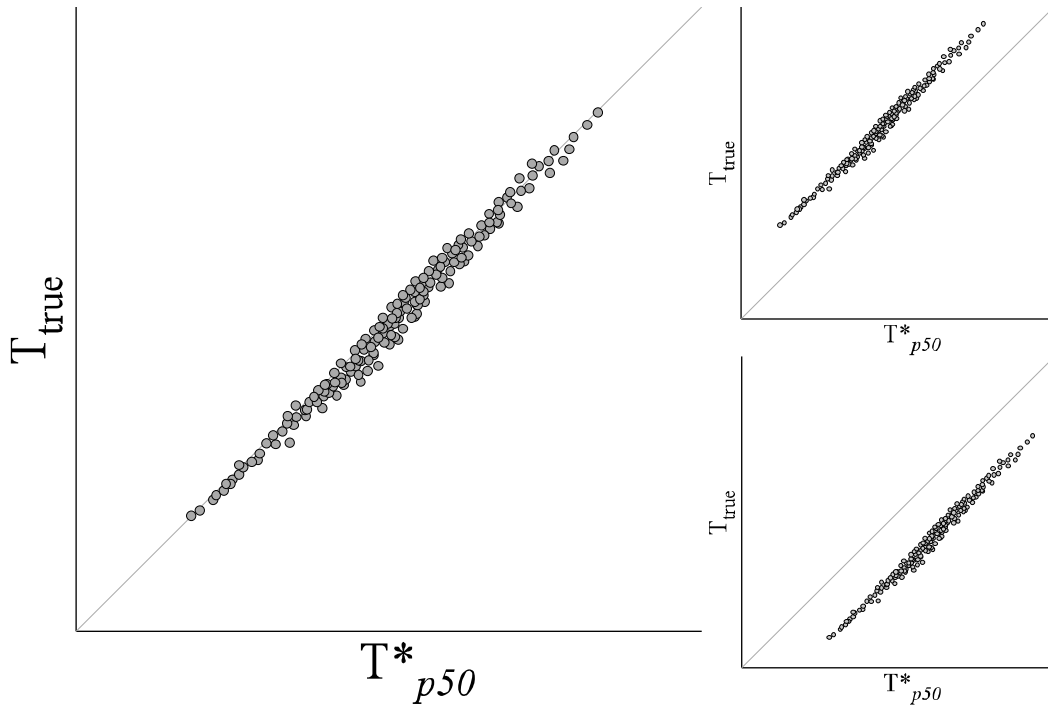


**Figure 2-2:** Schematic illustration of bias; (Left) Unbiased Estimator; (Upper Right) Biased estimator – Estimate less than true value; (Lower Right) Biased estimator – Estimate greater than true value.

### 2.2.2 Fair Uncertainty

Fair uncertainty is the precision with which the reference models estimate the truth. Recall that for a set of estimates to be unbiased, they should on average approximate the true value. For example, if half the estimates are greater than the truth and half the values are less than the truth, we would expect them on average to approximate the truth and thus be unbiased. However, this does not give an indication whether or not the estimates are fair. There needs to be a measure of fairness that will indicate if the spread of values are realistic. If the spread is not realistic then there is a problem with the fairness of the estimates. One way of determining if estimates are fair is to measure the frequency with which the true value falls within defined probability intervals or percentiles derived from the estimates. As stated earlier, we expect 50% of our estimates to be greater than the true value and 50% less than the true value. Moreover, we would expect a smaller percentage of true values fall within a smaller interval centred on the mean of the estimates. For example, one would expect 10% of the true values to fall within 10%

of the mean and 90% of the true values falling within 90% probability interval. If estimated probabilities follow these rules, then they can be regarded as a fair estimate of uncertainty.

Fairness can be quantified by the following equation;

$$E \left\{ Z \in Z^* \pm \frac{P}{2} \right\} = P^* = P \quad \forall P \in [0,1] \quad (2.2)$$

that states, the expected true value falls within an interval defined as the estimate bounded by plus or minus one half the percentile, and, that the actual fraction,  $P^*$ , is equal to the expected fraction,  $P$ , for all percentiles in the range 0 and 1. The expression  $\pm \frac{P}{2}$  is then simply the tolerance applied to  $Z^*$ . Consider 10  $P$  classes each with a width of 0.10 covering the range 0 to 1. As  $P$  increases the width of the interval  $Z^* \pm \frac{P}{2}$  increases and the likelihood that  $Z^*$  falls within the interval increases. For example, the tolerance associated with the probability interval  $P50$ , is  $\pm \frac{0.50}{2}$  or  $\pm 0.25$  so that the interval  $Z^* \pm \frac{P}{2}$  will include all true values that fall in the probability interval of the estimated values from 0.25 to 0.75. Similarly for the probability interval  $P90$ , the tolerance is  $\pm \frac{0.90}{2}$  or  $\pm 0.45$ , and the interval associated with the  $P90$  will be 0.05 to 0.95, with the assumption that 90% of the true values should fall within this interval defined by the estimates. Figure 2-3 shows examples of fair and unfair estimates. As with bias, we can achieve fairness through calibration.

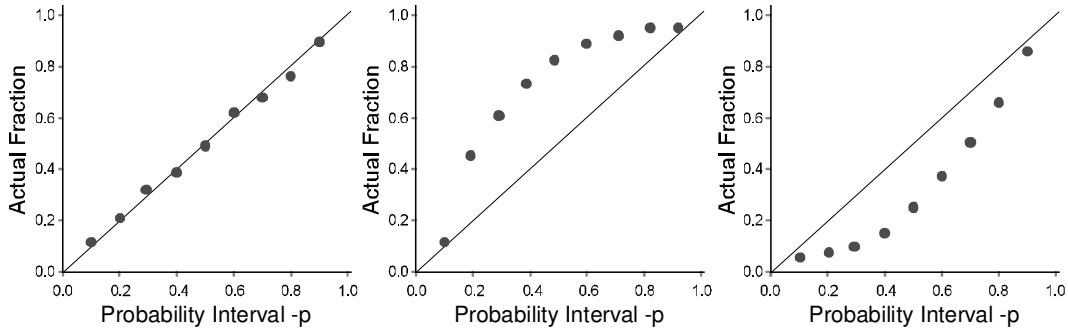


**Figure 2-3:** An illustration of accuracy plots, (Left) fair estimate, actual proportion is equal to the assigned proportion. (Centre) unfair estimate, too many estimates fall within the assigned  $p$ -interval. (Right) unfair estimate, too few estimates fall within the assigned  $p$ -interval.

### 2.2.3 Low Uncertainty

Finally, the third criterion required of a good estimate is low uncertainty. The lower the uncertainty associated with an estimate, the better. Quantifying uncertainty allows for direct comparison of estimates generated using different parameters. Low uncertainty is quantified by measuring the spread of the p80 interval. The measure is standardized by dividing by the p50 yielding a unitless measure and allows reference models to be compared regardless of size.

$$Uncert = \frac{P_{90} - P_{10}}{P_{50}} \quad (2.3)$$

where  $P_{10}$ ,  $P_{50}$  and  $P_{90}$  are the tonnages associated with those particular probability intervals. Consider two distributions of estimates that are both accurate and precise. When ascertaining uncertainty, the distribution of estimates which has the lowest uncertainty will be considered the best.

## 2.3 Distance Function

### 2.3.1 Distance Function (DF)

The distance function is at the heart of the methodology and is used to calculate and assign a distance to each sample location. The distance function is applied and modified for calibration.

Suppose for instance, the first sample is non-vein and has an indicator of 0, VI(0). The distance function is the distance to the nearest sample with indicator of 1, VI(1). This sample could exist next to the original sample if located at the contact between vein and non-vein or in a nearby drillhole if located at some distance from the vein, Figure 2-4. The actual distance is then modified depending on the value of the indicator VI. Consider the DF;

$$DF = \begin{cases} \left( \sqrt{dx^2 + dy^2 + dz^2} + C \right) & \forall VI = 0 \\ \left( \sqrt{dx^2 + dy^2 + dz^2} + C \right) \cdot -1 & \forall VI = 1 \end{cases} \quad (2.4)$$

where,  $\sqrt{dx^2 + dy^2 + dz^2}$  is the Euclidean distance between the current point and the closest point with a different VI,  $C$  is the uncertainty parameter, and the value -1 is the indicator constant applied to values where the VI is equal to 1. When the indicator VI is 0, or non-vein, the DF returns a positive value equal to the distance plus the uncertainty parameter  $C$ . If the indicator VI is 1 signalling the presence of vein, the DF returns a value equal to the distance plus the uncertainty parameter  $C$  and is given a negative sign.

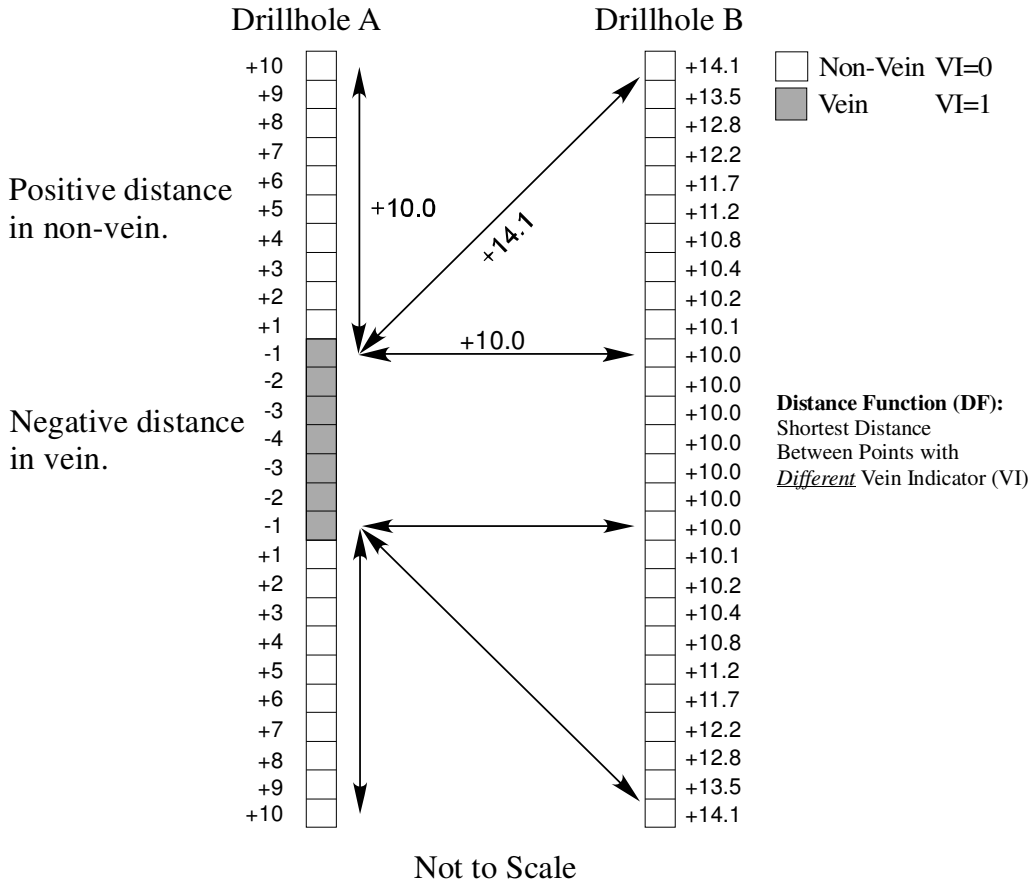


**Figure 2-4:** Schematic of distance function. Numbers indicate the distance assigned by the DF.

The distance from  $-C$  to  $+C$  is defined as the width of uncertainty or the uncertainty bandwidth.

### 2.3.1.1 Uncertainty Bandwidth Parameter $C$

The parameter  $C$  must be calibrated so that the width of uncertainty is neither too large nor too small.

Consider two drillholes, Figure 2-5, one with a vein intercept, the other without, that are separated by some distance,  $ds$ , the drill spacing. The true vein boundary, or iso-zero boundary of the vein must exist at some location between the two drillholes. We therefore define the distance,  $ds$ , as the maximum geologically reasonable distance that can be assigned to  $C$  and is equal to the drillhole spacing. For example, the vein shown in Hole A in Figure 2-5, could terminate at a point very close to the sampled location. This is possible although not very likely. Simi-

larly, the vein could extend to a point which is just short of the sampled location in Hole B, again, not likely, but possible.

The uncertainty parameter  $C$  is not designed to define the location of the iso-zero boundary but rather to define a reasonable bandwidth of uncertainty associated with the iso-zero surface boundary. The upper limit of the uncertainty bandwidth will be equal to the drill spacing.

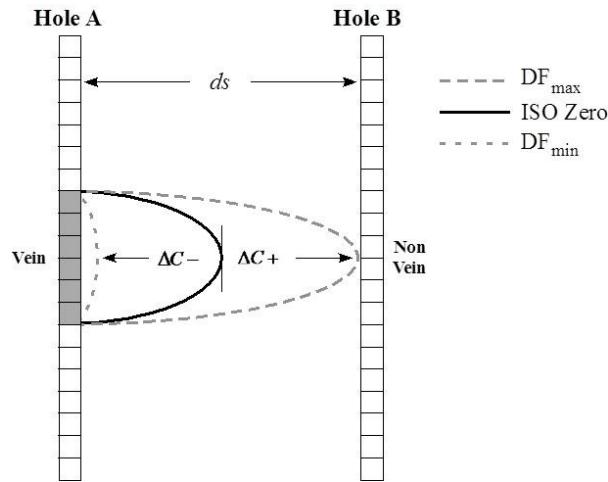


**Figure 2-5:** Schematic of the uncertainty bandwidth defined by  $C$ .

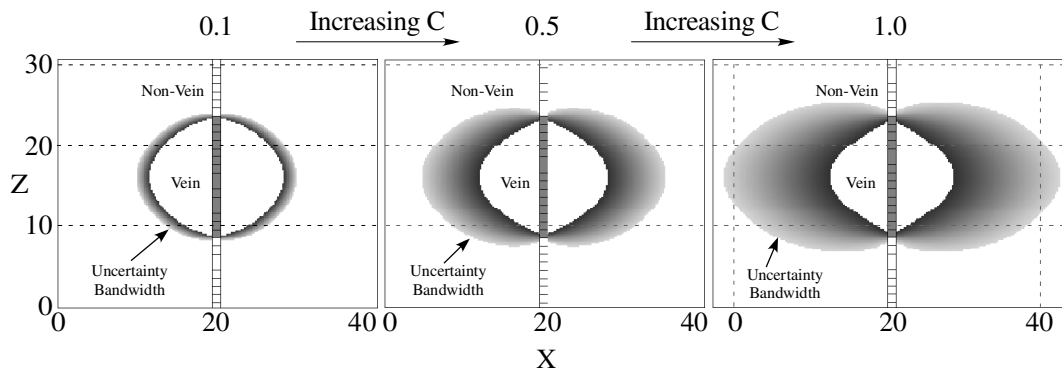


**Figure 2-6:** Examples of  $C$  parameters, increasing  $C$  from left to right.

The schematic in Figure 2-6 demonstrates the effect of increasing  $C$ . Figure 2-7 shows the effect when  $C=0$ , that is, when the uncertainty bandwidth has zero

thickness and in the case of Figure 2-8, a thickness of 8 corresponding to the  $C$  range of -4 to +4.

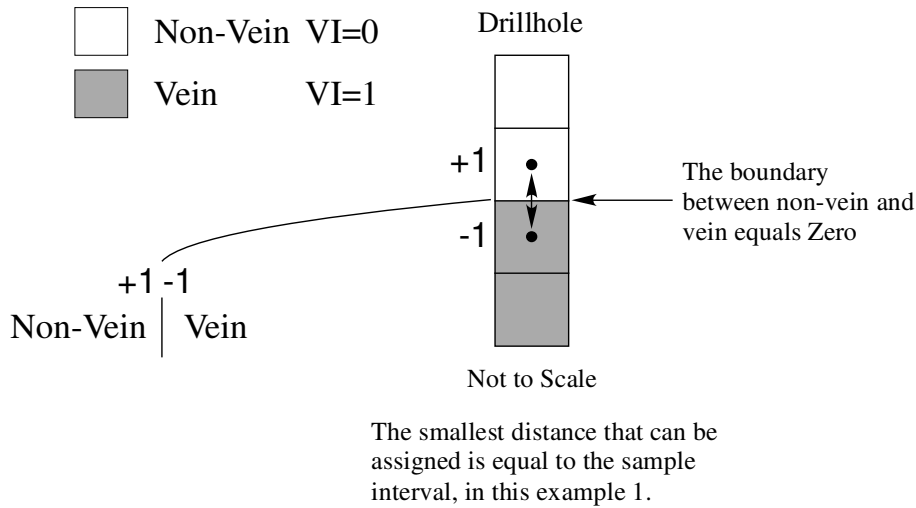


**Figure 2-7:** When  $C=0$  the uncertainty bandwidth has zero thickness.

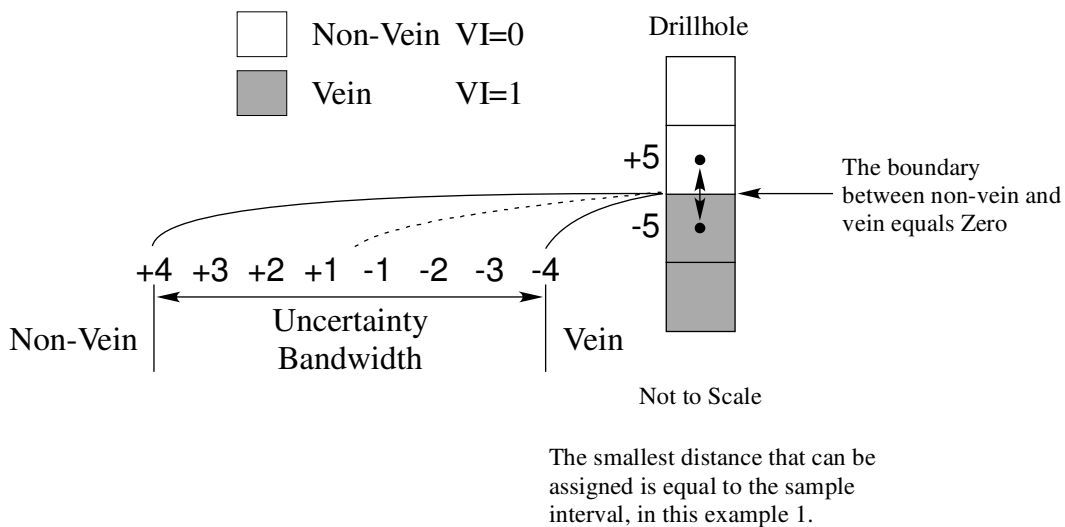


**Figure 2-8:** When  $C=4$  the uncertainty bandwidth has a thickness of 8, -4 to +4.

The drill spacing could represent a large bandwidth for widely spaced data which would produce large tonnage uncertainty. A symmetric erosion and dilation

through a constant C could possibly lead to a bias. There must be a parameter to center the width of the uncertainty band. The parameter chosen to center the uncertainty bandwidth is beta ( $\beta$ ).

### 2.3.2 Modified Distance Function ( $DF_{\text{mod}}$ )

The DF discussed in 2.3.1 is modified in a second step by applying a bias parameter,  $\beta$ , used to center the distribution of estimates. The bias parameter is applied to the original DF as shown in Equation 2.5.

$$DF_{\text{mod}} = \begin{cases} (dist + C) / \beta & \forall VI = 0 \\ (dist + C) \cdot \beta & \forall VI = 1 \end{cases} \quad (2.5)$$

When the indicator VI is 0, or non-vein,  $DF_{\text{mod}}$  returns a positive value equal to the original DF divided by  $\beta$ . If the indicator VI is 1, again signalling the presence of vein,  $DF_{\text{mod}}$  returns a negative value equal to the DF multiplied by  $\beta$ . Thus all positive  $DF_{\text{mod}}$  values are located outside of the vein structure and all negative  $DF_{\text{mod}}$  values are located inside the vein structure with the contact between the two equal to zero. The values returned by  $DF_{\text{mod}}$  are the values used in the interpolation process.

Figure 2-9 illustrates the relationship of C to the DF and modified DF. As C increases, there is a symmetrical increase in both the DF and modified DF. That is, both increase at the same rate and the ratio between DF and  $DF_{\text{mod}}$  remains the same for both positive (non-vein) and negative (vein) values of DF and  $DF_{\text{mod}}$ .

Figure 2-11 illustrates the relationship of  $\beta$  to the DF and modified DF. As  $\beta$  increases, the DF remains the same and  $DF_{\text{mod}}$  decreases for positive values and increases for negative values in the sense it becomes more negative. As a result the slope or ratio between DF and  $DF_{\text{mod}}$  decreases for positive values of DF and  $DF_{\text{mod}}$ , i.e. Non-vein, and increases for negative values of DF and  $DF_{\text{mod}}$ , i.e. vein.

### 2.3.2.1 The ISO-ZERO surface

The iso-zero surface is the interpolated contact between vein and non-vein. Recall that distance values outside the vein are positive and inside the vein are negative therefore the contact between the two would reasonably be zero. This zero point is known in the drilling and will be honoured by the

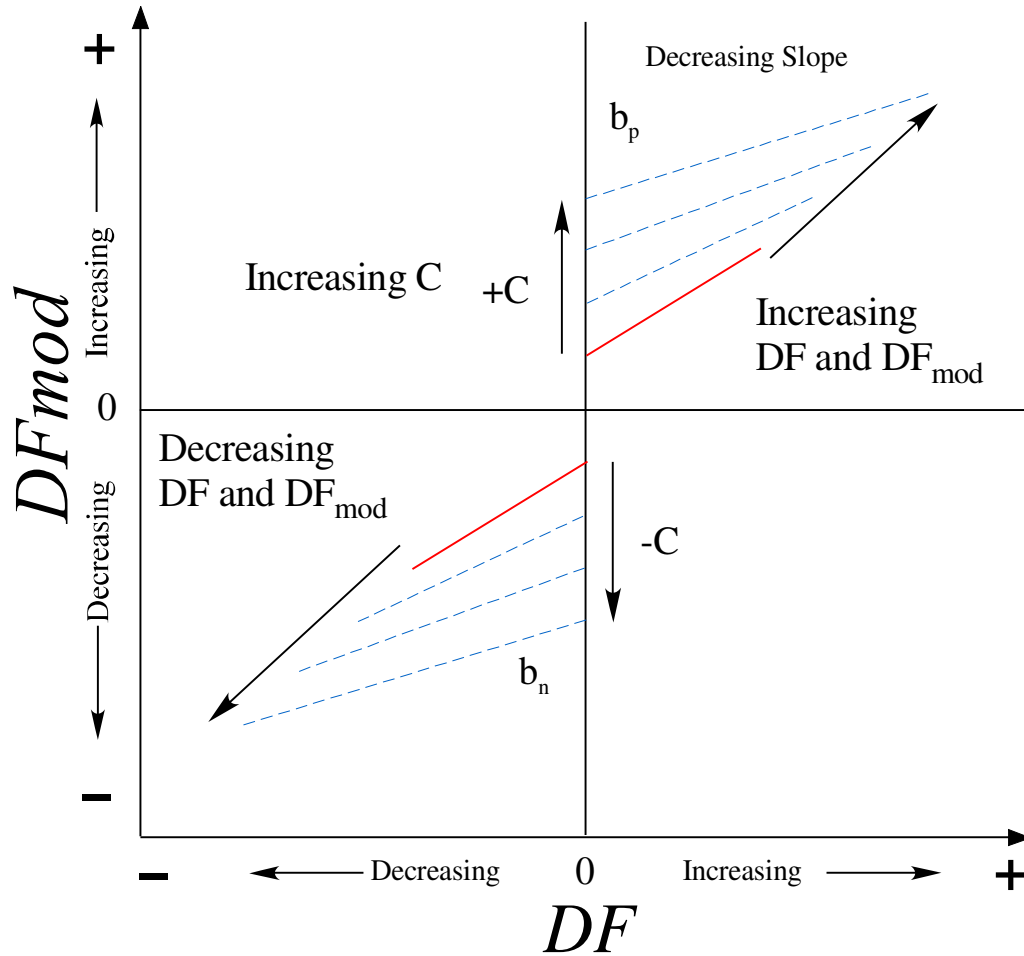
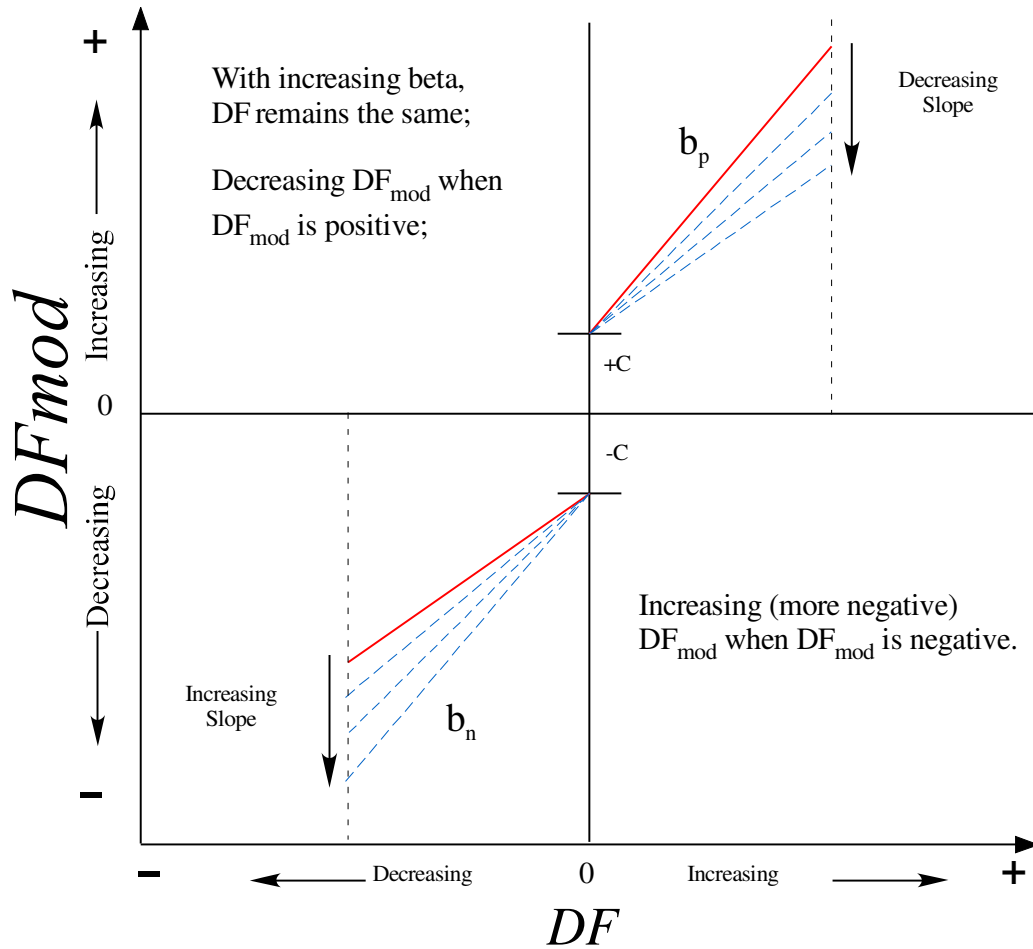
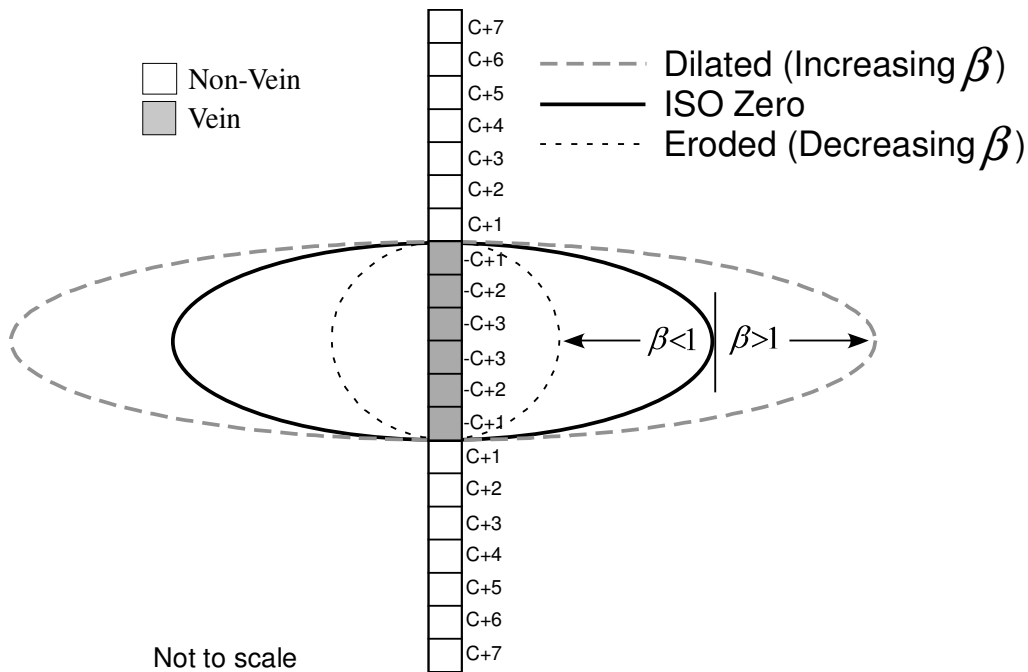


Figure 2-9: Effect of C on the DF and modified DF.



**Figure 2-10:** Effect of  $\beta$  on the DF and modified DF.

At locations away from sampled locations, however, there will be uncertainty as to where the actual position of the contact surface is located. The shape and size of the iso-zero surface is controlled by  $\beta$  and has the effect of dilating the iso-zero for the larger values of  $\beta$  shown as the outer dashed ellipse in Figure 2-11, or eroding the iso-zero surface for decreasing values of  $\beta$  as depicted by the inner dotted line in Figure 2-11.



**Figure 2-11:** Effect of  $\beta$  on the iso-zero surface. With increasing  $\beta$ , the surface expands, with decreasing  $\beta$  the surface contracts.

### 2.3.2.2 Bias Correction Parameter Beta

The beta parameter ( $\beta$ ) allows shifting of the interpolated set of realizations towards the center and an unbiased distribution, the 45° (1:1) line on an accuracy plot, Figure 2-12.

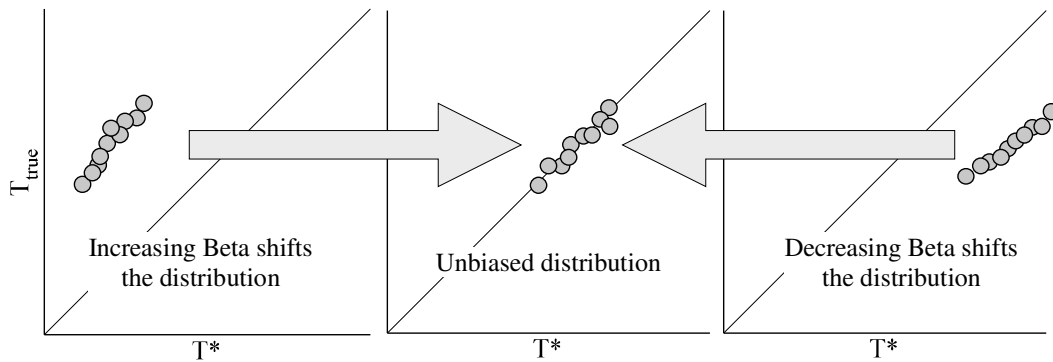


**Figure 2-12:** Behaviour of Beta on the distribution of a set of interpolated realizations

The  $\beta$  parameter is a number typically between 0.1 and 2 and is dependent on drillhole spacing. If the drill spacing tends to overestimate the tonnage, then  $\beta$  values greater than 1 are used to shift the distribution to the left towards the 45°

line, Figure 2-12 right. On the contrary, if drill spacing tends to underestimate the tonnage, then  $\beta$  values less than 1 are used to shift the distribution to the right, Figure 2-12 left. The closer the set of realizations are to the 45° line, the closer  $\beta$  will be to 1. The implementation of  $\beta$  imposes a control on the final surface and makes it possible to adjust the iso-zero surface so that fair and unbiased estimates can be obtained. The calibration of  $\beta$  is discussed in chapter 3.

### 2.3.3 Distance Function Thresholds

The tonnage is taken from the uncertainty bandwidth, the size of which is determined by the uncertainty constant  $C$  and the minimum and maximum limits of the bandwidth determined from both from  $C$  and  $\beta$ .

The inner limit of the uncertainty band,  $DF_{\min}$  is calculated as;

$$DF_{\min} = -\frac{1}{2} C \cdot DS \cdot \beta \quad (2.6)$$

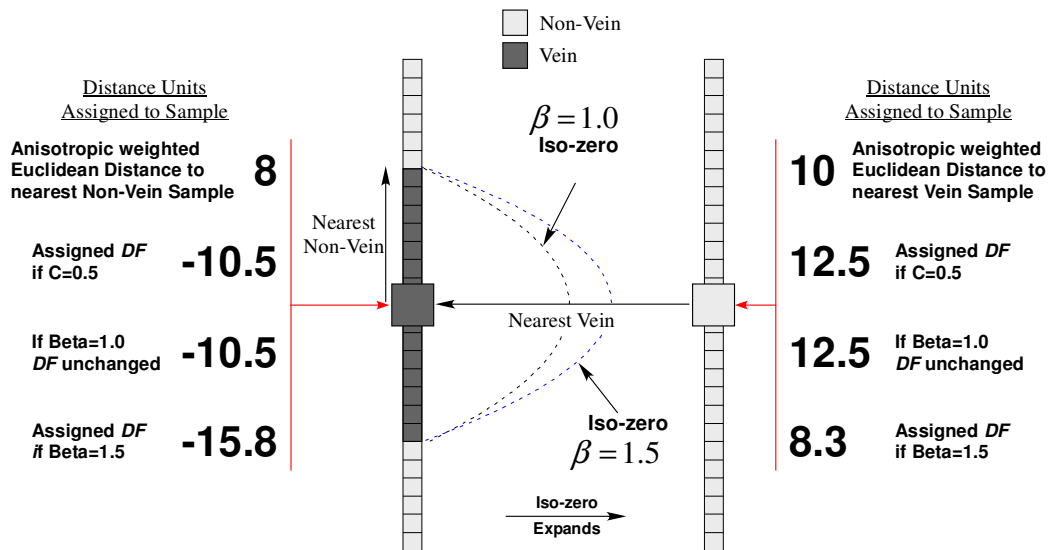


Figure 2-13: As Beta increases from 1, the iso-zero surface expands.

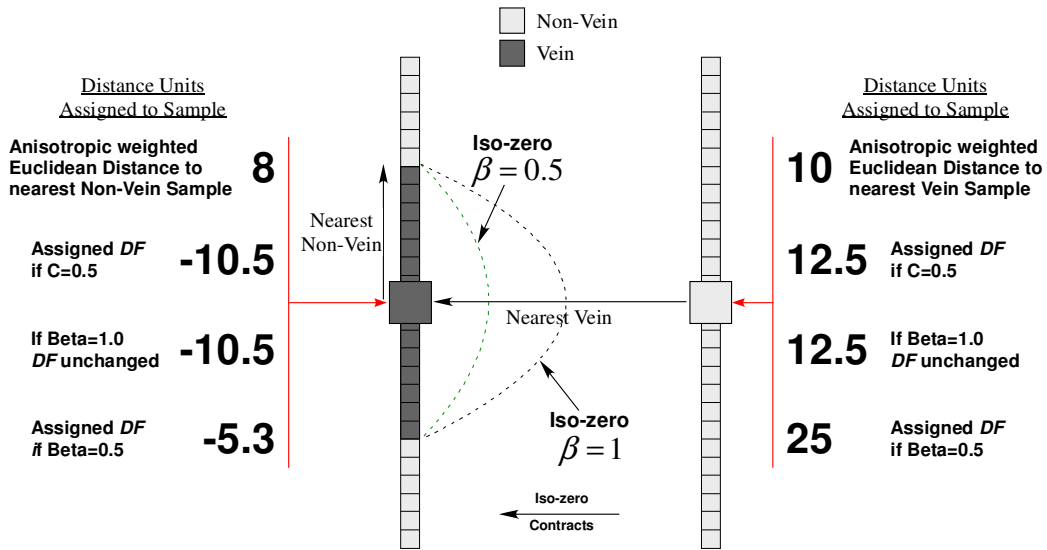
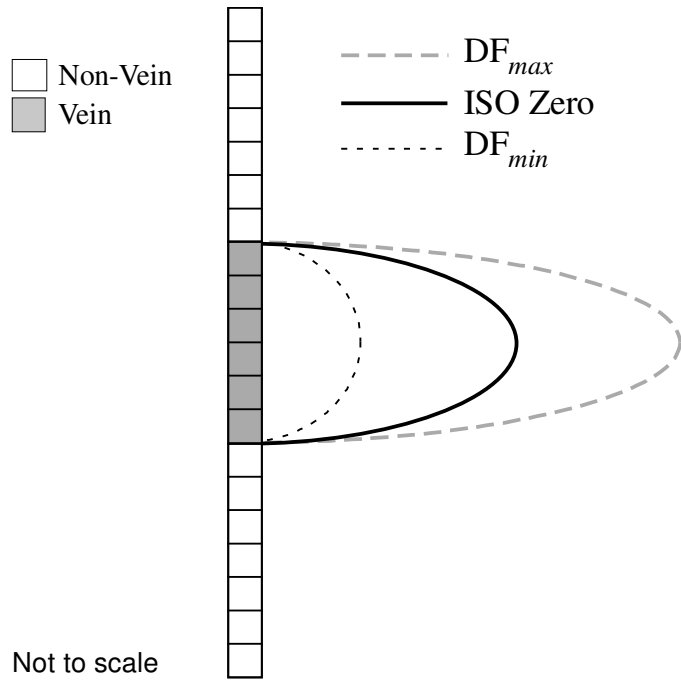


Figure 2-14: As Beta decreases from 1, the iso-zero surface shrinks.

where  $DS$  is the drill spacing and is the lower limit defined as one half the distance function of the portion inside the vein structure. The outer limit of the uncertainty band,  $DF_{max}$  is calculated as:

$$DF_{max} = \frac{1}{2} \frac{C \cdot DS}{\beta} \quad (2.7)$$

and is the maximum limit defined as one half the distance function of the portion outside the vein structure. The concept is shown in Figure 2-15.



**Figure 2-15:** Uncertainty Bandwidth limits, DFmin inner limit, DFmax outer limit.

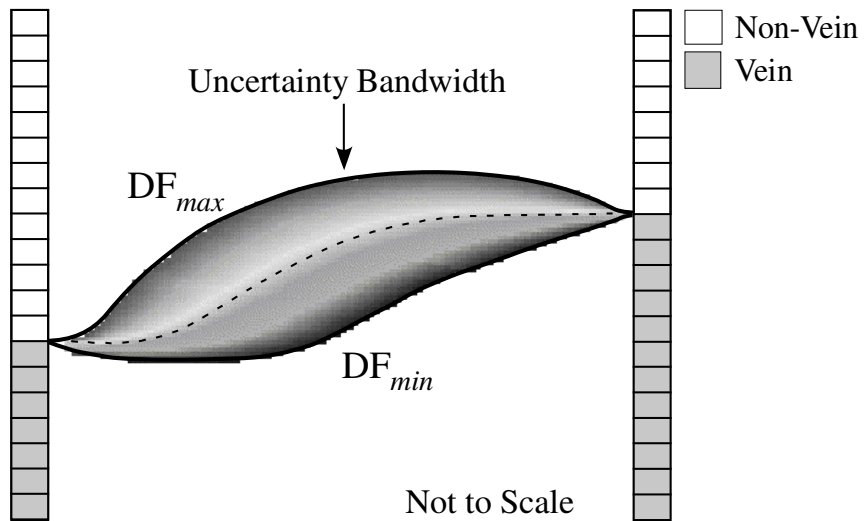


**Figure 2-16:** Schematic of uncertainty bandwidth between drillholes.

The probability thresholds within the bandwidth are defined as a  $p$  - probability value. The bandwidth interval is rescaled to  $[0,1]$  so that  $DF_{min} = 0$  and  $DF_{max} = 1$ . The solid line in Figure 2-15 is the  $p_{50}$  and has a  $p$  value of 0.5. The

$p$  values are used to extract tonnages for defined probability intervals by converting individual model cell values into  $p$  values.

The  $p$  value is calculated as;

$$p = \frac{z - DF_{\min}}{DF_{\max} - DF_{\min}} \quad (2.8)$$

where  $z$  is the estimated value. The total tonnage for a particular probability interval  $p_i$ , is the total number of cells where  $p \leq p_i$ . Recall the zone of uncertainty is located between  $DF_{\min}$  and  $DF_{\max}$ . If  $z < DF_{\min}$  then  $z$  is certainly located within the vein structure. If  $z > DF_{\max}$  then  $z$  is most certainly located outside the vein structure. By dividing the space between  $DF_{\min}$  and  $DF_{\max}$  into a  $[0,1]$  interval, we can readily extract tonnages from a mapped distance function for any probability interval.

A FORTRAN program *u\_tonnes* was written to extract the tonnage for each probability interval. The program tabulates the tonnage from  $p05$  to  $p95$  using a probability interval of 0.05 and writes the output to a file. Subsequent tabulations are appended to the file for each additional realization thus building a database of completed realizations.

## 2.4 Mapping of the Distance Function

Kriging is a commonly used interpolator. The kriging weights minimize the error variance of a linear estimate. Kriging is a smooth interpolator that does not reproduce short scale variability, however, for mapping the distance function it is ideal. The simple kriging estimate is defined by the equation:

$$d^*(\mathbf{u}) - m = \sum_{\alpha=1}^n \lambda_{\alpha} \cdot [d(\mathbf{u}_{\alpha}) - m] \quad (2.9)$$

where  $d^*(\mathbf{u})$  is the kriged estimate,  $m$  is the stationary mean over the area of interest, and for each location  $\alpha$ ,  $d(\mathbf{u}_{\alpha})$  is the data and  $\lambda_{\alpha}$  is the weight assigned to that data.

Since the mean is considered to be stationary throughout the study area, Equation 2.9 can be simplified by removing the mean. This is accomplished by equating;

$$y(\mathbf{u}_\alpha) = d(\mathbf{u}_\alpha) - m \quad (2.10)$$

which leaves the residual  $Y$  and the kriging Equation 2.10 becomes;

$$y^*(\mathbf{u}) = \sum_{\alpha=1}^n \lambda_\alpha \cdot y(\mathbf{u}_\alpha) \quad (2.11)$$

The simple kriging equation can also be written as;

$$d^*(\mathbf{u}) = \sum_{\alpha=1}^n \lambda_\alpha \cdot d(\mathbf{u}_\alpha) + \left[ 1 - \sum_{\alpha=1}^n \lambda_\alpha \right] \cdot m \quad (2.12)$$

where the terms related to the mean are collected on the right hand side. Equation 2.12 shows the relation between the weights,  $\lambda_\alpha$ , and the mean  $m$ . As the estimate becomes more distant from the data, the weights approach zero, along with the influence of the data, and the value of the estimate approaches the value of the mean. A very useful property when applied in conjunction with the distance function. Considering that the variable used for interpolation in this methodology is a measure of distance derived from the distance function, we can use distance to calibrate the SK mean. This methodology uses negative distance to refer to distances inside a closed geologic structure, whereas positive distances denote distance away from the structure. The simple kriging mean controls the estimate in areas where there is little or no information. By manipulating the SK mean, we can control the magnitude and sign of any point located some distance from the data. Since kriging is exact, the values at all data locations are honored.

#### 2.4.1 SK Mean

Three examples have been created to demonstrate how the SK mean applies to the DF. The data set is a randomly generated 2D set of 27 points assigned with a distance function variable. Some locations have been assigned a negative distance function indicating the presence of vein, the rest are positive and represent non-vein. The results are displayed in Figure 2-17. The kriged maps shown on the left

side of Figure 2-17 were generated using the same parameters with the exception of the SK mean. In each case, the uncertainty parameter  $C$  was given an arbitrary value of 2 so that the corresponding color bar ranges from  $-2$  to  $+2$ , that is  $-C$  to  $+C$ . The specific determination of the  $C$  value was not considered for this exercise. The purpose is to illustrate the relationship of the SK mean to  $C$  and the kriged results. The three examples shown in Figure 2-17 means of  $+5$ ,  $0$  and  $-5$ . For reference, the centre map kriged with a mean of zero is the base case. On the left of Figure 2-17, we see a map of the estimated values using a mean of zero, on the right, a histogram of the estimated values. The dotted vertical lines show the limits of  $-C$  and  $+C$ . Using a mean of zero shows the bulk of the estimated points are contained within our uncertainty bandwidth. This means the majority of the map is uncertain and that the only 'certain' estimated cells are those close to the data points.

Perhaps we know from acquired geologic knowledge that the majority of the area is likely to be non-vein, we can condition the SK mean to produce estimates that tend to be on the positive side, indicating non-vein. In the top example shown in Figure 2-17, a SK mean value of  $+5$  units was chosen. It is evident from the corresponding histogram (Figure 2-17, top right), that the distribution has shifted to the right. The majority of estimated cells are now greater than  $+C$ , and these points will be classified most certainly as non-vein.

Now consider the opposite, that the majority of the area is actually more likely to be vein, we now condition the SK mean so that estimates on the negative side are favoured. In the bottom example of Figure 2-17, a SK mean value of  $-5$  units was used. In this case, the distribution has shifted left and lies below the  $-C$  limit (Figure 2-17, bottom right). Most estimated cells points now have values less than  $-C$  and we are certain these points will be classified as vein.

There is a continuous succession ranging from lenses of waste contained in a predominantly ore matrix for mean values less than  $-C$ , to lenses of ore or vein contained within predominantly waste when values greater than  $+C$  are used. The context of this thesis, is single closed geological units that warrant the use of an

SK mean greater than the value of +C. Depending on the relationship of the size of the area of interest (A), compared to the size of the orebody (a), using the mean

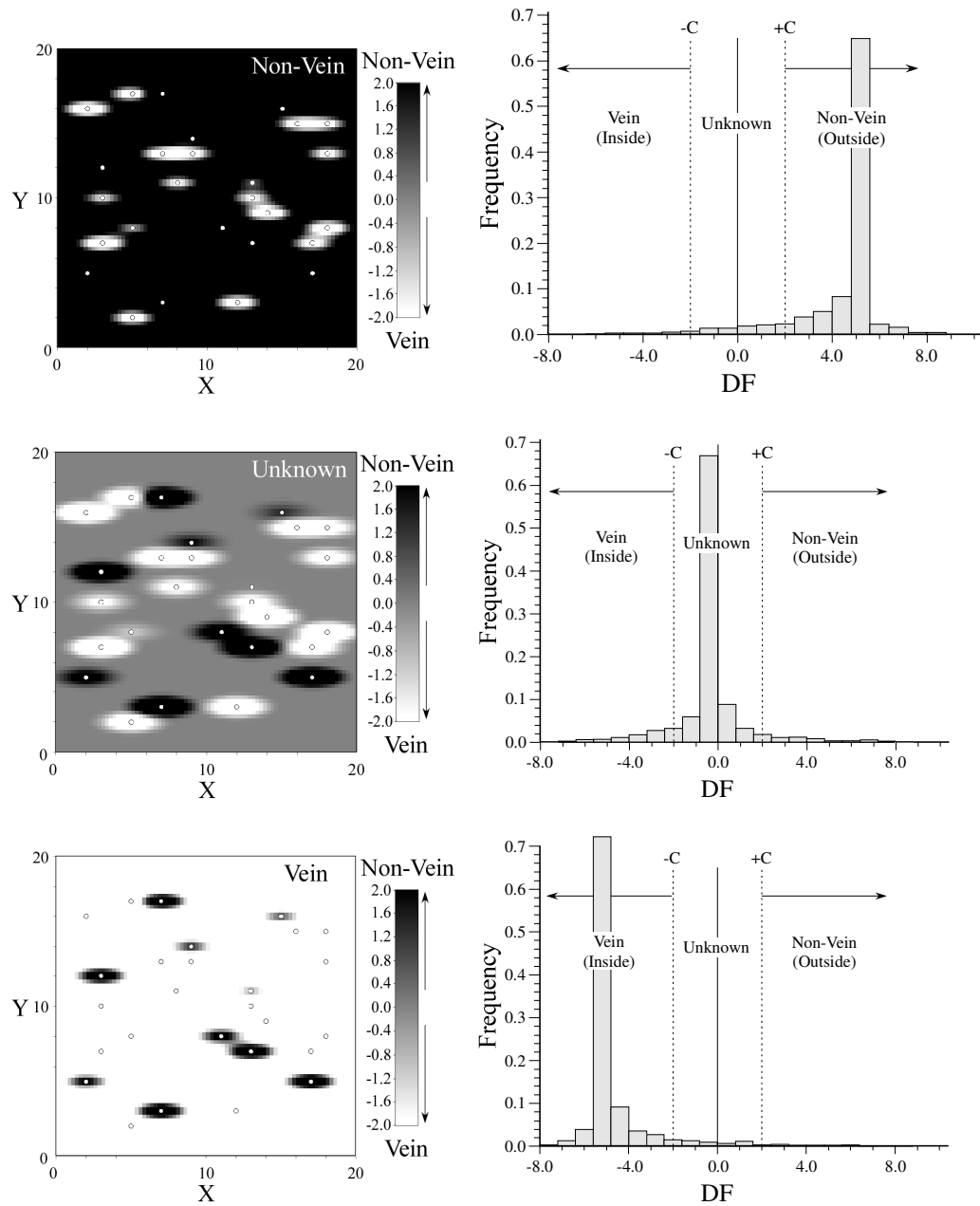


**Figure 2-17:** Effect of changing SK mean. Each realization uses the same parameters with the exception of the mean. (top) Mean = +5 units, (centre) Mean = zero, (bottom) Mean = -5 units.

of the data may not reproduce the desired geologic continuity. For example if the number of positive samples is much larger than the number of negative samples, i.e. long stings of positive waste samples with small vein structures, negative

samples, the mean will undoubtedly be positive. However, using the positive mean from the data may not reproduce the desired results. If this is the case, we can supply a different SK mean to condition the kriging to produce a result that is a better representation of the geology.

A remedy to this situation would be to confine the sampled area to that immediately surrounding the zone or orebody of interest thereby giving a better estimate of the mean.

#### 2.4.2 Variogram

The variogram is a necessary and essential part of the mapping process. The variogram supplies the spatial relationship between data pairs used by the kriging algorithm. The variogram defined by;

$$2\gamma(\mathbf{h}) = E\{[Z(\mathbf{u}) - Z(\mathbf{u} + \mathbf{h})]^2\} \quad (2.13)$$

It is the expected value of the squared difference between a sample  $Z(\mathbf{u})$  and a sample separated by a distance  $\mathbf{h}$ ,  $Z(\mathbf{u} + \mathbf{h})$ . When applying the variogram to the mapping algorithm we use the semivariogram,  $\gamma(\mathbf{h})$  which is one half the variogram. When modeling the DF we are interested in the short scale. That is, distances that are close to the vein boundary and in the range of the drillhole spacing. Since the idea is to map the boundary, any samples that are located more than half the drillhole spacing away are less important. The idea is to provide a variogram that will produce a smooth zone of uncertainty from drillhole to drillhole. The variogram range used in the variogram model to interpolate the DF is an important factor in the methodology.

Note that  $\beta$  is not the only parameter that controls the projection of the iso zero surface. The ranges specified by the variogram are important and will create the initial iso-zero surface, since it is unlikely that the initial surface will be free from bias. The larger the variogram ranges the farther the iso-zero will be projected as shown in Figure 2-18 and Figure 2-19.

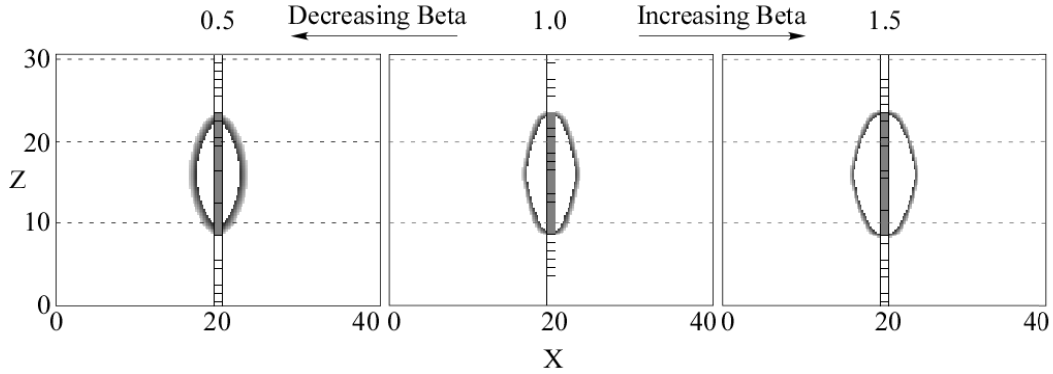


Figure 2-18: Effect of smaller variogram ranges.

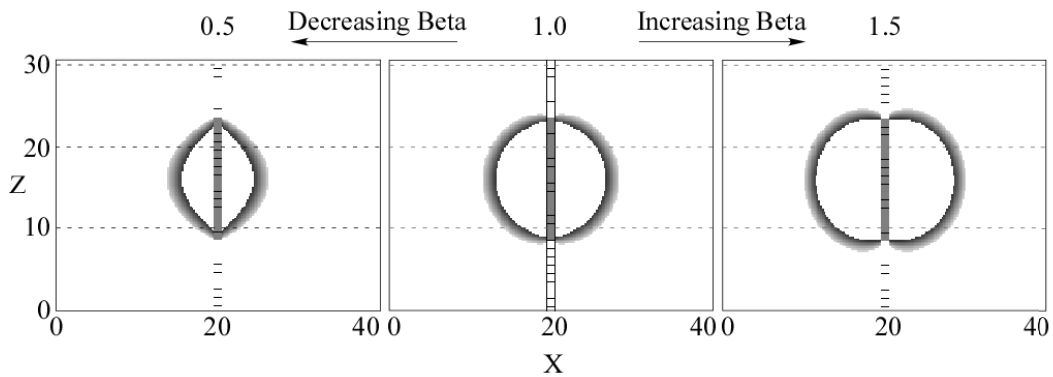


Figure 2-19: Effect of larger variogram ranges.

### 2.4.3 Anisotropy

In tabular vein type deposits there is a larger range of correlation along, strike and dip, than for thickness. This correlation often results in oreshoots, for example, oriented in the plane of the vein, that are thicker in the centre tapering towards the edges, Figure 2-20. Geometric anisotropy of an ore deposit is accounted for by modifying the distance function. The idea is to adjust the distance function to favour the direction maximum continuity rather than treating all directions equally. Recall the Euclidean part of the distance function;

$$dist = \sqrt{\Delta x^2 + \Delta y^2 + \Delta z^2} \quad (2.14)$$

The equation is modified to account for geometric anisotropy by dividing each direction by the anisotropic distance. The Euclidean distances in 2.14 can be re-

duced to distances corresponding to the strike direction,  $h_s$ , dip direction  $h_d$ , and the thickness direction,  $h_t$ . We can define three new variables,  $V_s, V_d$ , and  $V_t$ . These correspond to anisotropic distances in each of the strike, dip and thickness directions respectively.

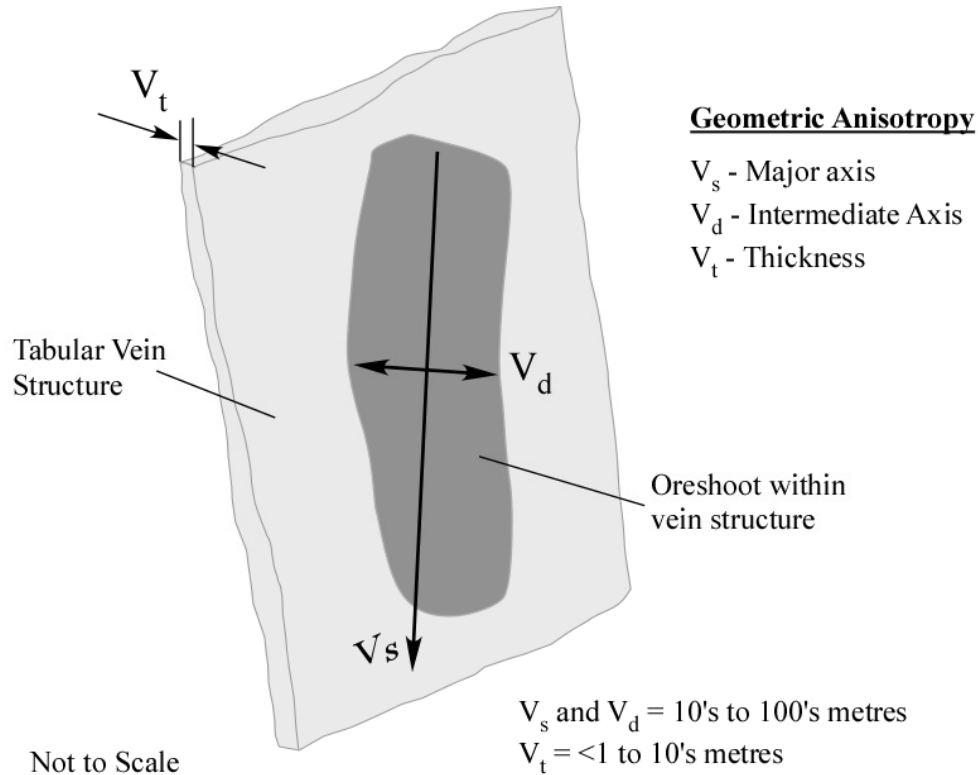
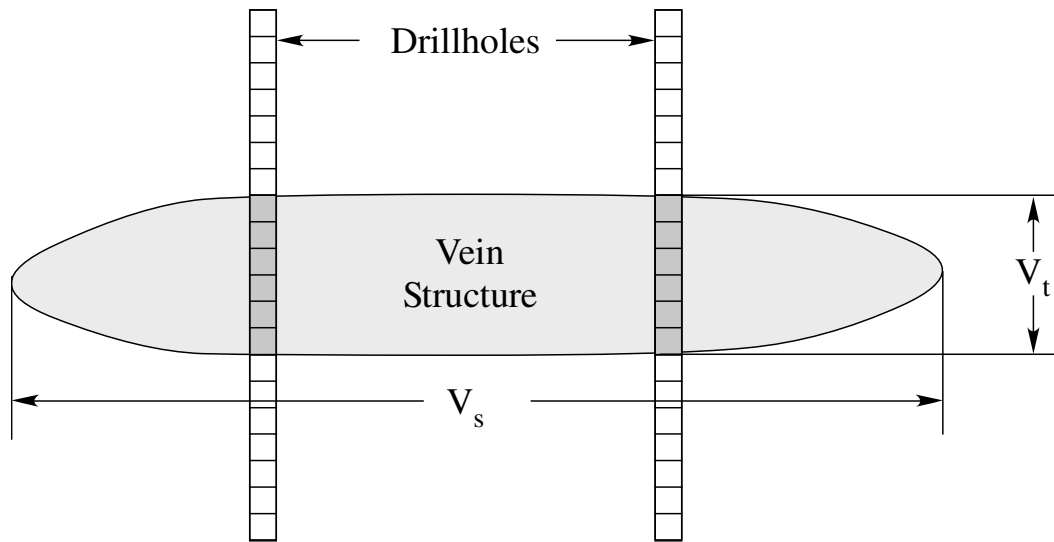


**Figure 2-20:** Example of geometric anisotropy in a tabular vein oreshoot.

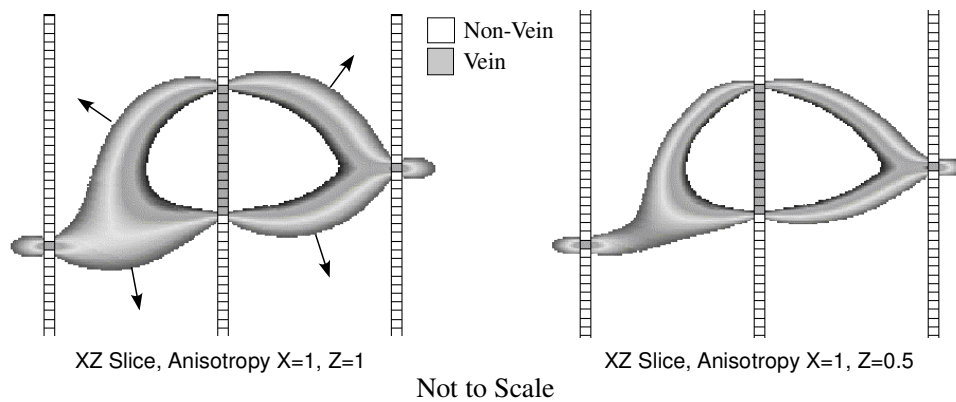
The illustration in Figure 2-21 shows a representation of an ore lens intercepted by two drillholes. The lens is assumed to have a shape approximate to that shown in the diagram. From this we extract an approximation of the strike of the lens,  $V_s$  and the thickness of the lens,  $V_t$ . These anisotropic directions including the third direction,  $V_d$ , are applied to Equation 2.14 such that;

$$dist = \sqrt{\left(\frac{h_s}{V_s}\right)^2 + \left(\frac{h_d}{V_d}\right)^2 + \left(\frac{h_t}{V_t}\right)^2} \quad (2.15)$$



Not to Scale

**Figure 2-21:** Geometric Anisotropy,  $V_s$  - along strike direction,  $V_t$  – thickness



Not to Scale

**Figure 2-22:** Geometric anisotropy applied to DF

This modification for geometric anisotropy allows the uncertainty bandwidth to have preference in the direction of maximum continuity. The left example in Figure 2-22 shows how the uncertainty bandwidth expands in a spherical envelope. Applying anisotropy to the DF, Figure 2-22 right, allows the DF to expand horizontally from hole to hole while constraining the tendency to expand in the vertical. Anisotropy tends to shrink the uncertainty bandwidth which ultimately lowers the uncertainty associated with the anisotropic model. The inner limit of the bandwidth is the same between both models shown in Figure 2-22. Therefore, each model will have the similar tonnages in the lower probability intervals.

## **2.5 Implementation Considerations**

### **2.5.1 Procedure Summary**

The general workflow is as follows. A set of reference models are created. The DF will be applied to strings of sample data emulating drillholes extracted from the models. Ideally, the deposits should be of known size and volume (tonnage). One solution is to create the reference models from scratch. The process begins with the unconditional simulation of a grid of a predetermined size. Next, a second simulation conditioned to a data set that ensures the simulation follows a few simple rules. Negative or positive values are maintained along the outer edge. This will later help with merging the two grids to produce closed 3D orebodies. A conditioning point set to a positive value is placed at the centre of the conditioned grid thus ensuring a positive centre. Once the two surfaces are created they can be merged to form a simulated synthetic 3D orebody. To merge the surfaces, the conditional surface must first be modified. Recall the conditional simulation, conditioning data is used to force the outer perimeter to be filled with negative values. The modifying procedure resets all cells with negative values to be reset to zero. After this is complete the resulting surface model will be a plane of zeros with a cluster of positive values located in the centre region of the grid. The cluster of positive values is essentially the vein deposit. The deposit is located in 3D space with respect to the unconditioned surface by adding the modified conditioned surface to the unconditioned surface. The true tonnage is calculated using the separation distance between the two surfaces. At each cell location in the grid the difference (thickness) between the surfaces is calculated and summed to give the true tonnage. Along the periphery, the surfaces are coincident and the difference is zero becoming more separated approaching the centre of the grid. The tonnage is recorded to be used for comparison at a later stage in the process. The process is repeated to create 50 separate synthetic vein reference models.

In advanced exploration projects the majority of subterranean information comes through diamond drilling campaigns. Drilling on regular equally spaced sections

is often the norm. The methodology presented here follows a similar approach. A program is used to drill (sample) the synthetic vein deposits on a regular rectangular grid. A GSLIB compatible file is produced which contains each drillhole in the grid discretized into sample intervals corresponding to the cell size of the simulated vein grid. Each sample point contains the  $xyz$  coordinates of the sample, the location of the footwall and hangingwall surfaces, and a vein indicator (VI) indicating whether the sample is located inside the vein(1) or outside the vein (0). The resulting drillholes are then modified using the distance function (DF). The DF calculates the distance between each drillhole sample and the closest sample with a different VI. Values for the parameters  $C$  and  $\beta$  are also applied at this time. The DF program output is a modified drillhole file composed of the  $xyz$  coordinates, Euclidean distance,  $DF_{mod}$  distance, VI and drillhole ID number. Drillhole data files are created for a range of drillhole spacings, and values of  $C$  and  $\beta$ . The drillhole data will be used to estimate the synthetic deposits using simple kriging.

The estimation process uses each drillhole data set as input to the kriging program. The resultant 3D models are used to calculate the estimated tonnage of the models that are then compared to the true tonnages. The entire process is automated using two bash script files. The first script creates the synthetic vein deposits and calculates the true tonnages; the second drills them, does the estimation and reports the tonnage. The tonnages are loaded into a custom EXCEL<sup>®</sup> spreadsheet and analyzed for precision and accuracy.

### **2.5.2 Soft Knowledge**

There is a place in this methodology for soft knowledge, that is, knowledge that is difficult to quantify or convey. Soft knowledge or expertise is an important topic of this methodology. There is some form of judgement required to determine if the methodology produces the desired results. Considering that the objective of the methodology is to calculate tonnage uncertainty by successfully modeling the geometry of a vein type deposit, it is important that the model reflect the image of what the orebody should look like. The width of uncertainty or the amount of un-

certainty is another issue where soft knowledge can be useful. The size of the uncertainty bandwidth to apply to a single deterministic model during half calibration is more likely based on some comfort level rather than a calculated value. An example of the need for soft knowledge is shown in Figure 3-27 found in section 3.6.2.

# Chapter 3

## Parameter Inference

Several key concepts behind the distance function approach were presented in Chapter 2. This chapter will discuss some of the important user defined parameters in the methodology and explain how to determine reasonable values for those parameters such that fair and unbiased results are obtained.

### 3.1 Data and Mean

The most important information extracted from the drillhole data is the rock type at each sampled location. Each sample is assigned a distance to the nearest sample that has the opposite rock type. The methodology presented here uses two rock types (vein and non-vein). Assay information and the length of the samples are not used. The methodology relies on the coordinates of the midpoint of the samples and the value of the modified DF. To properly use the DF we must define an area of interest large enough to enclose the entire orebody. Exploration drilling is often done only in and around the zone of interest. This may also apply to many of the holes that pass through the bounding box where there are sections of unsampled drillholes. In such cases, the addition of “dummy” sample intervals to the data is warranted. Sample intervals need to be added so that a complete set of sample intervals can be generated within the bounding box. There are no defined guidelines on the sample interval but depending on the existing data spacing, the average sample length could be considered as a lower limit.

The methodology presented here considers closed 3D orebodies. Enough drillhole length outside of the orebody should be included to ensure that the volume is closed. Also, a positive mean value must be chosen to ensure that kriging the DF values leads to a closed orebody. A mean equal to at least twice the drillhole spacing was used for the examples shown in this thesis.

## 3.2 Variogram and Anisotropy

The variogram is a measure of spatial variability between sample pairs. It is often referred to as a measure of dissimilarity between pairs of data separated by specific lag distances. The variogram is very important in kriging and simulation. Calculating the proper experimental variogram will also quantify the anisotropy associated with the data.

Two common types of anisotropy associated with ore deposits are geometric anisotropy and zonal anisotropy. Geometric anisotropy refers to anisotropy that exists when the variogram sill remains the same but the range varies with direction. Zonal anisotropy exists when the variogram sill varies with direction. With zonal anisotropy, the range in each direction can differ or remain the same. Both types of anisotropy can coexist in a deposit (Gringarten and Deutsch, 1999). In the case of tonnage uncertainty, geometric anisotropy is of interest and will be defined by the geometry of an ore deposit. Geometric anisotropy implies that a particular deposit is more continuous in one direction. We can often infer geometric anisotropy through knowledge acquired from geological mapping.

Variograms are used to analyze spatial data and are a measure of the spatial dependence between sample locations. The main parameter of the variogram is the range, that is, is the distance where pairs of data become uncorrelated. The variogram range is used when estimating the value at an unsampled location. The range parameter is derived from a model fitted to an experimental variogram.

## Simple Vertical Drillhole

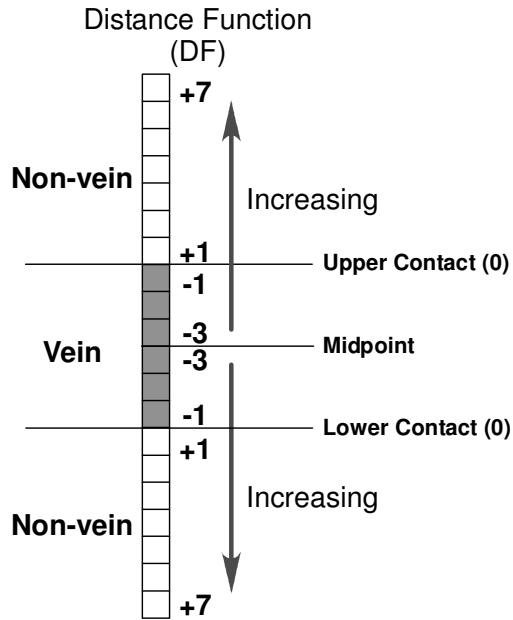


**Figure 3-1:** Schematic diagram of Distance Function. Distance increases away from vein/non-vein boundary.

In the simplest form, the distance function (DF) is calculated from a single drill-hole with a single intercept. The data configuration resulting from the DF will possess a cyclic pattern, uniformly decreasing then uniformly increasing. Variogram calculation on this arrangement of data will not produce a recognizable sill because paired data will always have some correlation with one another.

Consider the single intercept, Figure 3-1. The contacts of this intercept are assigned a distance of zero. As one moves up the hole away from the intercept, the distance values increase and are positively assigned. As one moves down the hole away from the contact, the values increase and are negatively assigned. After crossing the midpoint of the intercept, the maximum distance from the vein contact in either direction, the distance to the lower contact begins to decrease. The lower half of the hole, that is, from the midpoint to the bottom of the hole, is a mirror image of the upper half of the drillhole. This mirroring of the drillhole

causes a cycle in the variogram referred to as a hole effect. The hole effect is common in stratigraphically layered deposits.

### 3.2.1 Theoretical Variogram Model

Consider a single vertical drillhole of length ( $A$ ) that intersects a single vein-type (tabular) structure which has a thickness ( $a$ ). If the hole is discretized into equal sample intervals from top to bottom we are able to assign two variables at each sampled location; 1) a vein indicator (VI) corresponding to the presence of (1) or absence of (0) vein structure, and 2), the distance calculated by the DF.

#### 3.2.1.1 Drillhole Geometry

The result of the DF calculation is a column or string of uniformly distributed distances that can be divided into regions that can be associated with the variogram.

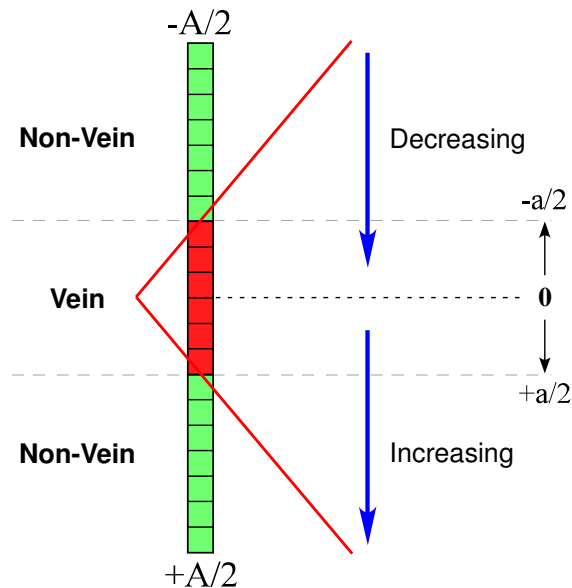


Figure 3-2: Drillhole geometry in simplified form.

The drill data can be divided into four regions corresponding to the following limits. The length ( $A$ ) of the drillhole can be divided into two parts separated at the midpoint of the vein, Figure 3-2. The upper half is defined as  $-A/2$  and the lower half as  $+A/2$ . Similarly the vein structure ( $a$ ), can be divided into  $-a/2$  and  $+a/2$  again at the midpoint of the intercept. The midpoint of the intercept or vein centre

(VC) in Figure 3-3, is defined as the zero point which separates the upper half of the drillhole from the lower half. Each half of the drillhole contains two regions, one non-vein and one vein. The regions in the upper and lower halves of the drillhole form mirror images of one another. The limits of the four regions, separated at the centre of the vein and the upper and lower vein contacts, are labelled Region I to IV.

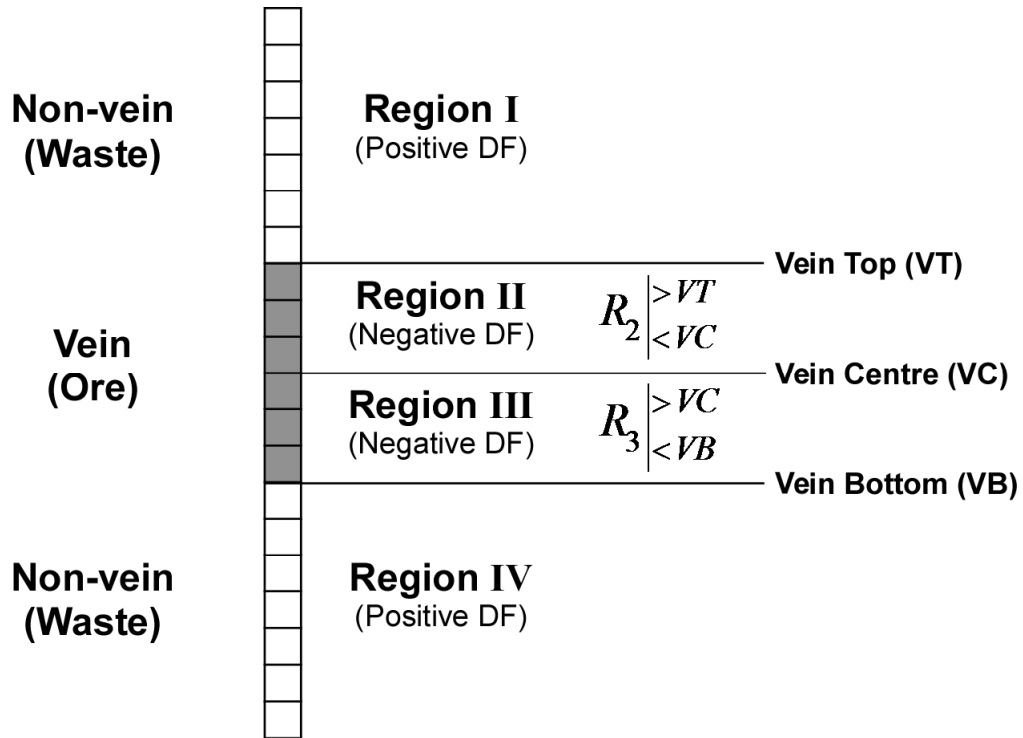


Figure 3-3: Defined drillhole regions.

Region 1 (RI) is a non-vein area extending from the upper limit of the drillhole,  $-A/2$ , to the vein boundary located at  $-a/2$ , Figure 3-2 and Figure 3-3. Following this is Region 2 (RII) composed of vein and extends from the upper contact of the vein,  $-a/2$ , to the midpoint of the vein (VC) which is also the zero point. Region 3 (RIII) is a mirror image of RII extending from the vein midpoint to the lower boundary of the vein located at  $+a/2$ . The final region, Region 4 (RIV), is the mirror of RI and extends from the lower vein contact at  $+a/2$  to the end of the drillhole at  $+A/2$ .

### 3.2.1.2 Variogram Geometry

Consider that the limits of the variogram span the length of the drillhole from  $-A/2$  to  $+A/2$  corresponding to the top and bottom of the drillhole, respectively. These limits define the minimum and maximum lag distance  $h$ . The vein structure can also be depicted on the variogram by plotting the positions of  $-a/2$  and  $+a/2$  with respect to the values  $-A/2$  and  $+A/2$ . When the lag distance  $h$  is greater than the vein thickness  $a$ , there will be no vein/vein pairs included in the calculation. Recall that samples classified as vein are negative and those classified as non-vein positive. Therefore one would expect the variance of vein/non-vein pairs to be greater than that of non-vein/non-vein pairs. Generally, it is expected that the vein thickness ' $a$ ' will be much less than the domain size  $A$ , therefore we should expect a lower average variance for vein/vein pairs than non-vein/non-vein pairs.

**Region one (RI)** is the region of most interest. It is the area bounded by a lag distances from 0 to  $A/2-a/2$ . Variances calculated in this region are for short lag distances where  $h < a/2$  and use all pair combinations, non-vein/non-vein, vein /non-vein and vein/vein. The region is not dominated by a single pair type however, as the domain size  $A$  increases with respect to vein size ' $a$ ', or vice versa, the type of dominate pairs change. Small values of ' $a$ ' with respect to domain  $A$ , non-vein/non-vein pairs dominate whereas for large values of ' $a$ ' vein/vein pairs dominate. Variance increases with increasing lag distance. When the lag distance is equal to the vein thickness, that is, when  $h=a$ , this marks the end of inclusion of vein/vein pairs. For all  $h > a$ , there are no vein/vein pairs included. Region 1 is most important since it will ensure that no pair combinations will be skipped, Figure 3-4.

**Region two (RII)** is the area located between lag distances of  $A/2-a/2$  and  $A/2$ , Figure 3-4. Since the minimum lag distance is equal to  $A/2-a/2$ , Region 2 will not contain any pairs from the same Region. Region 2 is dominated by vein /non-vein pairs for lesser lags, becoming predominantly non-vein/non-vein pairs for larger lags. In this region non-vein/non-vein pairs tend to have, on average, a lower vari-

ance than vein /non-vein pairs, we expect the variance to decrease with increasing lag distance.

**Region three (RIII)** is the area with lag distances between  $A/2$  and  $A/2+a/2$ , Figure 3-4. This region is dominated by vein /non-vein pairs. The position of the point  $h=a$  has a strong influence on the variance in this region and controls the ratio of vein/vein pairs included from RII - RIII and non-vein/non-vein pairs included from RI-RIV. As the lag distance  $h=a$  progresses through RIII, the ratio of vein-vein pairs increases and the ratio of non-vein/non-vein pairs decreases.

**Region four (RIV)** is the area with a lag distances greater than  $A/2+a/2$ , Figure 3-4. This area corresponds to large values of  $h$ . Values in Region 4 are paired only with values from Region I and thus are very similar. Since the distance function values are similar in these regions, the variance decreases rapidly eventually going to zero.

### 3.2.2 Numerical Verification

As shown in the preceding section, the variogram is divided into regions whose limits are defined by the domain  $A$ , and the thickness of the vein structure ' $a$ '. The subdivisions create two regions of positive slope above the vein centre and two regions of negative slope below the vein centre, as depicted in Figure 3-5.

The calculated variogram for lag distance  $h$  is defined as the expected value of the squared difference between pairs of data and is expressed as:

$$2\gamma(\mathbf{h}) = E\left\{[Z(\mathbf{u}) - Z(\mathbf{u} + \mathbf{h})]^2\right\} \quad (3.1)$$

The experimental variogram for the example is shown in Figure 3-5 and Figure 3-6 including the relative positions of the defined regions.

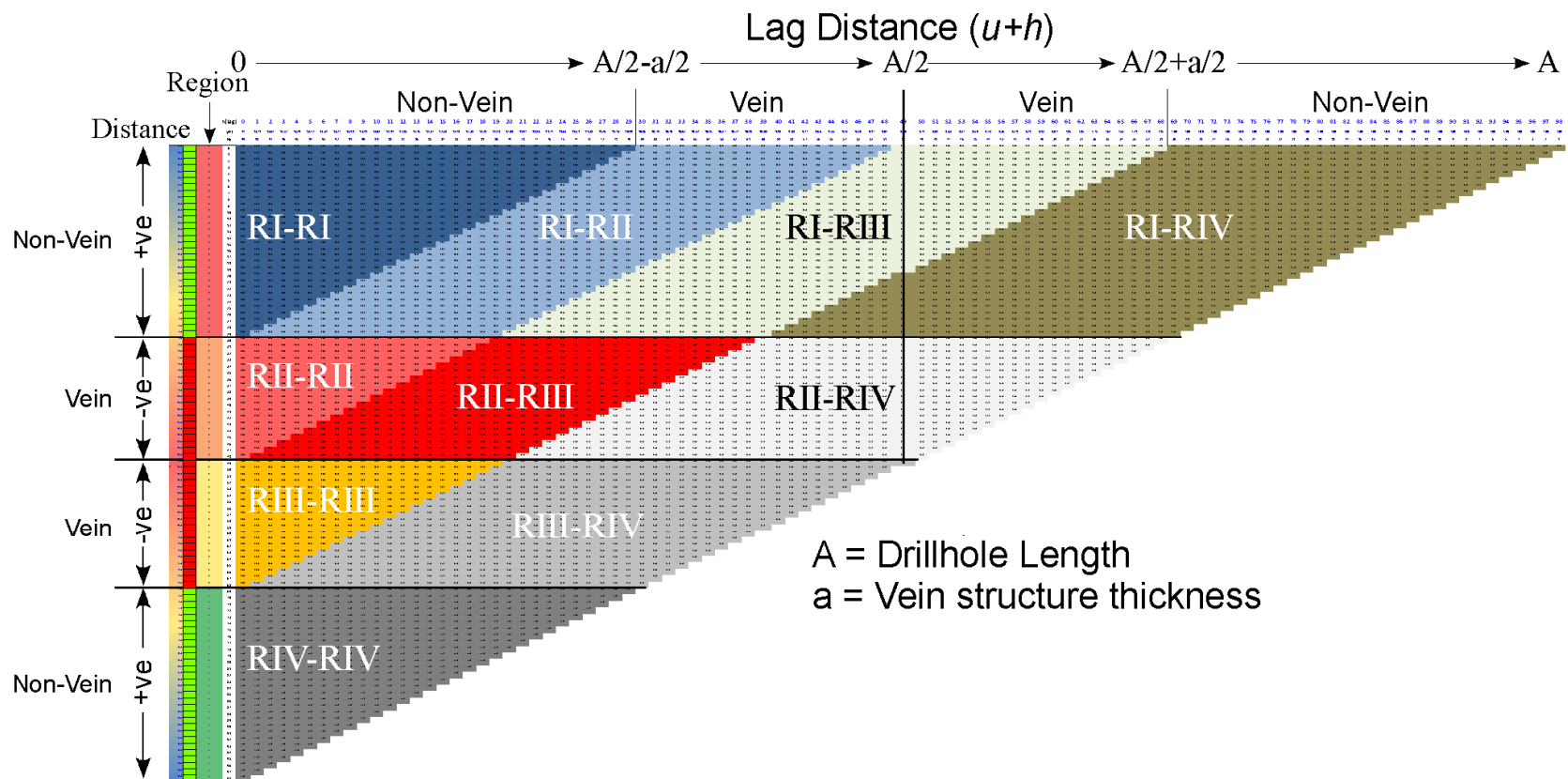


**Figure 3-4:**  $Z(u)$ ,  $Z(u+h)$  pairs by Region. Diagram depicts which rock types are paired and from which regions as the lag distance increases. For example, when the lag distance is between  $(A/2 + a/2)$  and  $(A)$ , the lag distance is longer than the thickness of the vein therefore no vein pairs exist. This is shown on the right outer edge of the diagram, RI-RIV, RII-RIV, RIII-RIV and RIV-RIV at the bottom.

### Experimental Variogram

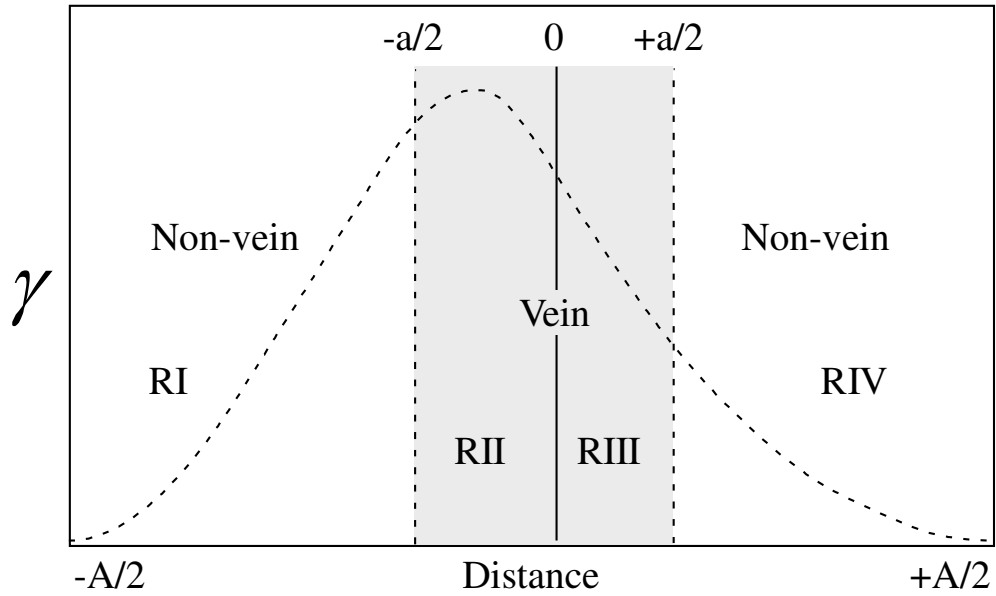


Figure 3-5: Schematic of experimental variogram regions with respect to the domain A.

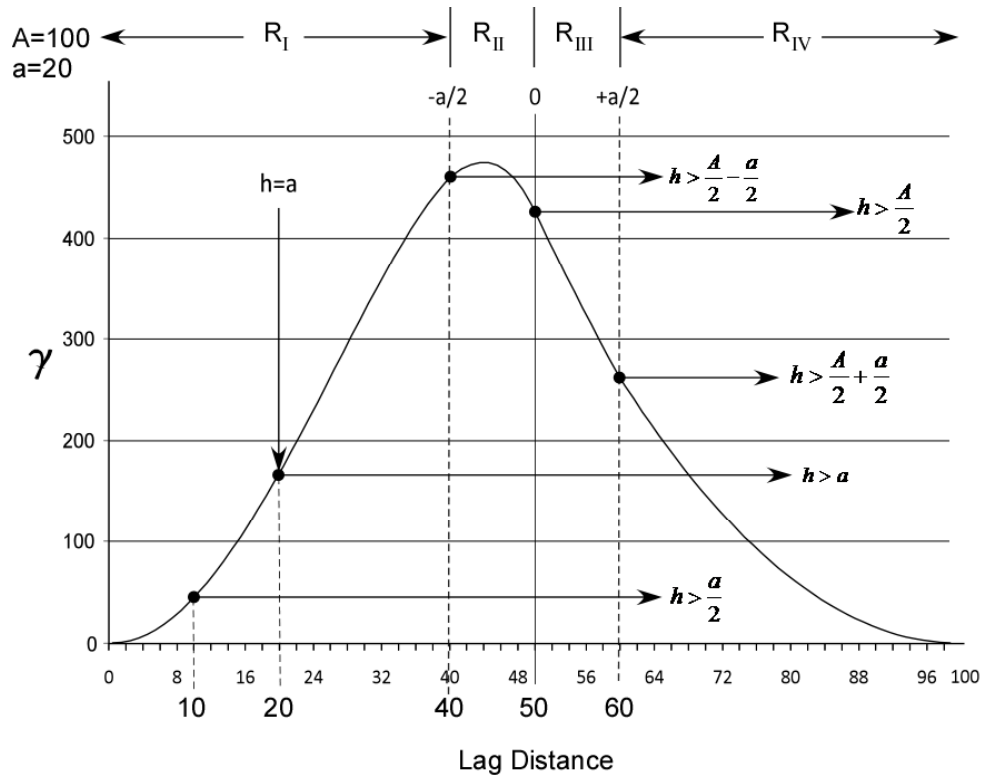


Figure 3-6: Experimental variogram example for lag  $h$  where drillhole length  $A=100$  and vein thickness  $a=20$ .

In integral form this can be expressed as the squared difference between pairs of data evaluated over the domain of interest.

$$2\gamma(\mathbf{h}) = \int_{U_{Lower}}^{U_{Upper}} [Z(\mathbf{u}) - Z(\mathbf{u} + \mathbf{h})]^2 du \quad (3.2)$$

The variogram is integrated over the finite domain of string data  $A$ , from  $-A/2$  to  $-A/2 - \mathbf{h}$  as shown in the following equation.

$$2\gamma(\mathbf{h}) = \int_{-A/2}^{A/2-h} [Z(\mathbf{u}) - Z(\mathbf{u} + \mathbf{h})]^2 du \quad (3.3)$$

The data  $Z(\mathbf{u})$  and  $Z(\mathbf{u} + \mathbf{h})$  can be replaced by the following linear equations;

$$Z(\mathbf{u}) = a_0 + a_1(\mathbf{u}) \quad (3.4)$$

and,

$$Z(\mathbf{u} + \mathbf{h}) = b_0 + b_1(\mathbf{u} + \mathbf{h}) \quad (3.5)$$

where  $a_0$  and  $b_0$  are the y intercepts of the curve and  $a_1$  and  $b_1$  the respective slopes. For each defined region I through IV, there will be a different slope and intercept combination. **Table 3-1** lists the combinations of intercept and slope for each region. The intercept is expressed in terms relating to the uncertainty constant  $C$  as depicted in Figure 3-7.

**Table 3-1:** Slope and intercepts by region

<b>Region</b>	<b>Intercept <math>a_0</math></b>	<b>Slope <math>a_1</math></b>
I	+C-a/2	-1
II	-C-a/2	-1
III	-C-a/2	1
IV	+C-a/2	1

From the parameters listed in Table 3-1, we can define four different equations corresponding to the four regions of the variogram.

$$Z(\mathbf{u}) = \begin{cases} +C - \frac{a}{2} - \mathbf{u} & \text{RI} \\ -C - \frac{a}{2} - \mathbf{u} & \text{RII} \\ -C - \frac{a}{2} + \mathbf{u} & \text{RIII} \\ +C - \frac{a}{2} + \mathbf{u} & \text{RIV} \end{cases}$$

In the small example here a constant slope is assumed, it is possible that the slope be variable, a case to be addressed in the following section on the beta parameter.

Recall the integral for a variogram over a finite domain, if  $Z(u)$  and  $Z(u+h)$  in Equation 3.3 are replaced with the equivalent equations  $a_0 + a_1(u)$  and  $b_0 + b_1(u+h)$  the resulting equation,

$$2\gamma(\mathbf{h}) = \int_{U_{lwr}}^{U_{upr}} [(a_0 + a_1(\mathbf{u})) - (b_0 + b_1(\mathbf{u} + \mathbf{h}))]^2 du \quad (3.6)$$

can be reduced to

$$\begin{aligned} 2\gamma(\mathbf{h}) = & (a_0 - b_0 - b_1\mathbf{h})^2 \cdot (U_{upr} - U_{lwr}) \\ & - (a_0 - b_0 - b_1\mathbf{h}) \cdot (a_0 - b_1) \cdot (U_{upr}^2 - U_{lwr}^2) \\ & + \frac{(a_1 - b_1)^2}{3} (U_{upr}^3 - U_{lwr}^3) \end{aligned} \quad (3.7)$$

Where  $a_0$  and  $a_1$  are the intercept and slope of the tail region and  $b_0$  and  $b_1$  are the intercept and slope of the head region, while  $U_{upr}$  and  $U_{lwr}$  are the upper and lower limits defined by the two regions,  $\mathbf{h}$  is the lag distance. Using the above equation the theoretical variogram was calculated and is shown in Figure 3-8.

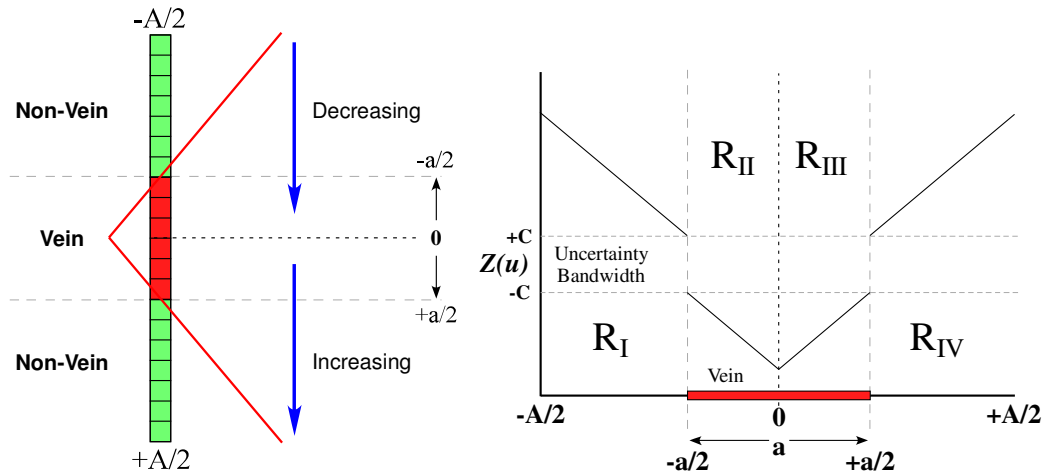


Figure 3-7: Relationship of Data (left) to variogram slopes and intercepts (right)

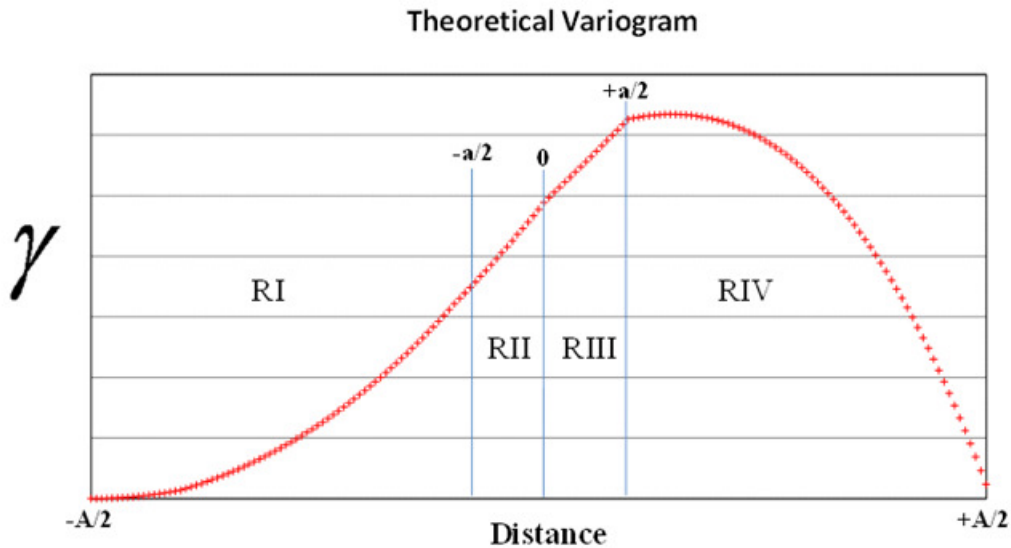


Figure 3-8: Theoretical Variogram calculated using Equation 3.7.

### 3.2.3 Comments on Multiple strings / Multiple intercepts

It is often the case that vein deposits contain more than a single vein structure. If multiple vein structures exist, they can vary in number from one drillhole to another. If multiple vein structures exist then the cyclic nature of the variogram will be reproduced over the range of  $A$  for each intercept, producing a non-damped hole effect. Hole effects in the variogram make the selection of a single range ambiguous and difficult. The experimental variogram will have to be calculated and fitted.

### 3.2.4 Practical Considerations

**Nugget Effect** - In theory, when  $h$  is zero the variance between pairs will be zero. In this example there are no tolerances used on lag distances and no search angles used. Therefore the nugget effect will be zero since the squared difference between any points with a zero separation will be zero and the sum of all squared differences in the zero class will also be zero. In practice the squared difference at zero lag can be non-zero due the closeness and the tolerances used.

**Shape** – In the example shown in Figure 3-8, the variogram has a bell shape caused by the presence of only one structure and the symmetrical nature of the drillhole data. With the addition of strings and multiple intercepts, the shape will become more sinuous repeating once for each additional structure. The first range is the most important and will be controlled by the size of the vein.

**Anisotropy** – The anisotropy will likely be approximated by other means such as acquired knowledge of the morphology of the deposit gained through drilling and mapping.

## 3.3 Parameter Guidelines

The following section presents some guidelines and comments on parameter selection and application of the various components discussed in Chapter 2 needed to achieve a calibration of  $C$  and  $\beta$ .

### 3.3.1 Variogram

The goal of the interpolation process with respect to tonnage uncertainty is to produce a smooth surface representing the possible variation in the surface from drillhole to drillhole. Two of the criteria discussed here, as applied to variogram modeling, are the nugget variance and the variogram ranges.

The nugget variance is the value of the variogram when the separation distance  $h$  is just greater than zero. It is recommended using a zero nugget variance for modeling tonnage uncertainty to ensure that the surfaces vary smoothly.

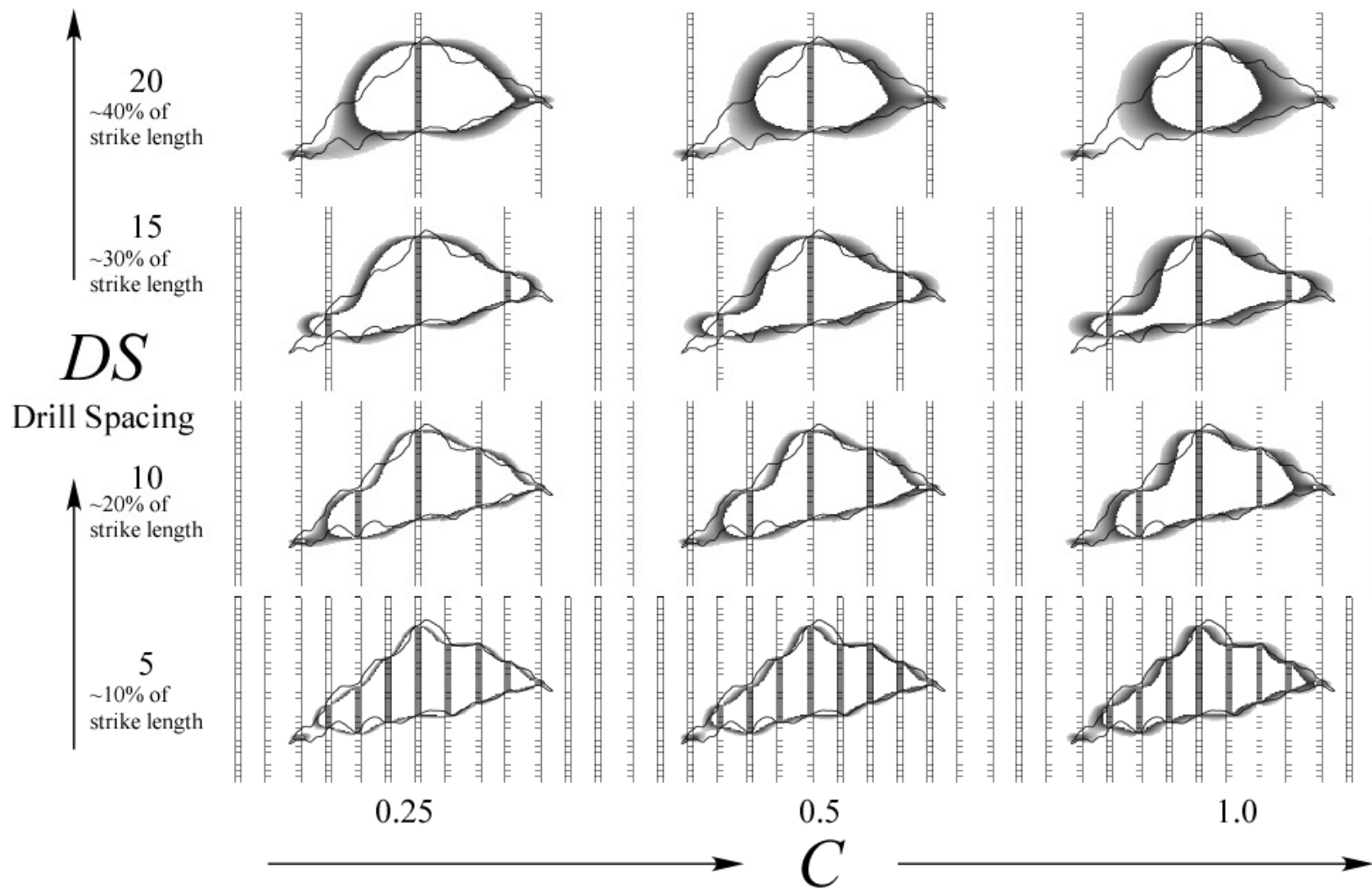
In the previous section the theoretical variogram was discussed with specific detail to the paired data and their respective vein types. The theoretical variogram reached the maximum sill for lag distances approaching  $A/2$  or one half the size of the domain. Deutsch (2005) suggests using variogram ranges set between one quarter and one half of the domain size in order to create a smooth surface between drillholes.

The examples used in this thesis were modeled using a single spherical model with zero nugget variance, maximum and minimum range of 35 units and a vertical range of 16. These ranges were found to provide the best smoothing and continuity between drillholes as depicted in Figure 3-9, and represent approximately one third of the size of the domain.

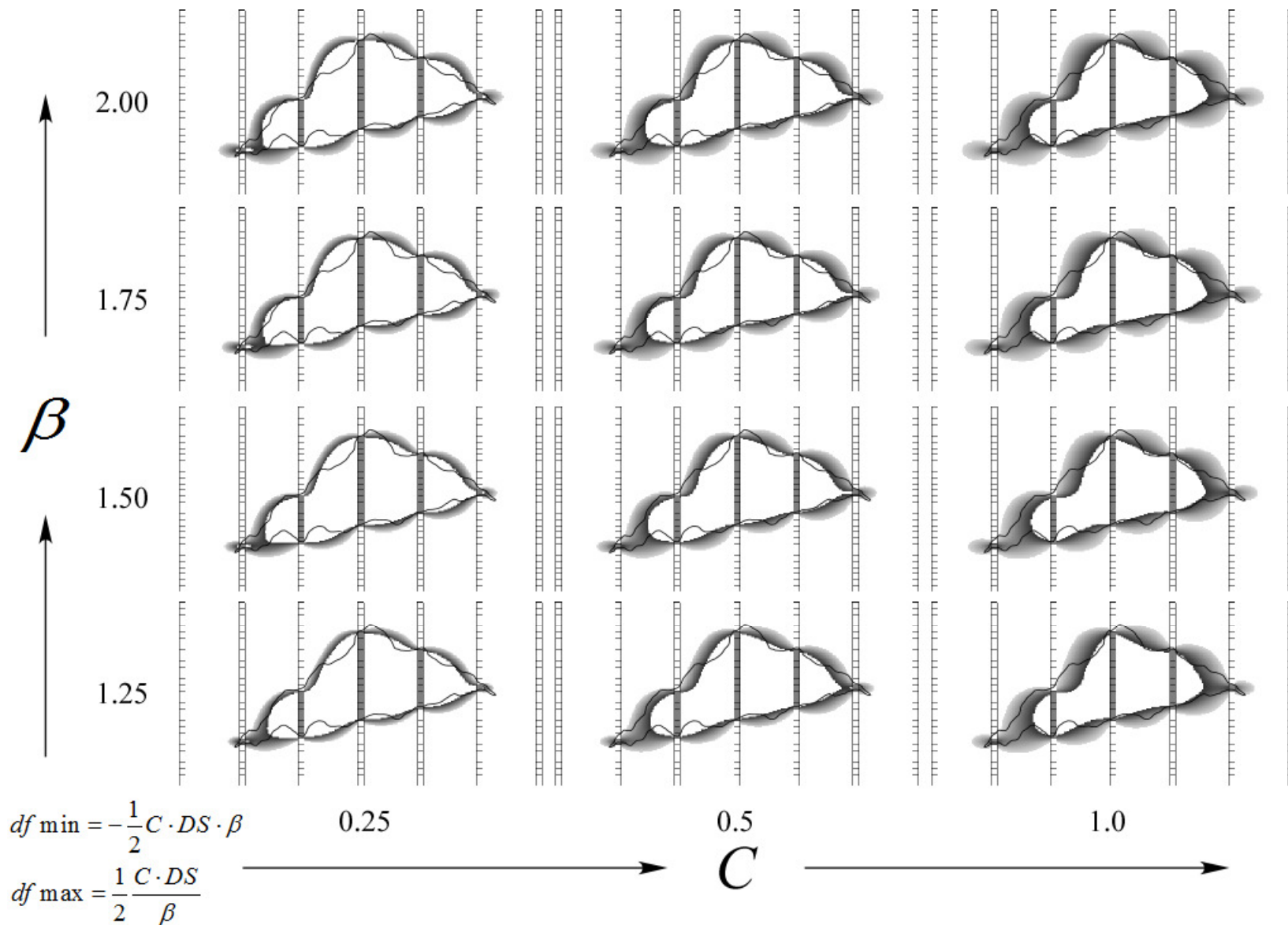
### 3.3.2 Unbiasedness parameter C

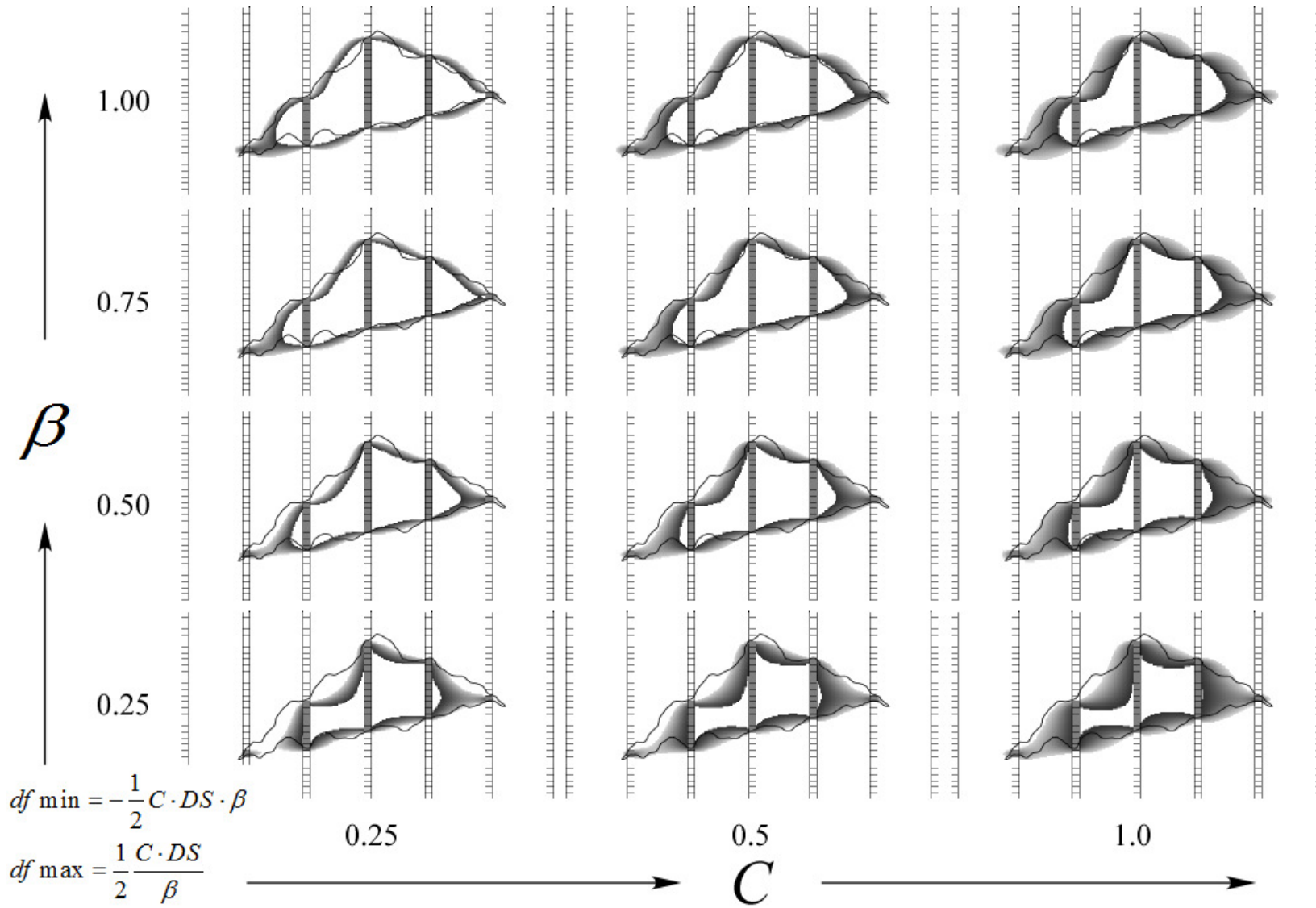
The unbiasedness parameter C, also referred to as the uncertainty parameter, varies from near 0 to 1. A value of 0 represents zero uncertainty and a value of 1 represents the maximum uncertainty bandwidth, a value equal to the drill spacing as specified in the *dfv4* parameter file. In Figure 3-9, C values equal to 0.25, 0.5 and 1.0 are shown as applied to drillhole spacing of 5, 10, 15 and 20 units. These examples were generated using a neutral  $\beta$  value of 1 and therefore does not impact the DF. The results show that with increasing drillhole spacing and C there is increased uncertainty. Figure 3-10 shows a matrix of  $\beta$  versus C plots. Values of  $\beta$  from 0.25 to 2 were used along with C values of 0.25, 0.5 and 1.0. The plots are used illustrate that with increasing  $\beta$  there is a tendency for the zone of uncertainty to expand. With increasing C, the location of the iso-zero boundary, i.e. the centre of the uncertainty bandwidth, remains fairly consistent, and only the thickness of the uncertainty band increases.

The uncertainty of our estimates should be fair, that is, the range of uncertainty should be neither too large nor too small. This will be checked below.



**Figure 3-9:** Examples of uncertainty in orebody volume. Each example is same orebody realization, and same vertical slice through the centre in the XZ plane. Distance function calculated using  $\beta$  equal to one. The solid outline is the true orebody outline.

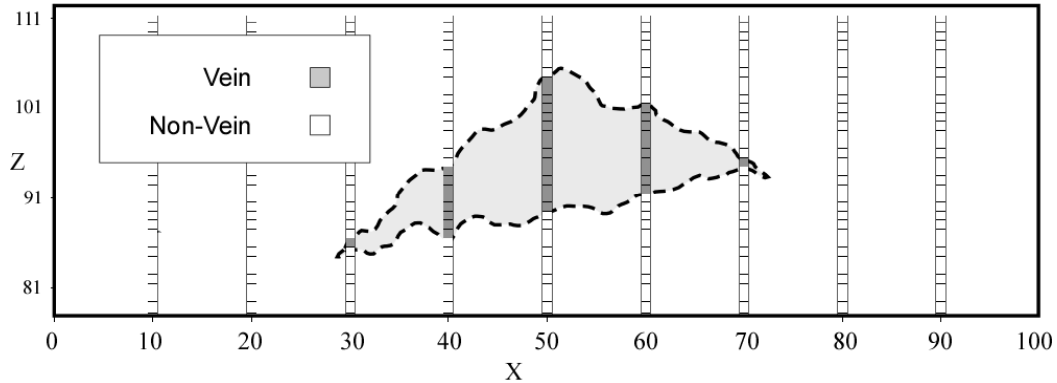




**Figure 3-10:** Examples of uncertainty using  $C$  and  $\beta$  combinations. Each example is same orebody realization, and same vertical XZ slice through the centre of the model. Distance function calculated using  $\beta$  values from 0.25 to 2.0. The solid outline is the actual orebody.

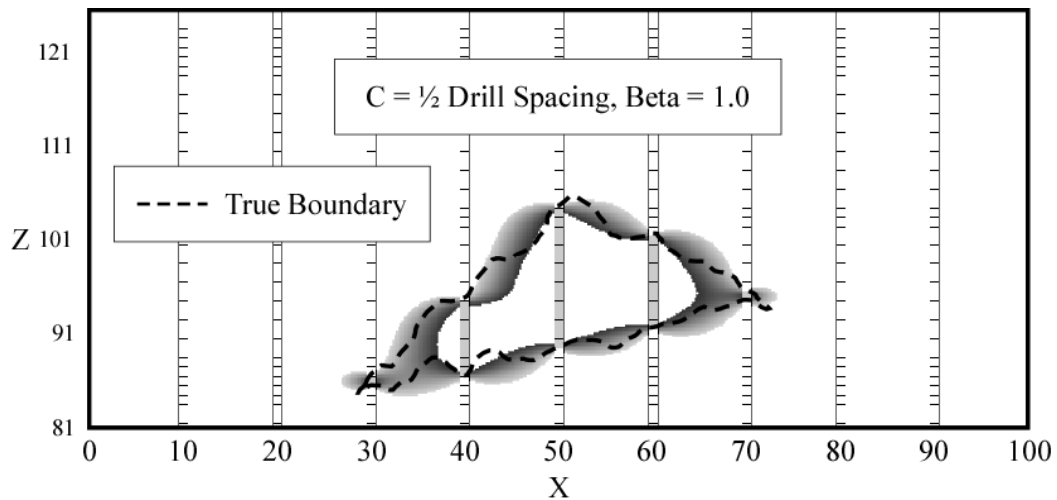
### 3.3.3 Fairness parameter Beta

The fairness parameter  $\beta$  controls the position of the iso-zero boundary located between conditioning points. The larger the value of  $\beta$  the larger boundary. Figure 3-11 shows a cross sectional view through an orebody and the true geometry



**Figure 3-11:** - Vertical section of the true orebody in the XZ plane through centre of simulated orebody.

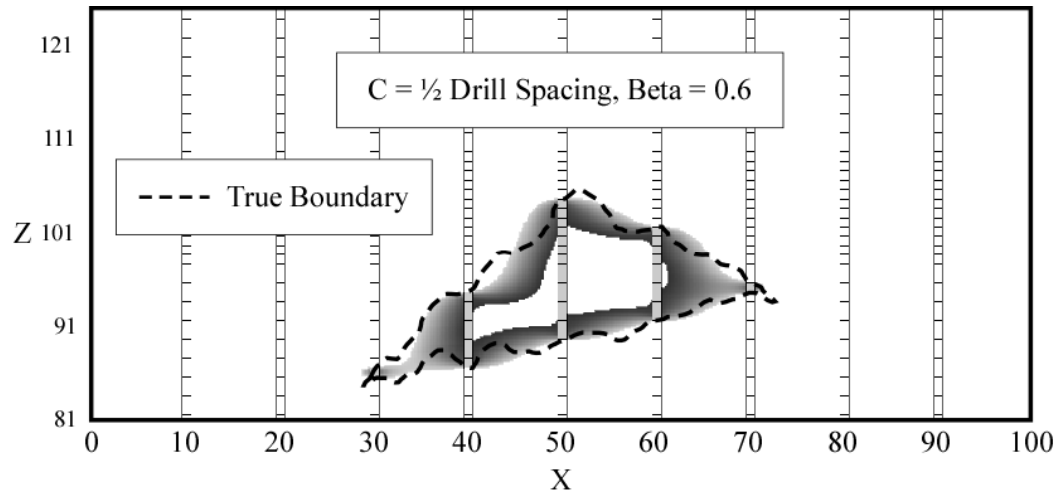
associated with it. The vertical strings shown in the figure represents drillholes evenly spaced every 10 units. Recall that  $\beta$  modifies the DF and that if  $\beta=1$ , the modified DF remains unchanged. Figure 3-12 shows an estimation using  $\beta=1$ . In Figure 3-13, a  $\beta$  of 0.6 was used and comparing that with the base case shown in



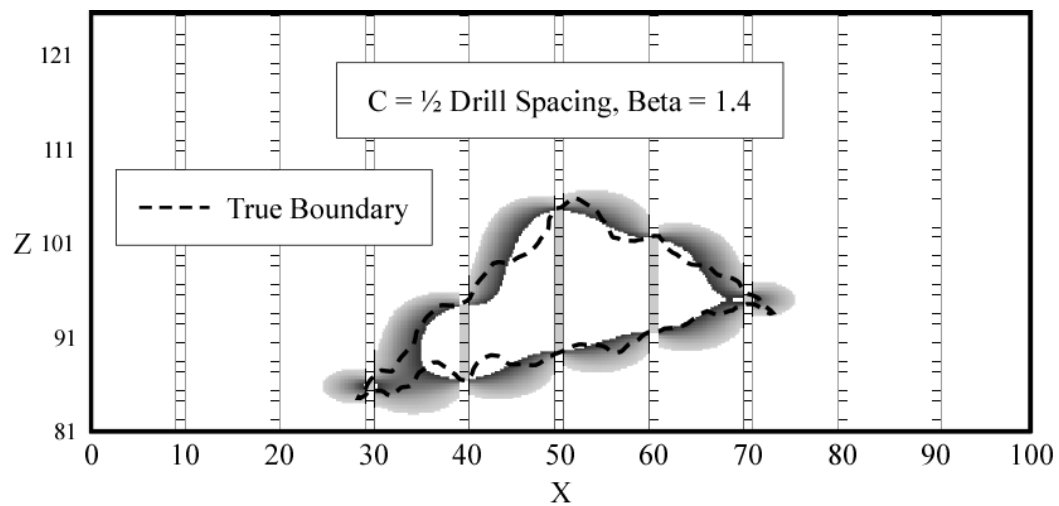
**Figure 3-12:** Vertical section in the XZ plane. Beta = 1, base case

Figure 3-12, we see that the iso-zero boundary and its associated bandwidth has contracted. Contrary to this, when  $\beta>1$ , shows that the iso-zero and bandwidth

expands, demonstrated in Figure 3-14 where a  $\beta$  equal to 1.4 was used for estimation.



**Figure 3-13:** Vertical section in the XZ plane. Beta = <1, Iso-zero contracts



**Figure 3-14:** Vertical section in the XZ plane. Beta >1, Iso-zero dilates

### 3.3.4 Anisotropy

The anisotropy for each simulated orebody was calculated using two vertical cross sections. The cross sectional dimensions through the centre of the orebody in XZ and YZ planes were used to calculate the average strike length and average vein thickness. A FORTRAN program was written to calculate and write the ani-

sotropy values of each realization to a file which is read when applying the distance function.

### 3.3.5 Simple Kriging Interpolator

Simple kriging was implemented with a version of the program *kt3d* that was modified to speed up the run time. The modified program *kt3d-df*, reads an input file produced by the program *dfopt* that creates a bounding box around the object and assigns a value of 0 to all cells located outside and 1 to all cells located inside the box. This enables *kt3d-df* to skip the estimation process for cells that are too far away and assign them a code of -999 indicating the cell has not been estimated. The size in number of cells of the 3D models estimated in *XYZ* directions is 100 by 100 by 80 for a total of 800,000 cells. The time to estimate this size of model using *kt3d* and the 10 unit drill spacing data set is just over four minutes. Recall that 50 realizations will be used so the total time needed is on the order of three and one half hours. The same run done using the bounding box and the modified kriging program is two minutes thirty seconds for a single run and just over two hours to complete the 50 runs for a total reduction in execution time of one hour twenty-five minutes, a 40% reduction in time.

### 3.3.6 SK Mean

The simple kriging mean can be used to help control the geologic connectivity as shown in Figure 3-15. Changing the SK mean has little effect of the width of the uncertainty band but helps connect the orebody between drillholes. The geological objects simulated in this thesis represent 3D closed solids which have nearly equal X and Y lengths. The vertical Z axis (thickness) is typically one third that of the X and Y dimensions. A simple kriging mean of twice the drill spacing was chosen to ensure the closed nature of the solids was maintained in estimation and that no “ore” would be estimated outside of the closed objects as depicted in Figure 3-15 where the mean used is equal to a negative value 4x the drill spacing.

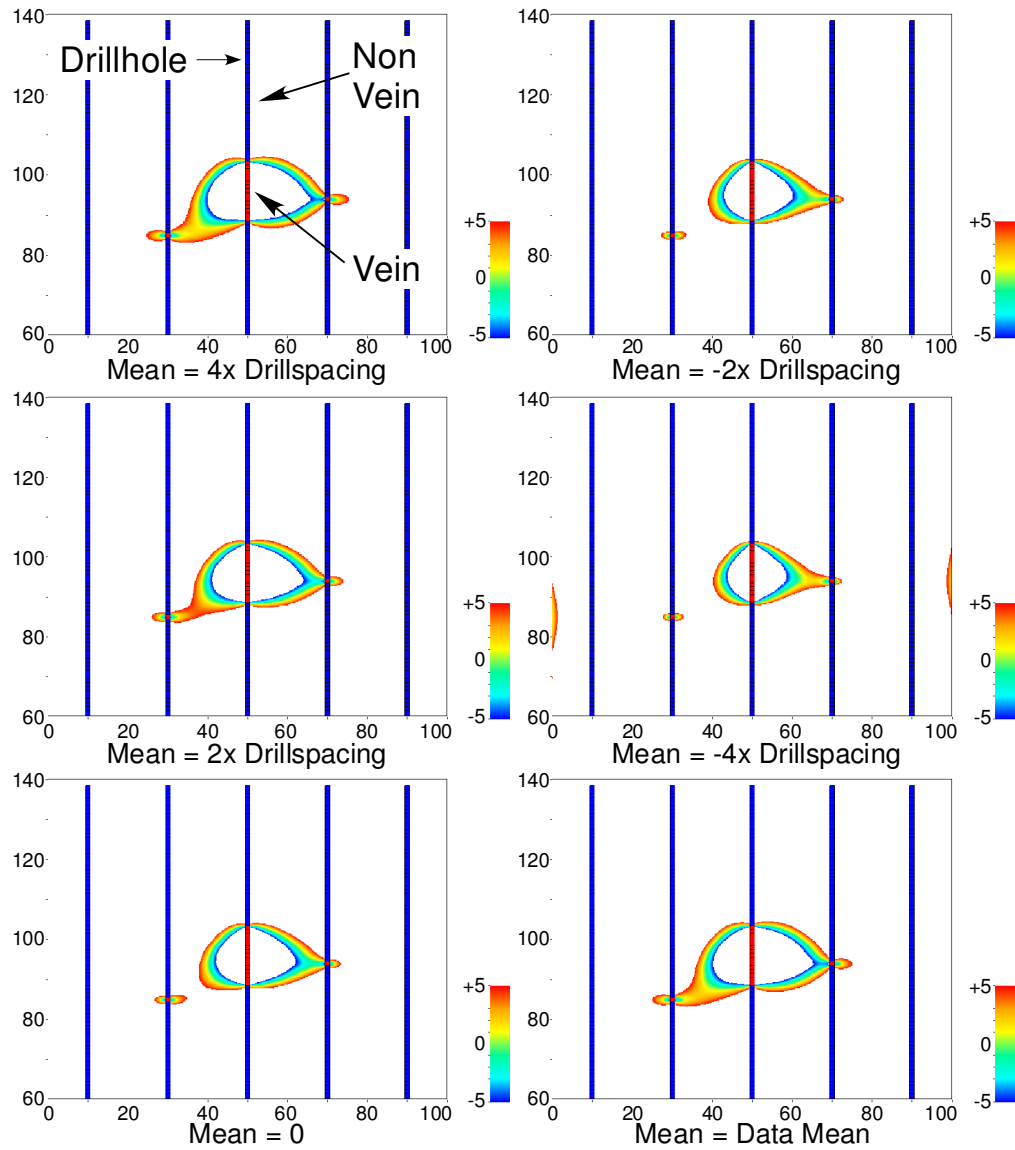


**Figure 3-15:** The effect of changing the SK mean on the DF. Vertical sections in the XZ plane.

### 3.4 Assessing Uncertainty

Accuracy is defined as the degree to which a measured value conforms to a specified standard. In this thesis the accuracy of the estimated tonnage is compared against the true tonnage. Precision is defined as a measure of reproducibility. Over a number of trials, precision is the number of times an experiment reproduces results within a predefined margin of error. Precision does not imply accuracy. Precision and accuracy must both be considered. It is of little value to produce

precise estimates if they are inaccurate. The desired result of an experiment is to have all results clustered together as close to the truth as possible and therefore be accurate and precise.

For any reasonable measure of uncertainty a set of estimates must be unbiased and fair. Bias is the expected value of the difference between the estimate and the truth;

$$bias = E\{T^* - T\} \quad (3.8)$$

If an estimator is unbiased, the expected value of the difference between the estimate and the truth will be zero and Equation 3.8 can be rewritten;

$$E\{T^*\} = E\{T\} \quad (3.9)$$

An unbiased estimate is a requirement for good uncertainty.

Figure 3-16 shows three different scatter plots. Figure 3-16 left, indicates a bias towards underestimation, all points in the data plot above the 45° line. Figure 3-16 centre, shows an unbiased scatter plot. The data group plots reasonably close to the 45° line with some estimates plotting above the line while other plot below the line. Finally, Figure 3-16 right, is an example of a bias toward overestimation where all points plot well below the line.

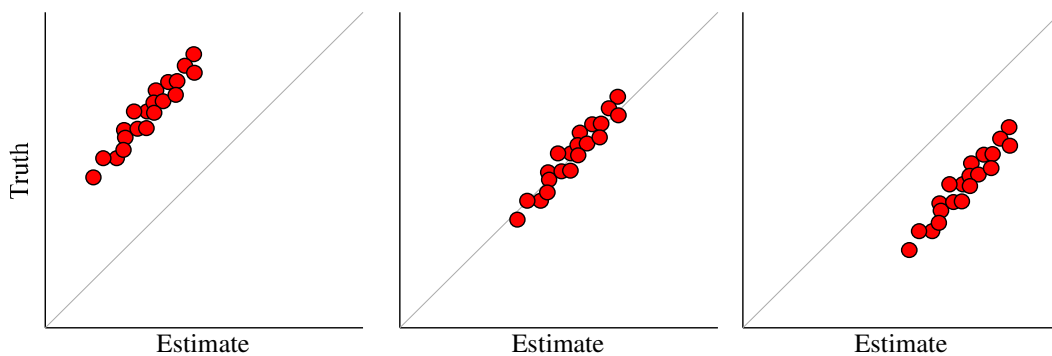


**Figure 3-16:** Schematic showing, Bias toward underestimation (left); Unbiased (centre); Bias toward overestimation (right);

### 3.4.1 Accuracy Plots

The accuracy of a set of estimated values is determined based on the fraction times the estimated value falls within a symmetrical predefined range.

$$p_{act} = \frac{Count\left(z_{est} \in \left[ z_{0.5-p/2}, z_{0.5+p/2} \right] \right)}{N} = p, \forall p \in [0,1] \quad (3.10)$$

The actual proportion  $p_{act}$  is defined as the number times an estimate,  $z_{est}$ , falls within the mean centred interval  $z_{0.5-p/2}$  through  $z_{0.5+p/2}$ , divided by the number of estimates  $N$ . A set of estimates is considered accurate if the actual fraction is equal to, or greater than the theoretical probability  $p$ . The closer  $p_{act}$  is to  $p$  for each probability interval from 0 to 1, the more accurate the estimates.

Consider a set of 50 estimates and a probability interval of p90. It is expected that 90% of the estimates will fall within the mean centred probability interval p90, defined as;

$$z_{0.5} \pm \frac{p}{2} = z_{0.5} \pm \frac{p_{90}}{2} = z_{0.5} \pm p_{45} \quad (3.11)$$

and defines the probability interval  $z_{.05} - z_{.95}$ . If there are 50 estimates, then the expected fraction would be 45 out of 50 estimates falling within the mean centred range  $z_{0.05}$  through  $z_{0.95}$ .

The target analogy is often used to explain accuracy and precision. In Figure 3-17, four different accuracy plot scenarios are presented. On the left side is a bullseye target showing a spread of twenty data points. The circles represent the probability intervals increasing from the inner p10 through the outer p90. The actual number of data landing in the each p-ring is calculated and compared to the theoretical number and plotted on the graph on the right side of Figure 3-17.

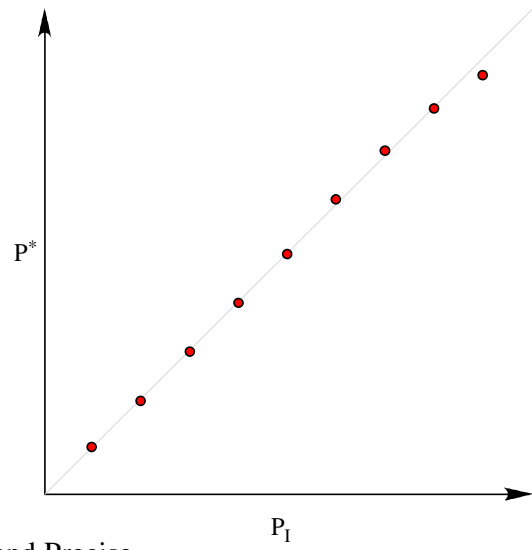
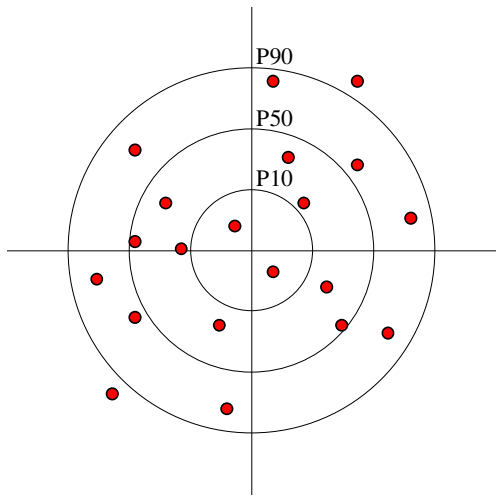
Starting with Figure 3-17a, visually the spread of data points on the target is consistent and even. There is no obvious bias visible in the data. Further examination will show that each ring of the target contains the appropriate number of data. Plotting the actual fraction against the probability interval produces the graph

shown on the right side of Figure 3-17. In Figure 3-17a, the points fall on the 45° line indicating that the result is accurate and precise, or unbiased and fair.

Moving to Figure 3-17b, visually the spread of data points on the target appears relatively consistent but more centrally concentrated than that shown in Figure 3-17a. Again, there is no obvious bias visible in the data other than its closeness to the centre of the target. Examination of the probability intervals reveals that each interval contains more data than it should. Plotting the actual fraction against the probability interval produces a plot of points that fall consistently above the 45° line indicating that the result is accurate and too precise and that the uncertainty bandwidth is too narrow. In such situations the tendency will be to overestimate.

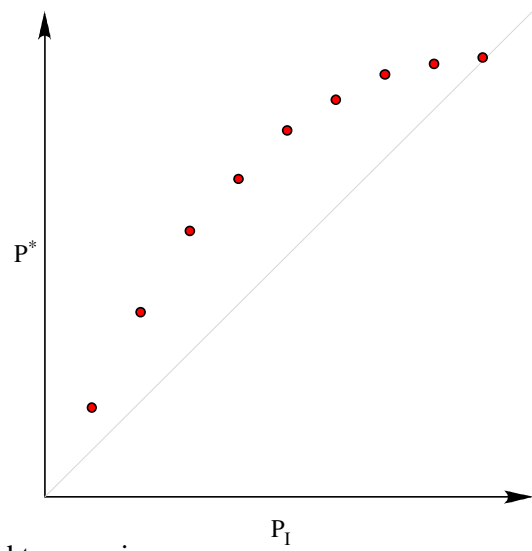
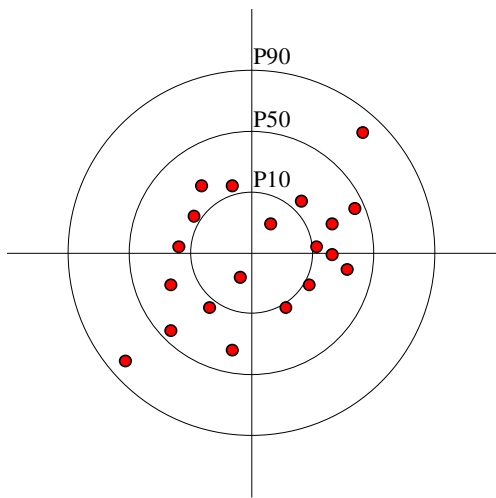
The opposite is shown in Figure 3-17c. This example also appears to be unbiased and with the exception of not having any points located close to the centre, appears to be uniform. In this instance, examination of the probability intervals reveals that each one contains less data than it should. The right hand side of Figure 3-17c reveals a that the plot of the actual fraction against the probability interval produces a plot where all points fall above the 45° line indicating that the result is accurate and imprecise meaning that that the uncertainty bandwidth is too wide. In such situations the tendency will be to underestimate.

Finally, Figure 3-17d shows a case which is neither accurate nor precise. In these cases the situation occurs where there are too many points plotting in the upper probability intervals and too few in the lower probability intervals, or vice versa. On the bullseye target the result is that points are centred on the p50 ring, or some other interval, with the number decreasing inward and increasing outward. On the line plot of the data the result is an “S” shaped plot. The dividing point between over estimation, points above the line, and under estimation, points below the line can occur at any point on the 45° line, in Figure 3-17d, this point is the p50 interval, and is shown this way for simplicity.



Accurate and Precise

**A**



Accurate and too precise

**B**

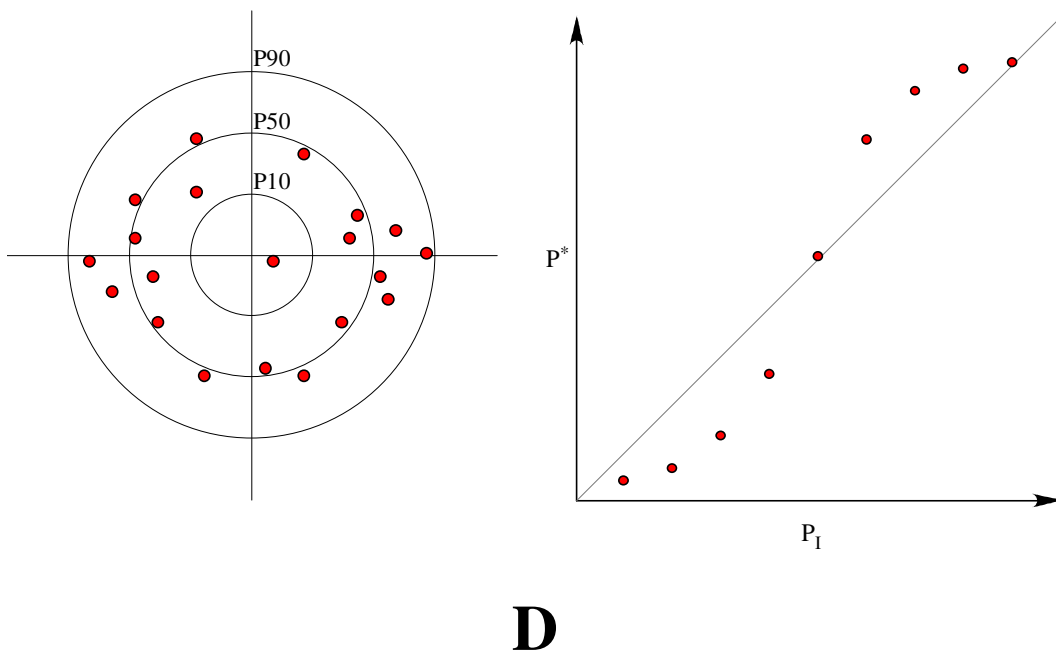
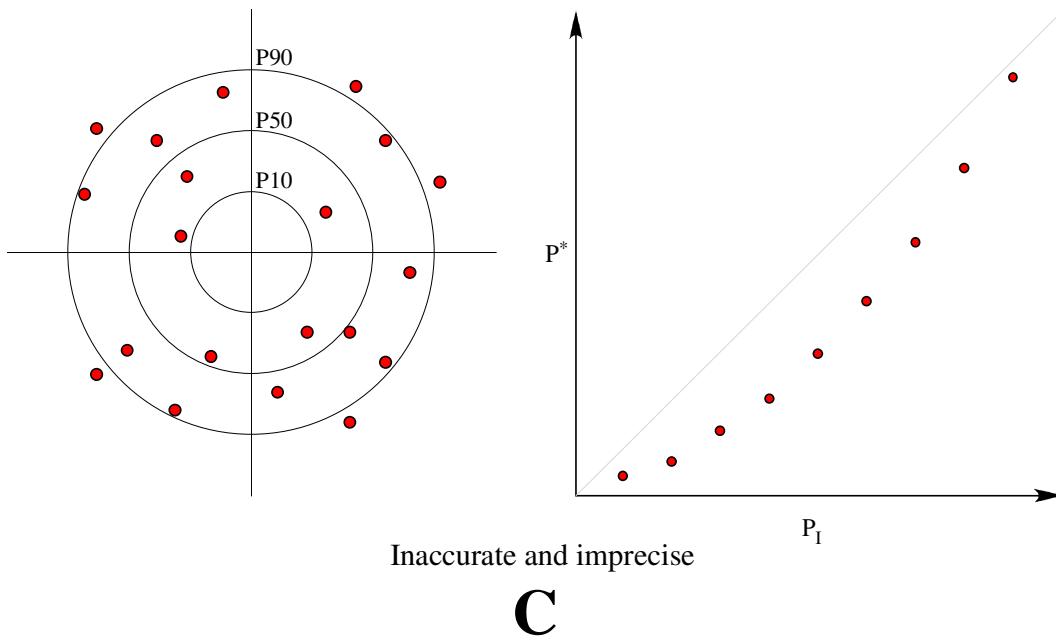


**Figure 3-17:** Accuracy and precision; A) Accurate and Precise, B) Accurate and too precise, C) Accurate and imprecise, and D) On average accurate and precise.

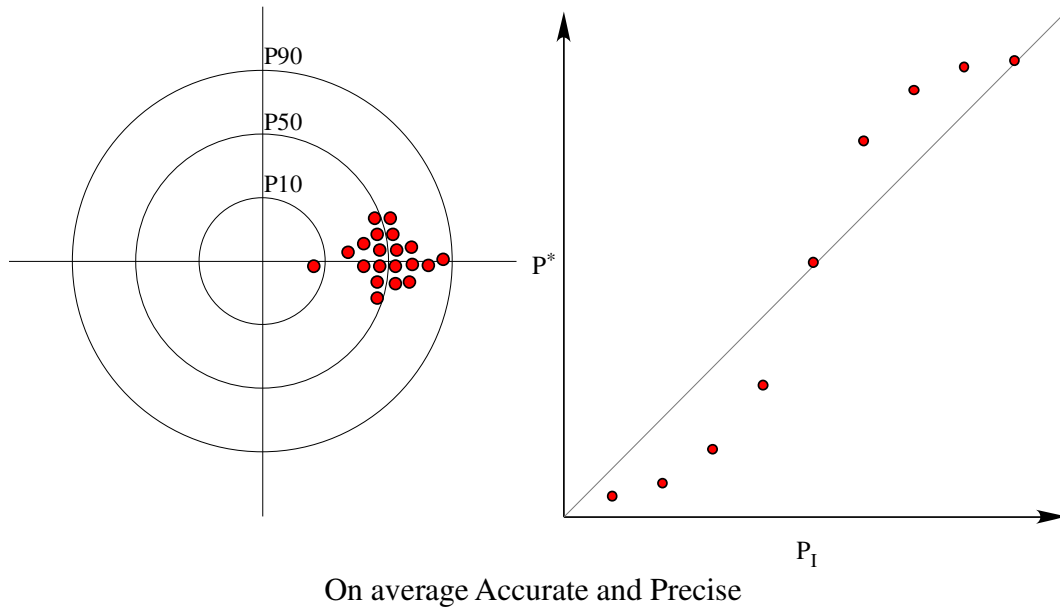


**Figure 3-18:** Same sample as **Figure 3-17 D**, different arrangement. Both are equally precise and on average accurate. This particular situation is difficult to control and is undesirable.

### 3.5 Calibration of Parameters

This section will discuss the calibration of the parameters  $C$  and  $\beta$  for accuracy and fairness.

#### 3.5.1 Objective function / criteria

Objective functions allow for the quantitative assessment of the parameters chosen for the estimation run. There are two principal objective functions used in this methodology,  $O1$  and  $O2$ . Generally, objective functions refer to functions that are to be maximized or minimized to obtain the optimal result. In this case, the objective functions are both set to zero to find the optimal value.

The objective function  $O1$  is a measure of the closeness to the truth or the accuracy of the estimate. It is defined as the expected value of the estimate ( $T^*$ ) minus the truth ( $T$ ), Equation 3.12, and approaches zero when the estimate approximates the truth. The function is standardized by dividing by the truth ( $T$ ).

$$O1 = \frac{E\{T^* - T\}}{E\{T\}} \quad (3.12)$$

When  $O1 > 0$ , on average  $T^*$  will be  $> T$  thus overestimating the tonnage. When  $O1 < 0$ , on average  $T^*$  will be  $< T$  and therefore underestimating the tonnage. Calculating  $O1$  for a different combinations of  $C$  and  $\beta$  produces the plot shown in Figure 3-19. Two points can be concluded from the plot, the first point shows that as  $\beta$  increases the value of also  $O1$  increases, and the second, that the values of  $O1$  are much more sensitive to  $\beta$  rather than  $C$ . The zero contour represents the condition where  $T^*=T$ .

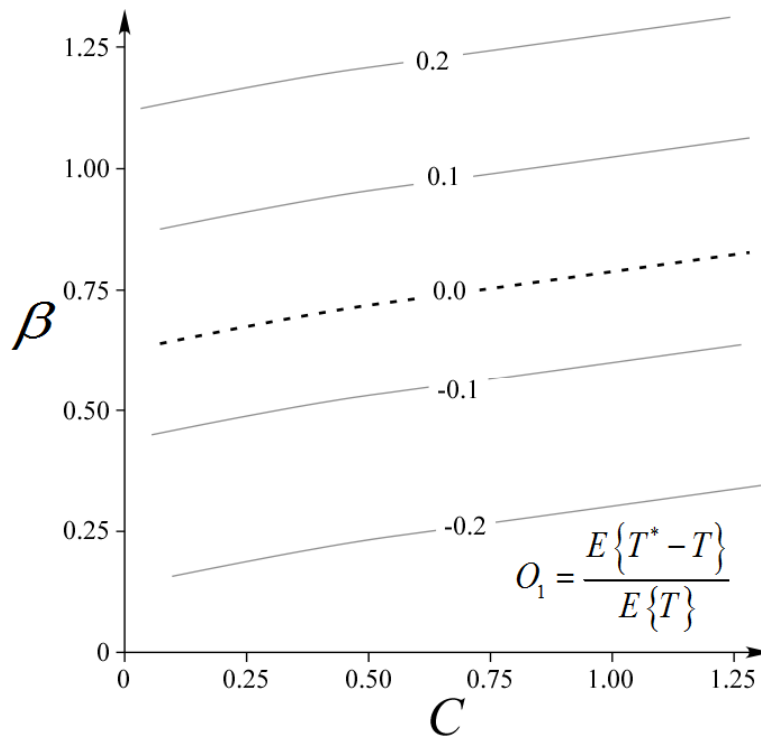


**Figure 3-19:** Contour plot depicting the relationship of  $O1$  to  $C$  and  $\beta$  .

The objective function  $O2$  is a measure of closeness of one estimate to another or the precision or fairness of an estimate. It is the sum of the difference between the number of times the estimate,  $P^*$ , falls within a defined probability interval,  $P_i$ , and the expected times it should fall within that interval. There are two varieties of the  $O2$  objective function,  $O2a$  and  $O2b$ .  $O2a$  is the squared difference, written as;

$$O2a = \frac{\sum_{i=1}^{n_p} (P_i^* - P_i)^2}{\sum_{i=1}^{n_p} P_i^2} \quad (3.13)$$

The second variety,  $O2b$ , is the non-squared version of  $O2a$  and can take a positive or negative value.

$$O2b = \frac{\sum_{i=1}^{n_p} (P_i^* - P_i)}{\sum_{i=1}^{n_p} P_i} \quad (3.14)$$

When  $O2b > 0$ , on average,  $P^*$  will be  $> P_i$  thus overestimating the tonnage, Figure 3-17B. The result is accurate, but too precise, suggesting the uncertainty bandwidth is too narrow. When  $O2b < 0$ , on average  $P^*$  will be  $< P_i$  thus underestimating tonnage, Figure 3-17C. Calculating  $O1$  for a different combinations of  $C$  and  $\beta$  produces the plot shown in Figure 3-20. Two points can be taken from the plot, (1) shows that  $O2b$  is not monotonic as  $\beta$  increases. For small  $\beta$  is increasing, at some point,  $O2b$  reaches its peak and begins decreasing as  $\beta$  continues to increase, (2) a single value of  $C$  can have multiple points where the  $O2b$  function is zero. The zero contour represents the point where  $P^* = P_i$ .

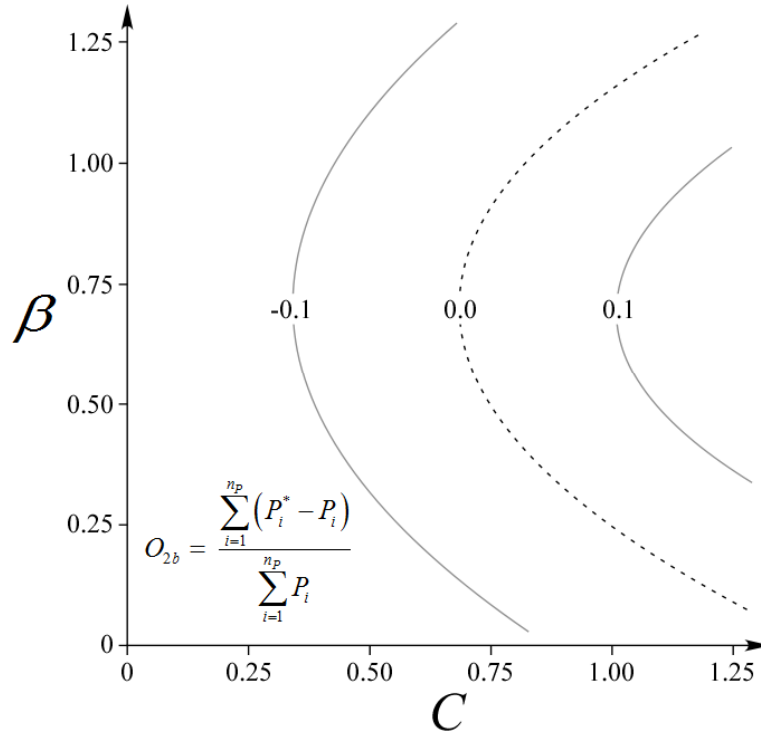


**Figure 3-20:** Contour plot depicting the relationship of  $O_{2b}$  to  $C$  and  $\beta$ .

Unbiased and fair estimates of tonnage can be produced by setting both objective functions,  $O_1$  and  $O_2$ , to zero. Presented in Figure 3-21 is a plot with  $O_{2b}$  superimposed on  $O_1$ . The location where the zero contours for  $O_1$  and  $O_{2b}$  intersect provide a unique solution and optimal values for both  $\beta$  and  $C$ .

If the objective function  $O_1$  is not zero, that is to say,

$$O_1 = \frac{E\{T^* - T\}}{E\{T\}} \neq 0 \quad (3.15)$$

then the methodology becomes unstable and attempts to calculate the  $O_{2a}$  and  $O_{2b}$  will most likely lead to false results. All data that does not fall on (or extremely close to) the line  $O_1 = 0$  must be disregarded.

Also, that the uncertainty is a strong function of  $\beta$  suggesting that small changes in  $\beta$  have a large effect on  $O_{2b}$ .

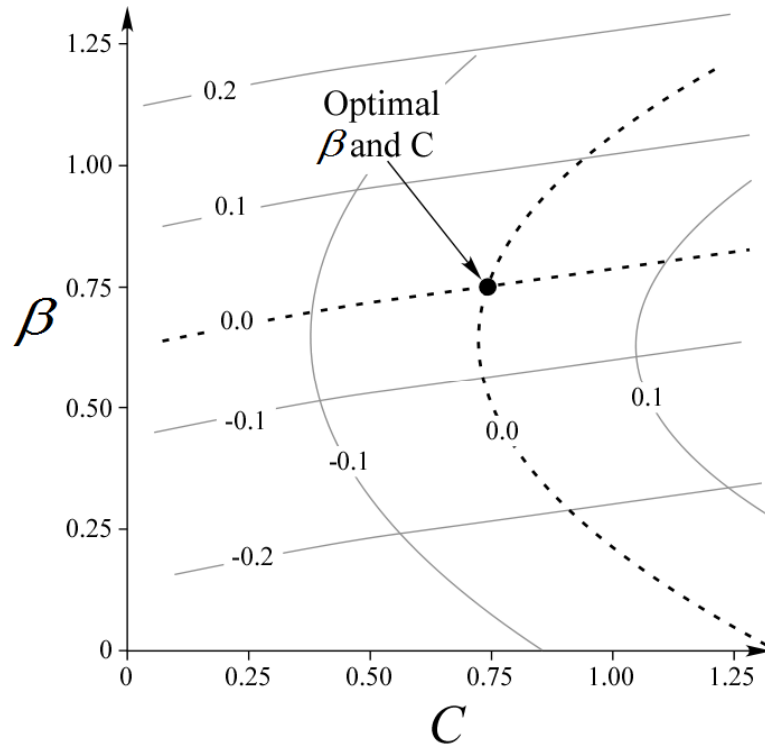


**Figure 3-21:** Optimization of  $C$  and  $\beta$ .

### 3.5.2 Parameter Optimization

Parameterization (the choice of  $\beta$  and  $C$ ) can be subdivided into three categories representing the degree of accuracy required versus the amount of time desired. The categories are (1) empirical selection, (2) light calibration and (3), full calibration.

#### 3.5.2.1 Empirical Selection

Empirical selection refers to the application of  $\beta$  and  $C$  based on the guidelines discussed in Section 3.3 previously in this chapter.

#### 3.5.2.2 Light Calibration

In a light calibration scenario, the interpolated models are compared to a single solid model (wireframe) representation of the orebody. A  $C$  value is chosen based on the interpretation of representative sections and the expert judgement of the

person(s) doing the modeling. The value of  $C$  is chosen so that a reasonable range of uncertainty is produced.

Once a reasonable value for  $C$  is chosen,  $\beta$  is modified until the  $p_{50}$  value of the interpolated model coincides with the tonnage of the constructed solid model.

### 3.5.2.3 Full Calibration

In a full calibration scenario, multiple wireframe solid models are needed to be constructed that will be used as the reference models. For each reference model an optimization program is used to calculate the optimal  $\beta/C$  combination that provides an unbiased and fair estimate of uncertainty. A single run requires the interpolation of all reference models using a single  $\beta/C$  combination. To calculate the optimal  $\beta/C$  combination under full calibration requires multiple iterations using different  $\beta/C$  combinations. The research completed during this thesis has determined the average number of iterations needed for full calibration is between 9 and 12. If the input parameters and reference models are not sensitive to changes in  $\beta$  and  $C$  it is possible that a full calibration could be completed in a minimum of 7 runs, however, as sensitivity to changes increases, the number of runs required to produce an optimal  $\beta/C$  combination will also increase. Because each iteration includes full interpolation of each model, full calibration requires considerable CPU time and increases with the size and number of models used.

### 3.5.3 Search Strategy C/Beta Space

A FORTRAN program *optdf.exe* was written for full optimization. The program searches the  $C$  and  $\beta$  space as defined by the user. The program reads a parameter file, (see Appendix A), that passes the minimum and maximum values for  $C$  and  $\beta$ . These values create a bounding box within which the optimization takes place, Figure 3-22: Initial four points used in Full Optimization of  $C$  and  $\beta$ . Starting with the minimum values  $(C_{\min}, \beta_{\min})$ , each reference model is interpolated using the values  $C_{\min}$  and  $\beta_{\min}$ . The values of the objective functions  $O1$  and

$O2b$  are calculated using the current values of  $C/\beta$  and the program moves to the next  $C/\beta$  combination,  $(C_{\min}, \beta_{\max})$ , and the process repeats.

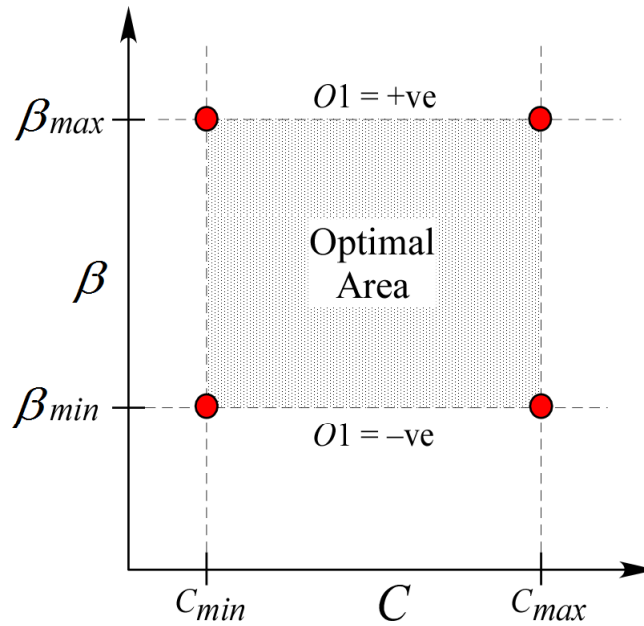


**Figure 3-22:** Initial four points used in Full Optimization of  $C$  and  $\beta$ .

Using the objective functions calculated at  $\beta_{\min}$  and  $\beta_{\max}$ , the value,  $\beta_A$ , the  $\beta$  value where the objective function  $O1 = 0$  is extrapolated and the complete set of reference models are recalculated using the  $C/\beta$  combination  $C_{\min}, \beta_A$ , Figure 3-23. This method requires that the initial selection of  $\beta_{\min}$  and  $\beta_{\max}$  be chosen so that the calculated objective function  $O1$  at each location,  $\beta_{\min}$  and  $\beta_{\max}$  will have a different sign. If they do not the optimization program terminates.

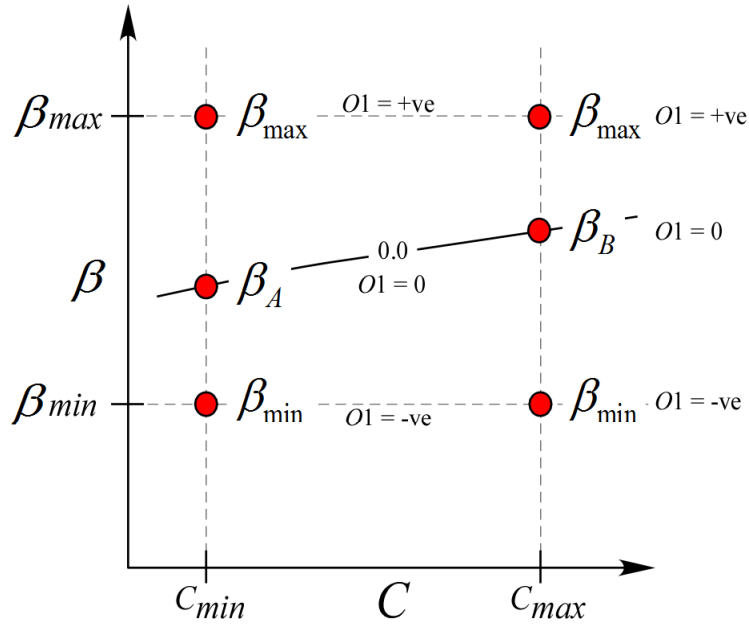


**Figure 3-23:** Full Optimization  $O1$

The process is repeated at  $C_{max}$  and the corresponding value of  $\beta$  where the objective function  $O1=0$  is calculated,  $\beta_B$ , Figure 3-23. At this stage in the optimization process we have completed six complete runs, corresponding to each point in Figure 3-23 interpolating the complete set of reference models.

The next process in full optimization is to find the point on the  $O1=0$  contour shown in Figure 3-23, where objective function  $O2b$  is also equal to zero. Recall that the objective function  $O2b$  is also calculated at  $\beta_A$  and  $\beta_B$ . The process begins by extrapolating the likely position along  $O1=0$  where  $O2b=0$  using the values of  $\beta_A$  and  $\beta_B$  as end members, Figure 3-24. For this example assume that the

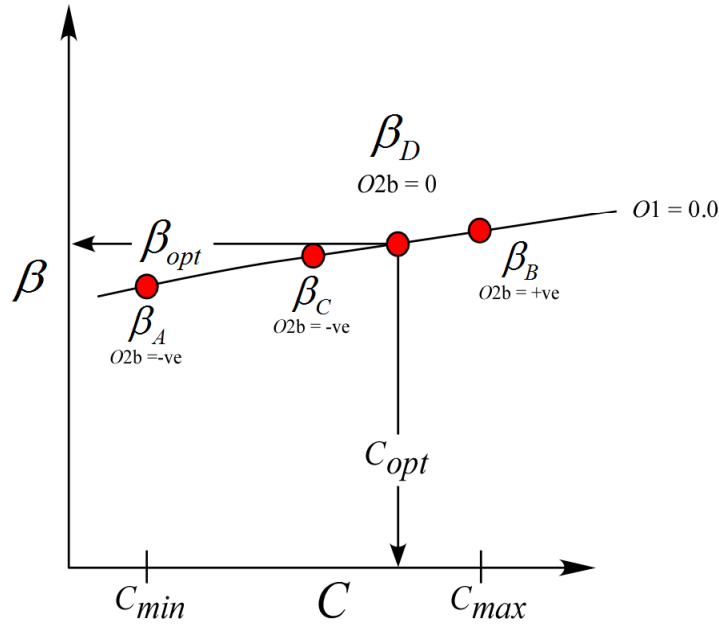


Figure 3-24: Full Optimization  $O2b$

combination of parameters,  $C_{min}$  and  $C_{max}$ , have the necessary requirement that the calculated values of objective function  $O2b$  at  $\beta_A$  and  $\beta_B$  have different signs. If they do not, then additional runs are needed until this requirement is met. Therefore, it is essential that the minimum and maximum values for  $C$  and  $\beta$  are carefully chosen to prevent unnecessary runs. The process begins by selecting the midpoint between  $\beta_A$  and  $\beta_B$  which lies on the zero contour,  $\beta_C$ . The values of  $C$  and  $\beta$  are calculated at  $\beta_C$  and used to re-interpolate the set of reference models. The Objective function  $O2b$  is calculated and depending on its value another point along the line is chosen and the process repeated. If the points are close enough and the relationship is close to linear, finding the position on the line where  $O2b = 0$  can be reasonably found. Referring to Figure 3-24, if the value of  $O2b$  at  $\beta_C$  is found to be negative, we know that the location of  $O2b=0$  lies to the right. We can extrapolate where the location of  $O2b=0$  is and re-interpolate the models and recalculate the objective function. If the objective functions are zero, within a tolerance, then the optimal values for  $C$  and  $\beta$  are reported, otherwise the process is repeated until the point where  $O2b$  on the  $O1=0$  contour is found.

The final step is calculating indicator models for selected p-intervals. A FORTRAN program *clipdf* was written to calculate the indicator models. The intervals usually chosen are the p10, p50, and p90. Calculating the indicator models is not a particularly CPU intensive operation however, the program *clipdf* has an option to produce a summary output file of the volume and tonnage for the 99 percentiles. This operation is CPU intensive requiring 99 loops through the model, one for each percentile. An option to skip the summary output was put in place if the summary is not required.

## 3.6 Implementation Considerations

### 3.6.1 Computational considerations

The time required for an operation depends on the level of calibration desired. At the lowest level, values for  $C$  and  $\beta$  are chosen and a model created. The time required for this level is determined by the size of model. A model with 4.8 million cells was completed in 40 minutes on a 3Ghz Pentium IV with 1Gb of random access memory.

If a more detailed calibration is considered then multiple models can be created using a single wireframe as a reference model. In this situation a single value of  $C$  is provided and models created for different levels of  $\beta$  until a model is produced in which the p50 tonnage matches that of the wireframe. The model will have a level of uncertainty defined by  $C$ . The time consuming part is the creation of multiple models.

Full calibration requires multiple reference models. Recall from Section 3.5.3 that full optimization requires a minimum of eight combinations of  $C$  and  $\beta$ . These eight combinations are run for each reference model. The primary issue with the full optimization method is time. The most time consuming process is the kriging. The test case presented here required about three hours per run, or about 30 hours in total. The computer used was a 3 GHz Pentium 4 with 1Gb of ram. There were 50 reference models kriged in each run for a total of 500 kriging runs. Each 3D

grid had a total of 800,000 cells. Changing the drill spacing or model size will have a significant impact on the time needed to carry out a similar optimization.

Significant time could be saved by reducing the number of models needed to produce a stable result. Initial indications suggest that the total number could be reduced by half to 25 as shown in Figure 3-25 which plots the cumulative value of  $O_2$  with increasing number of reference models. The graph shows the value of  $O_2$  becoming stable after about 25 reference models. The time reported here used a kriging optimization method not discussed. The technique places a bounding box around the complete orebody and instructs the kriging program to skip any cells located outside the limits of the box. More effective methods could be developed to improve efficiency. The speed of the optimization program itself could be improved through a redesign of the algorithm and improvements in the source code.

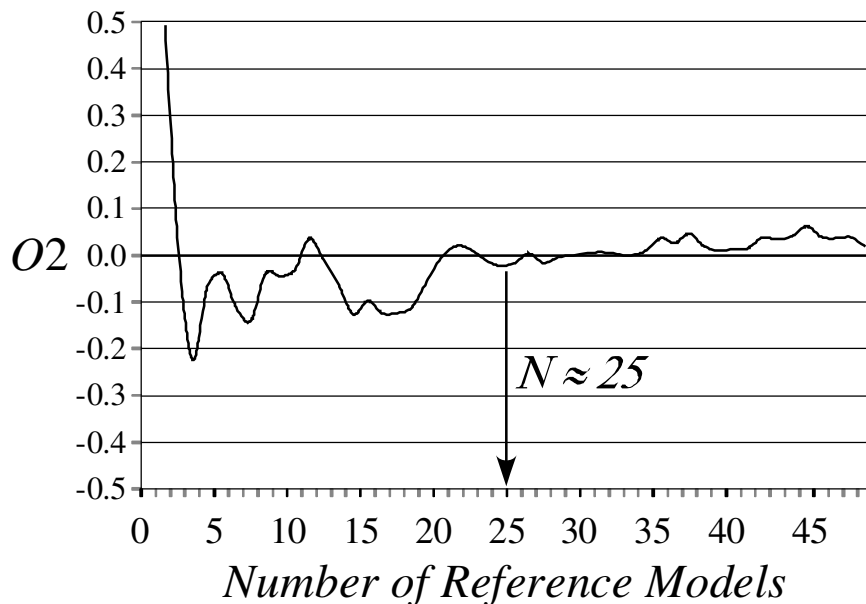
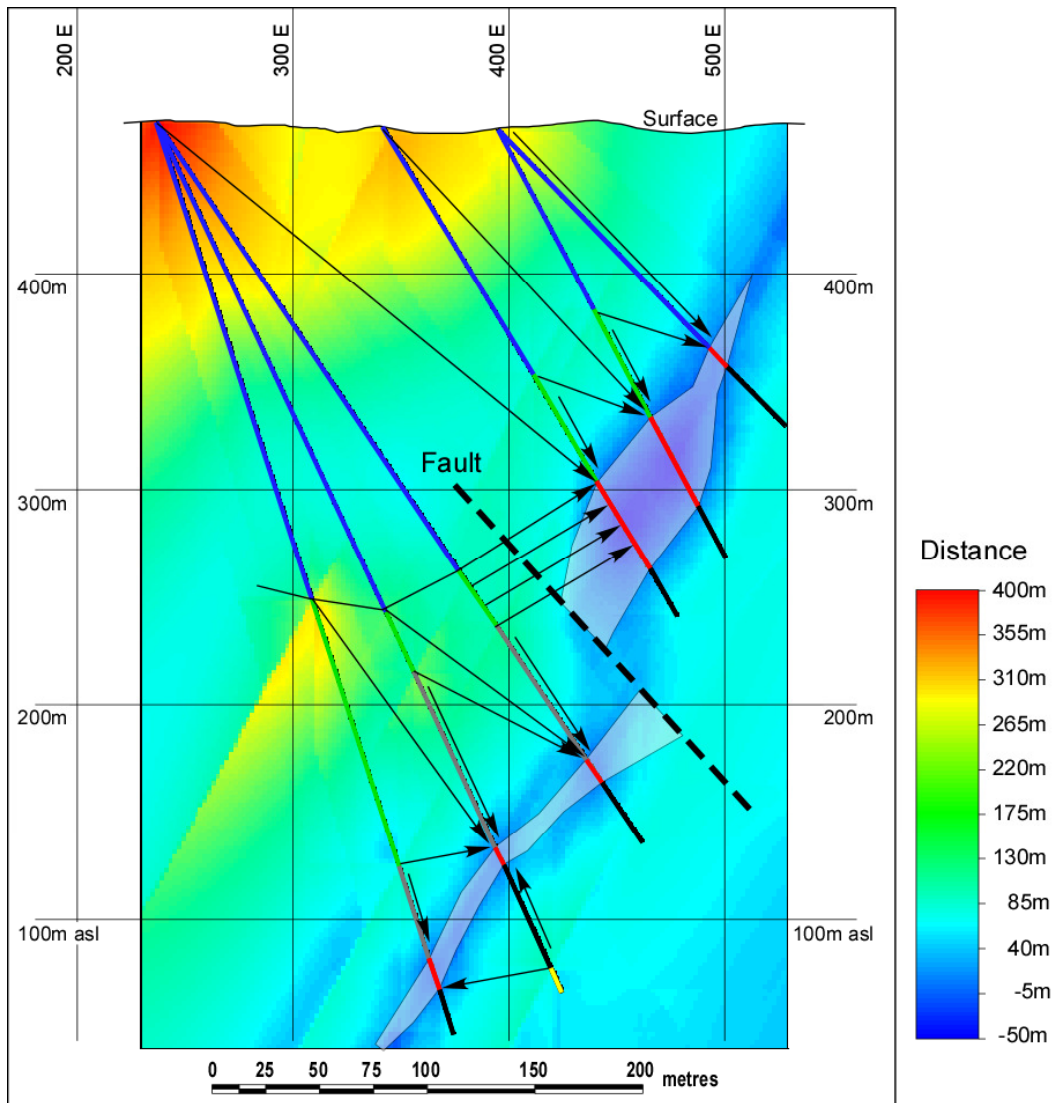


Figure 3-25: Plot of  $O_2$  versus number of reference models interpreted.

### 3.6.2 Practical Considerations

Practical considerations include data configuration and geological considerations.



**Figure 3-26:** Vertical cross section example. Arrows point to the closest sample used in calculation of the DF. Colored background represents a 2D model of the DF. Hotter colors are farther away from the vein. Cold colors (Darker blues) are closer to, or located inside vein. Note that in some instances the pairs cross structural boundaries. Also inclined holes and an inclined deposit can cause artefacts.

Consider the example in Figure 3-26. The illustration shows inclined holes and a narrow inclined orebody. The upper three holes are separated from the lower three holes by a fault. The arrows point to the contacts used to calculate the DF and cause a number of artefacts. The presence of geological structures also plays an important part. Structures such as faults, the dashed line in Figure 3-26, are hard

boundaries. The DF has no knowledge of these structures and could produce undesirable results, Figure 3-27.

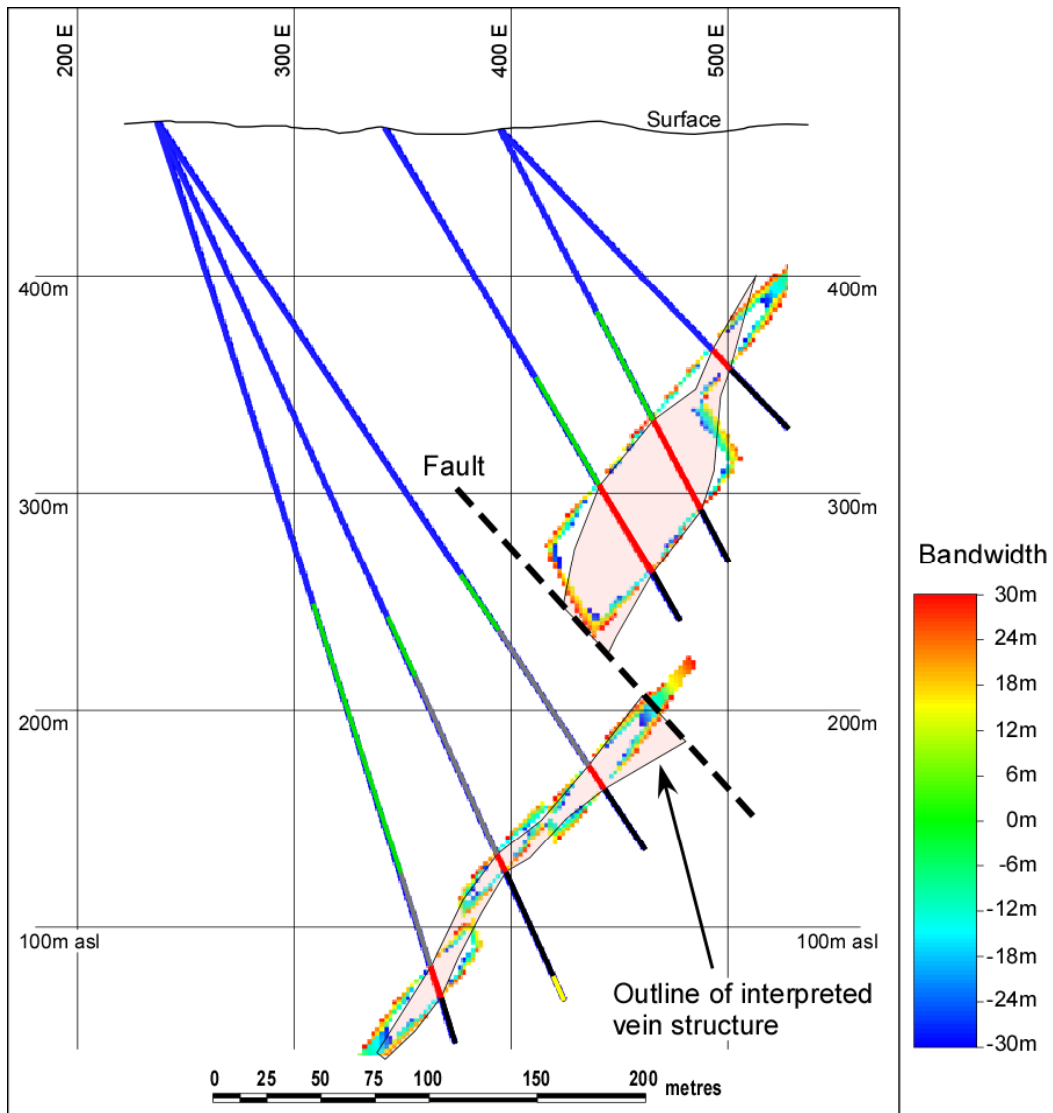


**Figure 3-27:** Modeled and clipped DF shown crossing an interpreted fault (Dashed Line) on the lower three holes. However on the upper three holes the DF terminates before the fault due to the absence of vein down dip. Outline of wireframe vein shown for reference.

# Chapter 4

## Synthetic Examples

Chapter 4 discusses the application of the methodology presented in Chapter 2 to a set of synthetic orebodies. Beginning with a brief introduction to the processes used to generate the synthetic reference orebodies. Section 4.2, will also describe the methodology used to sample and interpolate the orebodies. Section 4.3 presents application and calibration of the parameters. Section 4.4 concludes with a discussion on the accuracy and fairness of the results

### 4.1 Simulation and the Reference Models

A set of synthetic orebodies forms the basis for the method. The orebodies are created using Sequential Gaussian Simulation (SGS). SGS takes a random path through the model assigning a value at every location until every cell in the model has been visited. As part of the process, every newly estimated cell is added to the dataset and used for subsequent cells.

#### 4.1.1 Creating the Reference Models

The idea of using SGS to create synthetic orebodies is straightforward. Create two SGS generated realizations, one unconditionally simulated, the other conditioned to data, and add them together to produce a closed 3D object with finite volume and an adequate thickness, see Figure 4-1. The modifications applied to the realizations are used to locate and add some definition to the surfaces. The first surface created is an unconditionally simulated surface. The realizations are relatively flat. By using a multiplier we can add some vertical exaggeration to the realization. The unconditional simulation was multiplied by a value of 10.

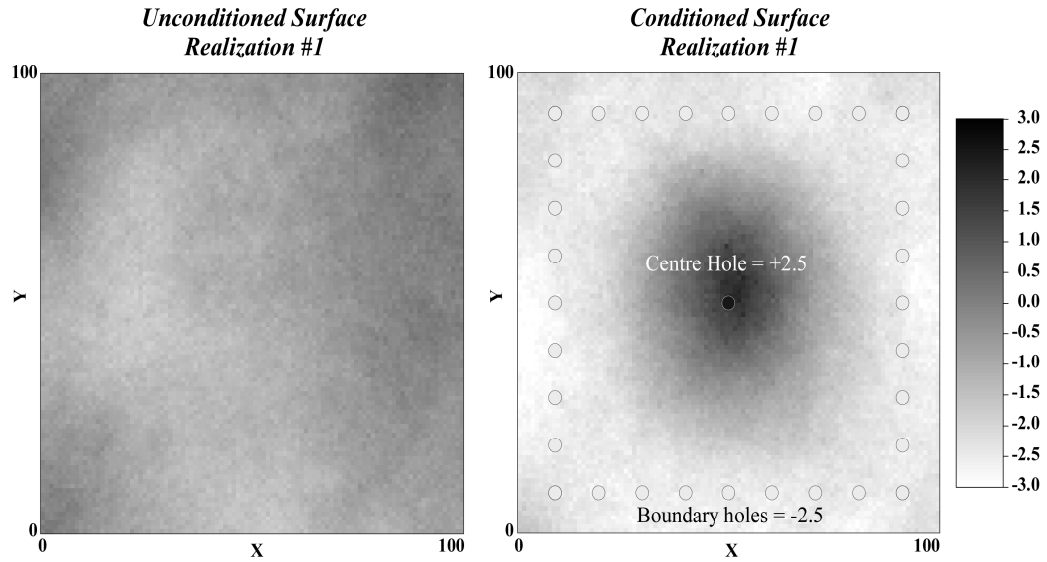


**Figure 4-1:** (left) unmodified unconditioned 2d surface, (right) unmodified data conditioned 2d surface showing location of conditioning data.

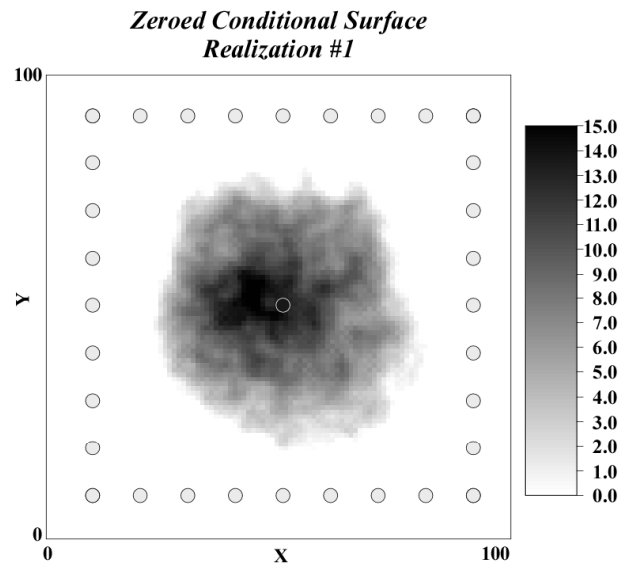


**Figure 4-2:** Modified conditional 2d surface, zeroed so outer fringes of area equal zero.

The realizations are translated to remove negative elevations. To locate the surface, each cell in the grid has 100 added to the cell value so that the surface is “centered” on the 100 elevation. The modified surface for realization 1 is shown in Figure 4-3 left.

The second SGS surface, Figure 4-1 right, shows the conditioned realization. This realization is conditioned to a data set consisting of a bordering ring of negative values (-2.5) and one central point (+2.5) as shown in the figure. This will ensure that the data is positive in the centre and negative along the periphery. As for the previous realization, we multiply by a constant to provide more relief to the realization than that of the standard normal distribution used in SGS. For this realization a multiplicative constant of 5 was used. Since the realization is conditioned to data with the range -2.5 to +2.5, the smaller constant of 5 was chosen because it is half of what was used for the unconditioned surface. An additive constant of 2 was used with this realization. It was not the intention to fully remove negative values from this realization. Since this realization will be added to the unconditional surface and there is the desire to have a closed geometric object we can use the negative values create the intersection between the two surfaces. Consider the nature of the conditioning data. A central “high” point and a ring of low points around the perimeter, this will cause SGS realizations to have high values in the centre becoming increasingly smaller toward the edges at some point becoming all negative. If we reset all the negative values to zero, we are left with a realization, Figure 4-2, which can be described as a dome sitting on a plane of zeros. If we add this realization to the unconditioned surface we will create a new surface that contains the same values of the unconditional surface around the edges, (unconditional + 0), and the value of the unconditional surface plus the conditional surface towards the centre, (unconditional + conditional). The result is two surfaces, Figure 4-3, coincident at the margins becoming separated towards the centre. The separation between the two surfaces is the thickness of the vein deposit and can be seen in the XZ cross section through the centre of the two surfaces, Figure 4-4.

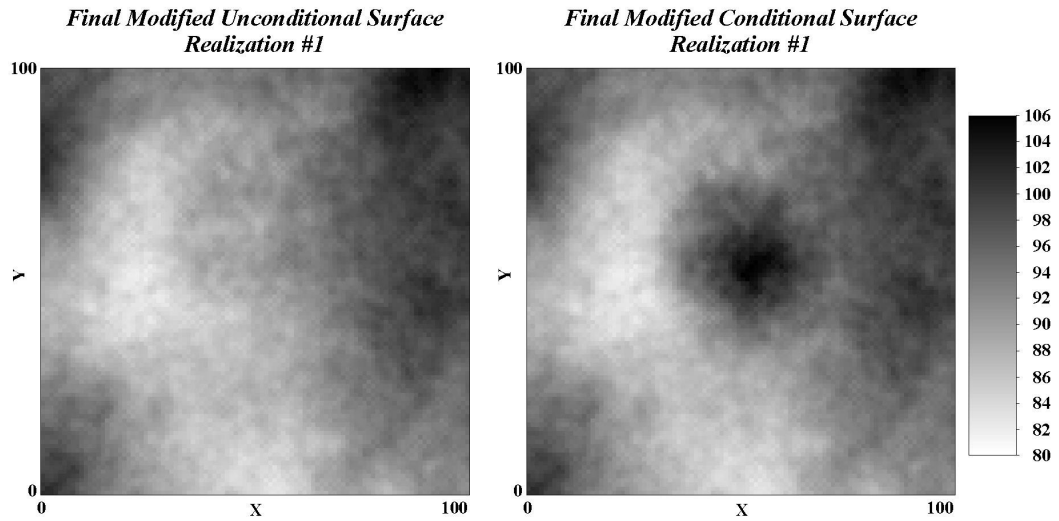


**Figure 4-3:** (left) Modified final conditional 2d surface, zeroed so outer fringes of area equal zero.

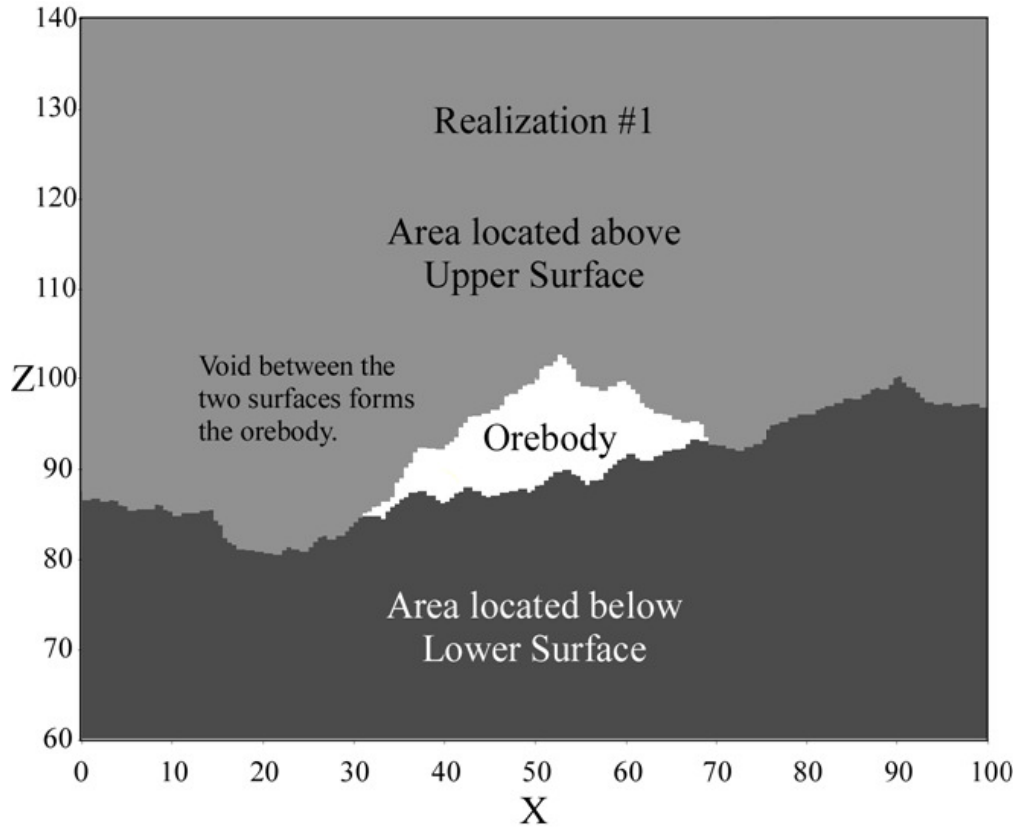


**Figure 4-4:** XZ Cross section through modified conditional and unconditional surfaces

The modification of the initial unconditional and conditional realizations created by the GSLIB program *sgsim.exe*, were done using the program *emode.exe*. This

program reads in a parameter file containing the names of the SGS realization files, the output modified realization files, and the multiplication and addition factors to be used for manipulation. The program also contains a smoothing subroutine to smooth out some of the short scale variations in the realizations. See Appendix A for an example of the *emode* parameter file.

#### 4.1.2 Smoothing

The modified SGS realizations have some erratic and unrealistic features as depicted by the top example in Figure 4-5. A smoothing algorithm was developed based on a 5 point moving average which arithmetically averages the four adjacent cells and the current cell as shown in the schematic in Figure 4-6.

The newly calculated cells are written to a separate file and not used in further averaging operations. To avoid any negative impact caused by using averaged values and original values together. The result of the smoothing is shown in the illustration at the bottom of Figure 4-5.

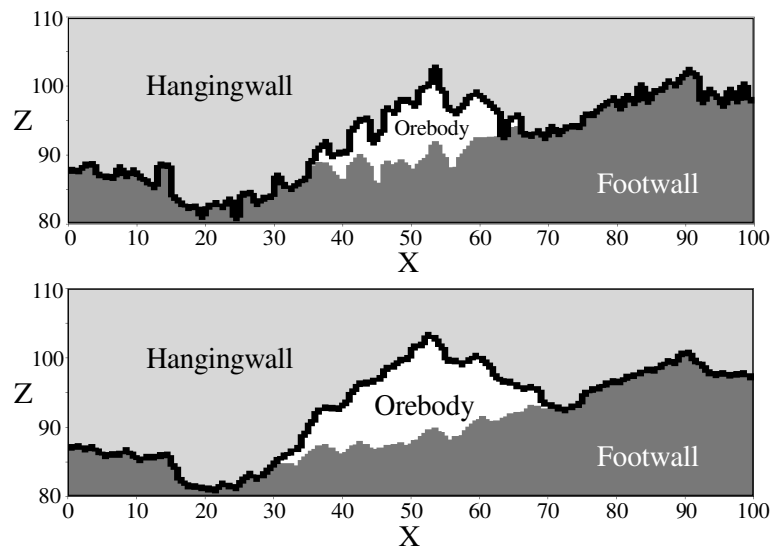


**Figure 4-5:** (top) Modified SGS surfaces without smoothing; (bottom) Modified surfaces using smoothing



sions along with the model top and bottom. The output file contains the *xyz* coordinates of the sample location, the elevations of the upper contact,  $Z_u$ , and the lower contact,  $Z_l$ , an indicator  $VI$  for holding the vein indicator value and a drill-hole identification number. An example of *drill5.exe* output is shown in Figure 4-7. The drillholes can be discretized to any value by specifying a  $z_{min}$  and  $z_{size}$  in surface grid parameter section of the parameter file. Since the surface grids are 2D, the  $z$  components are not used and can be changed, however, the number of levels must remain as 1.

At each location visited, the program queries the elevation of each of the surfaces. The elevations are stored as the upper elevation,  $Z_u$ , and the lower elevation,  $Z_l$  for that location. The program then checks the value of  $z$  and if  $z < Z_l$  or  $z > Z_u$ , that is, located below the lower surface or above the upper surface, the sample gets assigned a value of 0 and denotes the sample is located in non-vein. If the sample is located between  $Z_l$  and  $Z_u$ , it gets assigned a value of 1 signalling the presence of vein. See Appendix A for an example of the *drill5* parameter file.

#### **4.2.1.1 Drillhole Spacing**

Drill spacing is generally regarded as the average spacing between drillholes contained in a drillhole sample set. In the methodology presented here, drill spacing is used as the basis for defining the uncertainty constant  $C$ . The actual value of the uncertainty constant used in the DF calculation is not  $C$  but rather the specified drill spacing multiplied by  $C$ . For instance, consider the case where two orebodies with different dimensions are drilled using a rectangular grid of the same dimensions as the orebody. Each grid uses the same number of holes. The drill density would be the same regardless of the actual distance between holes. By standardizing the average drillhole spacing to  $C$  we can remove the physical dimension from the distance function equation. This has the benefit of having the exact same limits,  $[0,1]$  for  $C$  regardless of drill spacing. Therefore, specifying a  $C$  value of  $\frac{1}{2}$  has the same connotation regardless of project and means the same,  $\frac{1}{2}$  the effective drill spacing.

```

DH for Realization      1
7
x
y
zmin
Zu
Zl
VI
BHID
50.00   50.00  139.00  104.50   89.60   0   41
50.00   50.00  138.00  104.50   89.60   0   41
.....
50.00   50.00  106.00  104.50   89.60   0   41
50.00   50.00  105.00  104.50   89.60   0   41
50.00   50.00  104.00  104.50   89.60   1   41
50.00   50.00  103.00  104.50   89.60   1   41
50.00   50.00  102.00  104.50   89.60   1   41
50.00   50.00  101.00  104.50   89.60   1   41
50.00   50.00  100.00  104.50   89.60   1   41
50.00   50.00   99.00  104.50   89.60   1   41
50.00   50.00   98.00  104.50   89.60   1   41
50.00   50.00   97.00  104.50   89.60   1   41
50.00   50.00   96.00  104.50   89.60   1   41
50.00   50.00   95.00  104.50   89.60   1   41
50.00   50.00   94.00  104.50   89.60   1   41
50.00   50.00   93.00  104.50   89.60   1   41
50.00   50.00   92.00  104.50   89.60   1   41
50.00   50.00   91.00  104.50   89.60   1   41
50.00   50.00   90.00  104.50   89.60   1   41
50.00   50.00   89.00  104.50   89.60   0   41
.....
50.00   50.00   64.00  104.50   89.60   0   41
50.00   50.00   63.00  104.50   89.60   0   41
50.00   50.00   62.00  104.50   89.60   0   41
50.00   50.00   61.00  104.50   89.60   0   41
.....
.....
.....

```

**Figure 4-7:** Drill5.exe output example. The hole is located at the centre of the 100x100 surface grid, (50, 50). The upper surface is at 104.5 and the lower surface at 89.6. The Hole number is 41. If the sample elevation  $z$ , third column, is between  $Zu$  and  $Zl$ ,  $VI=1$ .

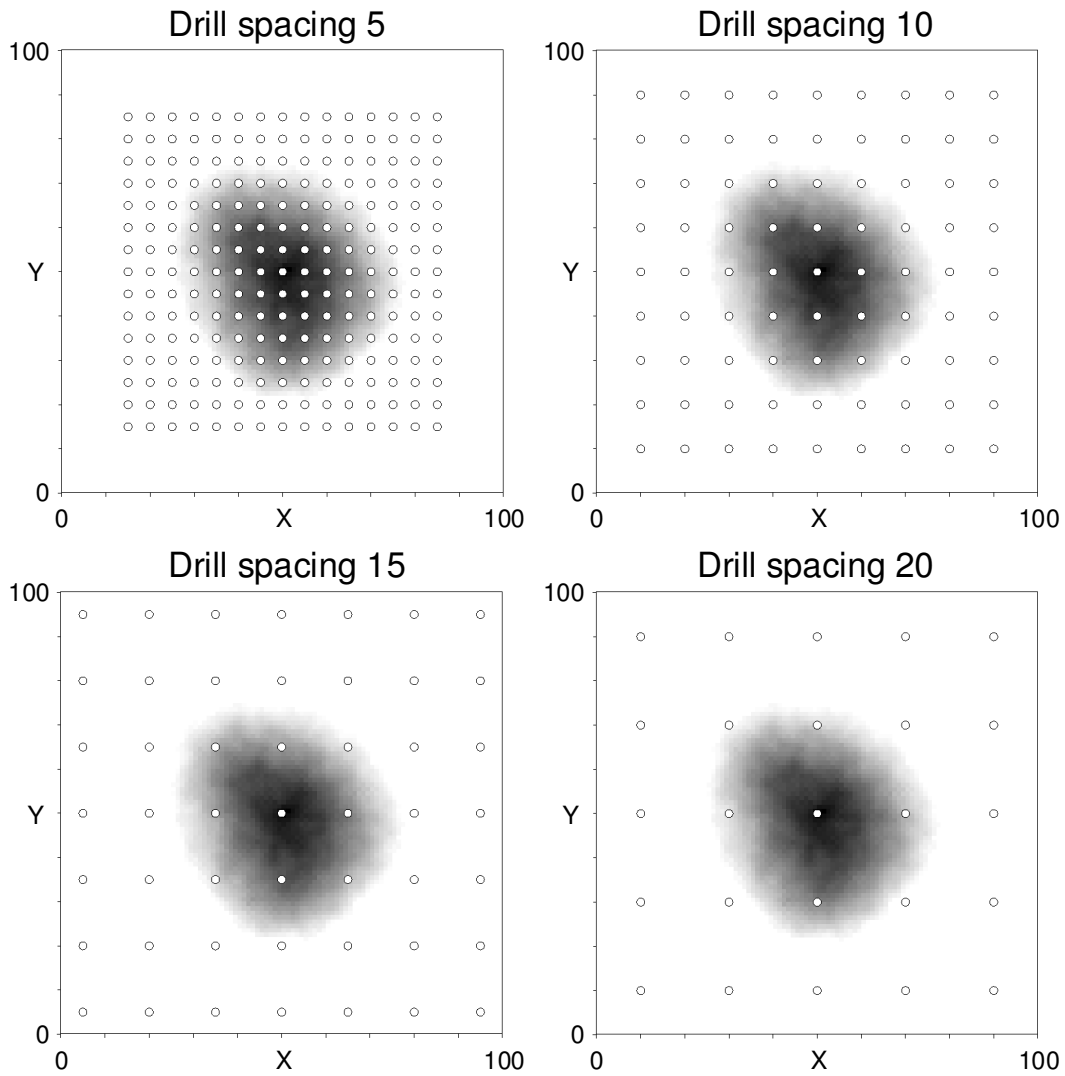


**Figure 4-8:** Drill spacing shown superimposed on Realization #1. Spacings are relative to deposit size

Each of the simulated orebody has a somewhat circular shape with an average areal extend of 48x48 units. The drill spacing considered for this study is shown in Table 4-1, and is not that different from the spacing one would find in actual drilling programs of this scope.

**Table 4-1:** Comparison of methodology drill spacing to those found in real world.

Simulated Orebody			Actual Example		
Spacing	Strike	%	Spacing	Strike	%
Units	Length	Size	Metres	Length	Size
5	48	10%	20	200	10%
10	48	21%	40	200	20%
15	48	31%	60	200	30%
20	48	42%	80	200	40%

#### 4.2.2 Application of the Distance Function

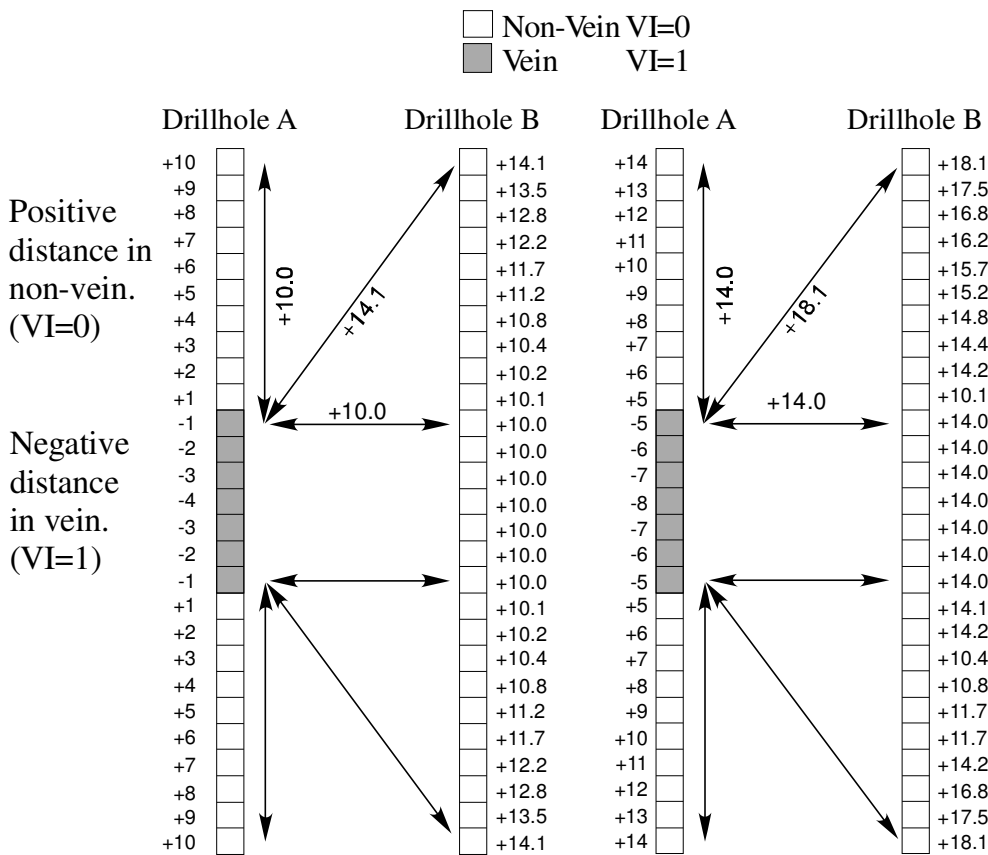
The distance function is applied to drill data using a FORTRAN program called *dfv4.exe*, see Appendix A for details. The program works with any GSLIB formatted program so long as it is formatted correctly which means the first three columns are the *xyz* coordinates of the sample and the eighth column is the indicator VI. The drillhole file can have any orientation. The drillholes do not have to be completely discretized from collar to end-of-hole (EOH), however, there must be sufficient contiguous samples in and around the zone of interest. The DF is calculated based on the anisotropy, discussed separately in Section 3.2.4.5, specified in the parameter file. Anisotropy is specified either through reference to an external file or by parameters set in the DF parameter file itself. The DF program assigns a distance based on three parameters, 1) uncertainty constant  $C$ , 2) beta and 3) the anisotropy.

Recall the unmodified distance function found in 2.15, where  $h_s$ ,  $h_d$  and  $h_t$  are the Euclidean distances between the selected data pairs, and  $V_s$ ,  $V_d$  and  $V_t$  is the associated anisotropy in each direction. The anisotropy is specified in one of two ways, 1) by specifying an anisotropy file in the *dfv4.exe* parameter file, or 2) by specifying the anisotropy factors directly in the *dfv4.exe* parameter file. The anisotropy file is created by the program *anis.exe* which calculates the geometric anisotropy of each realization of the synthetic models and outputs the results to a file. The DF is modified by  $Cp$  and  $\beta$  depending on the value of VI, Equations 4.1 and 4.2.

$$dF_{\text{mod}} = (dF + Cp) / \beta \quad \forall \text{VI}=0 \quad (4.1)$$

$$dF_{\text{mod}} = (dF + Cp) \cdot \beta \quad \forall \text{VI}=1 \quad (4.2)$$

The additive value  $Cp$  is calculated as  $C \cdot DS$  where  $C$  is the uncertainty constant and  $DS$  is the drill spacing specified in the parameter file. The result, distances that are tuned to the geometric anisotropy of the orebody. See Figure 4-9.



Not to Scale

**Distance Function (DF):** Shortest distance between points with *different* Vein Indicators (VI).

**Figure 4-9:** (left) Euclidean distances to samples with different VI values, negative values are VI =1, Positive values are VI=0. (right) Modified distances applied by the DF when  $Cp=4$  and  $\beta=1$ .

### 4.3 Calibration

In section 3.5 the process for full calibration was outlined. The full calibration process was applied using 50 synthetic models described above and the results tabulated for each of the four different drill spacings. The results show that the minimum number of iterations needed to find the optimal values for  $C$  and  $\beta$  varies from eight, for a drill spacing of ten units to eleven for the five and fifteen unit drill spacings.

**Table 4-2:** Full Calibration Results for 5 unit drill spacing

5 Unit Drillhole Spacing

Run	N	C	$\beta$	O1	O2
1	50	0.100	0.900	-0.053	-1.000
2	50	0.100	1.100	0.041	-0.924
3	50	0.100	1.013	0.002	-0.147
4	50	0.300	0.900	-0.052	-0.516
5	50	0.300	1.100	0.035	-0.031
6	50	0.300	1.020	0.001	0.653
7	50	0.250	1.018	0.001	0.573
8	50	0.213	1.017	0.001	0.484
9	50	0.185	1.016	0.001	0.409
10	50	0.164	1.015	0.001	0.298
11	50	0.121	1.014	0.002	0.049

**Table 4-3:** Full Calibration Results for 10 unit drill spacing

10 Unit Drillhole Spacing

Run	N	C	$\beta$	O1	O2
1	50	0.100	1.000	-0.084	-0.689
2	50	0.100	1.200	0.062	-0.671
3	50	0.100	1.115	0.001	-0.382
4	50	0.300	1.000	-0.091	-0.227
5	50	0.300	1.200	0.041	0.227
6	50	0.300	1.138	0.001	0.431
7	50	0.200	1.127	0.001	0.138
8	50	0.173	1.124	0.000	0.000

**Table 4-4:** Full Calibration Results for 15 unit drill spacing

## 15 Unit Drillhole Spacing

Run	N	C	$\beta$	O1	O2
1	50	0.100	1.200	-0.098	-0.587
2	50	0.100	1.400	0.068	-0.493
3	50	0.100	1.318	0.000	-0.316
4	50	0.300	1.200	-0.123	-0.213
5	50	0.300	1.400	0.022	0.391
6	50	0.300	1.370	0.001	0.400
7	50	0.188	1.341	0.000	0.102
8	50	0.200	1.344	0.000	0.156
9	50	0.167	1.335	-0.001	0.018
10	50	0.150	1.331	0.000	-0.036
11	50	0.163	1.334	0.000	0.013

**Table 4-5:** Full Calibration Results for 20 unit drill spacing

## 20 Unit Drillhole Spacing

Run	N	C	$\beta$	O1	O2
1	50	0.100	1.400	-0.074	-0.417
2	50	0.100	1.600	0.087	-0.343
3	50	0.100	1.498	0.007	-0.481
4	50	0.300	1.400	-0.108	0.014
5	50	0.300	1.600	0.033	0.426
6	50	0.300	1.560	0.006	0.421
7	50	0.200	1.529	0.004	0.111
8	50	0.183	1.524	0.005	0.037
9	50	0.150	1.514	0.005	-0.153
10	50	0.181	1.523	0.004	0.028

The full calibration results show that the optimized values of C do not greatly vary for the three larger drill spacings as shown in Figure 4-10 and that the value of  $\beta$  increases as drill spacing increases, Figure 4-11. Subsequent runs using a constant C value of 0.2 for each drill spacing show that the optimized values of  $\beta$  are not highly sensitive to C as also seen in Figure 4-11. This also suggests that selecting a value of C for partial calibration between 0.15 and 0.2 is appropriate.

### Optimized C Values vs. Drillspacing

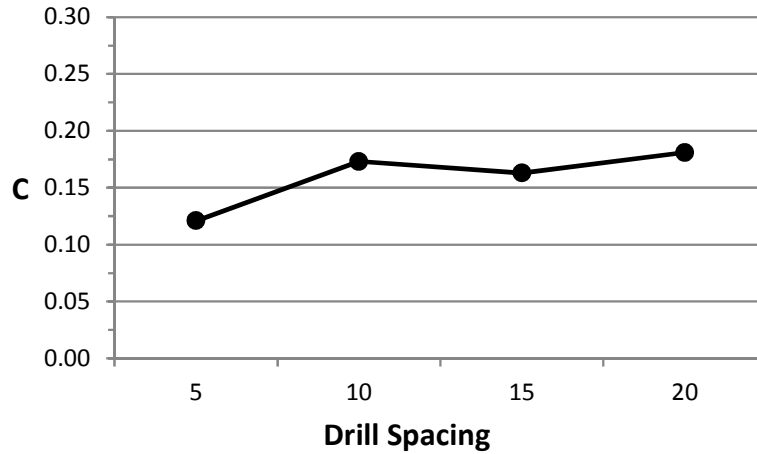


Figure 4-10 : Optimized values of C versus drill spacing

### Optimized Beta Values vs. Drillspacing

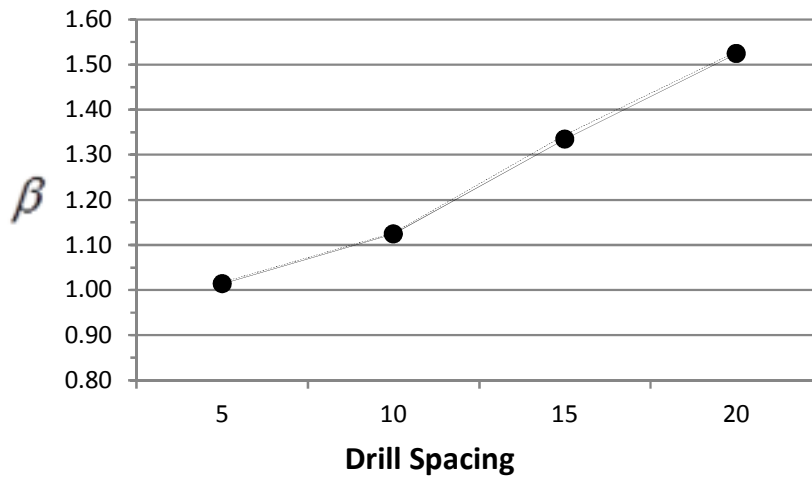


Figure 4-11 : Optimized values of  $\beta$  versus drill spacing (solid line); Values of  $\beta$  for a constant value of  $C = 0.2$  for each drill spacing.(dashed line)

## 4.4 Uncertainty Results

Results are shown for four different drill spacings. Spacings can be converted to real world terms. Based on the average size of the reference models, 48x48 units, a 5 unit spacing represents an orebody drilled on ~10% of its strike length, 10 unit spacing represents an orebody drilled on ~20% of its strike length, 15 unit spacing represents an orebody drilled on ~15% of its strike length, and finally a 20 unit

spacing represents an orebody drilled on ~40% of its strike length. In comparison to real world scenarios, consider an orebody of interest that has a strike length of 200 metres. The drillhole spacing used in the examples translates into drilling the real life orebody on 20, 40, 60 and 80 metre drill spacings. These are all reasonable sized drill spacings in any exploration project. The results show that as the drill spacing increases so does the uncertainty and the spread of points on the accuracy plots. The closer drill spacings of 20 and 40 are most likely too close for grass roots cases but help illustrate the methodology. As drill density increases the amount of uncertainty decreases and most likely the methodology would not be warranted. However, it would provide uncertainty not quantified with deterministic methods and perhaps a half calibration of a deterministic model could be implemented.

#### **4.4.1 Drill Spacing 5**

The 5 unit spacing is the most densely sampled example. The 5x5 grid utilized 225 drillholes incorporating 17,775 samples. The drillhole sample interval is 1 unit. Figure 4-13, Figure 4-14 and Figure 4-15 show accuracy plots for three points on the plot shown in Figure 4-12. Two points are located at the edge of the optimization area, point A corresponding to the  $C_{\min}$  endpoint of the O1 line, and point C, the  $C_{\max}$ , endpoint of the O1 line. A third point B, is the location of the calculated optimal values of C and  $\beta$ . All figures show accuracy plots with a narrow spread of points along the 45° line and within the 5% tolerance limits. This is expected from closely spaced drilling. The precision, shown on the right hand side in the figures show a curved trend for points A and C showing lower precision. The curve is subtle in Figure 4-13 because location A is close to the optimized location C.

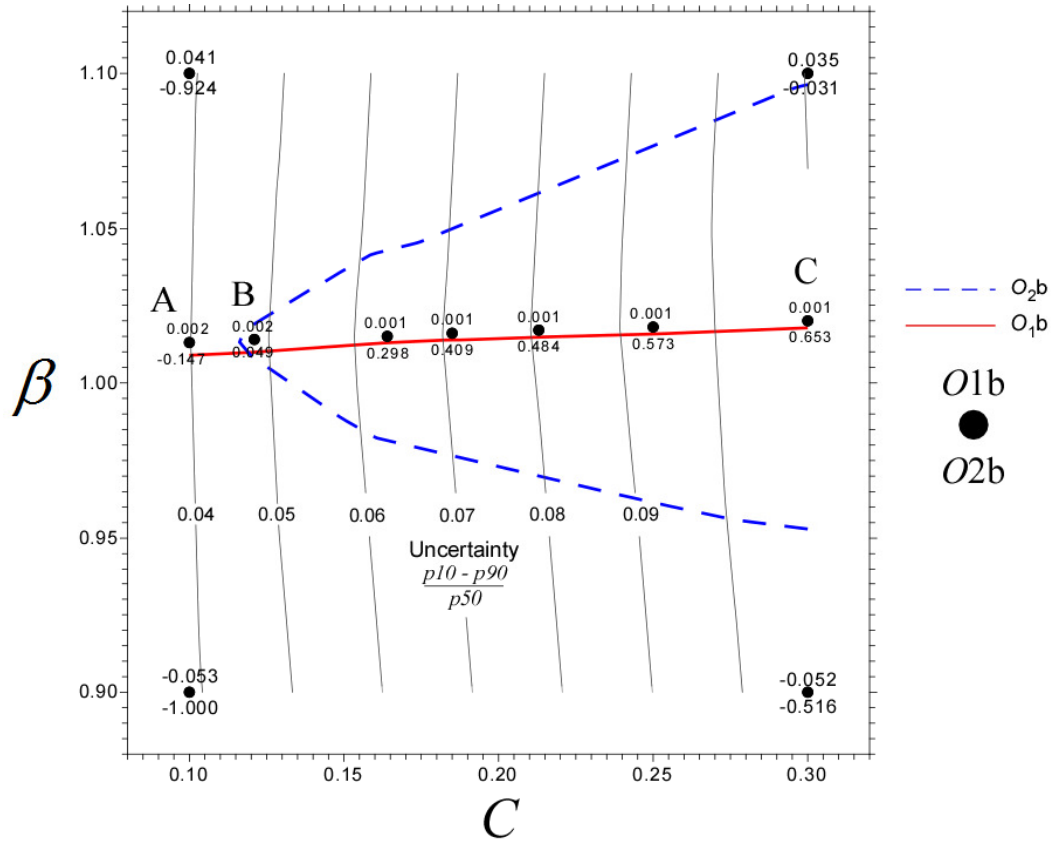


Figure 4-12:  $C/\beta$  space for 5 unit spacing. A)  $C_{\min}$  end member, B)  $C_{\max}$  end member and C) optimal  $C/\beta$ . Letters refer to accuracy plots below. Full set of plots are available in Appendix B.

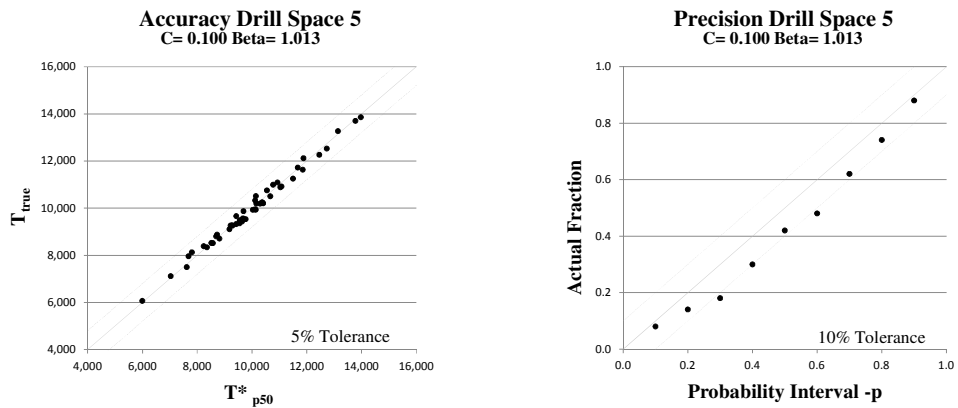


Figure 4-13: Accuracy plot for location A in Figure 4-16

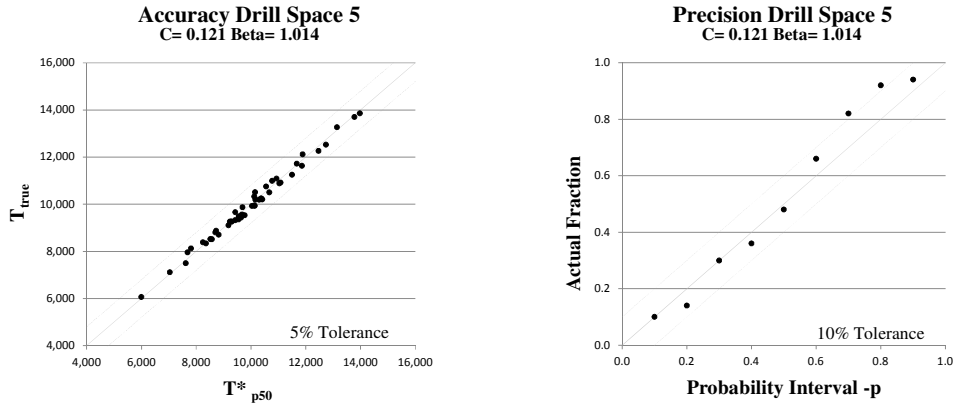


Figure 4-14: Accuracy plot for location B in Figure 4-16

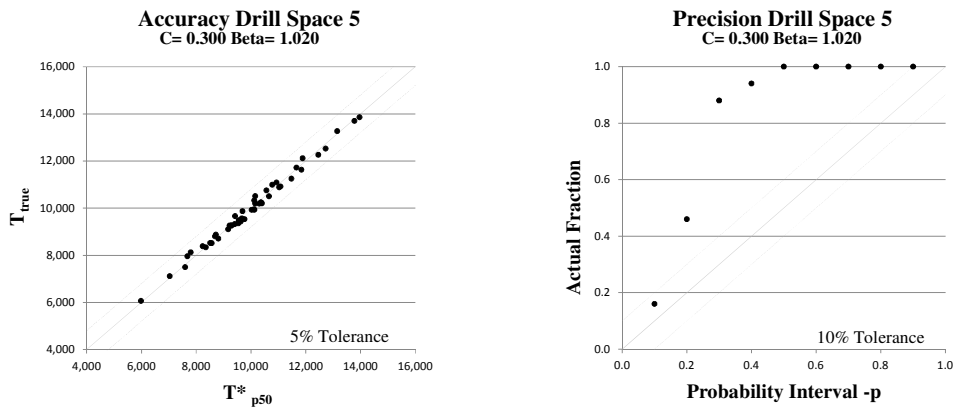
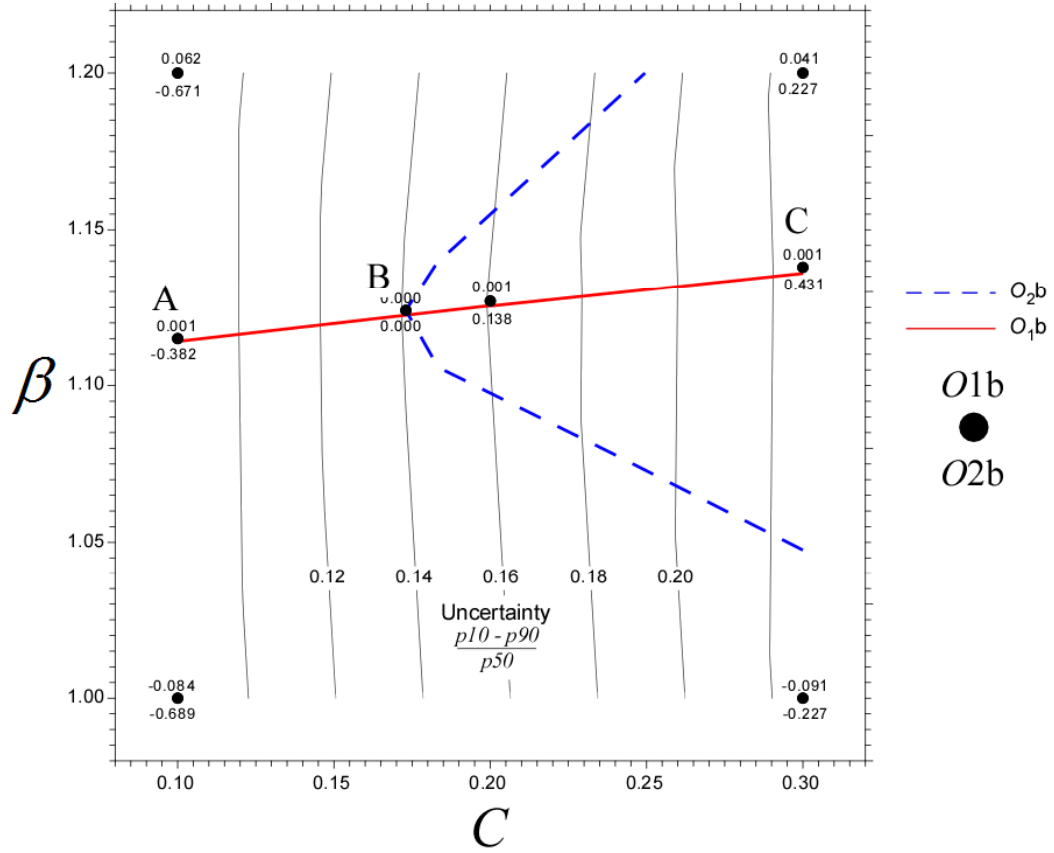


Figure 4-15: Accuracy plot for location C in Figure 4-16

#### 4.4.2 Drill Spacing 10

The 10 unit spacing represents a drillhole spacing equal to about 20% of the strike length of the orebody. The 10x10 unit example produced 81 drillholes incorporating 6,399 samples at a sample interval of 1 unit. Figure 4-17, Figure 4-18 and Figure 4-19 show accuracy plots for three points on the plot shown in Figure 4-16. The accuracy plots show a wider spread along the 45° line than the 5 unit plots with some, approximately 8%, of the points falling outside the 5% tolerance limits. The precision, shown on the right hand side in the figures show a pronounced curve for both points A and C with most points falling away from the 45° line indicating poor precision. However, the optimized values of C and

$\beta$  show acceptable precision with all points falling inside the tolerance limits and close to the 45° line, see Figure 4-18.



**Figure 4-16:**  $C/\beta$  space for 10 unit spacing. A)  $C_{\min}$  end member, B)  $C_{\max}$  end member and C) optimal  $C/\beta$ . Letters refer to accuracy plots below. Full set of plots are available in Appendix B.

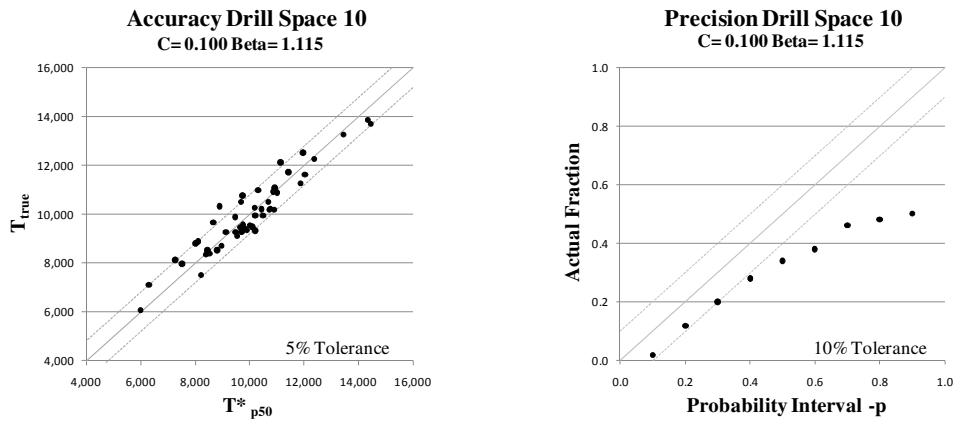


**Figure 4-17:** Accuracy plot for location A in Figure 4-16

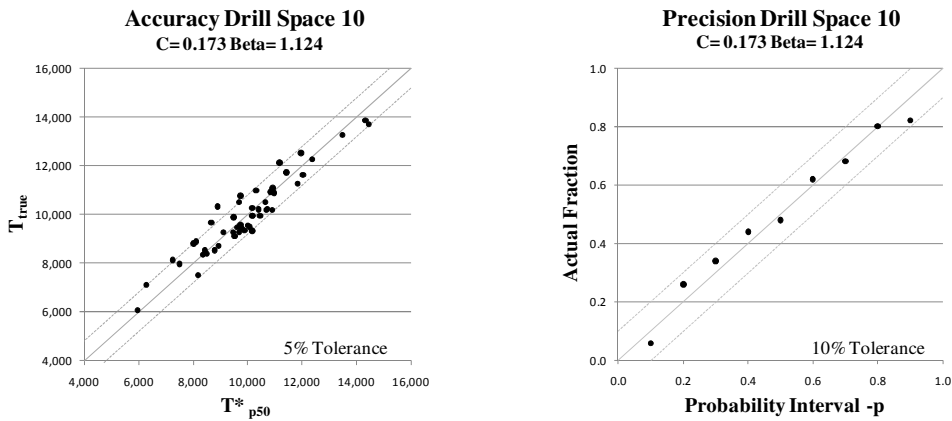


**Figure 4-18:** Accuracy plot for location B in Figure 4-16

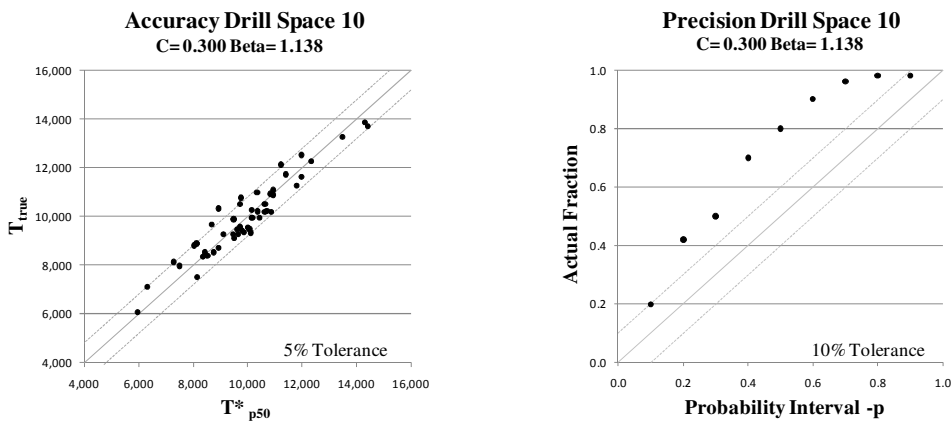


**Figure 4-19:** Accuracy plot for location C in Figure 4-16

### 4.4.3 Drill Spacing 15

The 15 unit drillhole spacing is the equivalent to about 30% of the strike length of the orebody which is 3 or 4 drillhole over its entire length. The 15x15 unit grid has 49 drillholes incorporating 3,871 samples at a sample interval of 1 unit. Figure 4-21, Figure 4-22, Figure 4-23 show accuracy plots for three points shown on the plot shown in Figure 4-20. The accuracy plots show a wider spread along the 45° line than the previous plots with ~30% of the points falling outside the 5% tolerance limits. The precision, shown on the right hand side in the figures show a

pronounced curve for both points A and C with most points falling away from the 45° line indicating poor precision. The optimized values of C and  $\beta$  show acceptable precision with all points falling inside the 10% tolerance limits and close to the 45° line, see Figure 4-22.

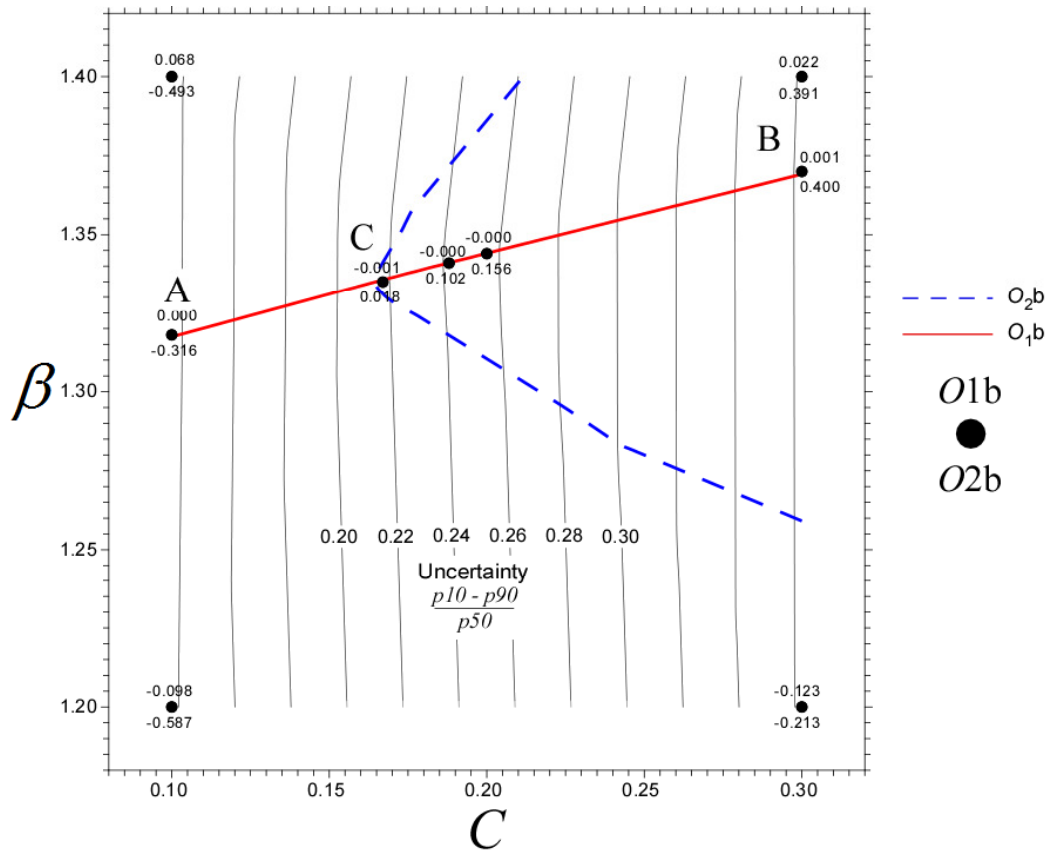


**Figure 4-20:**  $C/\beta$  space for 15 unit spacing. **A)**  $C_{\min}$  end member, **B)**  $C_{\max}$  end member and **C)** optimal  $C/\beta$ . Letters refer to accuracy plots below. Full set of plots are available in Appendix B.

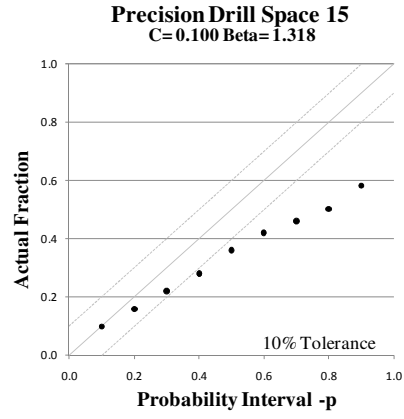
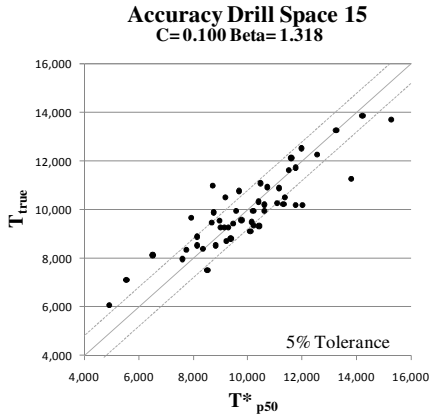


Figure 4-21: Accuracy plot for location A in Figure 4-20

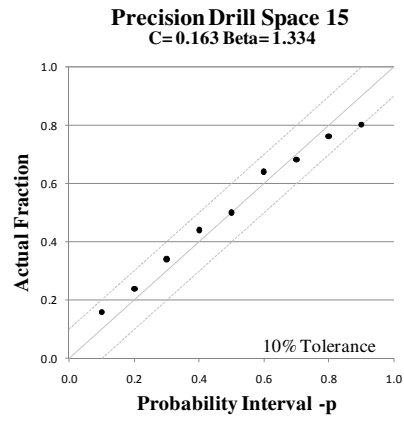
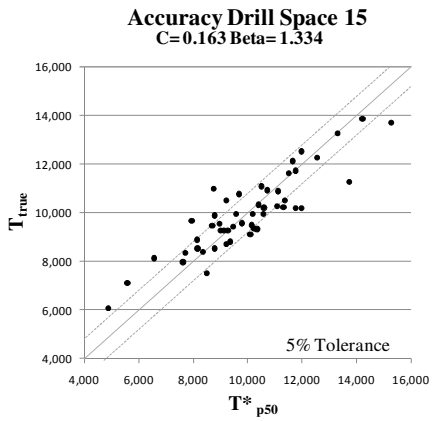


Figure 4-22: Accuracy plot for location B in Figure 4-20

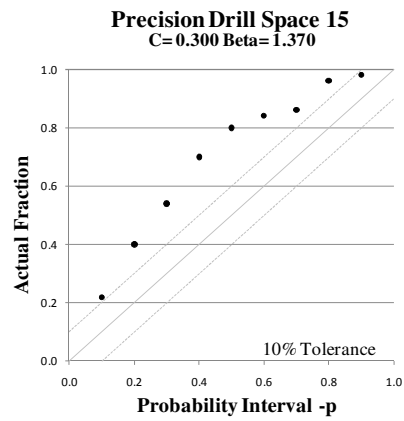
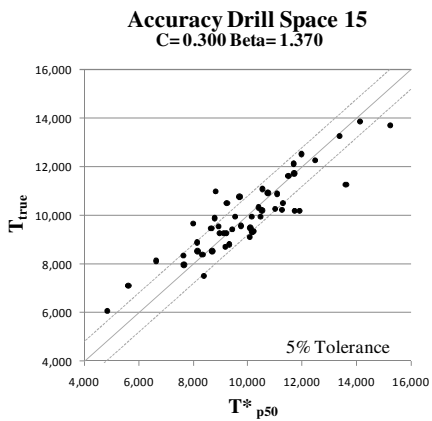
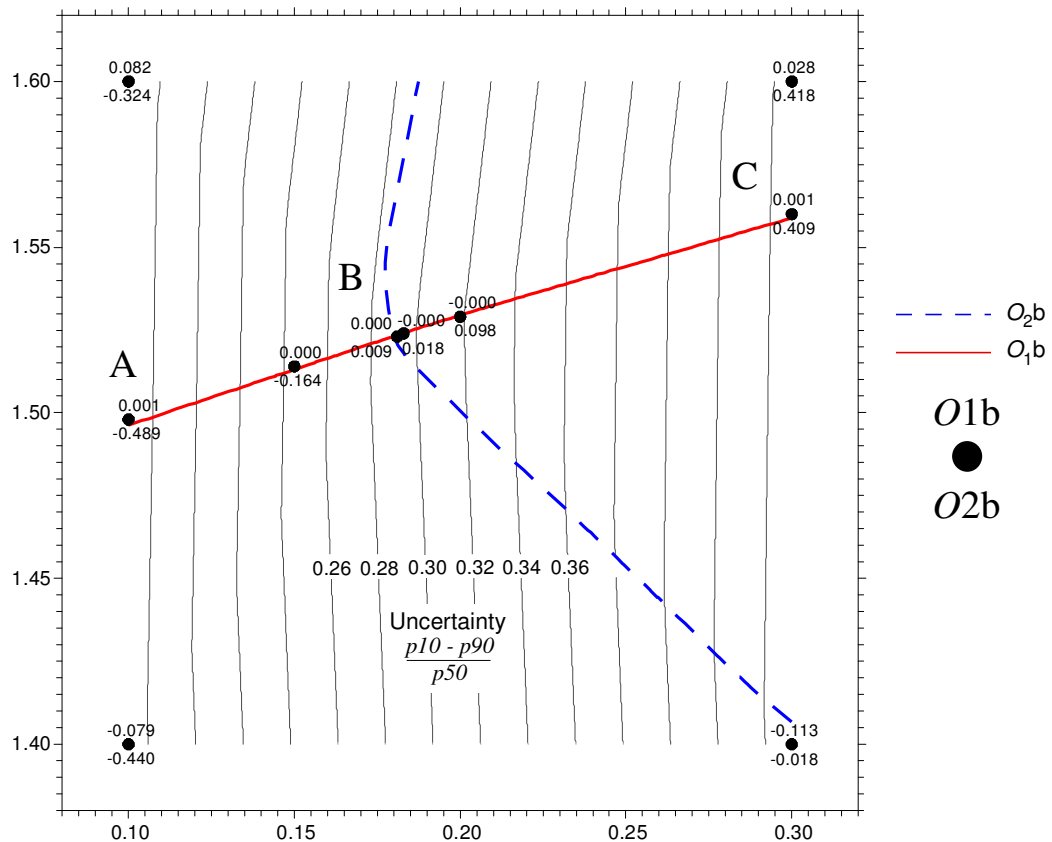


Figure 4-23: Accuracy plot for location C in Figure 4-20

#### 4.4.4 Drill Spacing 20

The 20 unit drillhole spacing is the most sparsely spaced set equivalent to about 40% of the strike length and represents only 2 to 3 drillholes over the entire strike length. The 20x20 unit grid has 25 drillholes containing 1,975 samples at a sample interval of 1 unit. Figure 4-25, Figure 4-26 and Figure 4-27 show accuracy plots for the three points shown on the plot shown in Figure 4-24. The accuracy plots shows the widest spread along the 45° line with ~50% of the points falling outside the 5% tolerance limits. The precision, shown on the right hand side in the figures show a pronounced curve for both points A and C with most points falling away from the 45° line indicating poor precision. The optimized values of C and  $\beta$  show acceptable precision with all points falling inside the 10% tolerance limits but are more erratic than previous plots, see Figure 4-26.



**Figure 4-24:**  $C/\beta$  space for 20 unit spacing. **A)**  $C_{\min}$  end member, **B)**  $C_{\max}$  end member and **C)** optimal  $C/\beta$ . Letters refer to accuracy plots below. Full set of plots are available in Appendix B.

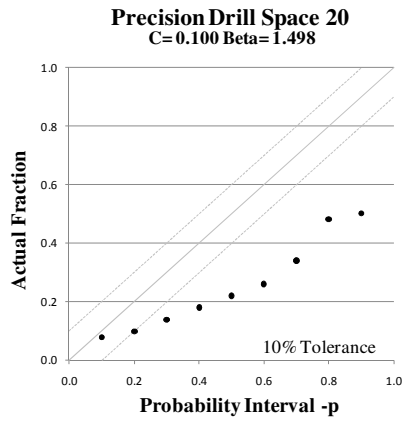
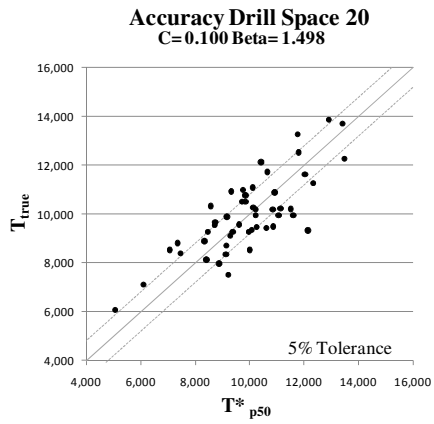


**Figure 4-25:** Accuracy plot for location A in Figure 4-24.

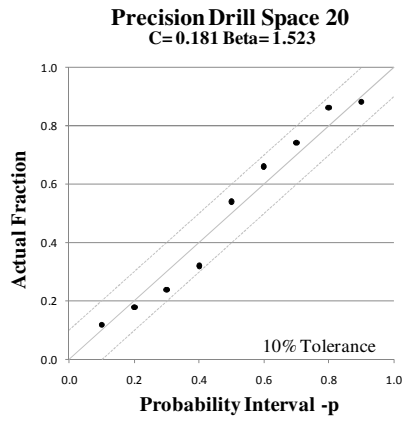
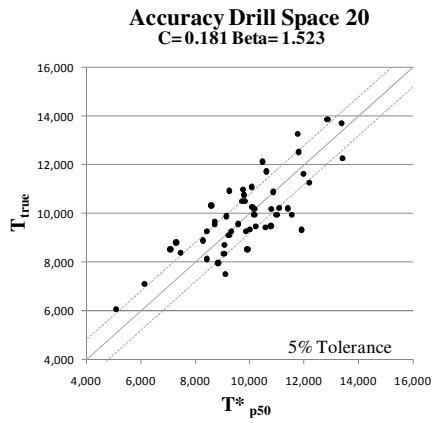


**Figure 4-26:** Accuracy plot for location B in Figure 4-24.

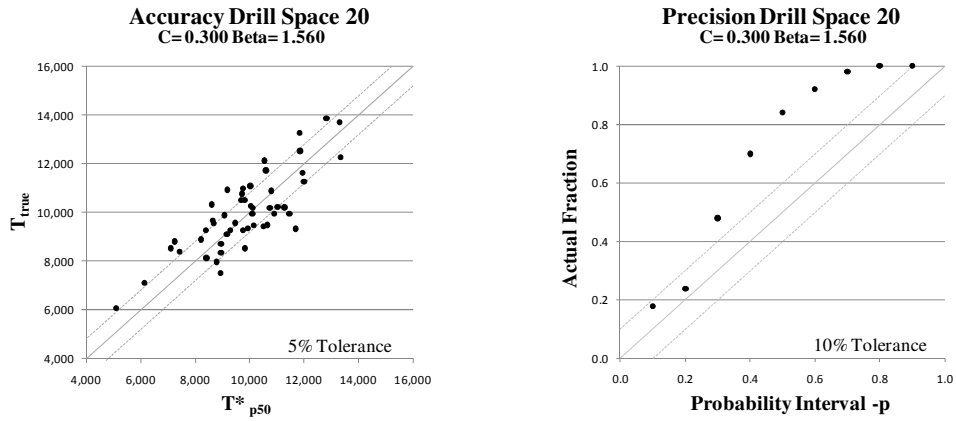
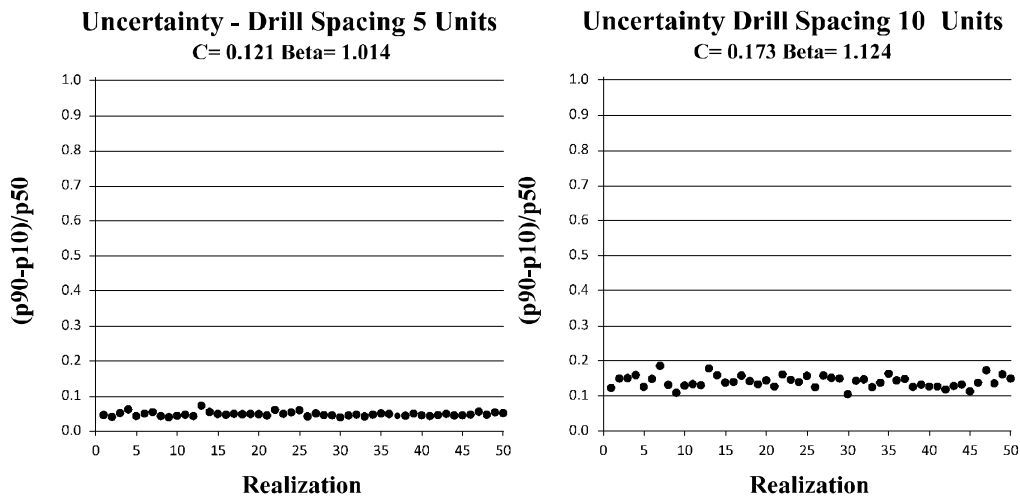
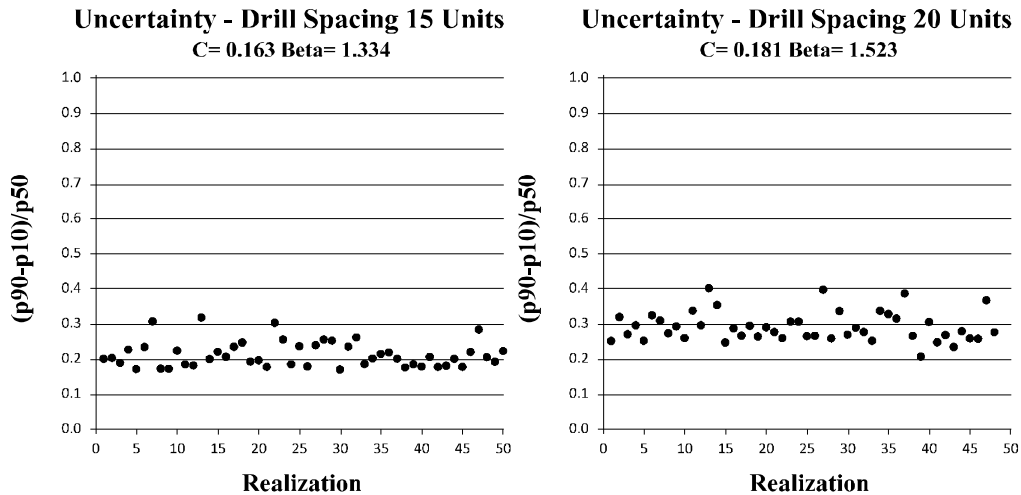


Figure 4-27: Accuracy plot for location C in Figure 4-24.

Recall from section 2.2.3 that uncertainty can be quantified by dividing the spread of the p80 interval by the p50 interval. A desirable quality of any estimate is low uncertainty. Uncertainty for each realization of the final optimized run for each of the four drill spacings is shown in Figure 4-28. The plots show as expected, that uncertainty increases and becomes more erratic as the drill spacing increases.





**Figure 4-28:** Uncertainty plots for final optimized  $C$  and  $\beta$  for; (A) 5 unit spacing (**top left**); (B) 10 unit spacing (**top right**); (C) 15 unit spacing (**lower left**); (D) 20 unit spacing (**lower right**).

## 4.5 Linkages & Implementation Challenges

The methodology presented here is best implemented in early stage exploration projects where there is limited and widely spaced drilling information. As the availability of data increases so does the knowledge of the geometry of the orebody and therefore the practicality of the method is diminished. In an operating mine, where there is usually an abundance of data, the methodology seems of little use as ore boundary limits are more defined through more dense drilling and mine excavation. However, in near-mine exploration, especially along strike and down dip, the methodology can be used to generate tonnage uncertainty in those sparsely drilled areas far removed from main mining activities. The methodology would also be applicable in feasibility or pre-feasibility studies when drilling is usually sparse.

Some of the challenges to apply this methodology are contained in the original data configuration. In many vein type deposits, drilling is stopped soon after the drillhole has exited the orebody, usually within meters of the contact. Although this scenario has not been tested, it is the belief of this author that the lack of data on the footwall side of the vein deposit could provide insufficient sample data that may produce erroneous results.

### 4.5.1 Multiple intercepts

It is common for vein type deposits to consist of more than a single vein structure. The methodology presented here does not explore multiple vein systems and how the DF would behave in those instances. The DF will need to incorporate a coding method to differentiate multiple vein intercepts especially if they belong to different domains.

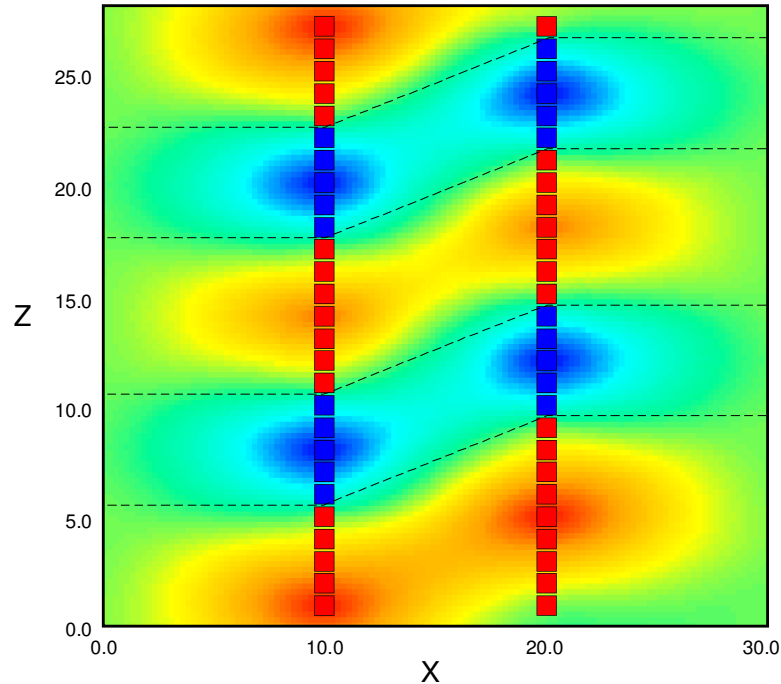


**Figure 4-29:** Simplified vertical XZ cross sectional schematic of multiple vein intercept scenario.

### 4.5.2 Anisotropy

As seen in section 2.4.3 the application of a geometric anisotropy can significantly impact the calculated result of the DF. Assumptions made about the actual anisotropy of the orebody in the presence of insufficient data could lead to poor or unacceptable results.

### 4.5.3 Widely Spaced Data

Data that is too widely spaced will present an additional challenge. A general lack of data could produce unrealistic models of the geometry of the deposit. As seen with the synthetic examples, as the drill spacing increases so does beta and the

uncertainty. It is possible that there exists a point where the drill spacing will produce a level of uncertainty that is unacceptable.

# Chapter 5

## Practical Application

### 5.1 Introduction

To demonstrate the viability of the methodology in an actual situation, the methodology was applied to a data set supplied to the University of Alberta by Inmet Mining Corporation of Toronto, Canada. The data set is from the Çayeli mine in northeastern Turkey, see Figure 5-1. The mine is a volcanogenic massive sulphide (VMS) but displays the characteristics of a vein type deposit. The part of the deposit modeled in this exercise consists of two mineralization types, 1) a hanging wall zone consisting of massive sulphide with >10% sphalerite termed '*clastic*' ore due to its structural characteristics, and 2), a footwall zone made up of a mix of massive sulphide and stockwork. The deposit strikes NNE with a length of more than 900m and a vertical extent in excess of 600m. The average thickness of the orebody is 20m, ranging from a few metres to 80m in the thickest sections. The deposit dips  $-65^\circ$  to the NNW. The data set is restricted to the Main Zone located in the upper mine above the 800m level.



**Figure 5-1:** Çayeli mine location map. (reproduced from “Technical Report on Mineral Resource and Mineral Reserve Estimates, Çayeli Mine, Turkey”, RPA, March, 2006)

The data set consists of 37 drillholes spaced across 13 sections on 40m centres. The author had no access to solid or wireframe models or the resource tonnage for individual zones making a comparison impossible.

### 5.2 Methodology

The Çayeli drillhole data was initially modified by adding sample intervals to non-sampled areas. The result is a dataset where each hole is sampled from collar to toe. This allows a complete string of distance data to be assigned to each drill-hole. The sample data was modified using the FORTRAN program *calcdf* which calculates the distance and assigns a modified distance to each sample interval. A partial calibration was used on the example data. Since no wireframe was supplied with the data set, one was created based on the defined vein geometry. The wireframe is shown in Figure 5-2. The wireframe tonnage was used as the average

tonnage or  $p50$  tonnage. The optimal value of  $\beta$  will be the value that best reproduces the tonnage for the wireframe for the  $p50$  interval. Indicator probability models are extracted for  $p10$ ,  $p50$  and  $p90$  intervals using the program *clipdf*. Figure 5-3 shows a section through the indicator model. Additional examples are contained in Appendix C.

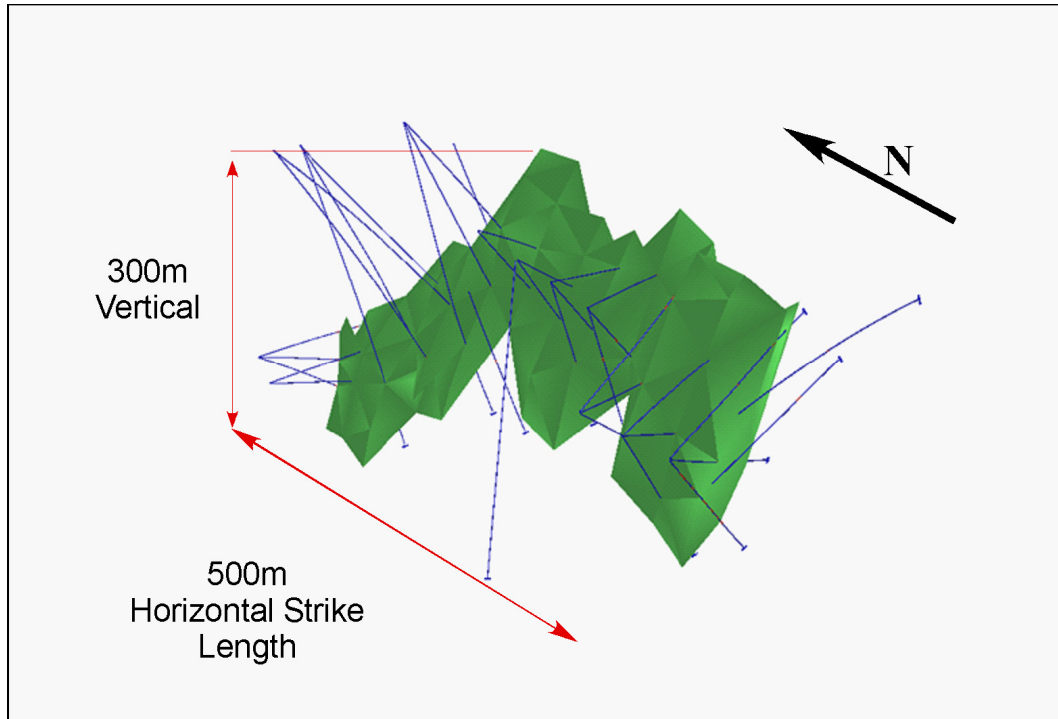


**Figure 5-2:** 3D View of wireframe used to calculate the  $p50$  interval tonnage.

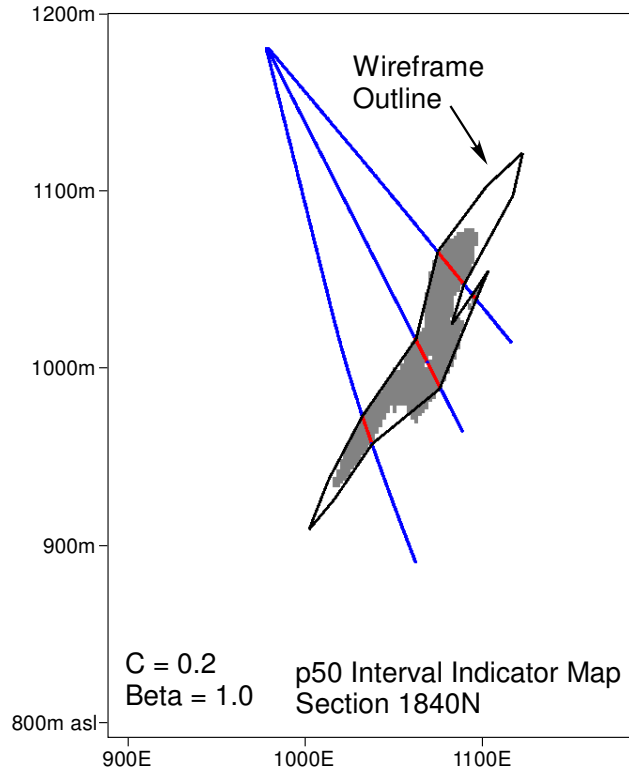


**Figure 5-3:** p50 Interval Indicator map of vertical section 1840N showing wireframe outline.

### 5.2.1 Selection of $C$ and $\beta$

The modifiers used in *calcdf* are based on the results of the synthetic trials discussed in Chapter 4. Figure 5-4 shows the full calibration results for the uncertainty parameter  $C$  for the various drill spacings used in the synthetic examples.

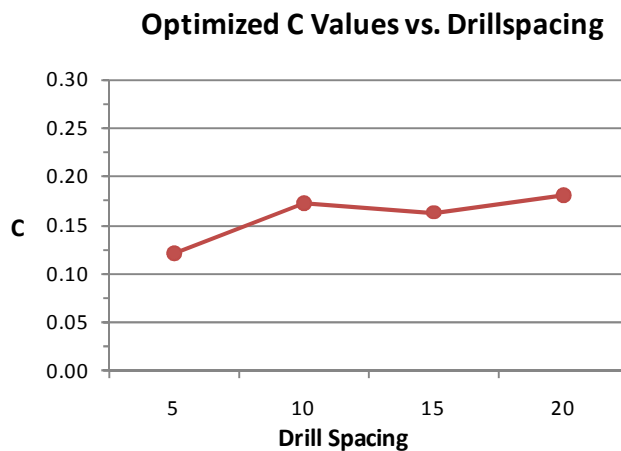


**Figure 5-4:** The optimized values of  $C$  for drillspacing.

Recall that the drill spacings discussed in Chapter 4 are based on the percentage of strike length and that a spacing of 20 units represents about 40% of strike length. For the Çayeli data, the average drill spacing is between 60m and 80m with a 500m strike length and down dip limit of 300m. In terms of unit spacing this is a similar drill density to the 10 to 20 unit spacing discussed in Chapter 4.

A quick examination of the synthetic results, Table 5-1 shows that for each drill-hole spacing a C value of 0.2 resulted in an *O1* objective function of close to zero suggesting an unbiased estimate.

**Table 5-1:** Comparison of Optimal values of C and Beta with selected values

Drill Space	C	$\beta$	O1	O2
5	0.121	1.014	0.002	0.049
5	0.200	1.017	0.001	0.450
10	0.173	1.124	0.000	0.000
10	0.200	1.127	0.001	0.138
15	0.163	1.334	0.000	0.013
15	0.200	1.344	0.000	0.156
20	0.181	1.524	0.000	0.000
20	0.200	1.529	0.000	0.100

Also of interest in Table 5-1 the closeness of the  $\beta$  values between the optimal value and the value for C=0.2. As drillhole spacing increases so does the need for a larger  $\beta$  as shown in Figure 5-5.

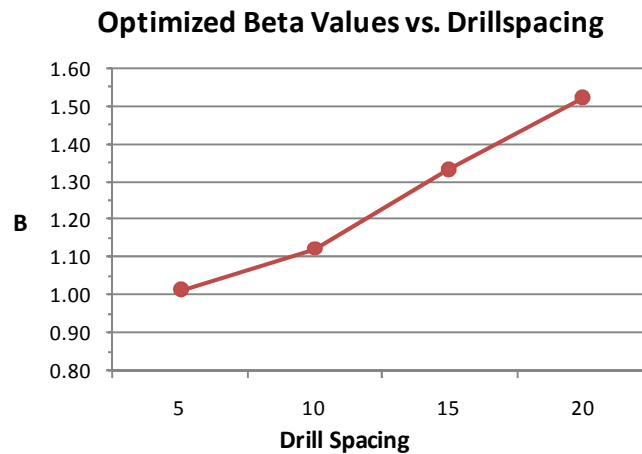


**Figure 5-5:** The optimized values of  $\beta$  for drillhole spacing.

Using the table as a guide, a C value of 0.2 was selected as a C value for the exercise and a selection of  $\beta$ 's since it is unclear from the table what value of  $\beta$  should be used. The example was calculated using  $\beta$  values ranging from 0.80 to 1.7.

### 5.2.2 Anisotropy

The anisotropy for the deposit was calculated using the model area extents as a partial representation of the deposit anisotropy. The model covers a strike length of 500m and a vertical (down dip) extent of 300m. Together with the average thickness of the deposit, 20m, a geometric anisotropy of  $x=1$ ,  $y=0.6$  and  $z=0.1$ , was applied to *calcdf*.

### 5.2.3 Variogram

Variogram used for the estimation was a single spherical model with zero nugget and an anisotropic search of 100m along strike (principal), 85m down dip (perpendicular) and 15m across the structure (z) which is close to the average thickness of the orebody. To ensure that sufficient data was found a large search in the principle direction was used equal to 2.5 times the drill spacing.

## 5.3 Results

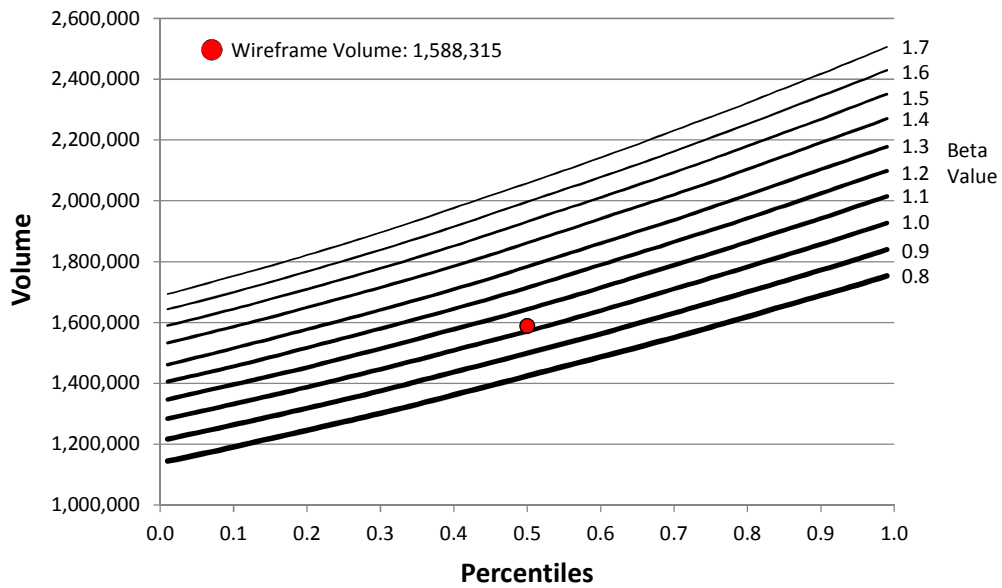
The results should reproduce the wireframe tonnage at the p50 interval and visual inspection of the uncertainty bandwidth. The process is trial and error and since no reference models exist for the practical example accuracy plots cannot be calculated. The results indicate that a  $\beta$  value of 1 is appropriate for a C value of 0.2 and the anisotropy ratios selected. The individual percentiles for each  $\beta$  value are plotted in Figure 5-6.

The uncertainty parameter was discussed in Chapter 2. Recall that the uncertainty parameter is chosen so that the width of the uncertainty bandwidth is neither too large nor too small. The uncertainty parameter is expressed as a percentage of drill spacing. In this example, a value of 0.2 represents 20% or 12m of the average drill spacing of 60m. Figure 5-7 shows vertical cross section 1840 north and the

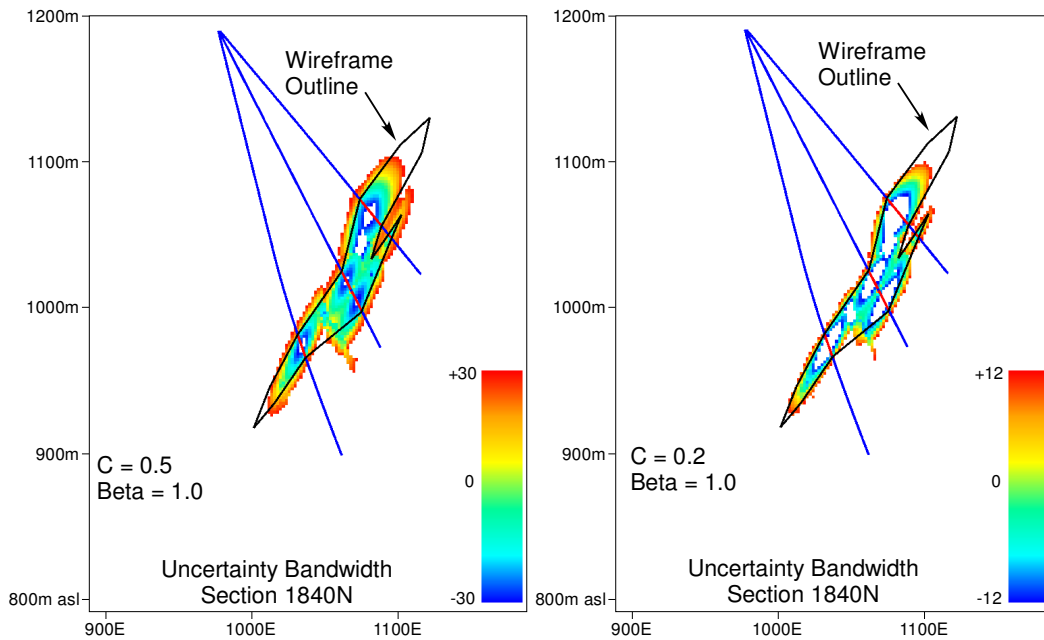
bandwidth associated with an uncertainty constant of 0.2 on the left and 0.5 on the right. Both figures represent a beta of 1.0. As stated earlier, an uncertainty constant of 0.2 was used for the final model of the practical example. This number was arbitrarily chosen based on the optimized results of the calibration studies done in Chapter 4, see Figure 5-4. The uncertainty bandwidth shown on the right in Figure 5-7 for a C of 0.5 is much larger than that for a C of 0.2.

Table 5-2 shows individual p-value volumes associated with both the C=0.2 and the C=0.5 bandwidths. The width of the 0.2 bandwidth has a volume equal to 643,000 or about 40% of the wireframe volume. The width of the 0.5 bandwidth is more than 1,000,000 or nearly 70% of the wireframe volume and is too large. Figure 5-8 shows the distribution of p-values for both uncertainty parameter values C=0.2 and C=0.5. The width of uncertainty for each can be seen in relation to the wireframe volume, which is shown as a circle. The distribution of volumes for C=0.5 uses a beta of 1.6. The p50 volume is close to the wireframe volume. With further modification the p50 for the C=0.5 case could be made to better match the wireframe volume but the purpose is to show the width of the uncertainty bandwidth so this volume is close enough to demonstrate the idea.

The resulting models produced by the method are used as the limits for mineralization. The indicator models produced by *clipdf* can be used to create volume shells for any p-value. The method offers more flexibility in the determination or selection of the resource tonnage. Rather than reporting the single tonnage associated with the wireframe model a tonnage range can be reported. Since the calibrated p50 or median tonnage is close to the wireframe tonnage, a measure of uncertainty to the wireframe tonnage based on the p50 tonnage can be applied.



**Figure 5-6:** Model volume results using an uncertainty constant of 0.2 and the specified beta. The red dot represents the wireframe volume.



**Figure 5-7:** Uncertainty bandwidth for C = 0.2 (left) and C=0.5 (right), vertical cross section 1840N.

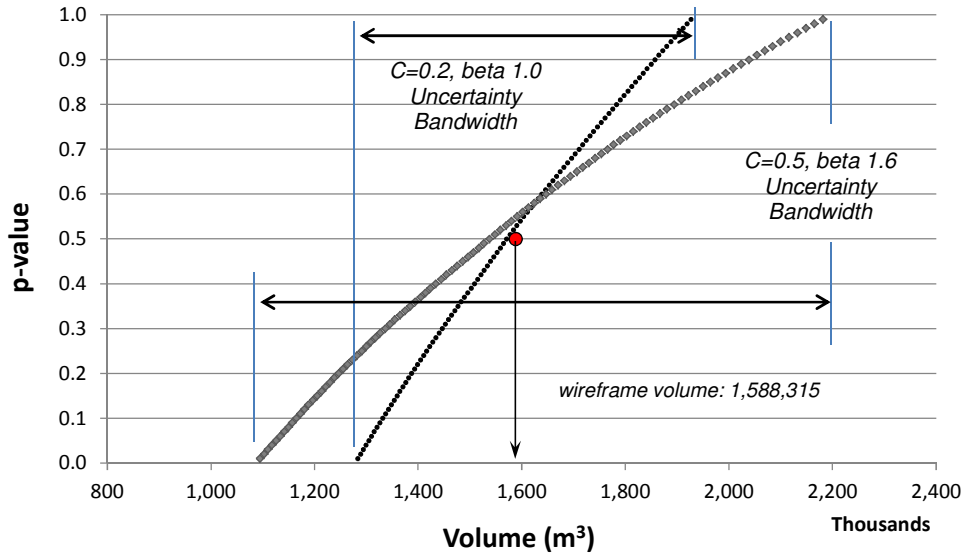


**Figure 5-8:** Range of volumes (uncertainty) associated with the C=0.2, beta = 1.0 model and the C=0.5, beta = 1.6 model. The red circle represents the wireframe volume.

**Table 5-2:** p-value Volumes

Percentile	C=0.2 Volume	C=0.5 Volume
<i>p99</i>	1,926,928	2,181,864
<i>p90</i>	1,857,088	2,039,232
<i>p75</i>	1,746,360	1,827,912
<i>p50</i>	1,570,936	1,537,808
<i>p25</i>	1,416,288	1,291,472
<i>p10</i>	1,331,608	1,165,144
<i>p1</i>	1,283,304	1,094,616
<i>Bandwidth</i>	643,624	1,087,248
<i>Wireframe</i>	1,588,315	1,588,315
<i>Relative Size*</i>	<b>41%</b>	<b>68%</b>

\* *Bandwidth / wireframe Volume*

A complete set of sections and plans through one of the models is contained in Appendix C.

# Chapter 6

## Conclusion

### 6.1 Conclusions

The tonnage of vein type deposits can be a significant source of uncertainty in mining projects. Tonnages of vein deposits are commonly calculated using wireframes built from the interpretation of geologic level plans and sections.

The construction of wireframe models is a deterministic process that is often time consuming. The wireframe models created provide a single tonnage estimate with no provision for the determination of the uncertainty associated with the estimate.

The purpose of modeling the boundary using a distance function is to provide a measure of the uncertainty in the tonnage. The novel method proposed in this thesis provides an estimate of the tonnage with uncertainty without the need to create a wireframe model. However, in the case of partial calibration it is desirable to have a wireframe for a base case volume.

The methodology was tested using 50 synthetic reference models with known true tonnages. The modeling process creates an uncertainty bandwidth that is calibrated to allow the calculation of tonnages corresponding to any probability value. Tonnages are calculated by summing the tonnages from all grid cells within the vein accounting for the chosen probability value.

The method when calibrated properly is shown to provide an estimate of vein deposit tonnage uncertainty that is both fair and accurate.

In Chapter 3, full optimization of the required parameters ( $C$  and  $\beta$ ) was presented. Chapter 4 showed how the framework is implemented with a synthetic example. The optimization process is time consuming, requiring a minimum of ten runs to completely optimize the needed parameters  $C$  and  $\beta$ . The time required increases with the size of the reference models and the number of reference models

used. The number of reference models required could be reduced through a sensitivity analysis. Further efficiency could be obtained through modification of the optimization process.

In Chapter 5, partial calibration was shown to produce encouraging results in the framework of an actual setting using a data set from the Çayeli mine in Turkey.

Although many refinements could be considered, the foundation has been established for a methodology to accurately and precisely evaluate tonnage uncertainty in vein-type deposits.

## **6.2 Future Work**

Vein type structures are constrained by the geology. A flat lying orebody may be contained within a specific lithological horizon, or a steeply dipping vein structure may be confined to a certain rock type close to a contact with another rock type. In these cases the methodology presented here may not produce the desired results. A closer investigation of structurally controlled zones, and how to incorporate that type of data into the distance function procedure is warranted.

The presence of bounding structures such as faults are common in vein type deposits. Structures such as faults and shear zones often truncate vein type structures. This situation was encountered in the practical example shown in Chapter 5. The vertical cross section in Figure 3-27 contains a major fault that truncates the mineralized zone. Future work will need to study the effects of structures such as faults on the methodology and how to incorporate them in the procedure to ensure that they are properly handled.

Another area of future work is case where not all available intercepts belong to the same geologic structure, that is to say, when the data is comprised of intercepts belonging to different structural entities. The schematics shown in Figure 6-1 show a simple section where one drillhole has two intercepts. The figure on the left assumes the intercepts belong to the same structure and the methodology presented here will produce a similar geometrical shape. However, if the inter-

cepts belong to different structures as depicted in the figure on the right, then the methodology will fail to produce the desired result. Therefore, there is a need to enhance the methodology to deal with multiple intercepts or vein structures.

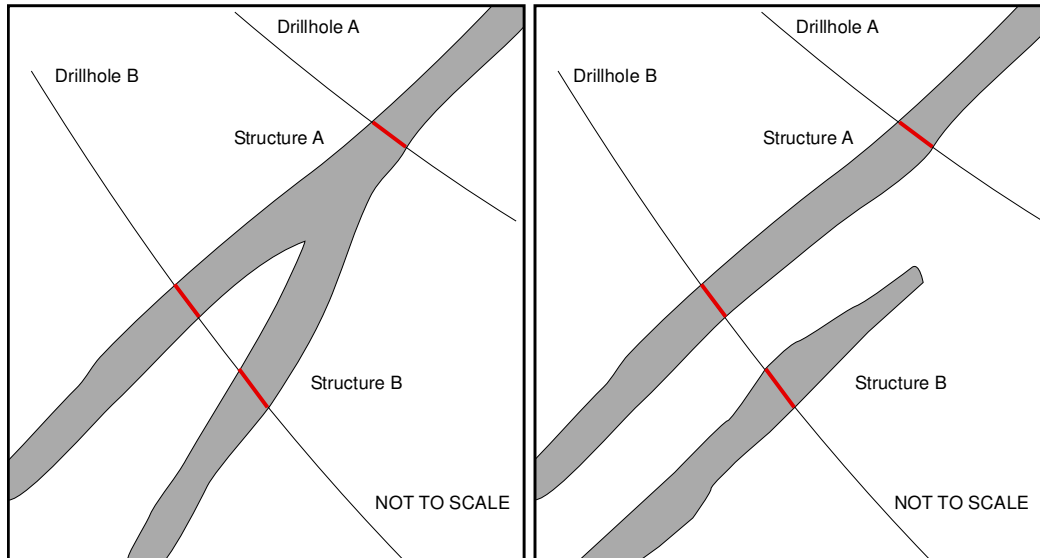


**Figure 6-1:** Vertical cross section schematic showing two possible interpretations. A) The two intercepts in drillhole B belong to the same structure. B) The two intercepts in drillhole B belong to different structures.

Many vein type deposits are more complex than a single planar vein in a single orientation. Deposits may have multiple veins at multiple orientations and multiple stages of development. The order of development and any cross cutting relationships that exist are important. Therefore the order in which the structures are interpolated is important. Figure 6-2 shows a simple schematic of two structures with different orientations and stages of development. Future work will need to study the effects of multiple structures and orientations on the distance function approach to vein tonnage uncertainty.

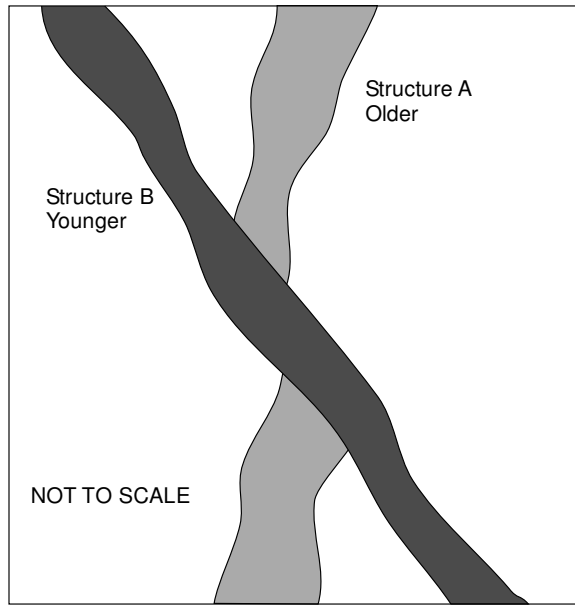


**Figure 6-2:** Vertical cross section schematic showing the cross cutting relationship of two vein structures. In this example structure A is also offset by structure B.

Finally, the methodology presented here assumed drilling on a regular rectangular grid. The effects and implications of drilling on an irregular grid need to be studied to determine if acceptable results are produced.

# Bibliography

1. Baumann, Ludwig, 1976, *Introduction to ore deposits*, New York, Wiley, 131 p.
2. Dennen, William H., 1989, *Mineral Resources: Geology, Exploration and Development*, New York, Taylor & Francis, 255 p
3. Deutsch, C.V. and Journel, A.G., 1998, *GSLIB: Geostatistical Software Library and User's Guide*, 2<sup>nd</sup> Edition, Oxford University Press.
4. Deutsch, C.V., 2005, *A Short Note on Prediction of Uncertainty in Tonnage and Grade of Vein Type Deposits*, paper #305. In Centre for Computational Geostatistics, Report 7.
5. Deutsch, C.V., *Direct Assessment of Local Accuracy and Precision*, In Geostatistics Wollongong '96, Volume 1, 115-125, E.Y. Baafi and N.A. Schofield, eds.
6. Dickinson, S.B., 1942. *The structural control of ore deposition in some South Australian Copper Fields*, No. 1. Geol. Surv. S. Aust., Bull., 20, 99 pp.
7. Dietrich, R.V., Skinner, B.J., 1979, *Rocks and Rock Minerals*, New York, Wiley, 319p.
8. Gilluly, J., 1968, *Principles of Geology* (3rd Edition), W. H. Freeman, San Francisco and London, 687 p.
9. Gringarten, E., Deutsch, C.V., *Methodology for Variogram Interpretation and Modeling for Improved Reservoir Characterization*, paper SPE56654 presented at the 1999 SPE Annual Technical Conference and Exhibition, Houston, Texas, October 3–6.
10. Kesler, Stephen E., 1994, *Mineral resources, economics, and the environment*, Toronto, Maxwell Macmillan Canada, 391p.
11. McLennan, J. and Deutsch, C., 2006, *Implicit Boundary Modeling (Boundsim)*, paper #102. In Centre for Computational Geostatistics, Report 8.
12. Panteleyev, A., 1986, *Ore Deposits #10. A Canadian Cordilleran Model for Epithermal Gold-Silver Deposits*, Geoscience Canada, Vol. 13, No. 2.
13. Park, C. F., MacDiarmid, R. A., 1975, *Ore Deposits* (3rd Edition), W. H. Freeman, San Francisco, 529 p.
14. Pawlowsky, Olea, and Davis, 1993, *Boundary Assessment Under Uncertainty: A Case Study*, *Mathematical Geology*, Vol. 25, No. 2.
15. Peters, Stephen G, 1993, *Nomenclature, concepts and classification of ore-shoots in vein deposits*, *Ore Geology Reviews*, 8, pp.3-22

16. Peters, William C., 1978, *Exploration and Mining Geology*, Toronto, John Wiley & Sons, 696 p.
17. Ryan, R.J., Smith, P.K., 1997, *Review of the mesothermal gold deposits of the Meguma Group, nova Scotia, Canada*, *Ore Geology Reviews*, 13, pp.153-183
18. Shcheglov, V. I., 1991, *Errors in Determining Boundaries of Stratified Deposits*, *Mathematical Geology*, Vol. 23, No. 1
19. Soares, Amilcar, 1990, *Geostatistical Estimation of Orebody Geometry: Morphological Kriging*, *Mathematical Geology*, Vol. 22, No. 7
20. Srivastava, R. Mohan, 2005, *Probabilistic Modeling of Ore Lens Geometry: An Alternative to Deterministic Wireframes*, *Mathematical Geology*, Vol. 37, No. 5

# Appendices

**Appendix A: Program summary, parameter files and scripts**

**Appendix B: Program results**

**Appendix C: Practical example figures**

# Appendix A: Program Summary, Parameter files and scripts

Listing of FORTRAN programs, associated parameter files and BASH script files.

## A.1 SIMULATION MODE PROGRAMS

Program: **E\_MODE3**

Modifies the output from SGSIM to construct the vein deposit. Each SGSIM realization must be must be modified and assembled into a simulated vein deposit. *E\_MODE3.EXE* modifies each conditional and unconditional simulation, adds them together and outputs the modified surface. Three output surfaces are created, a modified unconditional surface and two modified conditional surfaces, one added to the unconditional surface, and one subtracted from the unconditional surface. The program also creates a thickness map which can be used for verification and visualization of the virtual deposit.

INPUT:       **SGS\_U\_TEST.OUT** -The unconditional simulation realizations  
PART I:       Multiply by Factor A (10) and output to TEMP1A.OUT  
PART II:       Add Factor B (100) and output to TEMP1B.OUT  
PART III:      Smooth and output to MSGS\_1A.OUT

INPUT:       **SGS\_C\_TEST.OUT** -The conditional simulation realizations  
PART I:       Multiply by Factor A (5) and output to TEMP2A.OUT  
PART II:       Add Factor B (10) and output to TEMP2B.OUT  
PART III:      Smooth and output to MSGS\_1B.OUT  
PART IV:      Zero and output to TEMP2D.OUT  
PART V:       ADD to MSGS\_1A.OUT and output to MSGS\_1B.OUT  
PART VI:      SUBTRACT from MSGS\_1A.OUT and output to MSGS\_1C.OUT

OUTPUT:      Thickness Model   TSGS\_xA.OUT (U+C)  
OUTPUT:      Thickness Model   TSGS\_xB.OUT (U-C)

**Parameter File: emode.par**

Parameters for emode  
\*\*\*\*\*

```
START OF PARAMETERS:
d:\research\gslib\output\SGS_U_test.out      -Unconditional Surface
d:\research\gslib\output\SGS_C_test.out      -Conditional Surface
d:\research\gslib\output\1\SGS_1a.out        -Modified Unconditional Surface
d:\research\gslib\output\1\SGS_1b.out        -Output Upper Model UC + C
d:\research\gslib\output\1\SGS_1c.out        -Output Lower Model UC - C
d:\research\gslib\output\1\TSGS_1a.out       -Output Thickness Map UC + C
d:\research\gslib\output\1\TSGS_1b.out       -Output Thickness Map UC - C
10                                             -Unconditional Multiplication Factor
100                                            -Unconditional Additive Factor
5                                              -Conditional Multiplication Factor
2                                              -Conditional Additive Factor
```

**Program: TFTMAP**

Calculates the tonnage from the thickness maps produced by *E\_MODE3*. The values in the thickness map are multiplied by a tonnage factor (TF). The tonnage factor is equal to the cell x-size \* y-size \* specific gravity. Tonnages are appended to report after a completed iteration.

**IMPORTANT:** The program appends to the report file if it exists. To avoid having bogus entries the user must delete any existing file if needed.

INPUT: TSGS\_1A.OUT -Thickness created from E\_Mode3 output.  
OUTPUT: TMAP\_TABLE1.RPT -Tabulated report

**Parameter File: tmap.par**

Parameters for TMAP  
\*\*\*\*\*

```
START OF PARAMETERS:
D:\Research\gslib\output\1\TSGS_1a.out      -Thickness Map
D:\Research\gslib\output\1\TMAP_Table1a.rpt -Tonnage Report
1                                             -realization number
100 0.5 1                                     -nx, xmn, xsiz
100 0.5 1                                     -ny, ymn, ysiz
1 0.5 1                                       -nz, zmn, zsiz
1                                             -specific gravity
```

**Program: E\_TONNES2**

Calculates the true tonnage. The program calculates the vertical separation between the surfaces and multiplies it by a tonnage factor (TF). The tonnage factor is equal to the cell x-size \* y-size \* specific gravity. Tonnages are appended to report after a completed iteration.

**IMPORTANT:** The program appends to the report file if it exists. To avoid having bogus entries the user must delete any existing file if needed.

INPUT:	MSGGS_1A.OUT	-Modified Unconditional Surface
INPUT:	MSGGS_1B.OUT	-Modified Upper Model UC + C
INPUT:	MSGGS_1C.OUT	-Modified Lower Model UC - C
OUTPUT:	TONNAGE_TABLE1.RPT	-Tonnage Report
OUTPUT:	FSGS_1A_XXX.OUT	-Tonnage Model A
OUTPUT:	FSGS_1B_XXX.OUT	-Tonnage Model B

**Parameter File: etonnes.par**

```

Parameters for E_tonnes
*****

START OF PARAMETERS:
..\output\1\MSGGS_1a.out      -Modified Unconditional Surface
..\output\1\MSGGS_1b.out      -Modified Upper Model UC + C
..\output\1\MSGGS_1c.out      -Modified Lower Model UC - C
..\output\1\Tonnage_Table1.rpt -Tonnage Report
..\output\1\FSGS1_1.out       -Tonnage Model A
..\output\1\FSGS1_2.out       -Tonnage Model B
1                               -realization number
100 0.25 0.50                 -nx, xmn, xsiz
100 0.25 0.50                 -ny, ymn, ysiz
1 0.25 0.50                   -nz, zmn, zsiz
1                               -specific gravity

```

**Program: ANIS**

Calculates the anisotropy of a specified realization contained in the true thickness map produced by *E\_MODE3*. The program appends the data to the report file if it exists otherwise it creates the file. The anisotropy is calculated using the XZ and YZ cross sections through the centre of the map. Recall that simulated orebodies are centred on the grid due to the use of conditioning data used when simulating the orebodies.

**IMPORTANT:** The program appends to the report file if it exists so if required the user must delete the existing file to start fresh with a clean file.

INPUT:	TSGS_1A.OUT	-Thickness created from E_Mode3 output
OUTPUT:	TRUE_ANIS_1A.RPT	-Tabulated anisotropy report

**Parameter File: anis.par**

Parameters for Anis  
\*\*\*\*\*

START OF PARAMETERS:

```
d:\research\gslib\output\1\TrueA.out  -True thickness maps
d:\research\gslib\output\1\Anis.rpt   -Anisotropy Report
1                                       -Column with data
1                                       -realization number
400 0.25 0.50                          -nx, xmn, xsiz
400 0.25 0.50                          -ny, ymn, ysiz
1   0.25 0.50                          -nz, zmn, zsiz
```

## A.2 Subroutines

### Subroutine: **SMOOTH5**

Used in the program *E\_MODE*. The subroutine smoothes the SGS models to remove some of the roughness. The program uses a five point moving window. The algorithm uses the cells immediately preceding and following the working cell in the same row and the cells directly above and below the working cell. The result is the arithmetic average of the five cells. Filters are applied for cells located at the beginning or at the end of a row as well as for cells located along the bottom or top row. In these instances the average is based on 3 to 5 cells depending on the location. The calculated average value is not used in subsequent calculations.

### Subroutine: **SETZERO**

Used in the program *E\_MODE*. The subroutine zeros the background of the conditional model. Specifically, all cells with a value less than zero are reset to zero. When this model is added to or subtracted from the unconditional model, all cells in the final model will retain the value of the unconditional model, therefore, the models will have a zero difference in these areas and they will be coincident with one another.

### Subroutine: **ADDMOD**

Used in the program *E\_MODE*. The subroutine adds and/or subtracts the conditional model from the unconditional model and writes it to the final model output file.

### Subroutine: **TMAP**

Used in the program *E\_MODE*. The subroutine calculates and outputs a thickness Model which can be used for verification and visualization of the simulated vein deposit.

### A.3 ESTIMATION MODE PROGRAMS

Program: **DRILL5**

Drills the simulated orebody built from two surfaces. Output drillhole file contains the xyz coordinates, the elevations of the upper and lower surfaces, and the vein indicator (VI).

INPUT:	MSG5_1B.OUT	-Modified Upper Model UC + C
INPUT:	MSG5_1A.OUT	-Modified Unconditional Surface
OUTPUT:	DRILL.OUT	-Drillhole file

**Parameter File: drill5.par**

```
Parameters for drill5
*****

START OF PARAMETERS:
../output/1/MSG5_1b.out      -Upper Surface
../output/1/MSG5_1a.out      -Lower Surface
100 100 1                    -nx,ny,nz (Input surface dimensions)
0.50 0.50 0.125              -xmin,ymin,zmin (surface grid minimum)
1.0 1.0 0.25                 -xsiz,ysiz,zsiz (surface grid size)
5 10 20                      -nx,x-origin,x-spacing (Drill)
5 10 20                      -ny,y-origin,y-spacing (Drill)
140                          -Model top
60                          -Model bottom
1                            -Realization to Process
../output/1/DS20_SGS_A.out    -Output drillhole file
```

Program: **CALCDF**

The distance function. Calculates the distance from one sample to the closest sample with a different VI. Modifies the DF using the specified uncertainty constant C, and the specified  $\beta$  constant. The DF is also modified using the xyz anisotropy values stored in the anisotropy file. The output is used as the kriging input file.

INPUT:	DRILL.OUT	-Drillhole input file (from DRILL5)
INPUT:	ANIS.OUT	-Anisotropy file
OUTPUT:	MDRILL.OUT	-VF modified drillhole file

**Parameter File: calcdf.par**

```
Parameters for calcdf
*****

START OF PARAMETERS:
d:\research\gslib\output\1\tmp\DC10_10A.out - Input Drillholes
d:\research\gslib\output\1\True_Anis_1a.rpt - Anisotropy file
1 - Vein strike distance
1 - Vein dip distance
1 - Average Vein Thickness
10 - Drill Spacing
0.5 - Uncertainty Constant C
0.5 - beta parameter
1 - realization
d:\research\gslib\output\1\tmp\VF10_10A.out - Output file
```

**Program: DFOPT**

Used to optimize the kriging program *kt3d.exe*. The program takes advantage of the drift option in *kt3d.exe* to produce a file that flags all cells outside the area of the orebody defined by a bounding box so they are skipped during the kriging process. This greatly enhances the speed of a kriging run. The output file contains a flag, 0 or 1, which tells *kt3d.exe* whether to skip the block (0), or calculate the cell, (1). Skipped blocks are assigned a default value of -999.

INPUT: TRUE.OUT -True thickness map  
INPUT: VI.DAT -Vein Indicator  
OUTPUT: OPT.OUT -Optimized Model

**Parameter File: dfopt.par**

```
Parameters for dfopt
*****

START OF PARAMETERS:
D:/Research/gslib/output/1/True/A/TRUE.out -Input #1 True thickness map
D:/Research/gslib/output/1/tmp/VF.dat -Input #2 Vein Indicator
D:/Research/gslib/output/1/Ext5.opt -Output optimized model file
2 -Input #1 Column with data
9 -Input #2 Column with VI data
1 -realization number
100 0.5 1 -nx, xmn, xsiz
100 0.5 1 -ny, ymn, ysiz
1 0.5 1 -nz, zmn, zsiz
100 0.5 1 -nx, xmn, xsiz
100 0.5 1 -ny, ymn, ysiz
80 60.5 1 -nz, zmn, zsiz
```

Program: **U\_TONNES**

Calculates the tonnage for each proportion of C from -C to +C. There are 21 classes defined, from P0 to P100 corresponding to the value from -C (P0), to +C (P100). The value at P50 corresponds to the iso-zero surface. Tonnage is calculated as the cell volume multiplied by the specific gravity. After each iteration the tonnages are appended to report. Optionally, the program can write out the tonnage to a model file.

**IMPORTANT:** The program appends to the report file if it exists. To avoid having bogus entries the user must delete any existing file if needed.

INPUT:	MSGGS_1.OUT	-Modified Unconditional Surface
INPUT:	MSGGS_1A.OUT	-Modified Upper Model UC + C
INPUT:	MSGGS_1B.OUT	-Modified Lower Model UC - C
OUTPUT:	TONNAGE_TABLE1.RPT	-Tonnage Report
OUTPUT:	FSGS_1A_XXX.out	-Tonnage Model A
OUTPUT:	FSGS_1B_XXX.out	-Tonnage Model B

**Parameter File: *uton.par***

```
Parameters for U_Tonnes
*****

START OF PARAMETERS:
d:\Research\gslib\output\1\tmp\model.dat      -Input model
d:\Research\gslib\output\1\True_Tonnes.rpt    -Input True Tonnages
10                                             -Drill spacing
0.5                                           -Uncertainty Constant C
0.5                                           -beta
1 1 1                                         -dx,dy,dz Cell Sizes
1                                             -Specific Gravity
1                                             -Realization(not used)
d:\Research\gslib\output\1\Tonnage.rpt       -Append to tonnage report
```

Program: **OPTSEARCH**

Automated program to locate the optimal  $\beta$  and C combination for a data set. The file calls *inner.bsh* which calculates the set of realizations for a given C/ $\beta$  combination. Output summary file, *SUM*, contains the number of realizations used, C,  $\beta$ , and the objective functions, O1, O2a, O2b and OF. The input report file from *inner.bsh* contains the realization number, drill spacing, C,  $\beta$ , True tonnage, p0 through p1.0 (0.05 increments), the average estimated tonnage and the objective functions O1 and O2b. *Optsearch.exe* is given a maximum and minimum C and  $\beta$  and finds the optimal C/ $\beta$  combination within the defined space.

OUTPUT:	SUMMARY.SUM	-Output Summary file
---------	-------------	----------------------

INPUT: INNER.BSH -Bashfile to calc realizations  
 INPUT: INNER.RPT -Summary output from Bashfile

**Parameter File: optsearch.par**

```

Parameters for optsearch
*****

START OF PARAMETERS:
D:\research\gslib\output\1\reports\DS15b.sum -Output Summary file
D:\research\gslib\bashfiles\inner.bsh -Bashfile
D:\research\gslib\output\1\reports\DS15_b.rpt -Input Raw data
0.4 0.8 -Cmin,Cmax
0.4 0.8 -Bmin,Emax
  
```

Program: **CLIPDF**

Extracts indicator models from a model estimated using  $C$  and  $\beta$ . Multiple models can be extracted to the same file. The indicator models are specified using probability limits. For example, specifying 3 models at 0.1, 0.5, and 0.9 will extract indicator models representing the  $p_{10}$ ,  $p_{50}$  and  $p_{90}$  model limits. The program also output the volume and tonnage of the 99 percentiles, 0.01-0.99. For large models this can be time consuming. An option to disable the summary output is available. Cell sizes (dx,dy,dz) are used to calculate Volume. Tonnage is calculated by applying the specified specific gravity to the volume.

INPUT: MODEL.OUT -Input DF model  
 OUTPUT: VEININD.OUT -Output Indicator Model  
 OUTPUT: SUMVOL.OUT -Output Summary file

**Parameter File: clipdf.par**

```

Parameters for clipdf
*****

START OF PARAMETERS:
D:\Research\gslib\output\model.dat -Input model
D:\Research\gslib\output\veinind.dat -Output model
3 -Number of models to extract
0.1 0.5 0.9 -Model P values
10 -Drill spacing
0.3 -Uncertainty Constant C
1 -Beta
1 1 1 -dx,dy,dz Cell Sizes
1.0 -Specific Gravity
1 -Skip Summary (1=yes,0=no)
D:\Research\gslib\output\sumvoll.dat -Summary output
  
```

Program: **kt3d-mjm.exe**

A modification of the program *kt3d.exe* to speed the execution of the optimization of  $C$  and  $\beta$ . The modification makes use of the built-in external drift handling capability. An external file of cell indicator values, 0 or 1, is used to determine whether a cell is calculated or skipped. Skipped cells are assigned a value of -999, this value is universally used to indicate unestimated cells in GSLIB. The input file is generated using *DFOPT.EXE* previously discussed.

## A.4 Execution BASH scripts

Script: **inner.bsh**

Script called by **OPTSEARCH.EXE** used to automate the selection, drilling and estimation of an ore body.

**Script File: inner.bsh**

Page 1 of 3

```
# Drill Spacing - Run 10m Spacing
DSPACE=10
# C Constant - Run
CCONST="$1"
# Beta
BETA="$2"
# Mean to Use
SKMEAN=20
#realization
#cnt=1

echo $1
echo $2

cat<<END>1.tem
Parameters for drill5
*****

START OF PARAMETERS:
d:\research\gslib\output\1\MSG5_1b.out -Input Upper Surface
d:\research\gslib\output\1\MSG5_1a.out -Input Lower Surface
100 100 1 -nx,ny,nz (Input surface dimensions)
0.50 0.50 0.50 -xmin,ymin,zmin (surface grid minimum)
1.0 1.0 1.0 -xsiz,ysiz,zsiz (surface grid size)
9 10 10 -nx,x-origin,x-spacing (Drill)
9 10 10 -ny,y-origin,y-spacing (Drill)
140 -zmax (Top)
60 -zmin (Bottom)
REAL -Realization to process
d:\research\gslib\output\1\tmp\DCUCT_10A_REAL.out -Output file
END

cat<<END>2.tem
Parameters for dFV4
*****

START OF PARAMETERS:
d:\research\gslib\output\1\tmp\DCUCT_10A_REAL.out -Input Drillholes
d:\research\gslib\output\1\True_Anis_1a.rpt -Anisotropy file
1.0 -Vein strike distance
1.1 -Vein dip distance
0.3 -Average Vein Thickness
DSX -Drill spacing
UCT -Uncertainty Constant C
BTA -beta
REAL -realization
d:\research\gslib\output\1\tmp\VFUCT_10A_REAL.out -Output Drillholes

END
```

```

cat<<END>3.tem
      Parameters for dfopt
      *****

START OF PARAMETERS:
d:\research\gslib\output\1\True\A\FSGS_1A_REAL.out  -Input #1 True thickness map
d:\research\gslib\output\1\tmp\VFUCT_10A_REAL.out  -Input #2 VF VI
d:\research\gslib\output\1\ext10_REAL.opt          -Output optimized model file
2                                                    -Input #1 Column with data
9                                                    -Input #2 Column with data
1                                                    -Input Realization number
100 0.5 1                                           -nx, xmn, xsiz
100 0.5 1                                           -ny, ymn, ysiz
1 0.5 1                                             -nz, zmn, zsiz
100 0.5 1                                           -nx, xmn, xsiz
100 0.5 1                                           -ny, ymn, ysiz
80 60.5 1                                           -nz, zmn, zsiz

END

cat<<END>4.tem
      Parameters for KT3D
      *****

START OF PARAMETERS:
d:\research\gslib\output\1\tmp\VFUCT_10A_REAL.out  -file with data
0 1 2 3 8 0                                         -columns for DH,X,Y,Z,var,sec var
-1.0e21 1.0e21                                     -trimming limits
0                                                    -koption: 0=grid, 1=cross, 2=jackknife
xvk.dat                                             -file with jackknife data
1 2 0 3 0                                           -columns for X,Y,Z,vr and sec var
0                                                    -debugging level: 0,1,2,3
d:\research\gslib\debug\kt3d.dbg                   -file for debugging output
d:\research\gslib\output\1\tmp\SKUCTBTA.dat        -file for kriged output
100 0.5 1.0                                         -nx, xmn, xsiz
100 0.5 1.0                                         -ny, ymn, ysiz
80 60.5 1.0                                         -nz, zmn, zsiz
1 1 1                                               -x,y and z block discretization
2 24                                                -min, max data for kriging
0                                                    -max per octant (0-> not used)
35.0 35.0 16.0                                     -maximum search radii
0.0 0.0 0.0                                         -angles for search ellipsoid
0 SKM                                               -ktype: 0=SK,1=OK,2=non-st SK,3=exdrift
0 0 0 0 0 0 0 0 0 0                                -drift: x,y,z,xx,yy,zz,xy,xz,zy
0                                                    -0, variable; 1, estimate trend
d:\research\gslib\output\1\ext10_REAL.opt          -gridded file with drift/mean
1                                                    -column number in gridded file
1 0.0                                                -nst, nugget effect
1 1.0 00.0 0.0 0.0                                 -it,cc,ang1,ang2,ang3
35.0 35.0 16.0                                     -a_hmax, a_hmin, a_vert

END

```

```

cat<<END>5.tem

                Parameters for U_Tonnes
                *****

START OF PARAMETERS:
d:\research\gslib\output\1\tmp\SKUCTBTA.dat           -Input model
d:\research\gslib\output\1\True_Tonnage_1A.rpt       -Input True Tonnages
DSX                                                    -Drill spacing
UCT                                                    -Uncertainty Constant C
BTA                                                    -beta
1 1 1                                                 -dx,dy,dz Cell Sizes
1                                                      -Specific Gravity
REAL                                                  -Realization
d:\research\gslib\output\1\reports\CUCTBTA.rpt       -Append to tonnage report
END

for ((cnt =1; cnt <=50; cnt++))
do
  # Start Drilling
  sed -e "s/REAL/${cnt}/g" \
  1.tem > par.temp1
  sed -e "s/UCT/$CCONST/g" \
  par.temp1 > par.temp1a
  echo par.temp1a | d:/research/gslib/source/drill15

  # Start VF Calcs
  sed -e "s/REAL/${cnt}/g" \
  2.tem > par.temp2
  sed -e "s/UCT/$CCONST/g" \
  par.temp2a > par.temp2b
  sed -e "s/BTA/$BETA/g" \
  par.temp2b > par.temp2c
  echo par.temp2c | d:/research/gslib/source/dfv4

  # Start DF Optimize
  sed -e "s/REAL/${cnt}/g" \
  3.tem > par.temp3
  sed -e "s/UCT/$CCONST/g" \
  par.temp3 > par.temp3a
  echo par.temp3a | d:/research/gslib/source/DF-opt

  # Start KRIGING Calcs
  sed -e "s/REAL/${cnt}/g" \
  4.tem > par.temp4
  sed -e "s/UCT/$CCONST/g" \
  par.temp4 > par.temp4a
  sed -e "s/BTA/$BETA/g" \
  par.temp4a > par.temp4b
  sed -e "s/SKM/$SKMEAN/g" \
  par.temp4b > par.temp4c
  echo par.temp4c | d:/research/gslib/source/kt3d-mjm

  # Start TONNAGE Calcs
  sed -e "s/REAL/${cnt}/g" \
  5.tem > par.temp5
  sed -e "s/DSX/$DSPACE/g" \
  par.temp5 > par.temp5a
  sed -e "s/UCT/$CCONST/g" \
  par.temp5a > par.temp5b
  sed -e "s/BTA/$BETA/g" \
  par.temp5b > par.temp5c
  echo par.temp5c | d:/research/gslib/source/U_tonnes2
done

```

# Appendix B: Program Results

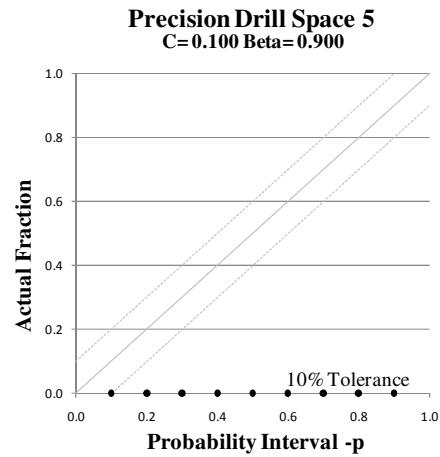
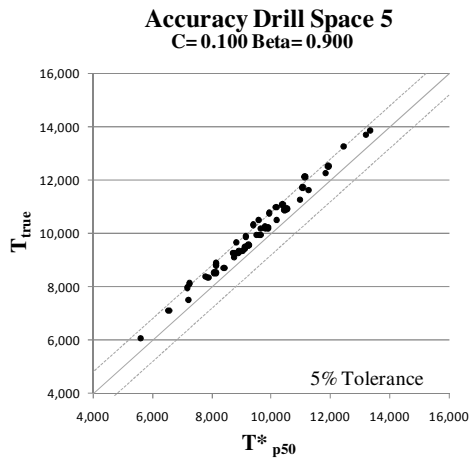
## B.1 5 Unit Drillhole Spacing

Table B.1: Run Results

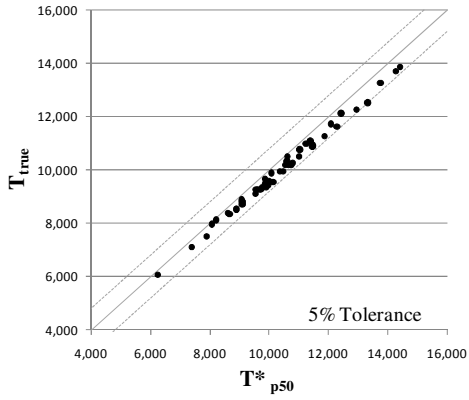
5 Unit Drillhole Spacing

Run	N	C	$\beta$	O1	O2
1	50	0.100	0.900	-0.05	-1.00
2	50	0.100	1.100	0.04	-0.92
3	50	0.100	1.013	0.00	-0.15
4	50	0.300	0.900	-0.05	-0.52
5	50	0.300	1.100	0.04	-0.03
6	50	0.300	1.020	0.00	0.65
7	50	0.250	1.018	0.00	0.57
8	50	0.213	1.017	0.00	0.48
9	50	0.185	1.016	0.00	0.41
10	50	0.164	1.015	0.00	0.30
11	50	0.121	1.014	0.00	0.05

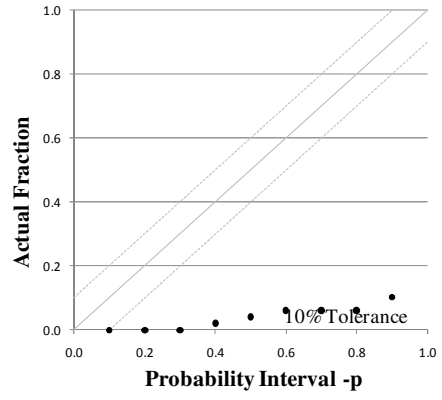
### Accuracy and Precision Plots – 5 Unit Spacing in order of run number



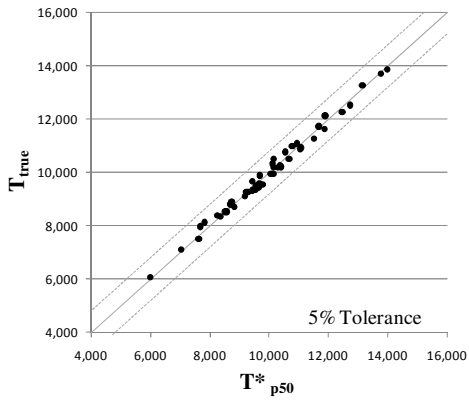
**Accuracy Drill Space 5**  
C=0.100 Beta= 1.100



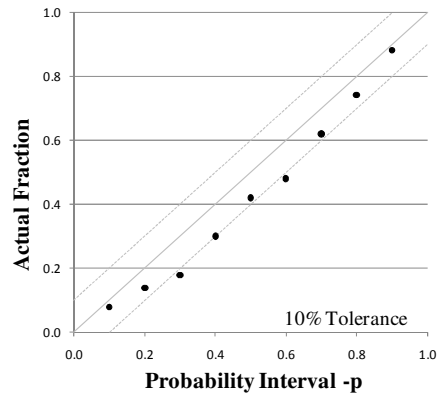
**Precision Drill Space 5**  
C=0.100 Beta= 1.100



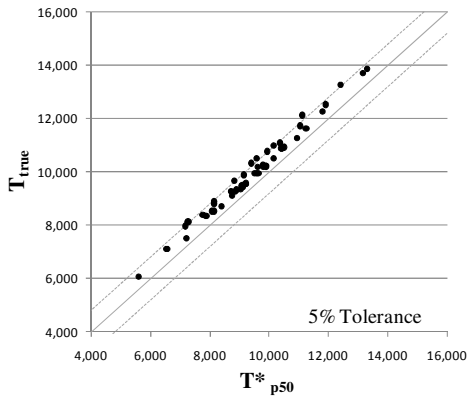
**Accuracy Drill Space 5**  
C=0.100 Beta= 1.013



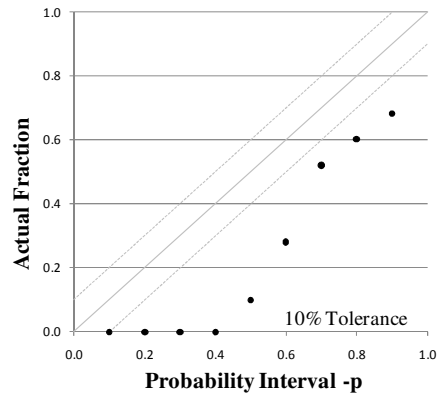
**Precision Drill Space 5**  
C=0.100 Beta= 1.013



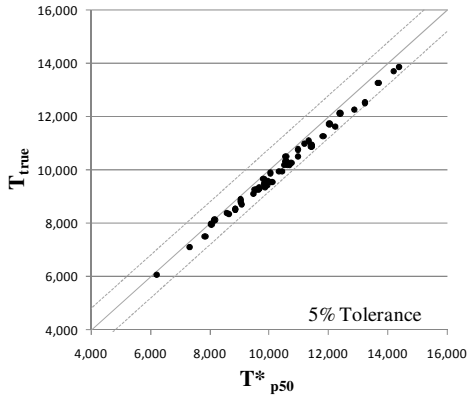
**Accuracy Drill Space 5**  
C=0.300 Beta= 0.900



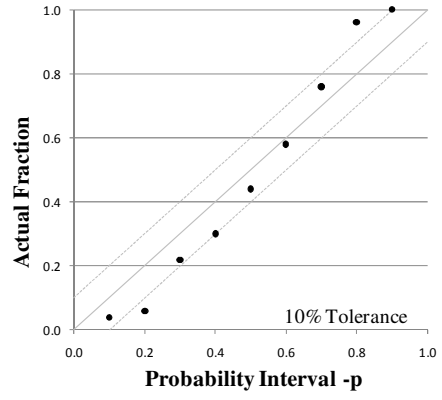
**Precision Drill Space 5**  
C=0.300 Beta= 0.900



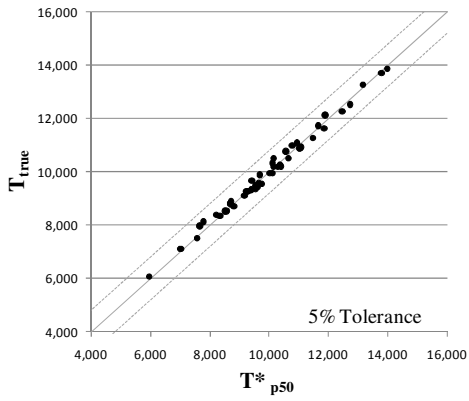
**Accuracy Drill Space 5**  
C=0.300 Beta= 1.100



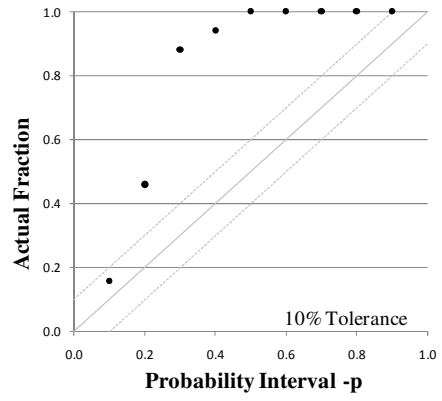
**Precision Drill Space 5**  
C=0.300 Beta= 1.100



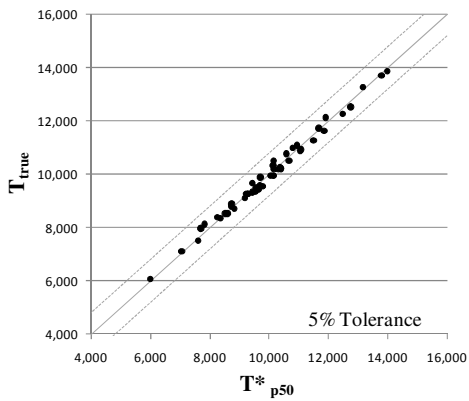
**Accuracy Drill Space 5**  
C=0.300 Beta= 1.020



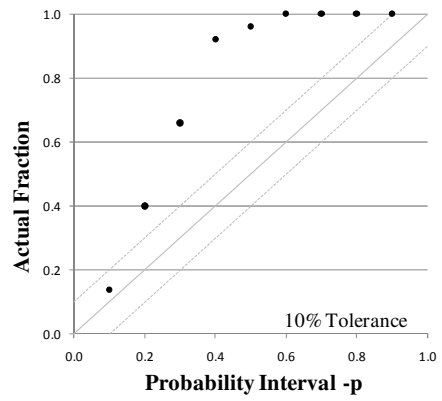
**Precision Drill Space 5**  
C=0.300 Beta= 1.020



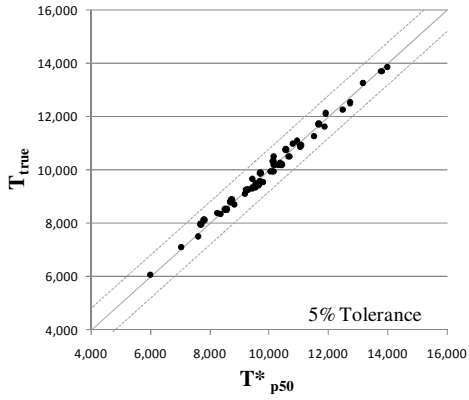
**Accuracy Drill Space 5**  
C=0.250 Beta= 1.018



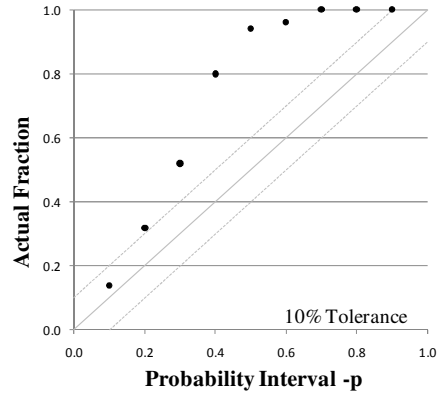
**Precision Drill Space 5**  
C=0.250 Beta= 1.018



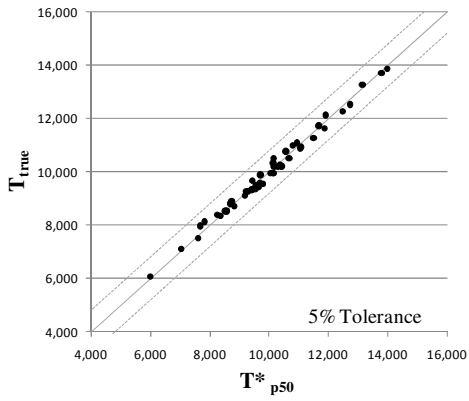
**Accuracy Drill Space 5**  
C=0.213 Beta= 1.017



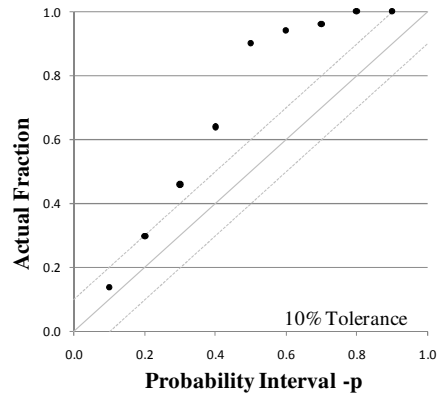
**Precision Drill Space 5**  
C=0.213 Beta= 1.017



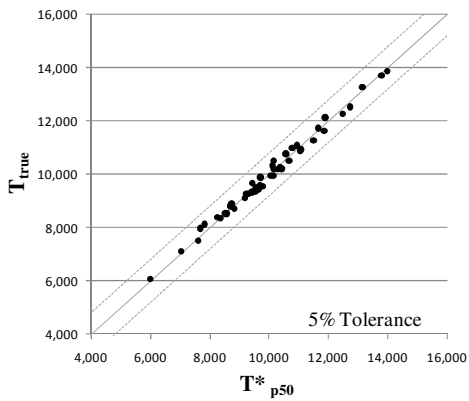
**Accuracy Drill Space 5**  
C=0.185 Beta= 1.016



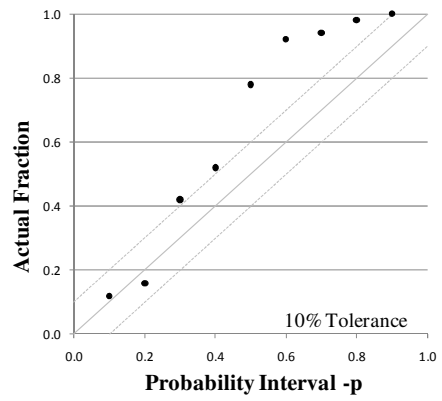
**Precision Drill Space 5**  
C=0.185 Beta= 1.016



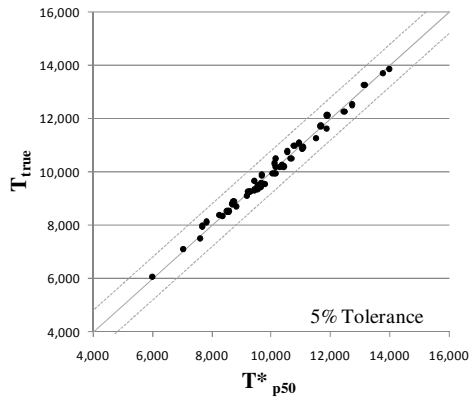
**Accuracy Drill Space 5**  
C=0.164 Beta= 1.015



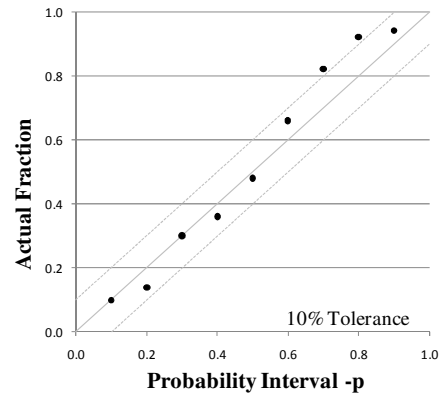
**Precision Drill Space 5**  
C=0.164 Beta= 1.015



**Accuracy Drill Space 5**  
 $C=0.121$   $\text{Beta}=1.014$



**Precision Drill Space 5**  
 $C=0.121$   $\text{Beta}=1.014$

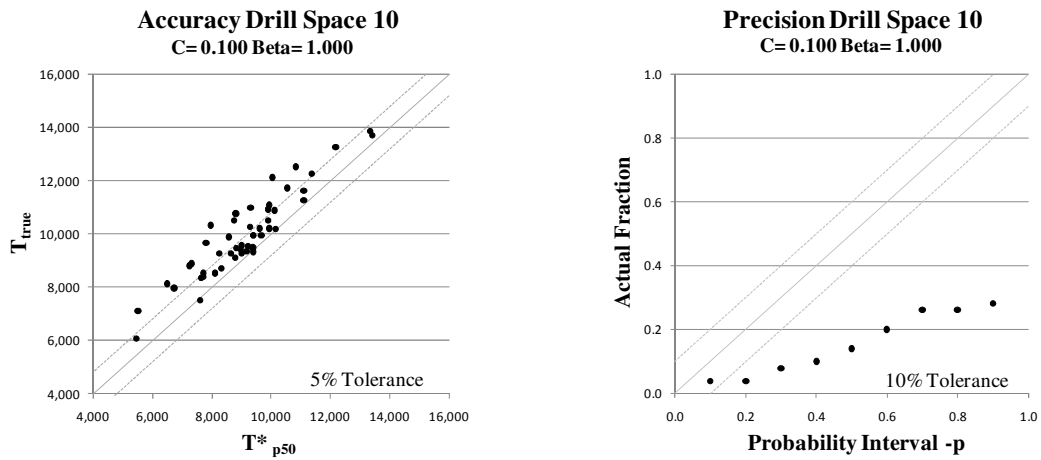


## B.2 10 Unit Drillhole Spacing

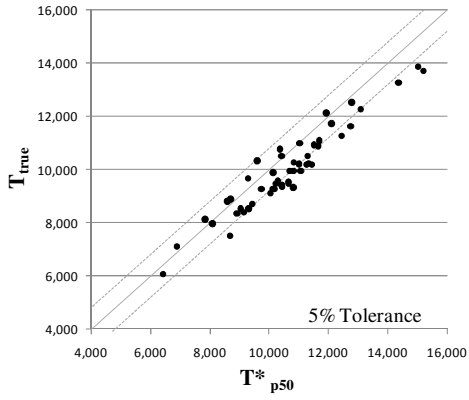
Table B.2: Run Results

10 Unit Drillhole Spacing						
Run	N	C	$\beta$	O1	O2	
1	50	0.100	1.000	-0.08	-0.69	
2	50	0.100	1.200	0.06	-0.67	
3	50	0.100	1.115	0.00	-0.38	
4	50	0.300	1.000	-0.09	-0.23	
5	50	0.300	1.200	0.04	0.23	
6	50	0.300	1.138	0.00	0.43	
7	50	0.200	1.127	0.00	0.14	
8	50	0.173	1.124	0.00	0.00	

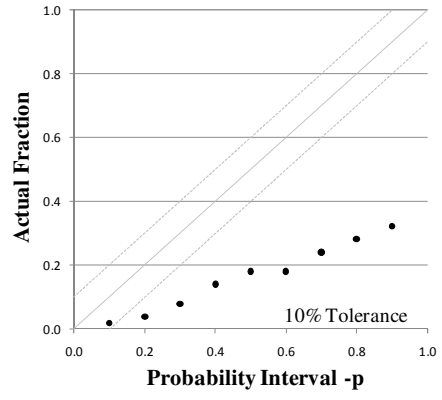
### Accuracy and Precision Plots – 10 Unit Spacing in order of run number



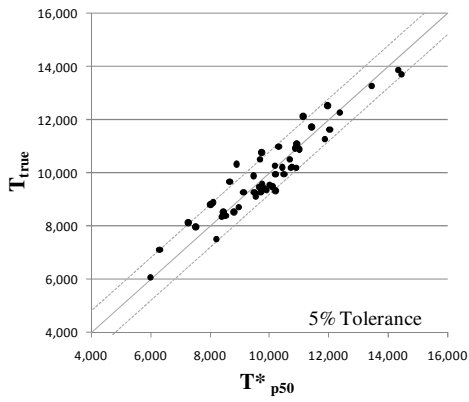
**Accuracy Drill Space 10**  
**C=0.100 Beta= 1.200**



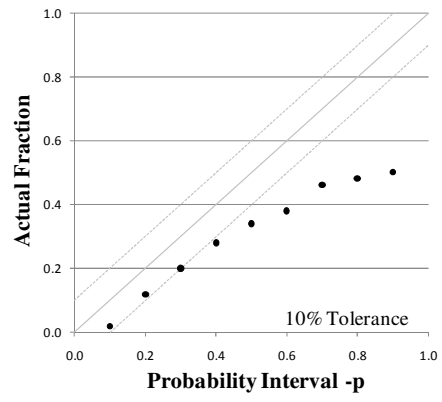
**Precision Drill Space 10**  
**C=0.100 Beta= 1.200**



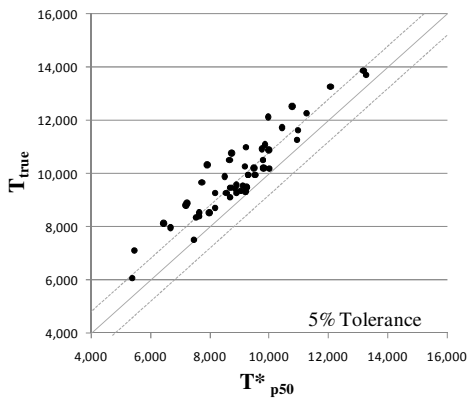
**Accuracy Drill Space 10**  
**C=0.100 Beta= 1.115**



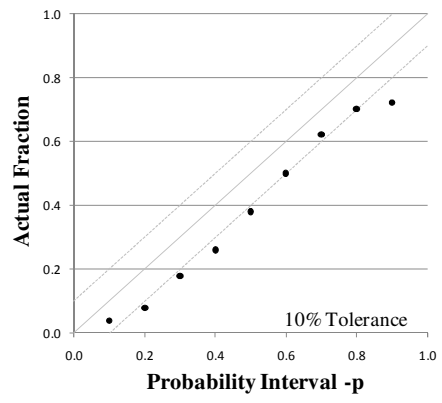
**Precision Drill Space 10**  
**C=0.100 Beta= 1.115**



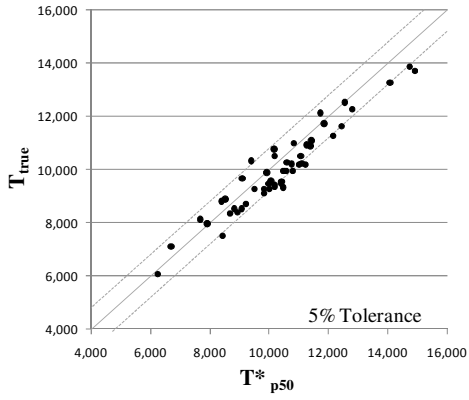
**Accuracy Drill Space 10**  
**C=0.300 Beta= 1.000**



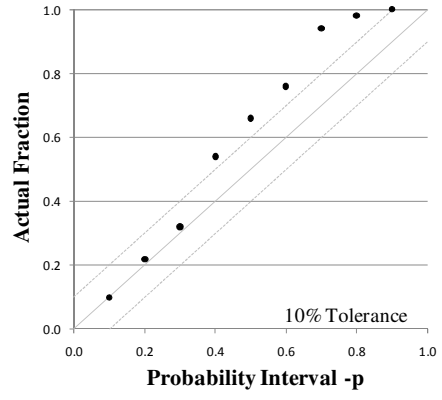
**Precision Drill Space 10**  
**C=0.300 Beta= 1.000**



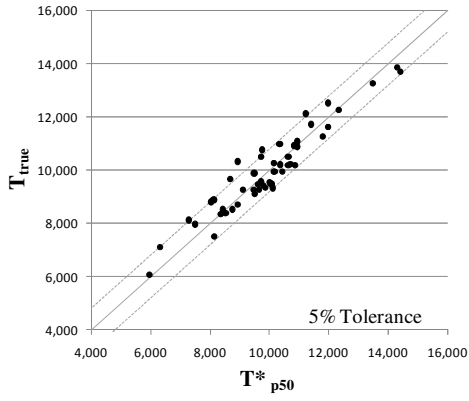
**Accuracy Drill Space 10**  
C=0.300 Beta=1.200



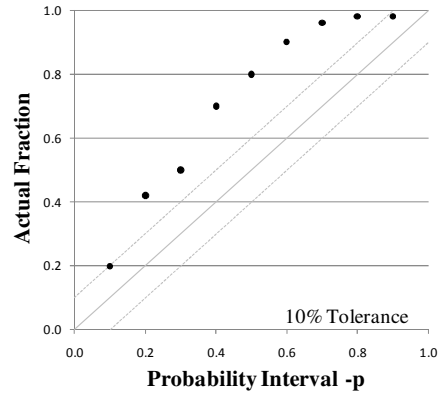
**Precision Drill Space 10**  
C=0.300 Beta=1.200



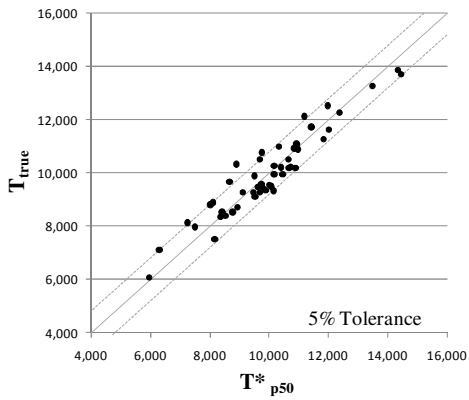
**Accuracy Drill Space 10**  
C=0.300 Beta=1.138



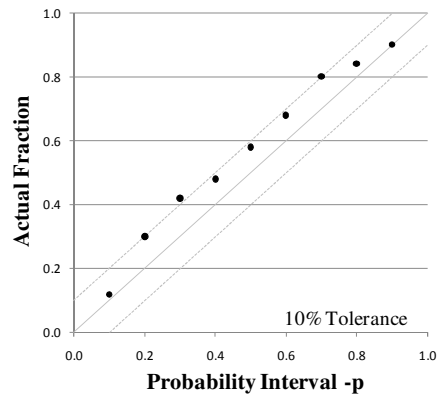
**Precision Drill Space 10**  
C=0.300 Beta=1.138



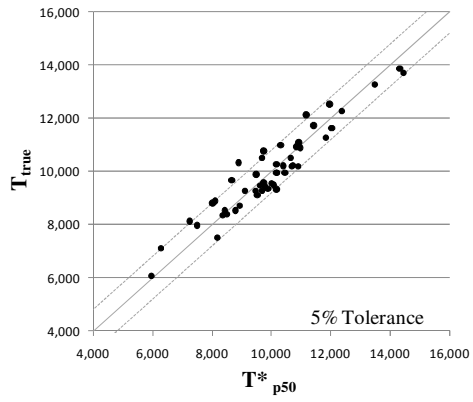
**Accuracy Drill Space 10**  
C=0.200 Beta=1.127



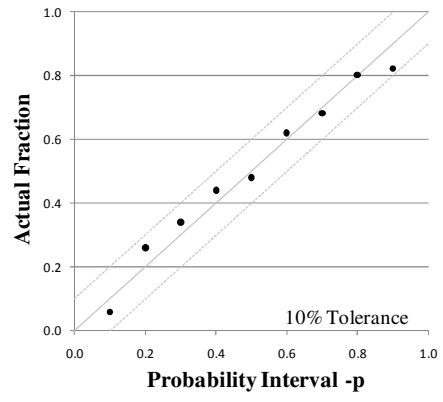
**Precision Drill Space 10**  
C=0.200 Beta=1.127



**Accuracy Drill Space 10**  
C=0.173 Beta= 1.124



**Precision Drill Space 10**  
C=0.173 Beta= 1.124



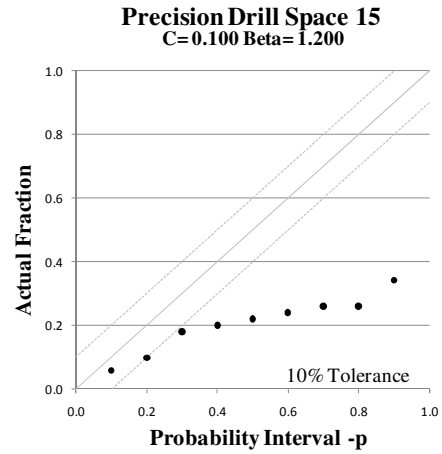
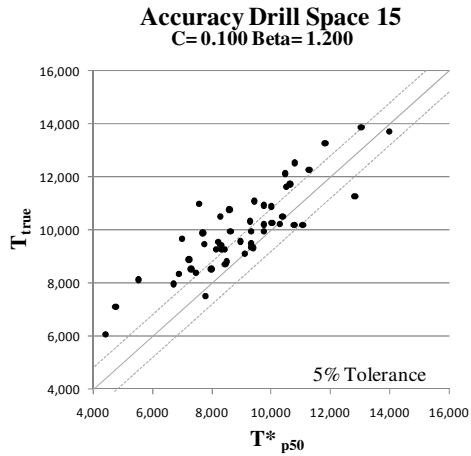
### B.3 15 Unit Drillhole Spacing

Table B.3: Run Results

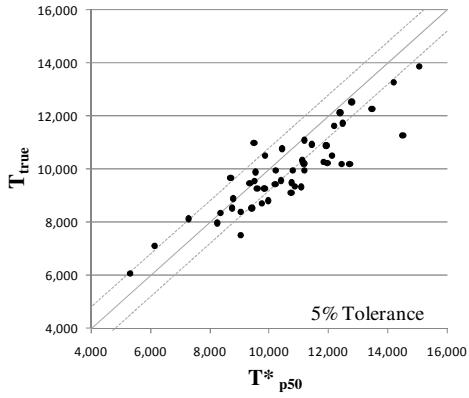
15 Unit Drillhole Spacing

Run	N	C	$\beta$	O1	O2
1	50	0.100	1.200	-0.10	-0.59
2	50	0.100	1.400	0.07	-0.49
3	50	0.100	1.318	0.00	-0.32
4	50	0.300	1.200	-0.12	-0.21
5	50	0.300	1.400	0.02	0.39
6	50	0.300	1.370	0.00	0.40
7	50	0.188	1.341	0.00	0.10
8	50	0.200	1.344	0.00	0.16
9	50	0.167	1.335	0.00	0.02
10	50	0.150	1.331	0.00	-0.04
11	50	0.163	1.334	0.00	0.01

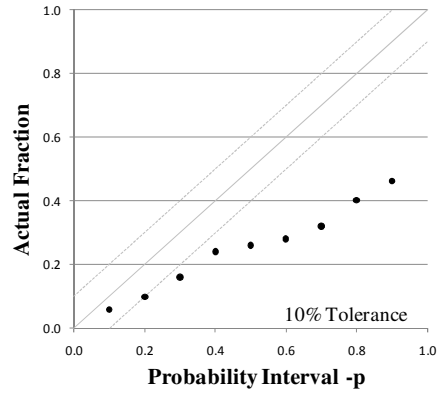
#### Accuracy and Precision Plots – 15 Unit Spacing in order of run number



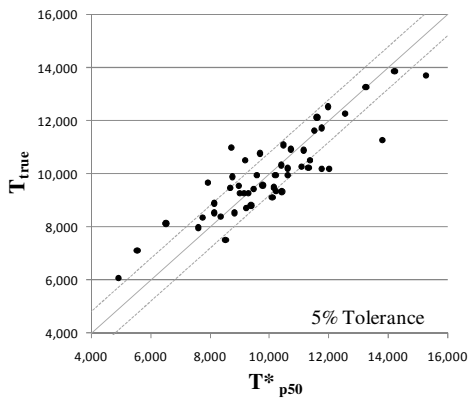
**Accuracy Drill Space 15**  
C=0.100 Beta= 1.400



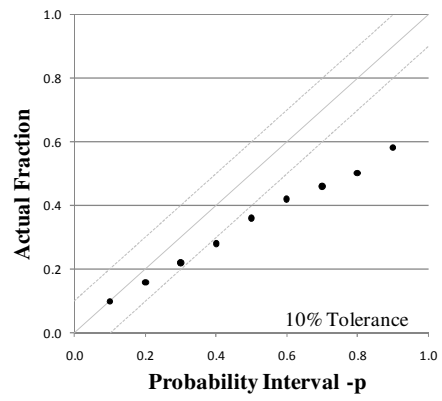
**Precision Drill Space 15**  
C=0.100 Beta= 1.400



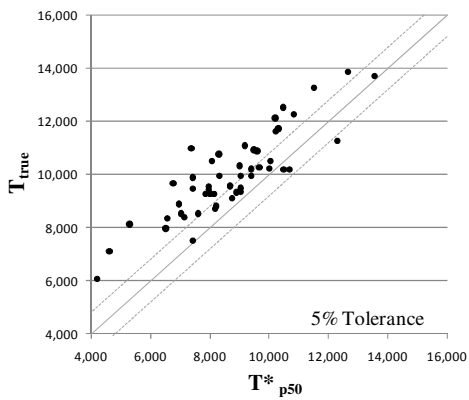
**Accuracy Drill Space 15**  
C=0.100 Beta= 1.318



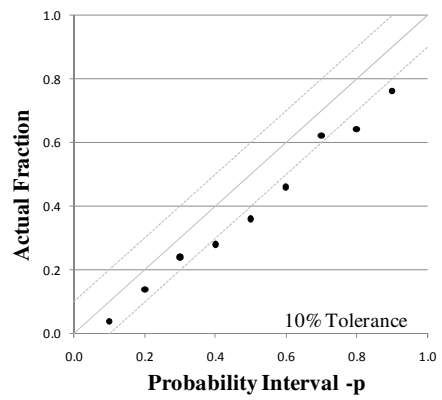
**Precision Drill Space 15**  
C=0.100 Beta= 1.318



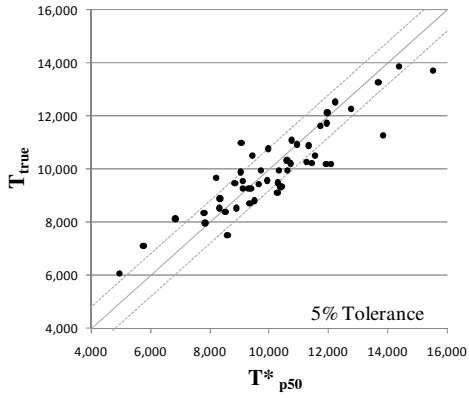
**Accuracy Drill Space 15**  
C=0.300 Beta= 1.200



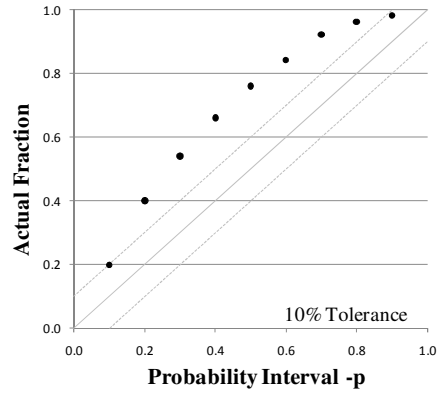
**Precision Drill Space 15**  
C=0.300 Beta= 1.200



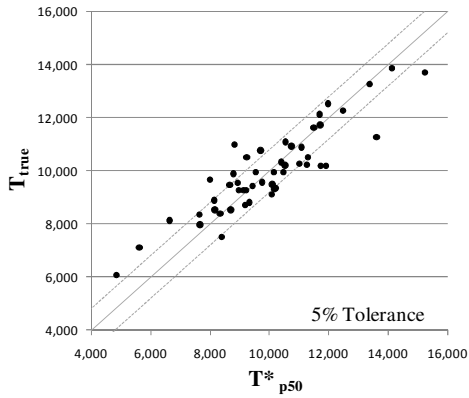
**Accuracy Drill Space 15**  
C=0.300 Beta= 1.400



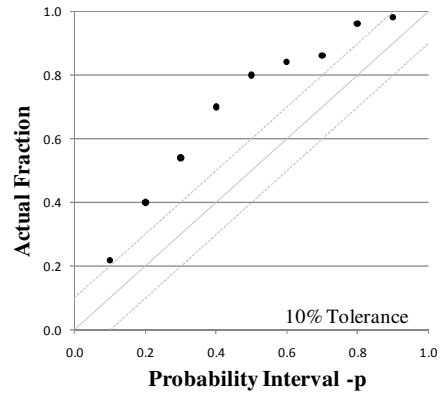
**Precision Drill Space 15**  
C=0.300 Beta= 1.400



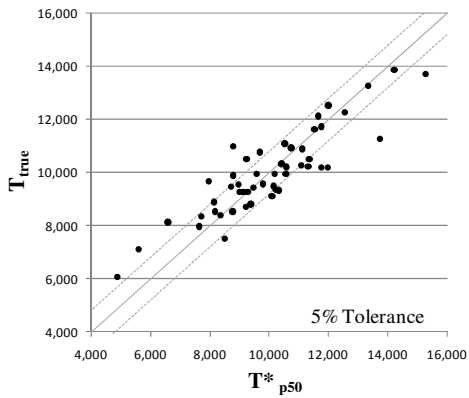
**Accuracy Drill Space 15**  
C=0.300 Beta= 1.370



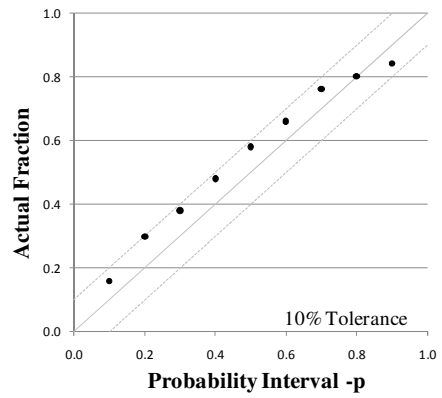
**Precision Drill Space 15**  
C=0.300 Beta= 1.370



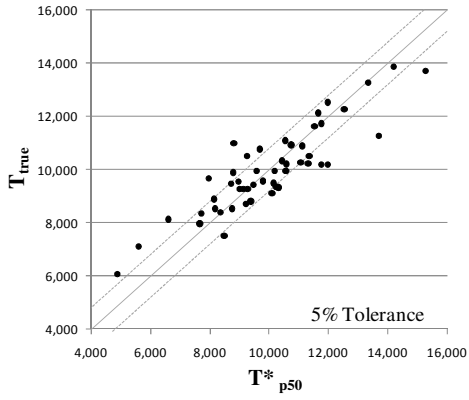
**Accuracy Drill Space 15**  
C=0.188 Beta= 1.341



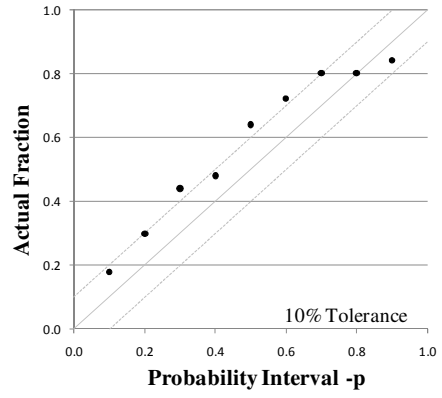
**Precision Drill Space 15**  
C=0.188 Beta= 1.341



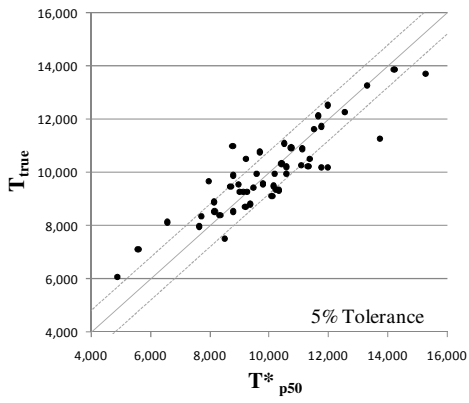
**Accuracy Drill Space 15**  
C=0.200 Beta= 1.344



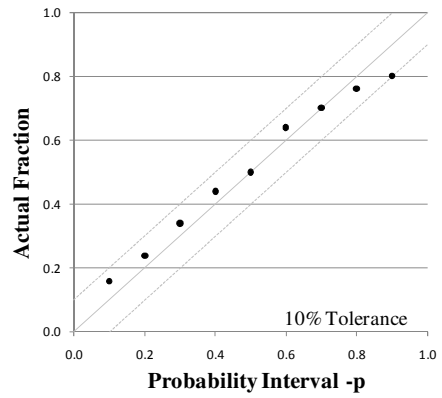
**Precision Drill Space 15**  
C=0.200 Beta= 1.344



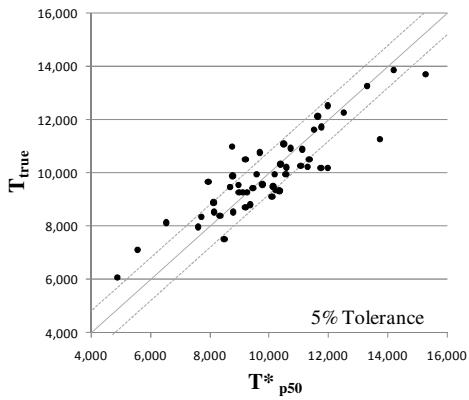
**Accuracy Drill Space 15**  
C=0.167 Beta= 1.335



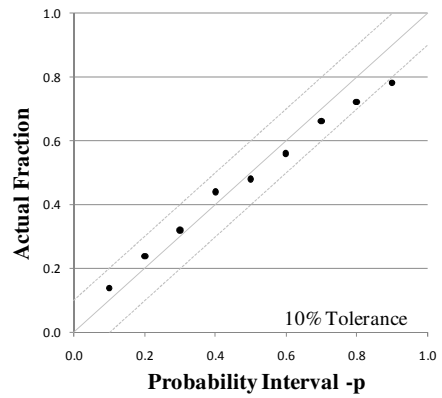
**Precision Drill Space 15**  
C=0.167 Beta= 1.335

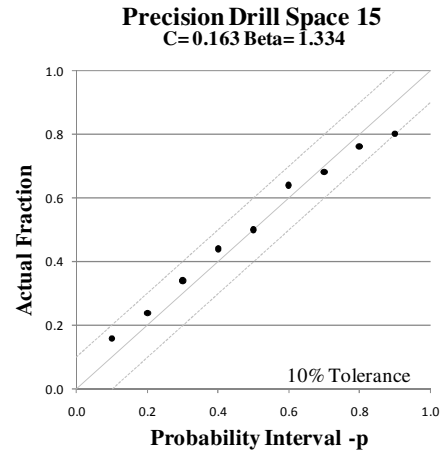
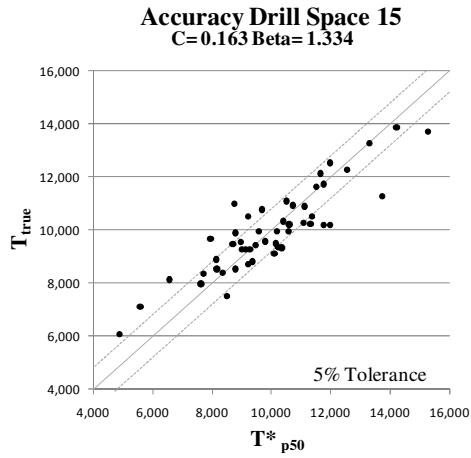


**Accuracy Drill Space 15**  
C=0.150 Beta= 1.331



**Precision Drill Space 15**  
C=0.150 Beta= 1.331





## B.4 20 Unit Drillhole Spacing

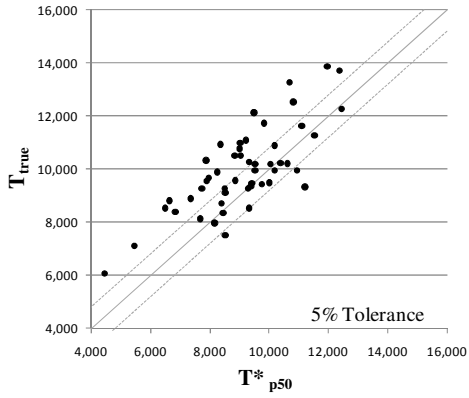
Table B.4: Run Results

20 Unit Drillhole Spacing

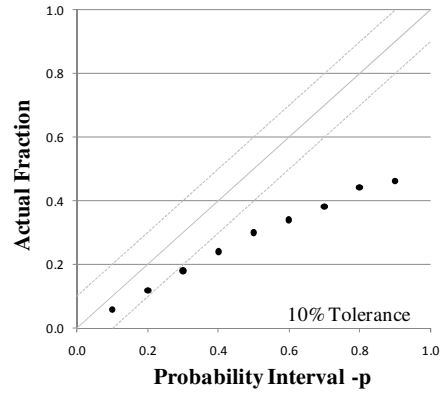
Run	N	C	$\beta$	O1	O2
1	50	0.100	1.400	-0.08	-0.44
2	50	0.100	1.600	0.08	-0.32
3	50	0.100	1.498	0.00	-0.49
4	50	0.300	1.400	-0.11	-0.02
5	50	0.300	1.600	0.03	0.42
6	50	0.300	1.560	0.00	0.41
7	50	0.200	1.529	0.00	0.10
8	50	0.183	1.524	0.00	0.02
9	50	0.150	1.514	0.00	-0.16
10	50	0.181	1.524	0.00	0.00

Accuracy and Precision Plots – 20 Unit Spacing in order of run number

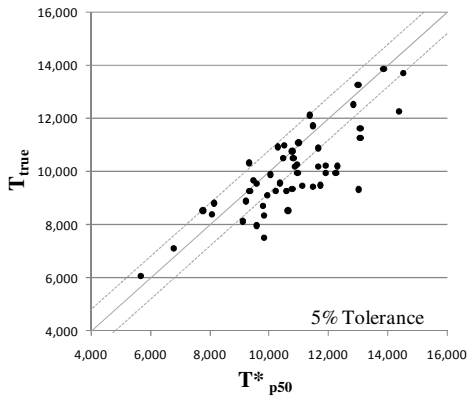
**Accuracy Drill Space 20**  
C=0.100 Beta= 1.400



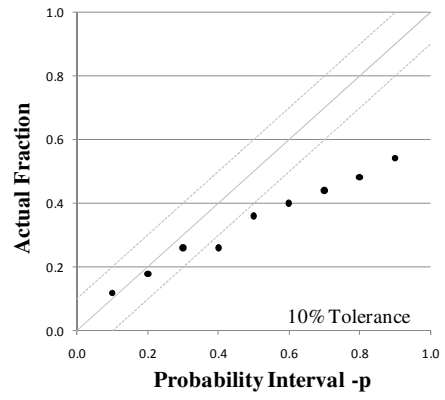
**Precision Drill Space 20**  
C=0.100 Beta= 1.400



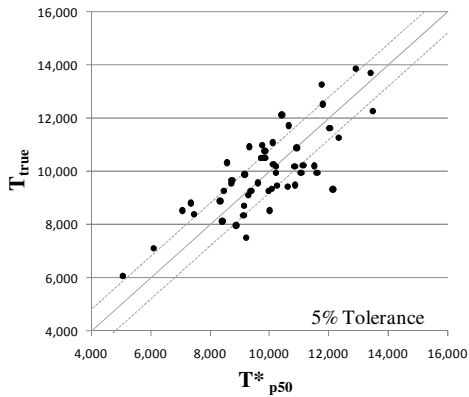
**Accuracy Drill Space 20**  
C=0.100 Beta= 1.600



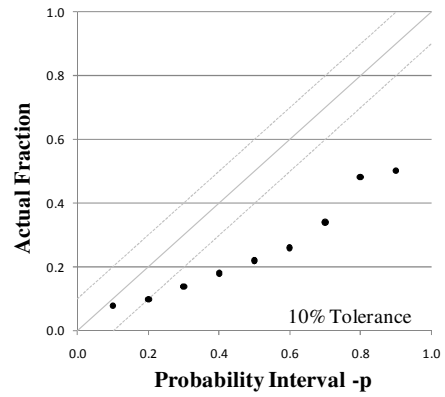
**Precision Drill Space 20**  
C=0.100 Beta= 1.600

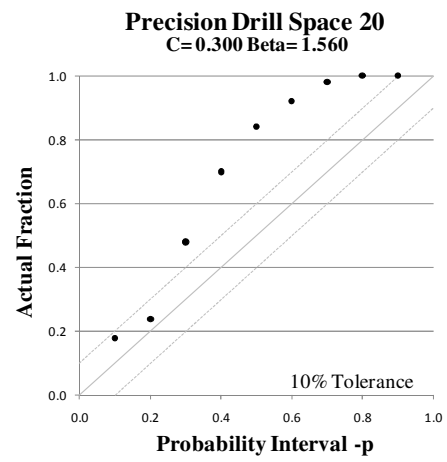
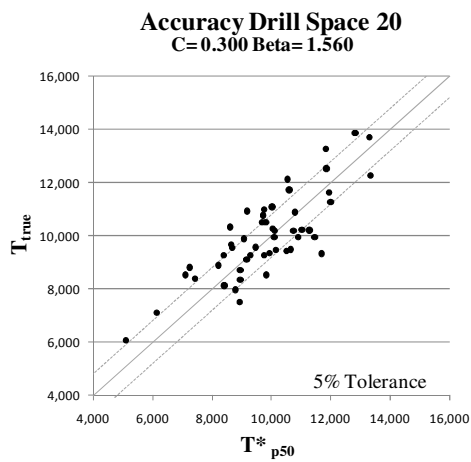
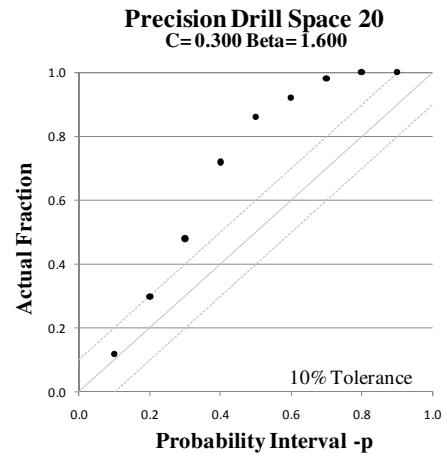
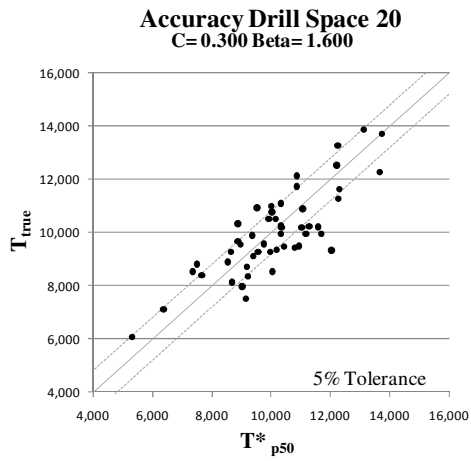
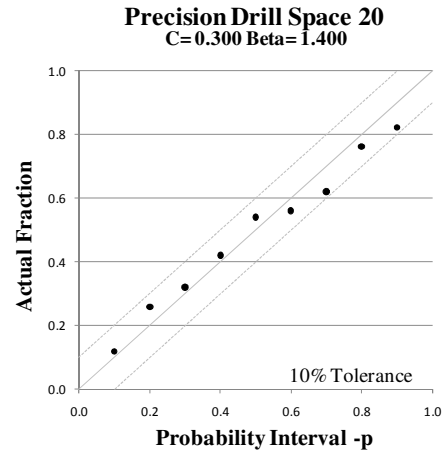
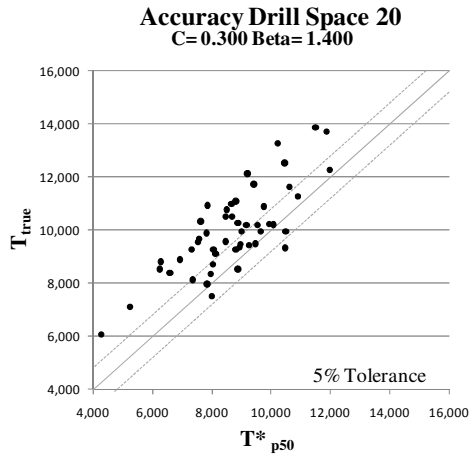


**Accuracy Drill Space 20**  
C=0.100 Beta= 1.498

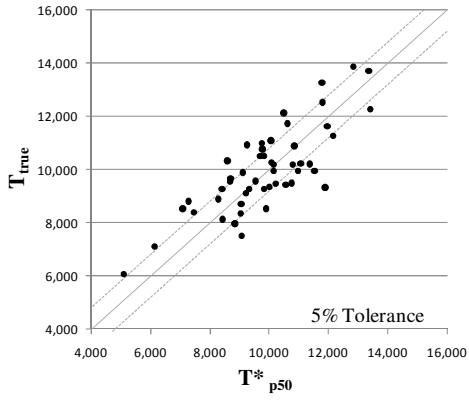


**Precision Drill Space 20**  
C=0.100 Beta= 1.498

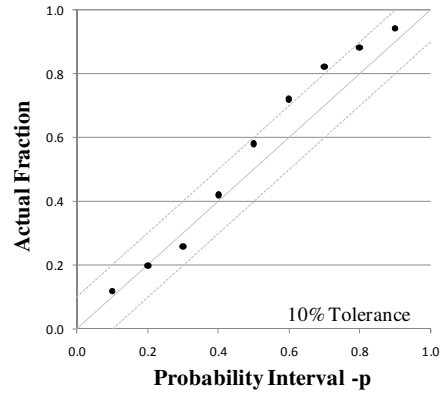




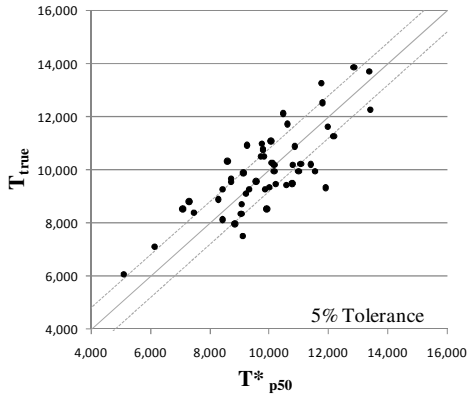
**Accuracy Drill Space 20**  
 $C=0.200$   $\text{Beta}=1.529$



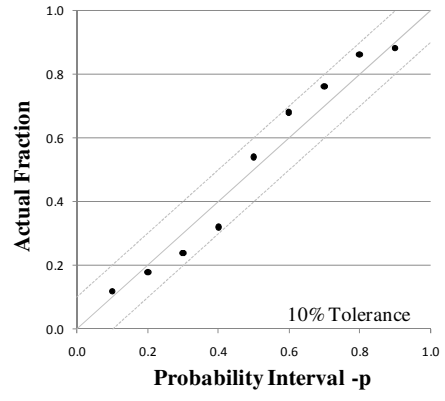
**Precision Drill Space 20**  
 $C=0.200$   $\text{Beta}=1.529$



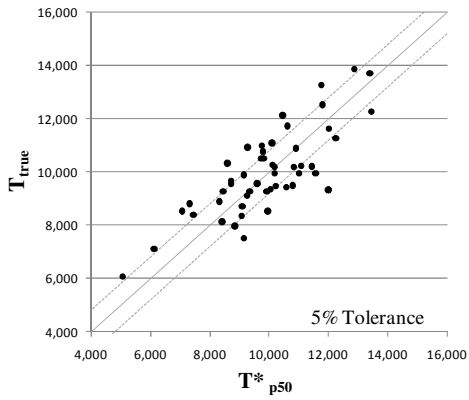
**Accuracy Drill Space 20**  
 $C=0.183$   $\text{Beta}=1.524$



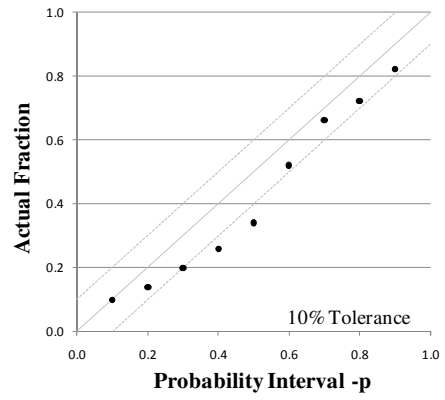
**Precision Drill Space 20**  
 $C=0.183$   $\text{Beta}=1.524$



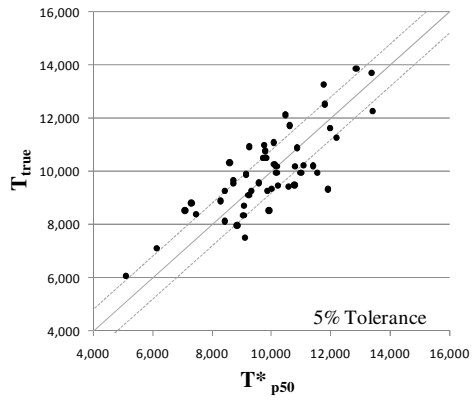
**Accuracy Drill Space 20**  
 $C=0.150$   $\text{Beta}=1.514$



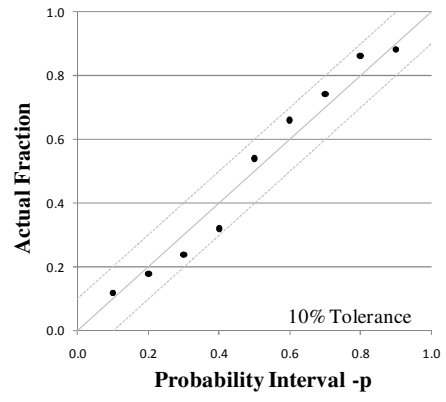
**Precision Drill Space 20**  
 $C=0.150$   $\text{Beta}=1.514$



**Accuracy Drill Space 20**  
 $C=0.181$   $\text{Beta}=1.523$



**Precision Drill Space 20**  
 $C=0.181$   $\text{Beta}=1.523$



# Appendix C: Practical Example Figures

## C.1 3D View

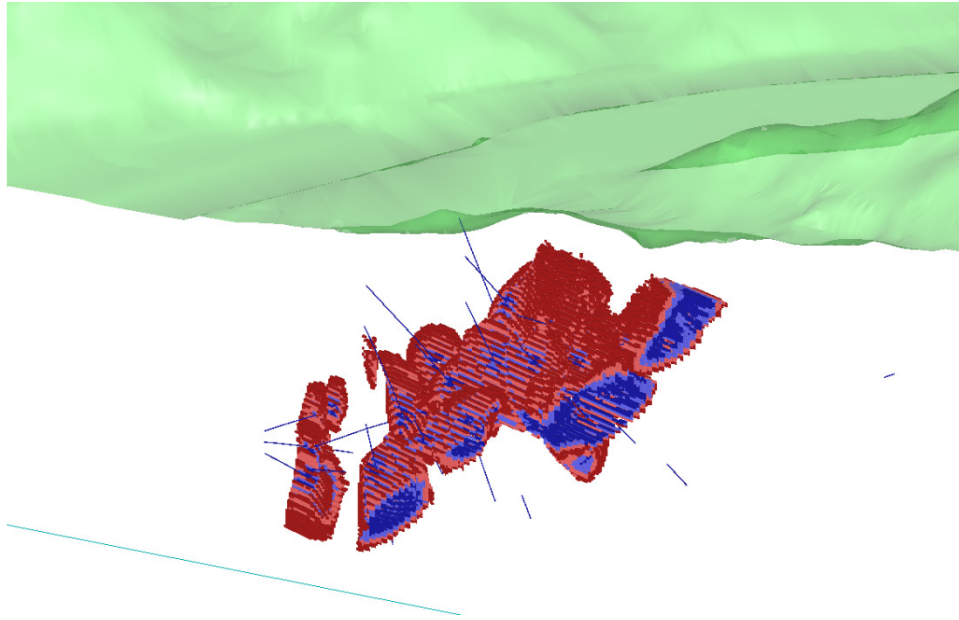


**Figure C-1:** Oblique slice through DF model (Not to Scale).

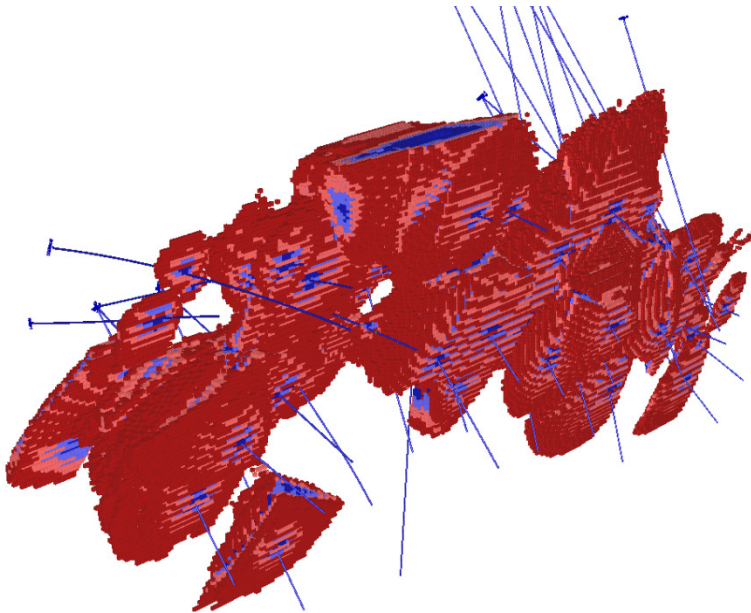


**Figure C-2:** Isometric View of DF Model bounded by  $-C$  and  $+C$  (Not to Scale).

## C.2 Vertical Cross Sections of the DF

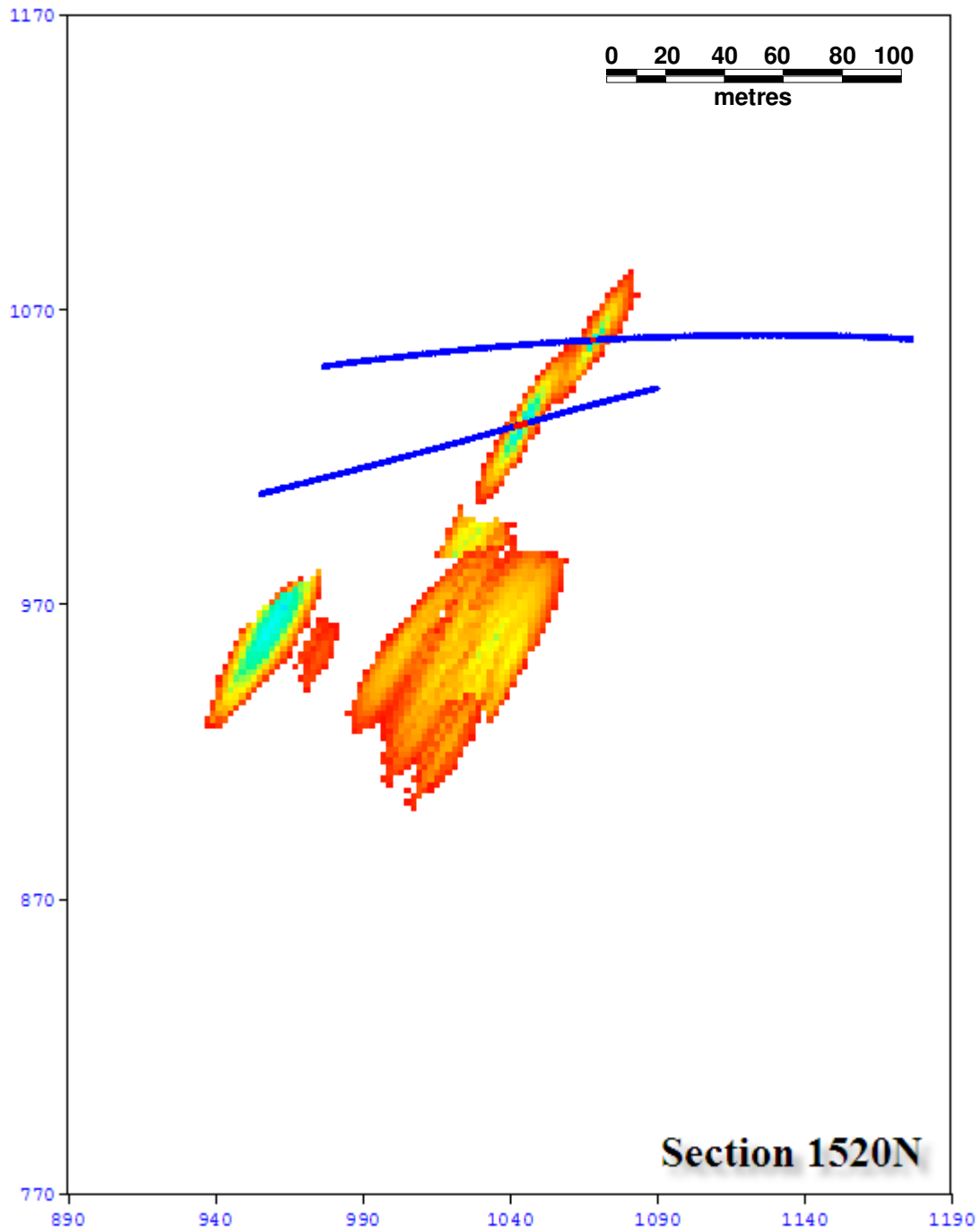
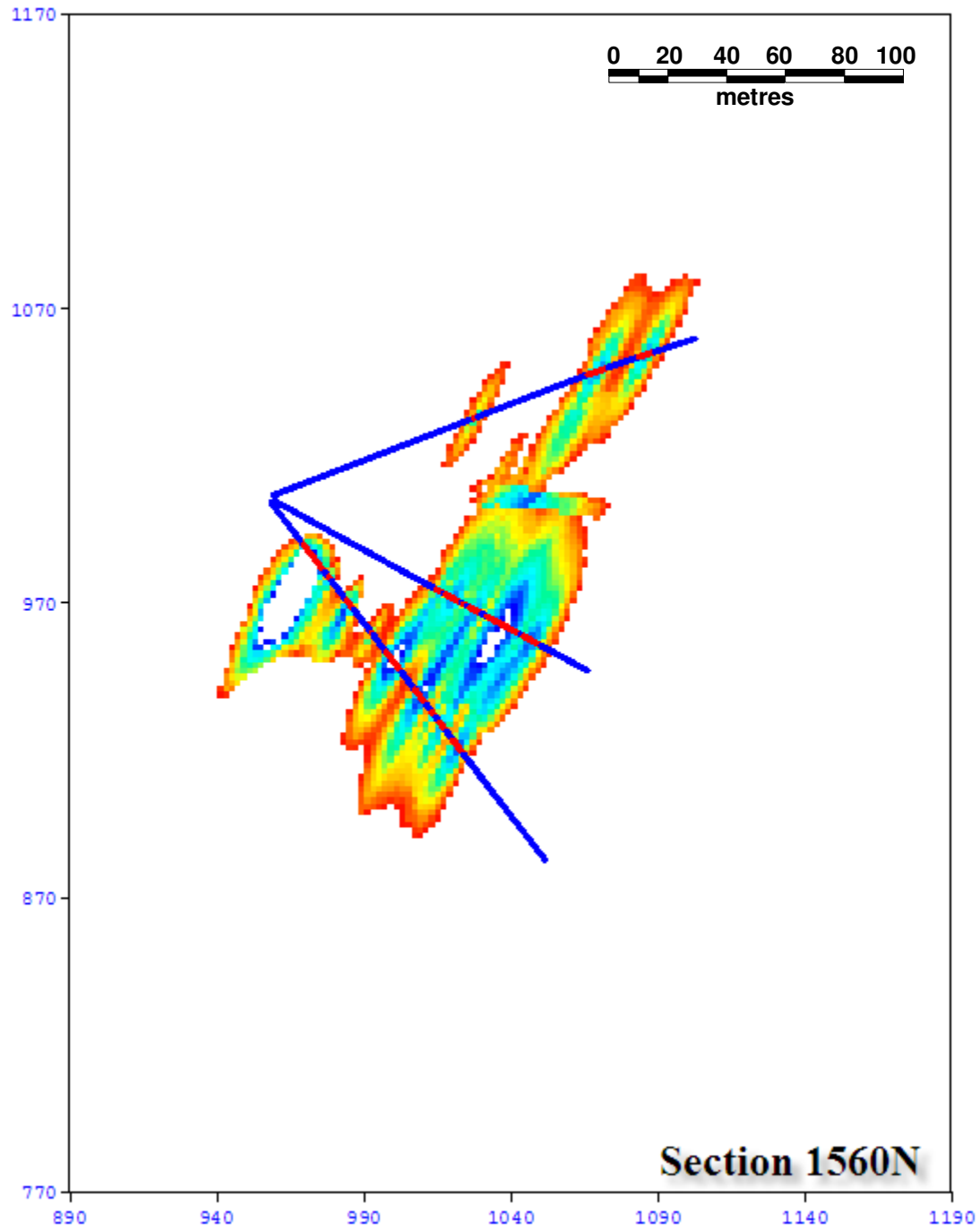
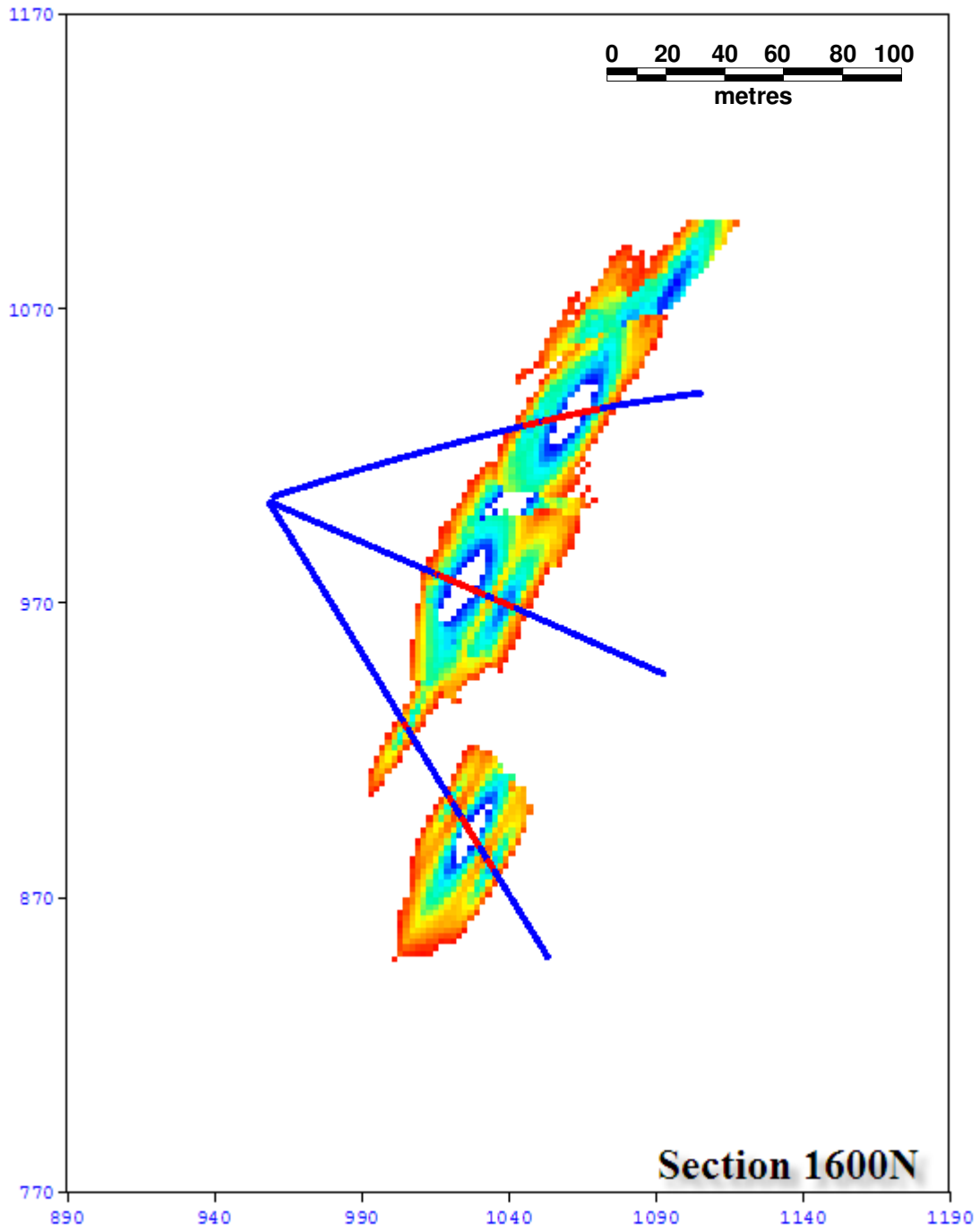


Figure C-3: Distance function model on vertical cross section 1520N.



**Figure C-4:** Distance function model on vertical cross section 1560N.



**Figure C-5:** Distance function model on vertical cross section 1600N.

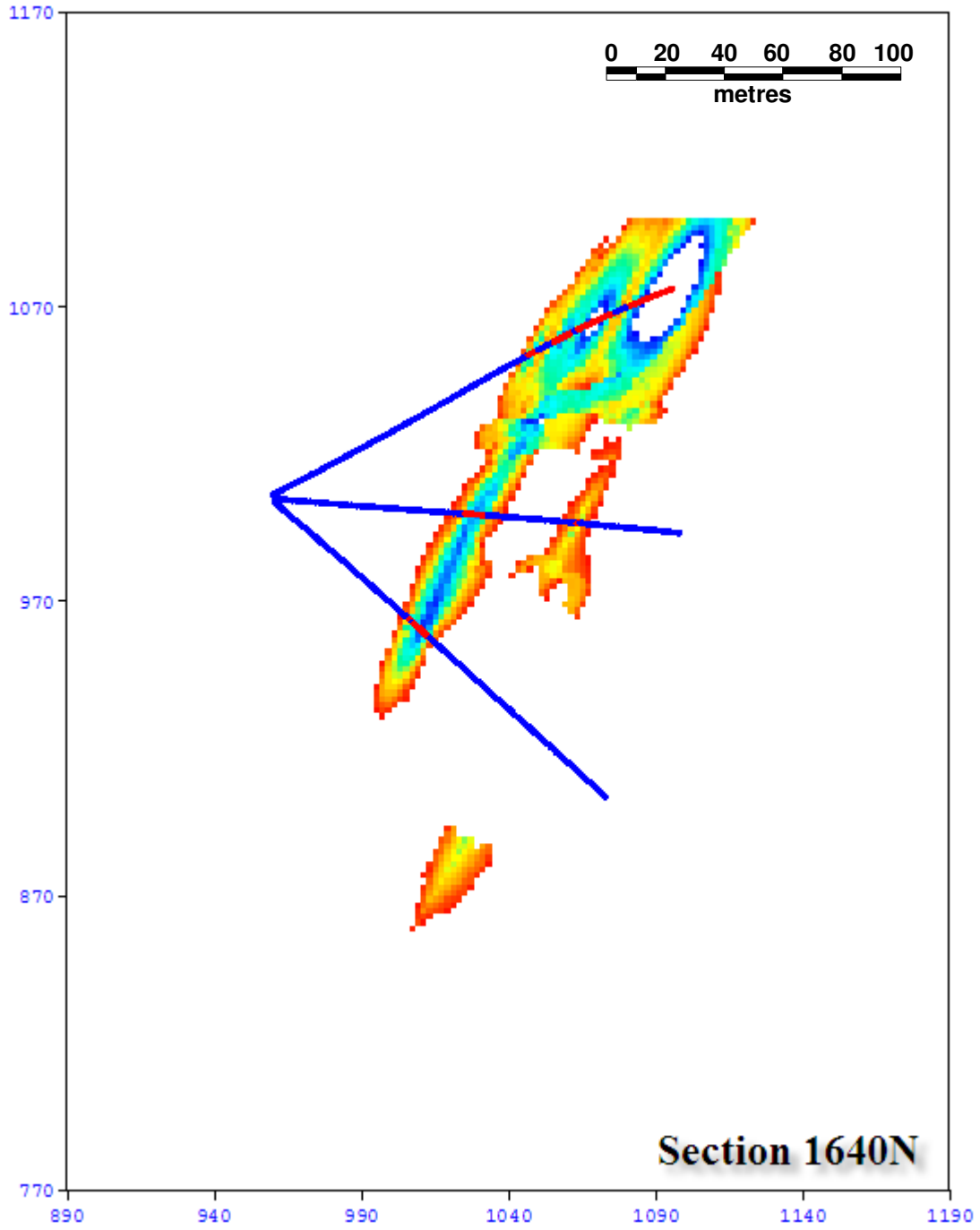


**Figure C-6:** Distance function model on vertical cross section 1640N.

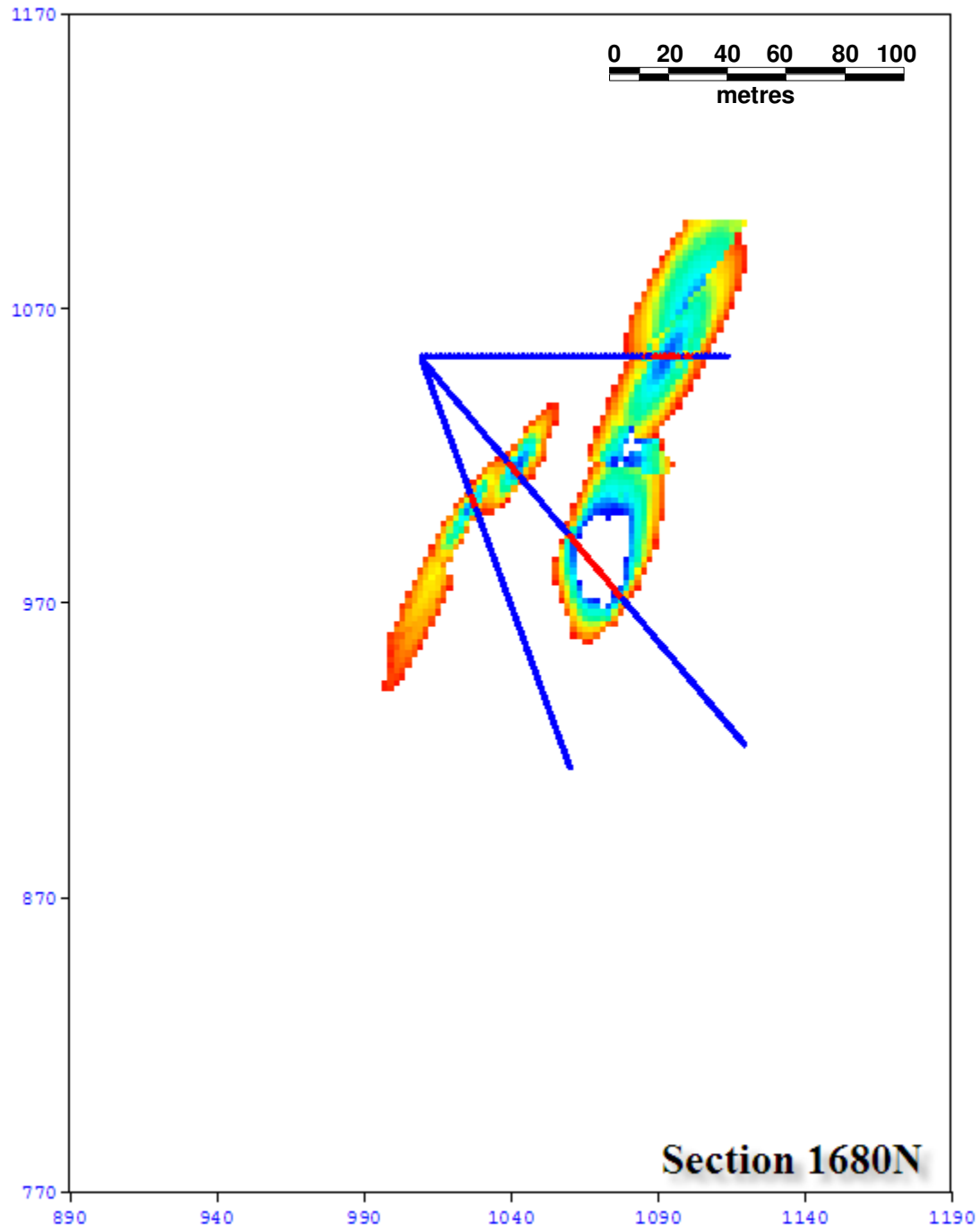


**Figure C-7:** Distance function model on vertical cross section 1680N.

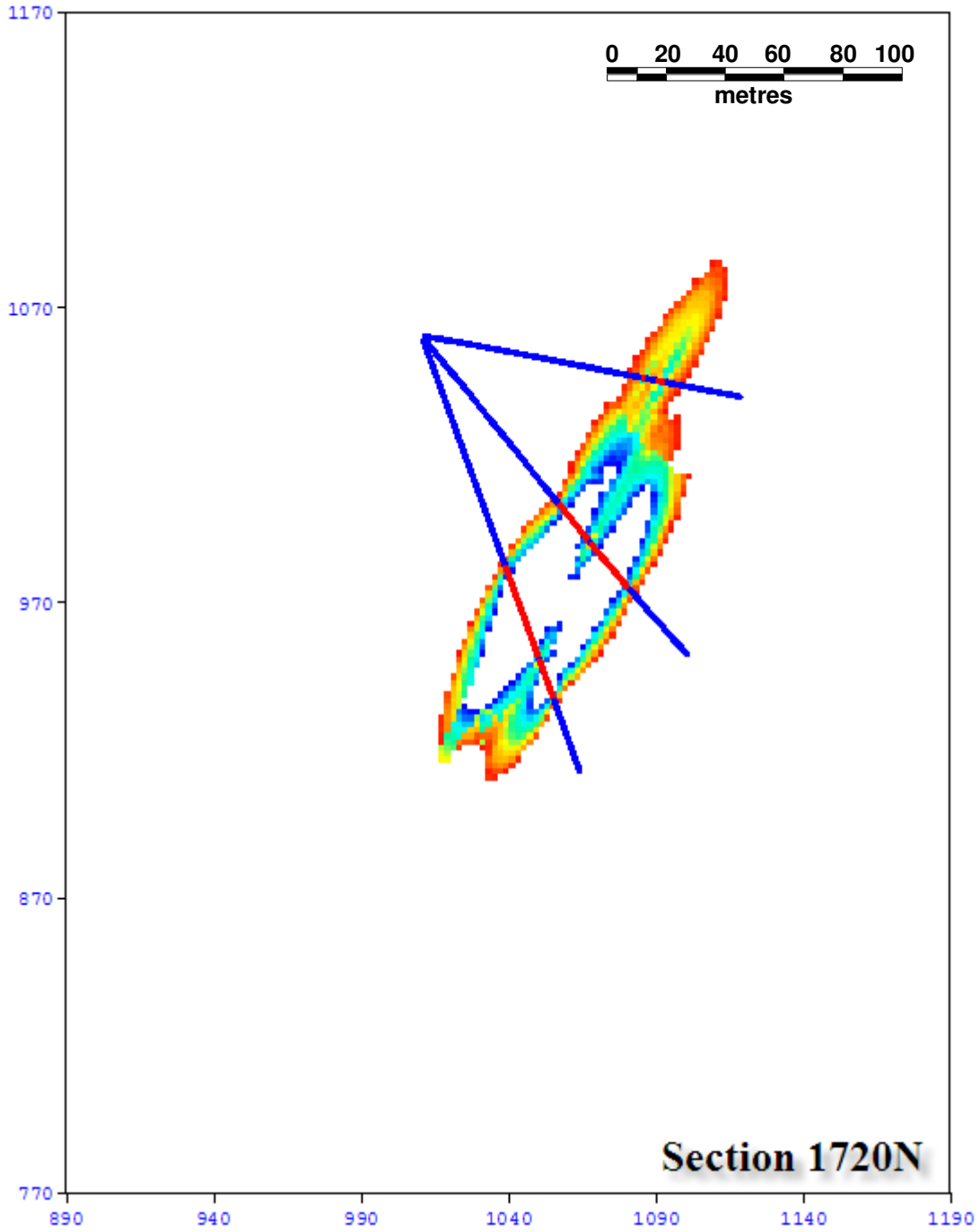


**Figure C-8:** Distance function model on vertical cross section 1720N.

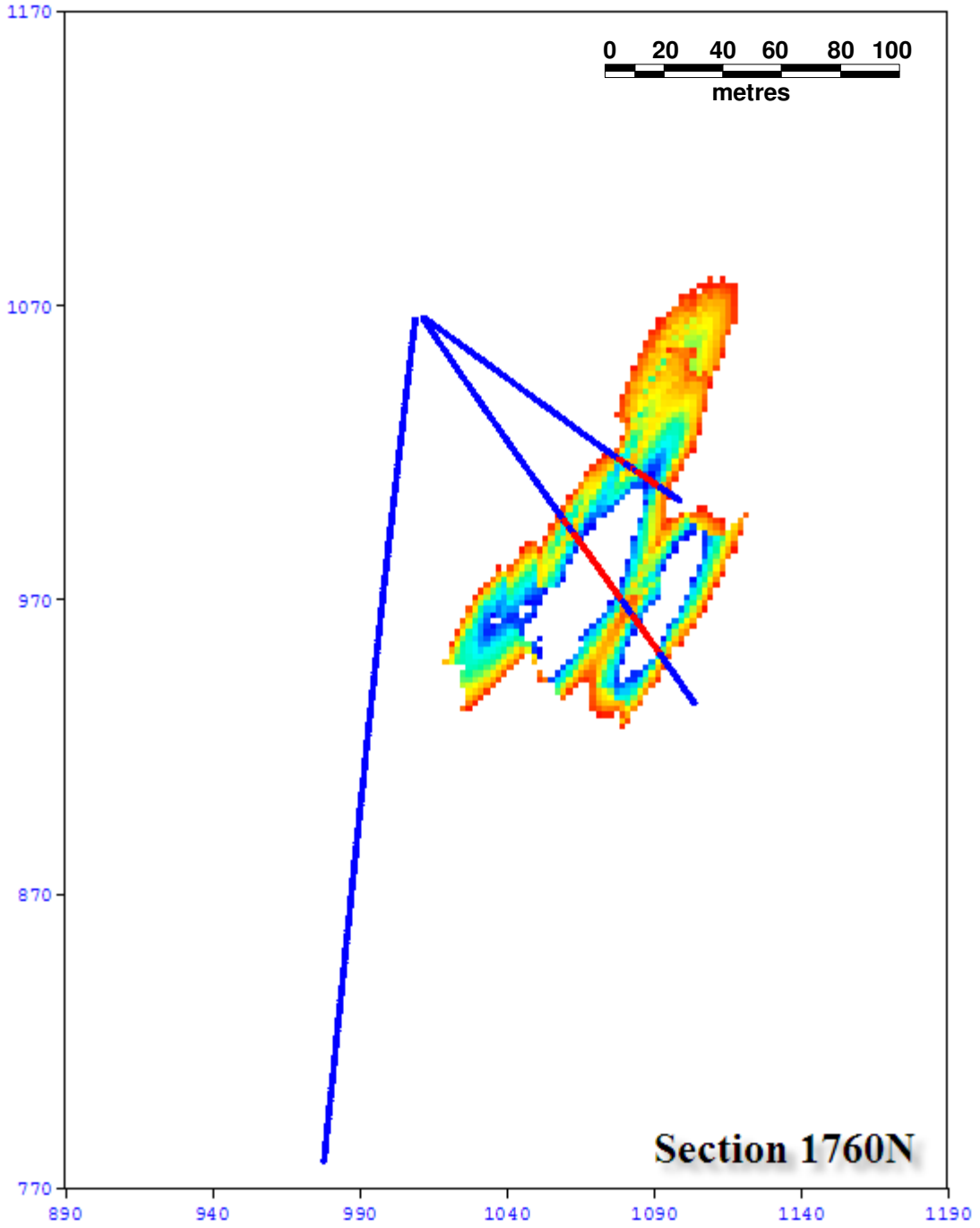


**Figure C-9:** Distance function model on vertical cross section 1760N.

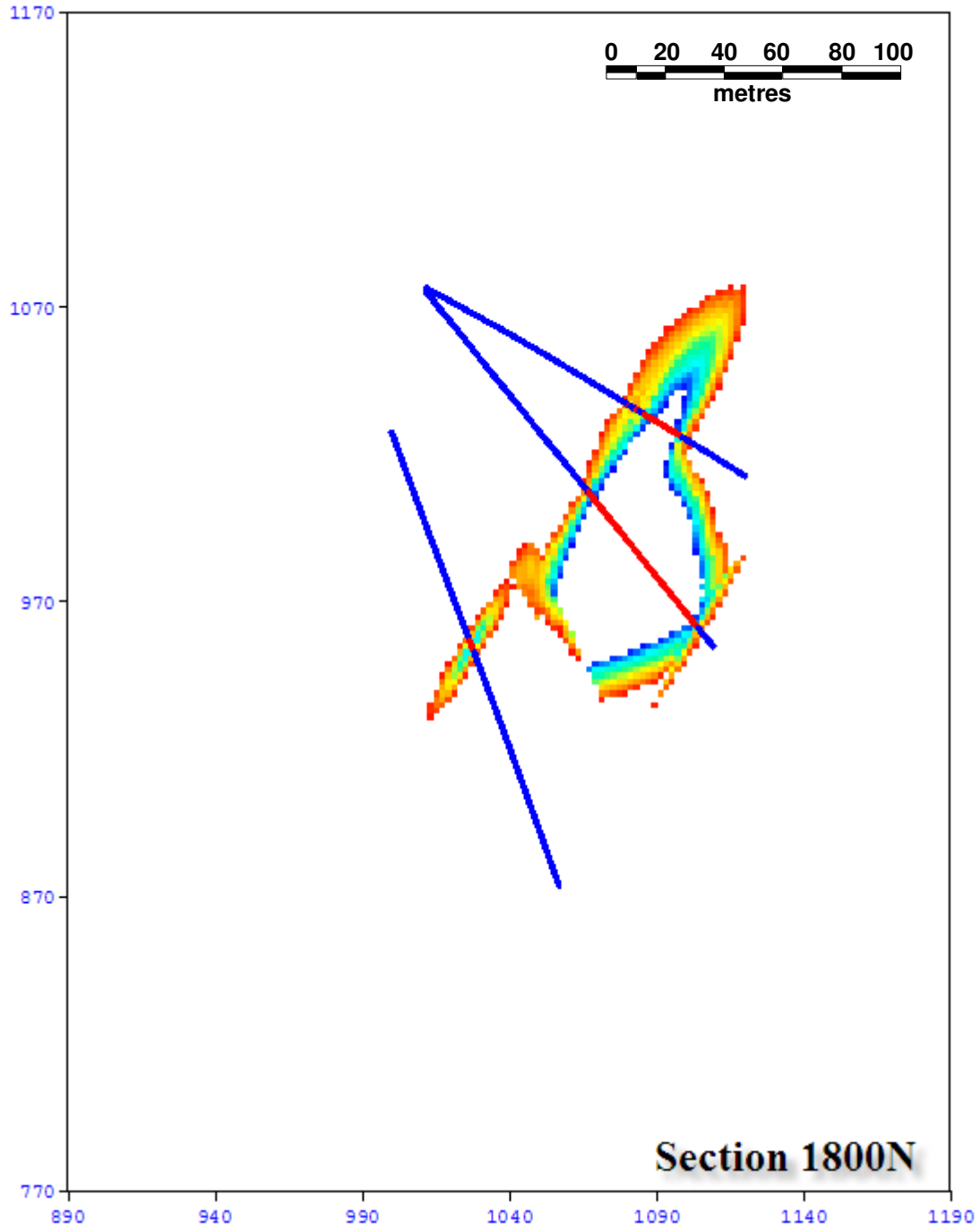


**Figure C-10:** Distance function model on vertical cross section 1800N.

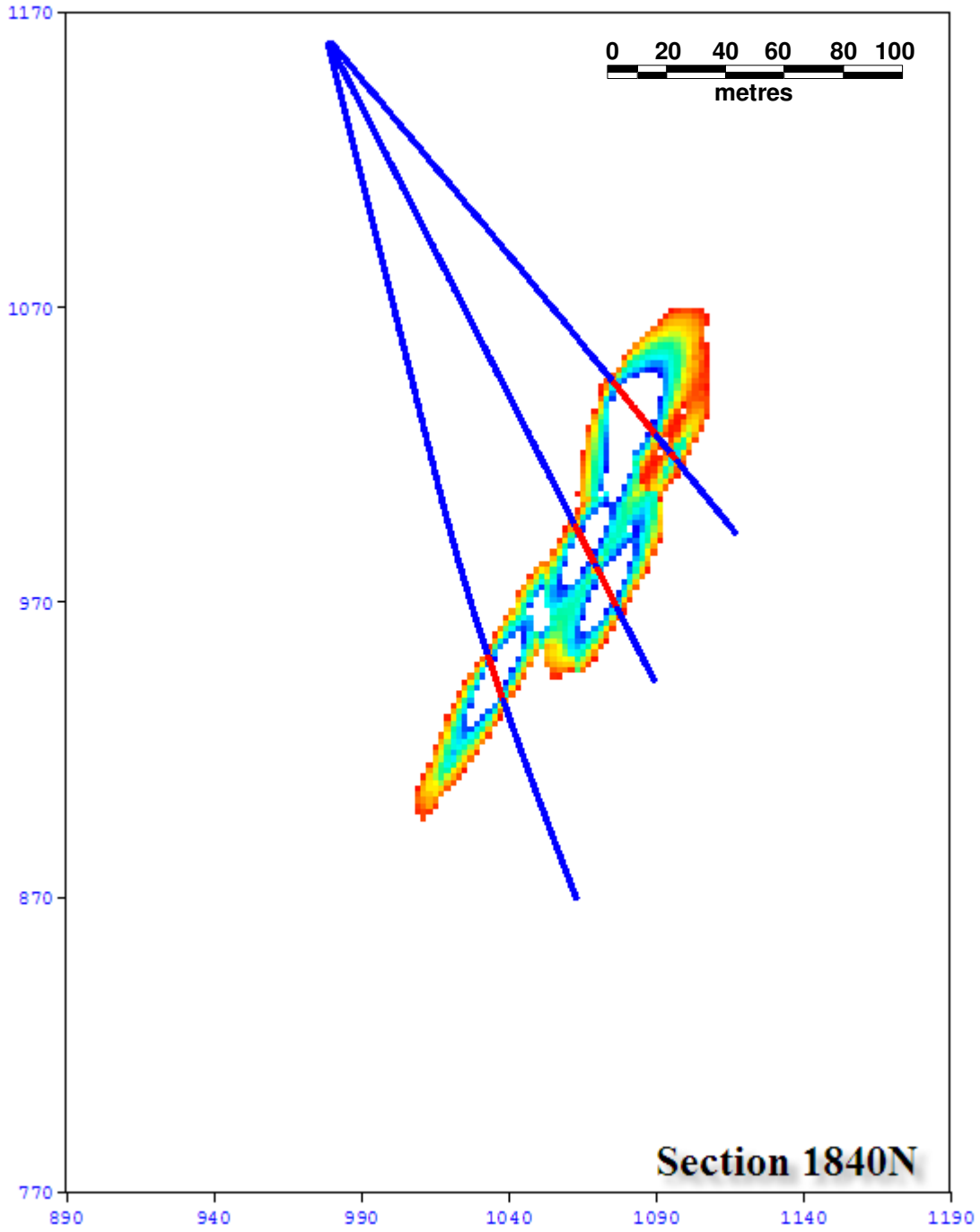


**Figure C-11:** Distance function model on vertical cross section 1840N.

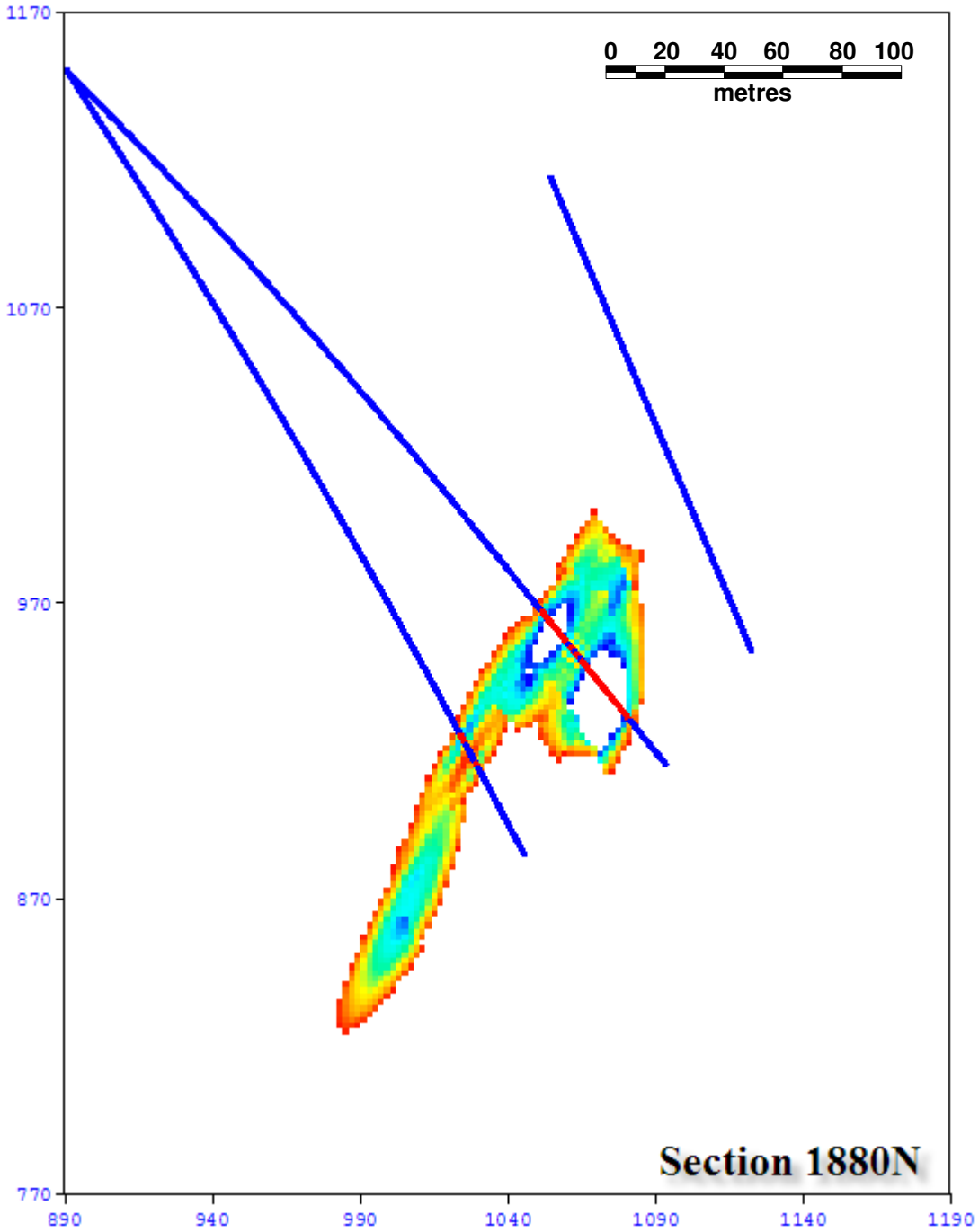


**Figure C-12:** Distance function model on vertical cross section 1880N.

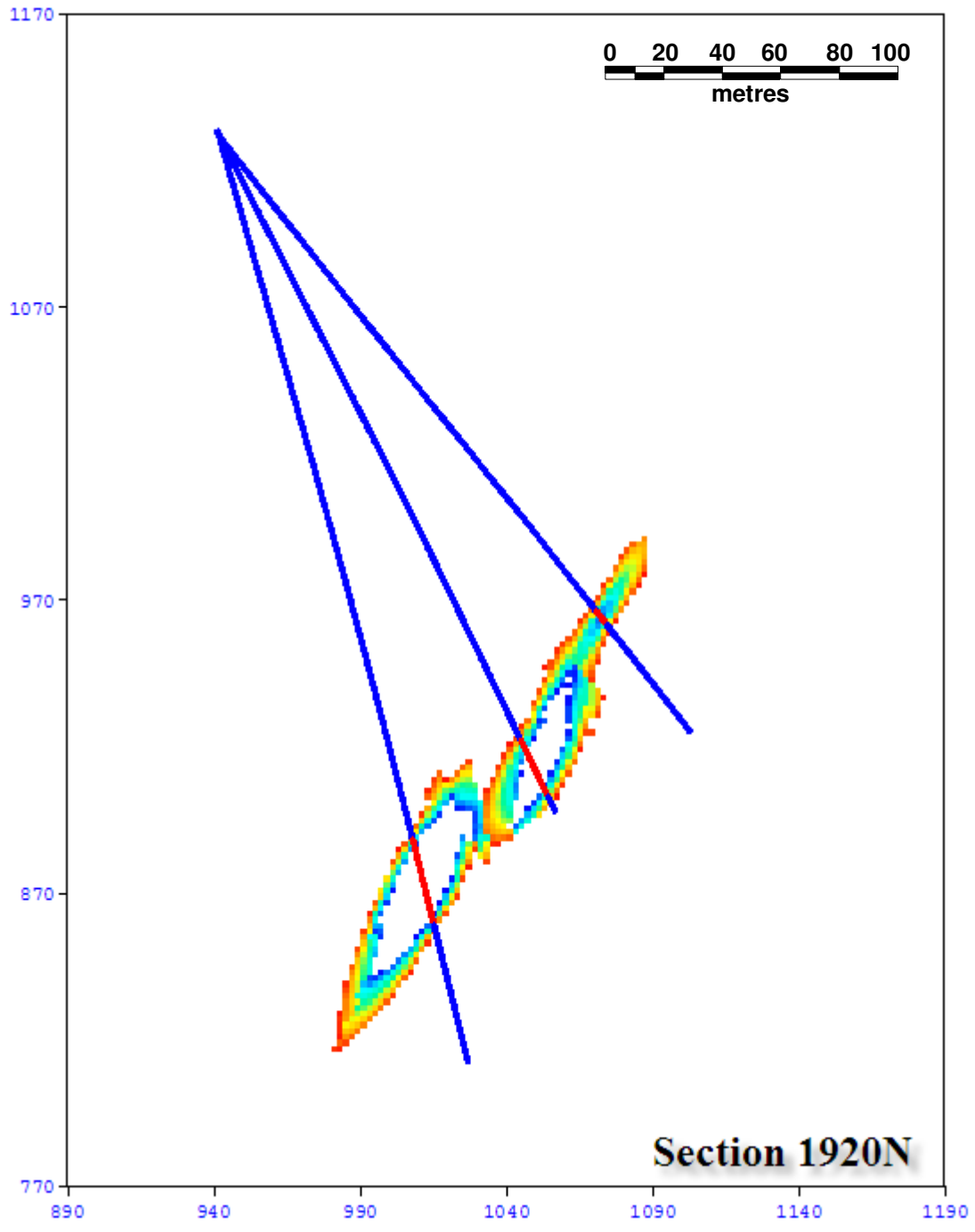


**Figure C-13:** Distance function model on vertical cross section 1920N.

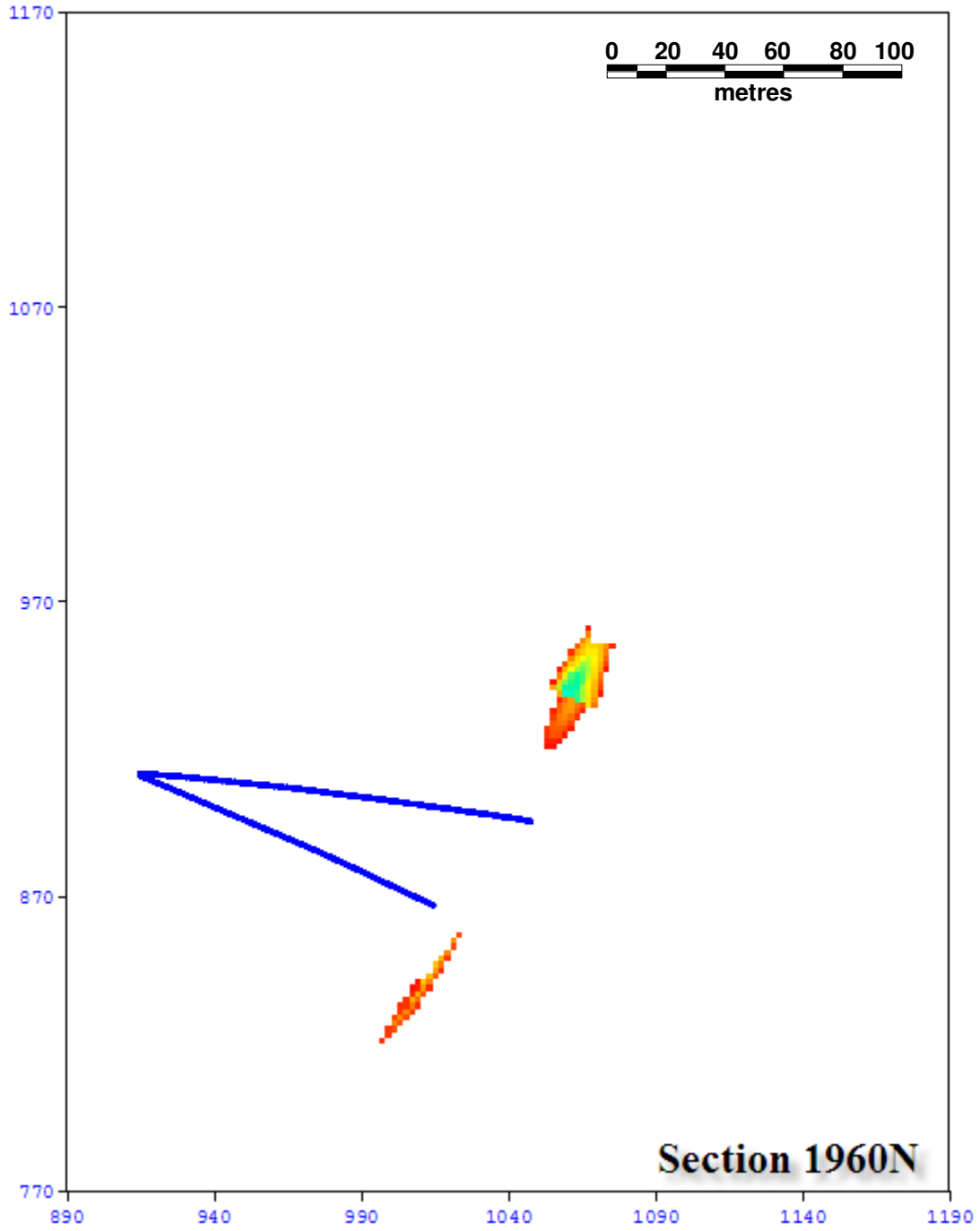


**Figure C-14:** Distance function model on vertical cross section 1960N.

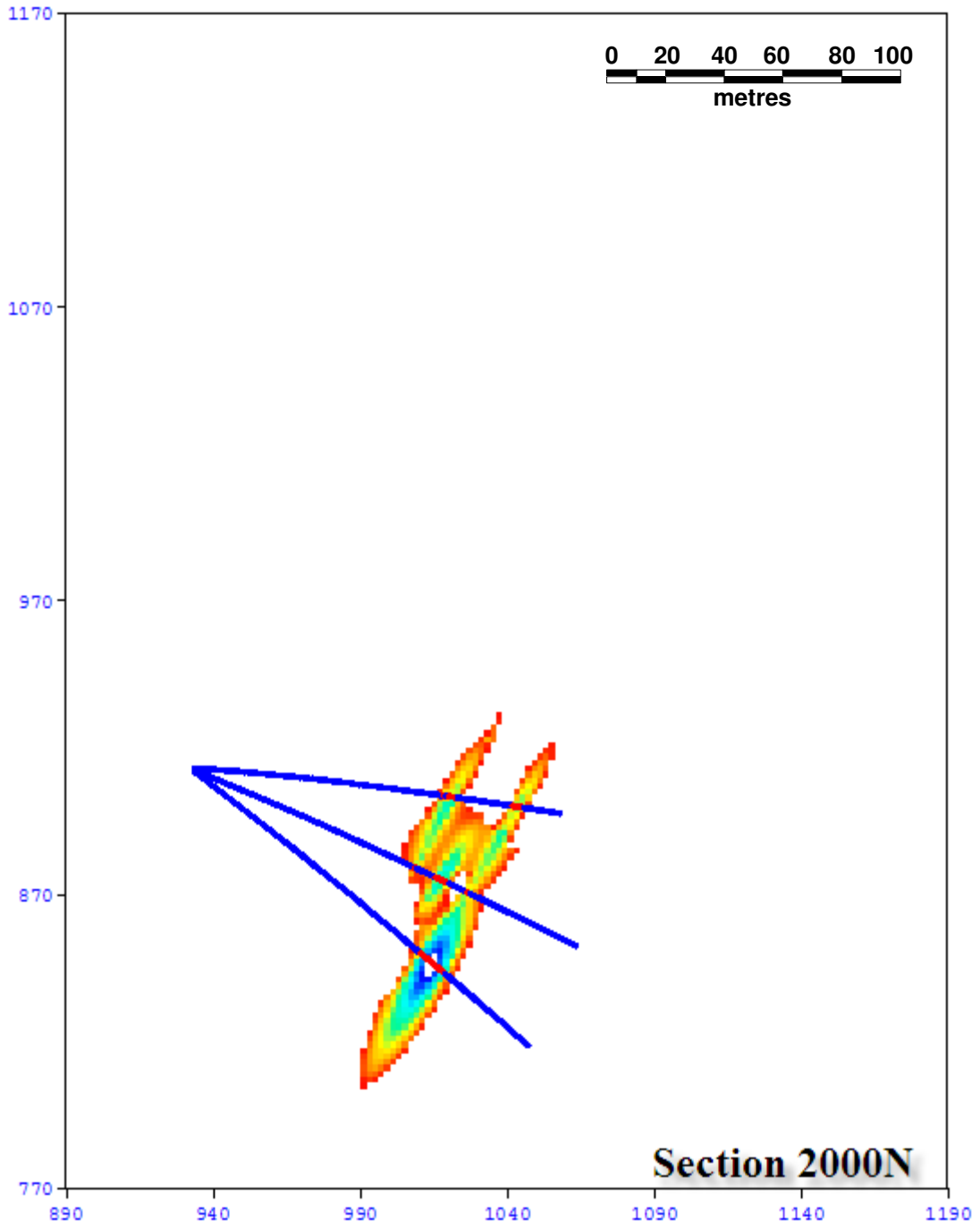


Figure C-15: Distance function model on vertical cross section 2000N.

### C.3 Horizontal Level Plans of the DF

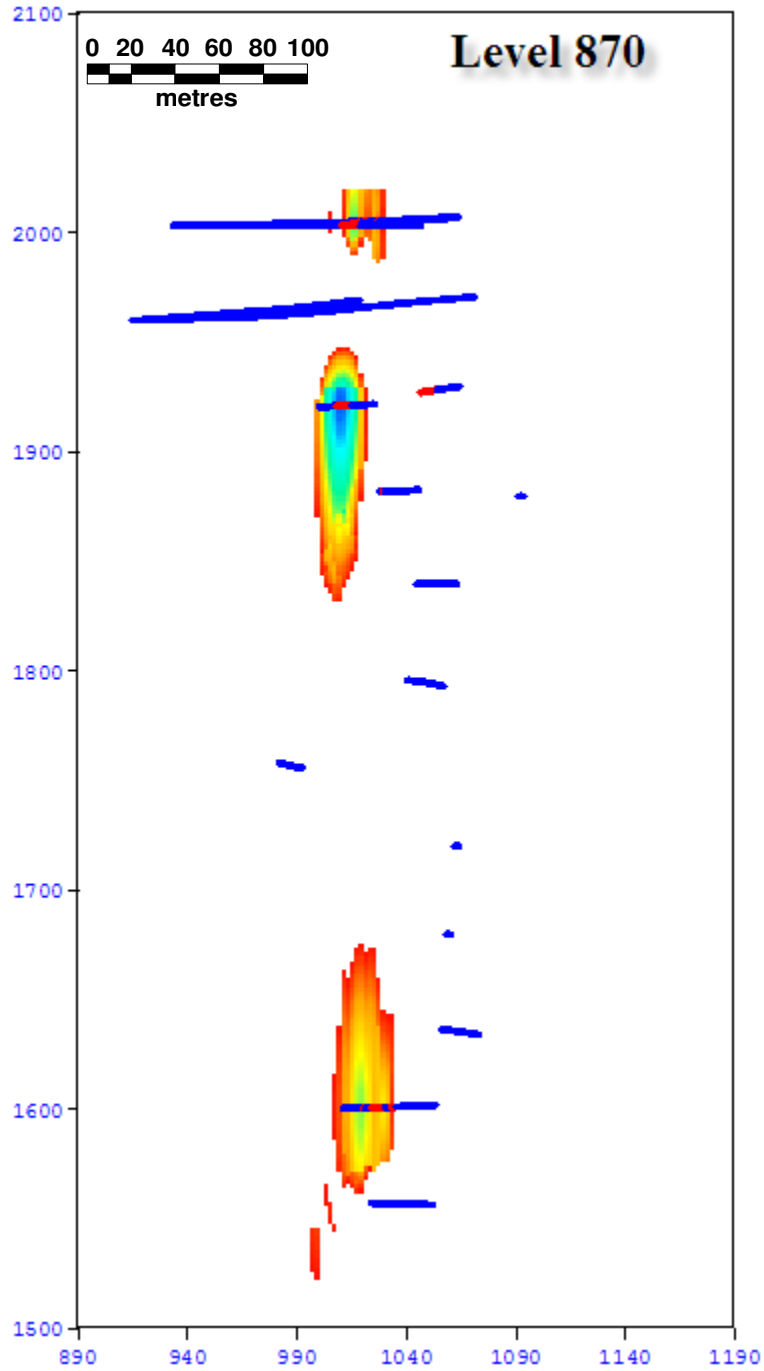
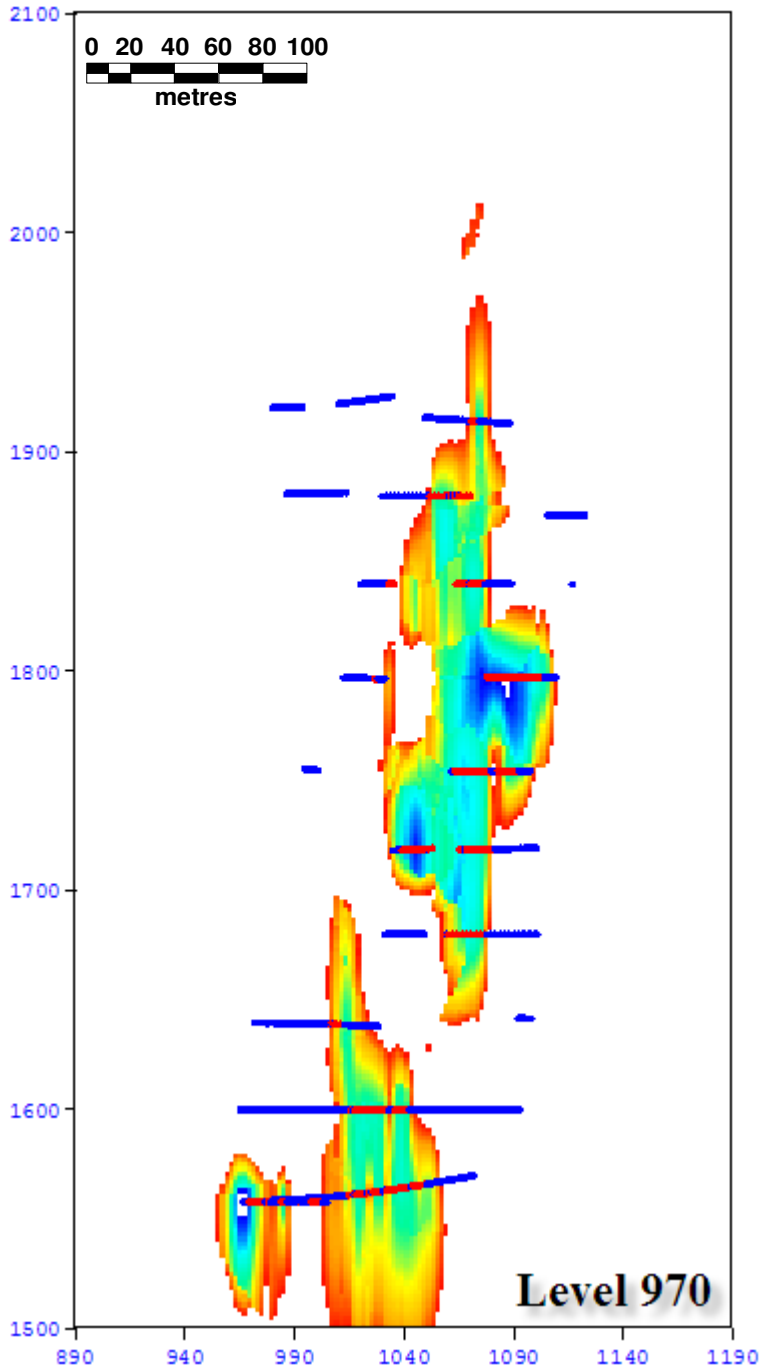
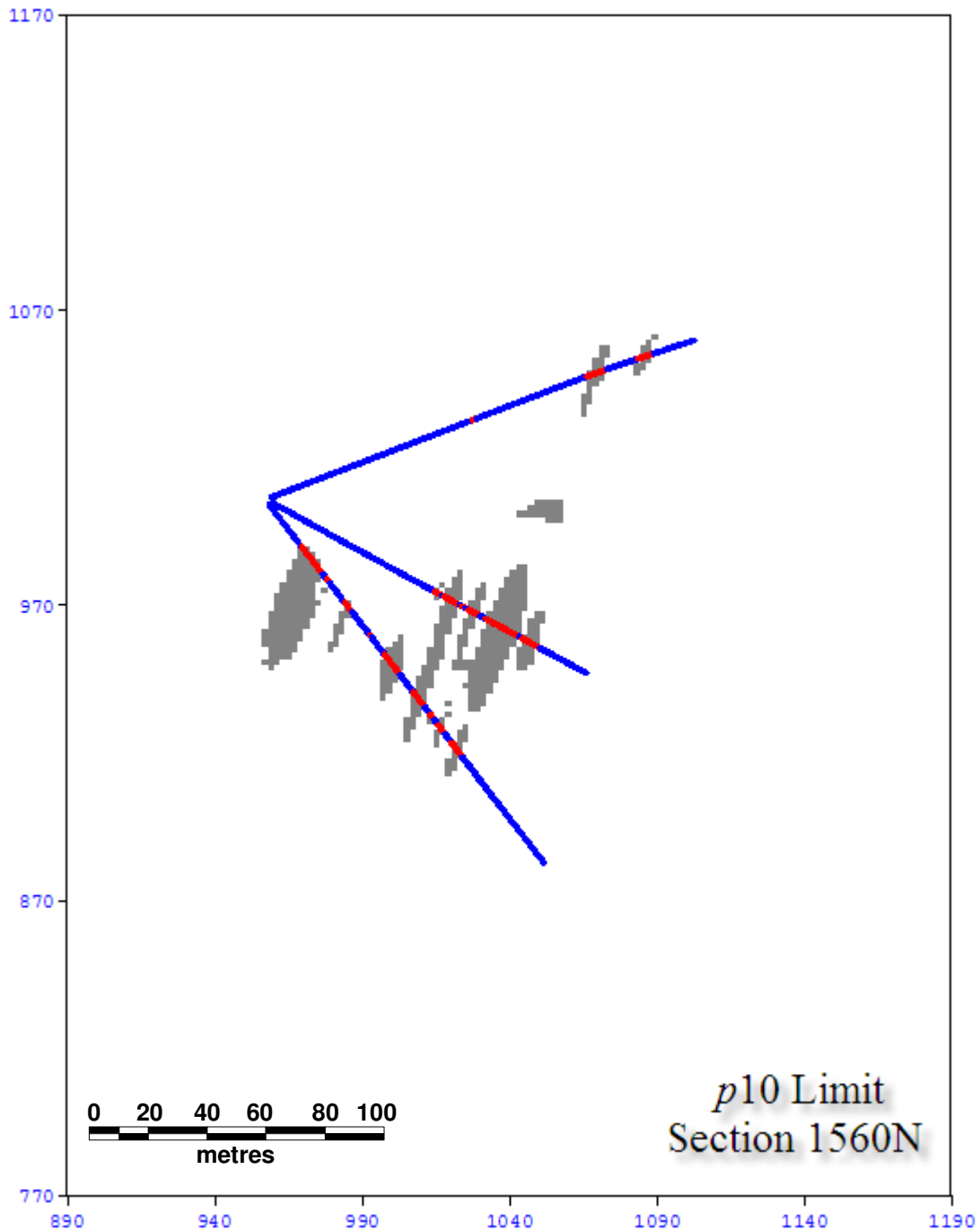


Figure C-16: Horizontal level plan elevation 870m showing DF.



**Figure C-17:** Horizontal level plan elevation 970m showing DF.

## C.4 Indicator Models Vertical Cross Section 1560N



**Figure C-18:** Vertical cross section 1560N,  $p_{10}$  Indicator Probability model created using *clipdf.exe*.

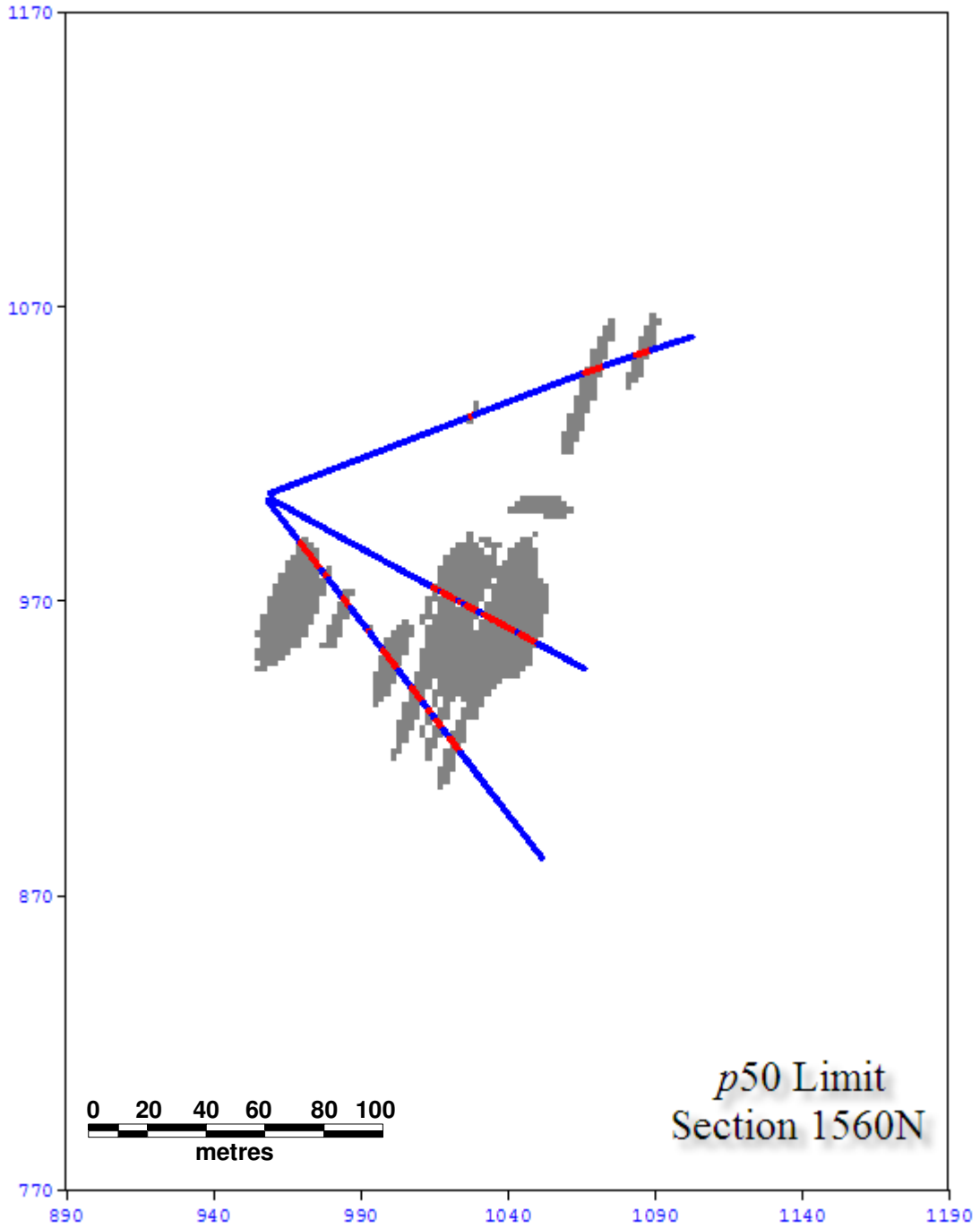


**Figure C-19:** Vertical cross section 1560N,  $p_{50}$  Indicator Probability model created using *clipdf.exe*.

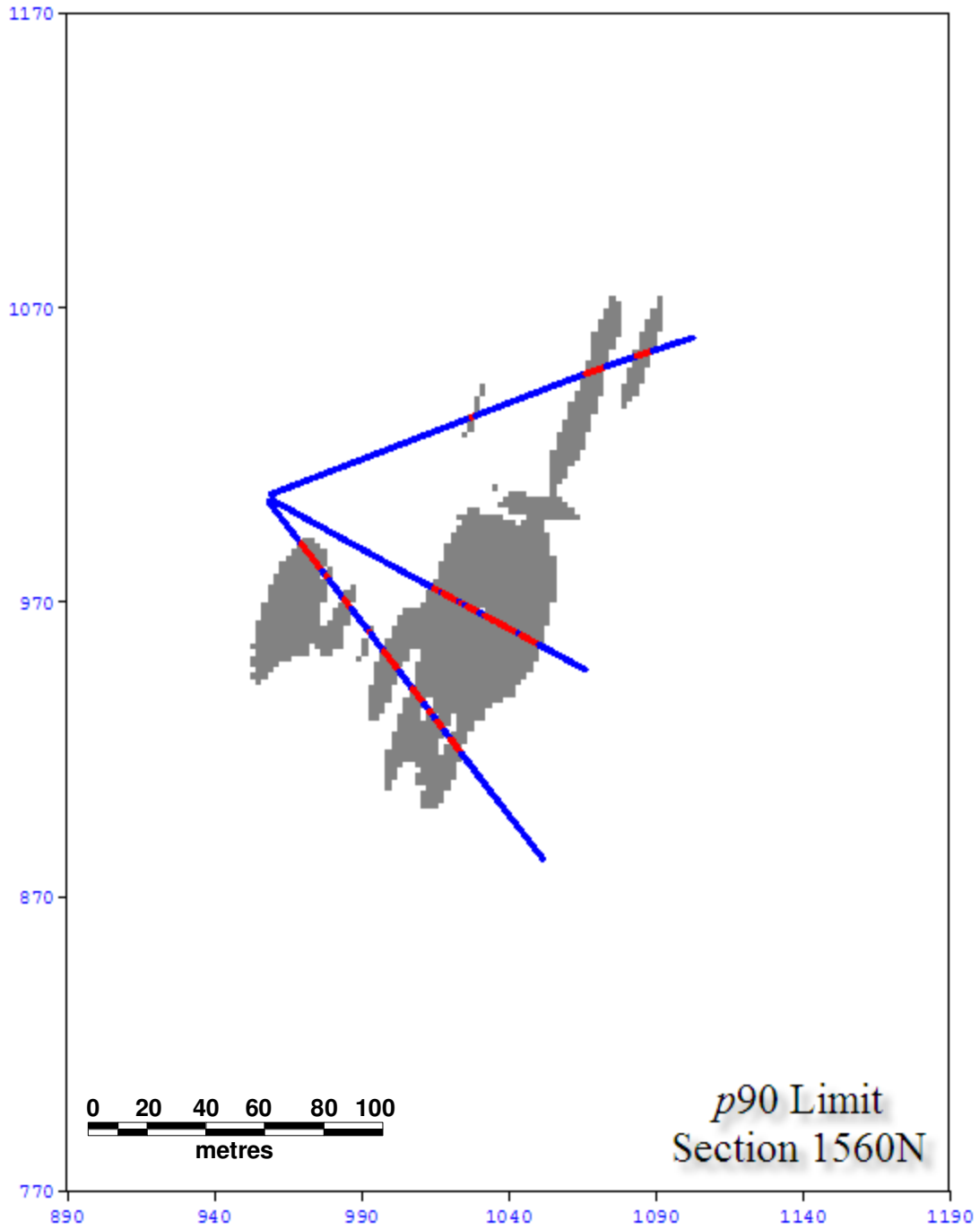


**Figure C-20:** Vertical cross section 1560N,  $p_{90}$  Indicator Probability model created using *clipdf.exe*.